

Photocopy and Use Authorization

In presenting this dissertation in partial fulfillment of the requirements for an advanced degree at Idaho State University, I agree that the Library shall make it freely available for inspection. I further state that permission to download, photocopy, and/or print my dissertation for scholarly purposes may be granted by the Dean of the Graduate School, Dean of my academic division, or by the University Librarian. It is understood that any copying or publication of this dissertation for financial gain shall not be allowed without my written permission.

Signature _____

Date _____

Optimization of Neutron and Gamma Ray Layered Shielding for Hot Cells Containing Used
Nuclear Fuel

by

Aaron Michael Thompson

A dissertation

submitted in partial fulfillment

of the requirements for the degree of

Doctor of Philosophy in Nuclear Science and Engineering

Idaho State University

Summer 2018

Copyright 2018 Aaron M Thompson

To the Graduate Faculty:

The members of the committee appointed to examine the dissertation of AARON M THOMPSON find it satisfactory and recommend that it be accepted.

Chad Pope, PhD,
Major Advisor

Jay Kunze, PhD,
Committee Member

George Imel, PhD,
Committee Member

Leslie Kerby, PhD,
Committee Member

Hossein Mousavinezhad, PhD,
Graduate Faculty Representative

Dedication

To my beloved Buttercup. I will always be your Dread Pirate Roberts. Without you and your support I never would have survived the “Fire Swamp” of my doctoral program. Forever and always... “As you wish!”

Also, to my darling daughters, four: Katelyn, Kira, Eliana, and Anora. Thank you for the laughter, giggles, jokes, wit, and most of all, support that helped me keep my sanity in check.

Acknowledgements

My deepest appreciation goes to my research advisor, Chad Pope, PhD for his invaluable friendship, expertise, and funding for materials to complete the experiments. I extend this appreciation to my committee members, Jay Kunze, PhD, George Imel, PhD, Leslie Kerby, PhD, and Hossein Mousavinezhad, PhD for their willingness to serve on my committee and to provide priceless advice in completing the work. Thank you to Idaho State University Graduate School and the Department of Physics, Health Physics, Electrical Engineering and Nuclear Engineering, and the staff of both for their diligence and assistance in making sure all the “i”s were dotted and “t”s were crossed.

Sarah Black deserves a special mention for her contributions to this work. She developed the Matlab® code used to create and automate the input files for the shielding optimization. Her efforts and assistance were paramount to the timely completion of this work. I am honored to have had her as a team member.

The Nuclear Engineering Laboratory is staffed by many wonderful people. Maxwell Daniels, MS, the reactor supervisor, and his staff were invaluable in the experimental phases assisting with space requirements, set up and tear down of experiments, and use of radionuclide sources. I give my gratitude to Max and his staff.

A special thanks to Caryn Havlovick, PhD for helping with the production of concrete shielding, Kelly Brown of Gem State Machining for manufacturing special components of the neutron collimator, Kevin Claver and the ISU technical safety office (TSO) for assistance with detectors and detector components, as well as gamma source training, and Maxwell Daniels and the reactor staff for their assistance in neutron experiments.

Thank you to Los Alamos for the use of PeakEasy 4.94 to process and analyze spectra generated during the experiments.

I express my deepest gratitude to the U. S. Army for providing this marvelous opportunity to further my education and to obtain this degree. Without the Army granting the time and financial resources toward this pursuit, it would not have happened.

Vita

Aaron M Thompson was born in Austin, Texas and raised in Manhattan, Kansas by loving, kind parents who taught him well in moral and ethical decision making as well as encouraged him to pursue his dreams through hard work and perseverance.

Aaron completed a Bachelor of Science (BS) in chemistry at the University of Iowa in 1997. He continued his education at Kansas State University completing a Master of Science (MS) in Nuclear Engineering in 2006. His thesis was titled, "Developmental Work on a Laser Sampled Electro-Optic Neutron Detector." He has continued his learning through many training and educational opportunities provided by the U.S. Army.

Following completion of Aaron's MS he was direct commissioned as an officer, First Lieutenant, in the U.S Army; Nuclear Medical Science Officer (72A). He was first assigned to work at U.S. Army Center for Health Promotion and Preventive Medicine (USACHPPM) at Aberdeen Proving Grounds in Maryland where he worked in environmental health physics.

He was deployed to Kuwait for six months to serve as the U.S. Army Material Command radiation safety officer for Southwest Asia. He was responsible for all radioactive commodities entering and leaving the theater of operation as well as recycling, repurposing, or disposing of unwanted or damaged radioactive commodities.

Upon return from deployment Aaron was assigned to the 20th Support Command Chemical, Biological, Radiological, Nuclear, and High Yield Explosives (CBRNE) at Aberdeen Proving Ground in Maryland. He served in two positions at this assignment. First, he served as the Command Force Health Protection officer providing guidance to the commander and troops on preventive medicine measures. Second, he served as the Health Physics Operations officer on the Nuclear Disablement Team (NDT). He was responsible for providing radiation safety measures and guidance to the team.

Aaron was then assigned to the U.S. Army Medical Department Center and School (AMEDDCS), CBRN Science Branch at Joint Base San Antonio - Fort Sam Houston in San Antonio Texas. He was the primary instructor for nuclear weapons and radiological effects. He also served as the Radiation Safety Officer for the school. While at this assignment he became the course manager for the Radiological Hazards Operators Training and Field Exercise, the premier course for training new 72As for deployment health physics, taught at and with Idaho National Laboratory. He was the course manager for two years and an instructor for three additional years.

Aaron was selected by the U.S. Army to return to school to complete a Doctoral (PhD) degree in Nuclear Engineering. He chose to complete this work at Idaho State University in Pocatello, Idaho. This opportunity was provided by the Long Term Health Education and Training (LTHET) program of the U.S. Army Medical Department. The work leading to completion of this degree follows herein.

Contents

LIST OF FIGURES	XI
LIST OF TABLES	XV
LIST OF EQUATIONS	XIX
LIST OF UNITS, ACRONYMS, AND SYMBOLS	XXI
ABSTRACT.....	XXIV
1 INTRODUCTION	1
2 RADIATION: PRINCIPLES AND INTERACTIONS	2
2.1 RADIATION PROTECTION PRINCIPLES	2
2.2 RADIATION INTERACTIONS WITH MATTER	4
2.2.1 <i>Gamma-ray Interactions with Matter</i>	4
2.2.2 <i>Neutron Interactions with Matter</i>	10
3 SHIELDING	16
3.1 SHIELDING MATERIALS AND RADIATION TYPE	16
3.2 SHIELDING OPTIMIZATION STUDIES	17
3.3 SHIELDING IN LAYERS	19
3.4 HOT CELL SHIELDING.....	20
3.5 CONCRETE: THEN AND NOW	21
4 COMPUTATION AND SIMULATION.....	24
4.1 MONTE CARLO	24
4.1.1 <i>Monte Carlo N-Particle (MCNP)</i>	26
4.1.2 <i>SCALE</i>	26
4.2 VARIANCE REDUCTION.....	27
4.2.1 <i>MCNP Variance Reduction Methods</i>	28
4.2.1.1 Cell Importance	29
4.2.1.2 Weight Windows	30
5 DISCUSSION.....	31
5.1 SHIELDING MATERIAL SELECTION	31
5.2 RADIONUCLIDE SOURCE SELECTION	34
5.3 RADIATION DETECTOR SELECTION.....	39
6 POINT KERNEL (HAND AND SIMULATION CALCULATIONS).....	42
6.1 DESIGN	42
6.2 RESULTS AND ANALYSIS	43
7 SHIELDING EXPERIMENT AND SIMULATION	47
7.1 EXPERIMENTAL DESIGN	47
7.2 GAMMA-RAY EXPERIMENT	47
7.2.1 <i>The First Attempt</i>	47
7.2.2 <i>The Second Attempt</i>	54
7.2.2.1 Counting System Checks	56
7.2.2.2 Experimental Results	60

7.2.2.3	Error Analysis.....	62
7.3	GAMMA-RAY SIMULATION.....	63
7.3.1	Tally Selection.....	64
7.3.2	Atom Densities	66
7.3.3	Geometry Refinements.....	68
7.3.4	Simulation Results with Comparison to Experimental Results.....	69
7.4	NEUTRON EXPERIMENT	76
7.4.1	Collimator/Storage Drum	77
7.4.1.1	Design.....	77
7.4.1.2	Construction	79
7.4.2	The Equipment	83
7.4.2.1	Counting System Checks	85
7.4.3	Results	86
7.4.4	Error Analysis	88
7.5	NEUTRON SIMULATION	92
7.5.1	Tally Selection.....	93
7.5.2	Atom Densities	99
7.5.2.1	Shielding Materials.....	99
7.5.2.2	Source Material.....	100
7.5.2.3	Detector Gas	101
7.5.3	Geometry Refinements.....	102
7.5.3.1	Addition of Walls	102
7.5.3.2	Detector Inactive Regions.....	103
7.5.3.3	Drum/Collimator Refinements	104
7.5.4	Simulation Results with Comparison to Experimental	105
8	SHIELDING OPTIMIZATION.....	107
8.1	OPTIMIZATION DESIGN	107
8.2	RESULTS	112
8.2.1	Gamma-Ray Monolithic Concrete Shield.....	112
8.2.2	Gamma-Ray Multi-Layered Multi-Material Shield.....	113
8.2.3	Neutron Monolithic Concrete Shield.....	114
8.2.4	Neutron Multi-Layered Multi-Material Shield.....	115
8.2.5	Weight Comparison and Rudimentary Cost Estimate	117
9	CONCLUSIONS.....	120
9.1	POINT KERNEL CALCULATIONS AND SIMULATIONS	120
9.2	EXPERIMENTS AND SIMULATIONS	120
9.3	OPTIMIZATION	122
10	FURTHER WORK.....	125
10.1	IMPROVEMENTS TO EXPERIMENTS.....	125
10.2	IMPROVEMENTS TO SIMULATIONS	126
10.3	FUTURE RELATED WORK IDEAS	127
11	REFERENCES	128
12	APPENDIX A: ATOM DENSITIES	132
12.1	POINT KERNEL AND CODE VALIDATION.....	132
12.2	EXPERIMENTAL SIMULATION MODEL ATOM DENSITIES	133
12.2.1	Gamma-ray Experiments.....	133
12.2.2	Neutron Experiments.....	136

12.2.3	<i>Hand Calculation Examples</i>	140
12.3	SHIELDING OPTIMIZATION.....	144
12.3.1	<i>Gamma-ray Models</i>	144
12.3.2	<i>Neutron Models</i>	146
13	APPENDIX B: SHIELDING MATERIAL INFORMATION.....	150
13.1	CONCRETE.....	150
13.2	STAINLESS STEEL 304 (McMASTER CARR).....	151
13.3	BORATED POLYETHYLENE (SHIELDWERX).....	152
13.4	TUNGSTEN CARBIDE (H. B CARBIDE).....	153
14	APPENDIX C: CURRENT SOURCE STRENGTHS AND SOURCE CERTIFICATES ...	154
14.1	CURRENT GAMMA RAY EMISSION RATE.....	154
14.2	¹³⁷ Cs CERTIFICATE.....	155
14.3	AMBe CERTIFICATE.....	156
14.4	CURRENT NEUTRON EMISSION RATE.....	159
15	APPENDIX D: DETECTOR DATA SHEETS.....	160
15.1	NAI(TL) SCINTILLATION DETECTOR FOR GAMMA-RAYS.....	160
15.2	³ He PROPORTIONAL COUNTING DETECTOR FOR NEUTRONS.....	164
16	APPENDIX E: POINT KERNEL HAND CALCULATION EXAMPLE.....	166
17	APPENDIX F: MONTE CARLO NEUTRON PARTICLE (MCNP) INPUT FILES	170
17.1	POINT KERNEL MODELS.....	170
17.2	GAMMA RAY EXPERIMENT MODELS.....	172
17.2.1	<i>Unshielded Setup</i>	172
17.2.2	<i>Shielded Setups</i>	176
17.2.2.1	Single Material, Single Layer.....	176
17.2.2.2	Multi-material, Multi-layered.....	180
17.2.3	<i>Gaussian Energy Broadening</i>	184
17.3	NEUTRON EXPERIMENT MODELS.....	185
17.3.1	<i>Unshielded Setup</i>	185
17.3.2	<i>Shielded Setups</i>	191
17.3.2.1	Multi-material, Multi-layered.....	191
17.4	GAMMA RAY HOT CELL OPTIMIZATION MODELS.....	198
17.4.1	<i>Concrete Only</i>	198
17.4.2	<i>Multi-material, Multi-layered</i>	204
17.5	NEUTRON HOT CELL OPTIMIZATION MODELS.....	209
17.5.1	<i>Concrete Only</i>	209
17.5.2	<i>Multi-material, Multi-layered</i>	214
18	APPENDIX G: OTHER CODES UTILIZED IN CONJUNCTION WITH MCNP	220
18.1	MATLAB® CODES FOR SHIELDING OPTIMIZATION INPUT FILE GENERATION.....	220
18.1.1	<i>Gamma-ray Concrete Shielding</i>	220
18.1.2	<i>Gamma-ray Multi-layered Shielding</i>	223
18.1.3	<i>Neutron Concrete Shielding</i>	228
18.1.4	<i>Neutron Multi-layered Shielding</i>	231
18.1.5	<i>Example Continue Run and Data Analysis</i>	234
18.2	SCRIPTS AND BATCH FILES.....	236

18.2.1	<i>Example .bat File for Windows System</i>	236
18.2.2	<i>Example Read File for .bat</i>	236
18.2.3	<i>Example .sh File for Linux System</i>	236
18.3	SPECIAL TREATMENT FOR TALLY GAUSSIAN ENERGY BROADENING COEFFICIENTS	236
19	APPENDIX H: SCALE INPUT FILES.....	238
19.1	POINT KERNEL MODELS	238
20	APPENDIX I: SCALE MESSAGE PASSING INTERFACE (MPI) BUILD	241
20.1	BUILDING SCALE MPI	242
20.1.1	<i>Installing Compilers and Third-party Libraries (TPLs)</i>	243
20.1.2	<i>Pre-configuration</i>	245
20.1.3	<i>CMake Configuration</i>	246
20.1.4	<i>Compilation and Installation</i>	249
20.2	INSTALLING DATA FILES	249
20.3	IMPLEMENTING PARALLEL PROCESSING.....	257

List of Figures

FIGURE 2-1 INTERACTIONS OF A SOURCE GAMMA-RAYS (ADAPTATION FROM COURSE NOTES BY JACK COURTNEY [37]).	5
FIGURE 2-2 THE PHOTOELECTRIC EFFECT.	6
FIGURE 2-3 COMPTON SCATTERING.	8
FIGURE 2-4 PAIR PRODUCTION AS MAY OCCUR NEAR A NUCLEAR FIELD.	9
FIGURE 2-5 ATTENUATION PROBABILITY OF THE VARIOUS PHOTON INTERACTIONS TO AND THEIR CONTRIBUTIONS TO TOTAL ATTENUATION PROBABILITY. SOURCE: WIKIMEDIA COMMONS.	9
FIGURE 2-6 INTERACTIONS OF SOURCE NEUTRONS (ADAPTATION FROM [37]).	11
FIGURE 2-7 INELASTIC NEUTRON SCATTERING.	11
FIGURE 2-8 ELASTIC NEUTRON SCATTERING.	12
FIGURE 2-9 NEUTRON ABSORPTION.	14
FIGURE 2-10: NEUTRON CROSS SECTION PLOT OF VARIOUS INTERACTIONS AND THE TOTAL CROSS SECTION FOR ^3He . PLOT IS COURTESY OF JAPAN ATOMIC ENERGY AGENCY NUCLEAR DATA CENTER, FROM JENDL-4.0 [38].	15
FIGURE 3-1 PRE-TENSIONING METHOD TO PRESTRESS CONCRETE. IMAGE FROM WIKIPEDIA.	22
FIGURE 3-2 POST-TENSIONING MULTI-TENDON ANCHOR FOR PRESTRESSING CONCRETE. IMAGE FROM WIKIPEDIA.	23
FIGURE 4-1 THE BASIC PROCESS OF ANALOG MONTE CARLO FOR THE LIFE OF A NEUTRON AND THE SELECTION OF RANDOM NUMBERS TO DESCRIBE ITS LIFE. DIAGRAM ADAPTED FROM MCNP LECTURE NOTES BY DR. CHAD POPE.	25
FIGURE 5-1 RECOMMENDED ENERGY SPECTRUM FROM AN $^{241}\text{AmBe}$ NEUTRON SOURCE USED IN EXPERIMENTAL MODELS [45].	36
FIGURE 5-2 GAMMA-RAY SPECTRUM ESTIMATED BY ORIGEN/SCALE FOR A WESTINGHOUSE 17X17 FUEL ASSEMBLY WITH VARIOUS BURNUP AND INITIAL ENRICHMENT.	37
FIGURE 5-3 FISSION NEUTRON SPECTRUM APPROXIMATED BY THE WATT DISTRIBUTION FOR ^{235}U (RED LINE) AND ^{239}Pu (BLUE LINE). (IMAGE FROM HTTP://NEUTRON.KTH.SE/COURSES/TRANSMUTATION/SPECTRA/SPECTRA.HTML)	38
FIGURE 6-1 DIAGRAM OF THE POINT KERNEL EXPERIMENTS.	42
FIGURE 7-1 SPECTRUM FROM THE ^{137}Cs CALIBRATION SOURCE.	49
FIGURE 7-2 A) PHOTOGRAPH OF AND B) DRAWING OF THE SET UP FOR THE J L SHEPHERD 1 Ci (3.7×10^4 MBq) CALIBRATOR SHOWING A SINGLE LAYER OF EACH MATERIAL AND THE 3X3 NAI DETECTOR.	51
FIGURE 7-3 SPECTRUM OBTAINED FROM 1 Ci (3.7×10^4 MBq) ^{137}Cs ON A Q&S 3X3 NAI DETECTOR HAVING TWO LAYERS OF EACH SHIELDING MATERIAL BETWEEN SOURCE AND DETECTOR.	52
FIGURE 7-4 SPECTRUM OBTAINED FROM 1 Ci (3.7×10^4 MBq) ^{137}Cs AND Q&S 3X3 NAI DETECTOR WITH ONE LAYER OF SHIELDING MATERIAL BETWEEN SOURCE AND DETECTOR.	52
FIGURE 7-5 BACKGROUND SPECTRUM TAKEN IN THE VAULT CONTAINING THE J L SHEPHERD CALIBRATOR AND IRRADIATOR USING THE Q&S 3X3 NAI DETECTOR.	53
FIGURE 7-6 A) A PHOTOGRAPH OF THE DETECTOR TO PIG SET UP USED. B) SHOWS A DRAWING OF THE SAME SET-UP BUT INCLUDING SHIELDING BLOCKS.	55

FIGURE 7-7 CALIBRATION SPECTRUM FOR THE BICRON 2x2 NAI DETECTOR USING ^{133}Ba AND ^{137}Cs SOURCES.	55
FIGURE 7-8 HISTOGRAM OF COUNTING SYSTEM CHECK DATA FREQUENCY, $F(E)$, AND PLOT OF COUNTING SYSTEM CHECK PROBABILITY, $P(E)$	59
FIGURE 7-9 PULSE HEIGHT SPECTRUM OBTAINED USING A BICRON 2x2 NAI DETECTOR AND A ^{137}Cs SOURCE.	60
FIGURE 7-10 SPECTRUM COLLECTED FOR THE EXPERIMENTAL RUN WITH A SHIELDING CONFIGURATION OF SSWCBPC.	62
FIGURE 7-11 CHANGES TO THE GEOMETRIC AND MATERIAL DESCRIPTIONS OF THE DETECTOR FROM BEGINNING TO END. A CUT AWAY FROM THE FULL DETECTOR IS PROVIDED FOR IDENTIFICATION OF INTERNAL PARTS.	69
FIGURE 7-12 PLOT OF GAMMA-RAY EXPERIMENTAL AND SIMULATION RESULTS WITH ASSOCIATED ERRORS.	71
FIGURE 7-13 A) TRACK LENGTH ESTIMATOR, F_4 TALLY OF THE GEOMETRY INDICATING THE RELATIVE FLUX OF PHOTONS. B) ZOOM OF THE SOURCE, SHIELDING, AND DETECTOR REGION OF THE PROBLEM FOR THE F_4 TALLY SHOWING RELATIVE FLUX OF PHOTONS THROUGHOUT THE PROBLEM.	74
FIGURE 7-14 A) A MODIFIED TRACK LENGTH ESTIMATOR, F_4 , TALLY SHOWING THE RELATIVE INTERACTION RATE FOR PHOTONS THROUGHOUT THE GEOMETRY. B) A CLOSE UP OF THE SOURCE, SHIELDING, DETECTOR REGION OF THE MODIFIED TRACK LENGTH ESTIMATOR INDICATING RELATIVE PHOTON INTERACTION RATE.	75
FIGURE 7-15 COMPARISON OF THE EXPERIMENTAL AND SIMULATED SPECTRA FOR A NO SHIELD CONFIGURATION OF THE EXPERIMENT.	76
FIGURE 7-16 COMPARISON OF THE EXPERIMENTAL AND SIMULATED SPECTRA FOR THE SSCBPWC SHIELDED CONFIGURATION OF THE EXPERIMENT.	76
FIGURE 7-17 DIAGRAM DEPICTING HOW THE ANGLE OF DIVERGENCE OF A COLLIMATOR IS DETERMINED FROM THE LENGTH AND DIAMETER OF A TUBE.	78
FIGURE 7-18: MCNP DEPICTION OF THE COLLIMATOR AND SOURCE CAPSULE CONTAINING THE AMBe SOURCE.	80
FIGURE 7-19 THE FULL DRUM WHILE COOLING WITH RODS ABOVE FOR ADDITIONAL WEIGHTING..	81
FIGURE 7-20 DRUM DURING COOLING WITH WEIGHTS AND SPACER TO PRESS THE TUBE LOW ENOUGH FOR THE LID.	82
FIGURE 7-21 TRANSPORTATION OF THE DRUM, APPROXIMATELY 500 POUNDS, TO THE UNIVERSITY USING AN ENGINE HOIST.	83
FIGURE 7-22 A) PHOTOGRAPH OF THE SET-UP WITH SHIELDING IN PLACE. B) DEPICTION OF THE SET-UP WITH SHIELDING IN PLACE.	85
FIGURE 7-23 COUNTING SYSTEM SPECTRUM GENERATED BY SCA WINDOWS OF 250 mV WIDTH. .	86
FIGURE 7-24 SPECTRUM OF THE NEUTRON EXPERIMENT WITH SHIELDING CONFIGURATION OF SSCBPWC. IT IS REPRESENTATIVE OF THE SHIELDED CONFIGURATIONS.	88
FIGURE 7-25 A) DEPICTS THE SOURCE IN THE DRUM AND THE DETECTOR ABOVE IN AN AIR ATMOSPHERE. B) SHOWS A CLOSE UP OF THE SOURCE TO PROVIDE A VIEW OF THE DETAIL. ...	92
FIGURE 7-26 A) COMPARISON OF EXPERIMENTAL AND SIMULATED NEUTRON/ ^3He REACTION SPECTRUM FOR THE UNSHIELDED SETUP AND B) THE SSCBPWC SHIELDED SETUP.	94

FIGURE 7-27 A) TRACK LENGTH ESTIMATOR NEUTRON TALLY FOR THE WHOLE GEOMETRY. B) ZOOM OF THE SOURCE AND DETECTOR.	97
FIGURE 7-28 A) MODIFIED TRACK LENGTH ESTIMATOR FOR NEUTRON TALLY SHOWING REACTION RATE FOR PROTON RECOIL ACROSS THE WHOLE GEOMETRY AND B) ZOOM TO THE AREA AROUND THE SOURCE AND DETECTOR.	98
FIGURE 7-29 A) MCNP PLOTTER DEPICTION OF THE FINAL ^3He DETECTOR GEOMETRY. B) DEPICTION OF THE FINAL DRUM/COLLIMATOR GEOMETRY.	105
FIGURE 7-30 PLOT OF NEUTRON EXPERIMENTAL AND SIMULATED RESULTS WITH ASSOCIATED ERRORS.	106
FIGURE 8-1 A) DEPICTION OF A CONCRETE SHIELD AS USED IN THE INITIAL SETUP OF THE OPTIMIZATIONS. B) DEPICTION OF THE MULTILAYERED SHIELD AS USED INITIALLY IN THE OPTIMIZATIONS.	110
FIGURE 8-2 A) DEPICTION OF THE CONCRETE SHIELD OF THE MODELS REPORTED. B) DEPICTION OF THE MULTILAYERED SHIELD USED IN REPORTED OPTIMIZATIONS.	111
FIGURE 8-3 PLOT OF THE GAMMA-RAY TALLY RESULTS FROM THE MONOLITHIC CONCRETE SHIELDING FOR VARIOUS THICKNESSES.	113
FIGURE 8-4 PLOT OF THE GAMMA-RAY TALLY RESPONSE FOR THE MULTILAYERED SHIELD VERSUS THE THICKNESS VARIATIONS OF TUNGSTEN CARBIDE AND BORATED POLYETHYLENE.	114
FIGURE 8-5 PLOT OF THE NEUTRON TALLY RESULTS FOR THE MONOLITHIC CONCRETE SHIELD.	115
FIGURE 8-6 PLOT OF THE NEUTRON TALLY RESULT FOR THE LAYERED SHIELD FOR VARYING THICKNESSES OF TUNGSTEN CARBIDE AND BORATED POLYETHYLENE.	116
FIGURE 9-1: COMPARISON OF THE OPTIMIZED SSCWCBP SHIELD TO THE CONCRETE SHIELD.	124
FIGURE 13-1 BORATED POLYETHYLENE SPECIFICATION SHEET FROM SHIELDWERX.	152
FIGURE 13-2 TUNGSTEN CARBIDE SPECIFICATION SHEET FROM H B CARBIDE.	153
FIGURE 14-1 A COPY OF THE 1 MCI ^{137}Cs SOURCE CERTIFICATE.	155
FIGURE 14-2 A COPY OF THE AMBe SOURCE CERTIFICATE – PAGE 1 OF 4. SOURCE STRENGTH SPECIFICATIONS.	156
FIGURE 14-3 A COPY OF THE AMBe SOURCE CERTIFICATE – PAGE 2 OF 4. CAPSULE SPECIFICATIONS.	157
FIGURE 14-4 A COPY OF THE AMBe SOURCE CERTIFICATE – PAGE 3 OF 4. SHIPMENT SURVEY RECORD.	158
FIGURE 14-5 A COPY OF THE AMBe SOURCE CERTIFICATE – PAGE 4 OF 4. SOURCE DESCRIPTION SUMMARY.	159
FIGURE 15-1 SODIUM IODIDE DETECTOR OVERVIEW PROVIDED BY SAINT GOBAIN CRYSTALS.[55]	160
FIGURE 15-2 INFORMATION REGARDING NAI(TL) DETECTORS. PAGE 1 OF 2. [56]	161
FIGURE 15-3 INFORMATION REGARDING NAI(TL) DETECTORS. PAGE 2 OF 2.	162
FIGURE 15-4 MODEL 2M2/2 NAI(TL) DETECTOR DIAGRAM PROVIDED BY SAINT GOBAIN.	163
FIGURE 15-5 MODEL P4-0812-217 He-3 DETECTOR SPECIFICATIONS PROVIDED BY GE REUTER STOKES.	164
FIGURE 15-6 MODEL P4-0812-217 GE REUTER STOKES ^3He DETECTOR DIAGRAM. PROVIDED BY GE REUTER STOKES.	165

FIGURE 16-1 ELEVATION PLOT OF THE MCNP GEOMETRY USED IN THE CODE VERIFICATION OF THE POINT KERNEL CALCULATIONS. IT PROVIDES A GRAPHICAL REPRESENTATION OF THE CONTRIVED PROBLEM.	167
FIGURE 20-1 SCALE 6.2 DATA INSTALLER WELCOME DIALOG.	250
FIGURE 20-2 SCALE LICENSE AGREEMENT.	251
FIGURE 20-3 SETTING TYPICAL DATA INSTALLATION PATH ON WINDOWS.	252
FIGURE 20-4 SETTING A TYPICAL DATA INSTALLATION PATH ON LINUX.	252
FIGURE 20-5 SETTING A TYPICAL DATA INSTALLATION PATH ON MAC.	253
FIGURE 20-6 DATA INSTALLER DIRECTORY CREATION ERROR MESSAGE.	253
FIGURE 20-7 DIRECTORY OVERWRITE DIALOG.	254
FIGURE 20-8 DATA SELECTION DIALOG.	254
FIGURE 20-9 MEDIA SELECTION DIALOG.	255
FIGURE 20-10 LOCATION OF THE “SETTINGS” OPTION IN FULCRUM.	256
FIGURE 20-11 SETTINGS DIALOG BOX.	257
FIGURE 20-12 FIRST LINE INPUT FILE ARGUMENT USED TO INITIATE PARALLEL PROCESSING.	258
FIGURE 20-13 LOCATION OF THE CUSTOMIZE OPTIONS IN FULCRUM.	259
FIGURE 20-14 CUSTOMIZE DIALOG BOX.	259

List of Tables

TABLE 5–I: GAMMA-RAY DETECTOR OPTIONS.	40
TABLE 5–II: NEUTRON DETECTOR OPTIONS.	41
TABLE 6–I: POINT KERNEL SOURCE PROPERTIES, MATERIAL DENSITIES, AND GEOMETRY SPECIFICATIONS.	44
TABLE 6–II: MATERIAL MASS ATTENUATION COEFFICIENTS AND BUILD-UP FACTORS.	44
TABLE 6–III: TABLE OF COMPUTED AND SIMULATED VALUES FOR THE CONTRIVED SHIELDING PROBLEM HAVING A 1 MeV PHOTON SOURCE AT THE CENTER OF A 20 CM SPHERICAL SHIELD WITH THE DETECTOR 100 CM AWAY.	46
TABLE 7–I: SOURCE, DETECTOR, AND EQUIPMENT DATA FROM INITIAL GAMMA-RAY EXPERIMENTAL SET-UP.....	48
TABLE 7–II: SOURCE, DETECTOR, AND EQUIPMENT DATA FOR THE GAMMA-RAY EXPERIMENTAL SET-UP PROVIDING RESULTS USED IN THIS WORK.	54
TABLE 7–III: RAW DATA FOR THE COUNTING SYSTEM CHECK.....	57
TABLE 7–IV: FREQUENCY AND PROBABILITY DATA. NIST TABLES REFERENCE: HTTPS://WWW.ITL.NIST.GOV/DIV898/HANDBOOK/EDA/SECTION3/EDA3674.HTM	58
TABLE 7–V: PULSE HEIGHT SPECTRUM DATA.	60
TABLE 7–VI GAMMA-RAY DATA.	61
TABLE 7–VII: EXPERIMENTAL ERROR ACCOUNTING FOR GAMMA-RAY EXPERIMENTS.	63
TABLE 7–VIII: DATA FOR GEB COEFFICIENT CALCULATION.....	66
TABLE 7–IX: MCNP F8 TALLY DATA WITH CALCULATED VALUES FOR COMPARISON TO EXPERIMENTAL. COMPUTED TO EXPERIMENTAL RATIOS ARE ALSO TABULATED.	72
TABLE 7–X: MCNP F4 TALLY DATA WITH CALCULATED VALUES FOR COMPARISON TO EXPERIMENTAL. COMPUTED TO EXPERIMENTAL RATIOS ARE ALSO TABULATED.	72
TABLE 7–XI: RELATIONSHIP BETWEEN LENGTH TO DIAMETER RATIO AND DIVERGENCE ANGLE. ..	78
TABLE 7–XII: NEUTRON EXPERIMENTAL EQUIPMENT LIST.....	84
TABLE 7–XIII: NEUTRON DATA.	87
TABLE 7–XIV: EXPERIMENTAL RELATIVE ERROR ANALYSIS FOR NEUTRON EXPERIMENTS.....	91
TABLE 7–XV: COMPARISON OF CO ₂ CONCENTRATION ON THE VARIANCE IN THE EXPECTED VALUE.	101
TABLE 7–XVI: COUNTS PER SECOND CALCULATED FROM MCNP F4 TALLY DATA AND COMPUTED TO EXPERIMENTAL RATIOS.	106
TABLE 8–I: COMPARISON OF SHIELDING WEIGHT AND COSTS.	118
TABLE 12–I: STANDARD COMPOSITION WEIGHT FRACTIONS USED IN CODE VERIFICATION INPUT FILES.	132
TABLE 12–II: REGULAR CONCRETE STANDARD COMPOSITION ATOM DENSITIES USED FOR GAMMA- RAY MODELS.	133
TABLE 12–III: LEAD STANDARD COMPOSITION ATOM DENSITIES USED FOR GAMMA-RAY MODELS.	133
TABLE 12–IV: ALUMINUM STANDARD COMPOSITION ATOM DENSITIES USED FOR GAMMA-RAY MODELS.	134

TABLE 12–V: DRY AIR STANDARD COMPOSITION ATOM DENSITIES USED FOR GAMMA-RAY MODELS.	134
TABLE 12–VI: STAINLESS STEEL 304 STANDARD COMPOSITION ATOM DENSITIES USED FOR GAMMA-RAY MODELS.	134
TABLE 12–VII: BORATED POLYETHYLENE HAND CALCULATED ATOM DENSITIES FOR GAMMA-RAY MODELS.	134
TABLE 12–VIII: TUNGSTEN CARBIDE HAND CALCULATED ATOM DENSITIES FOR GAMMA-RAY MODELS.	134
TABLE 12–IX: CESIUM CHLORIDE GLASS HAND CALCULATED ATOM DENSITIES FOR GAMMA-RAY MODELS. WEIGHT FRACTIONS WERE OBTAINED OF ELEMENTS COMPRISING MORE THAN 1% WERE OBTAINED FROM ECKERT & ZIEGLER.	134
TABLE 12–X: SODIUM IODIDE HAND CALCULATED ATOM DENSITIES FOR GAMMA-RAY MODELS. APPROXIMATE THALLIUM WEIGHT FRACTION WAS OBTAINED BY CORRESPONDENCE WITH SAINT GOBAIN.	135
TABLE 12–XI: MU METAL HAND CALCULATED ATOM DENSITIES FOR GAMMA-RAY MODELS. WEIGHT FRACTIONS, DENSITY, AND COMPOSITION WERE OBTAINED FROM WWW.MUMETAL.COM/MUMETAL-SPECIFICATIONS.PHP .	135
TABLE 12–XII: HAND CALCULATED ATOM DENSITIES USED IN THE GAMMA-RAY SIMULATIONS FOR THE CONCRETE USED AS SHIELDING MADE IN-HOUSE.	135
TABLE 12–XIII: HAND CALCULATED ATOM DENSITIES USED IN THE GAMMA-RAY SIMULATIONS FOR THE STAINLESS STEEL USED AS SHIELDING.	135
TABLE 12–XIV: REGULAR CONCRETE STANDARD COMPOSITION ATOM DENSITIES WITH ISOTOPIC ABUNDANCE MODIFICATIONS FOR NEUTRON MODELS.	136
TABLE 12–XV: STAINLESS STEEL 304 STANDARD COMPOSITION ATOM DENSITIES WITH ISOTOPIC ABUNDANCE MODIFICATIONS FOR NEUTRON MODELS.	136
TABLE 12–XVI: LEAD STANDARD COMPOSITION ATOM DENSITIES WITH ISOTOPIC ABUNDANCE MODIFICATIONS FOR NEUTRON MODELS.	137
TABLE 12–XVII: PVC STANDARD COMPOSITION ATOM DENSITIES WITH ISOTOPIC ABUNDANCE MODIFICATIONS FOR NEUTRON MODELS.	137
TABLE 12–XVIII: IRON STANDARD COMPOSITION ATOM DENSITIES WITH ISOTOPIC ABUNDANCE MODIFICATIONS FOR NEUTRON MODELS.	137
TABLE 12–XIX: DRY AIR STANDARD COMPOSITION ATOM DENSITIES WITH ISOTOPIC ABUNDANCE MODIFICATIONS FOR NEUTRON MODELS.	137
TABLE 12–XX: BORATED POLYETHYLENE HAND CALCULATED ATOM DENSITIES FOR NEUTRON MODELS. WEIGHT FRACTIONS OBTAINED FROM SHIELDWERX.	138
TABLE 12–XXI: TUNGSTEN CARBIDE HAND CALCULATED ATOM DENSITIES FOR NEUTRON MODELS. WEIGHT FRACTIONS OF MATERIALS ABOVE 1 W/O WERE OBTAINED FROM H. B CARBIDE..	138
TABLE 12–XXII: SHIELDING CONCRETE MIXED IN-HOUSE. ATOM DENSITIES ARE FROM STANDARD COMPOSITION MODIFIED FOR BOTH MEASURED DENSITY AND ISOTOPIC ABUNDANCE FOR NEUTRON MODELS.	138
TABLE 12–XXIII: SHIELDING STAINLESS STEEL 304 FROM McMASTER CARR. ATOM DENSITIES ARE FROM STANDARD COMPOSITION MODIFIED FOR BOTH MEASURED DENSITY AND ISOTOPIC ABUNDANCE FOR NEUTRON MODELS.	139

TABLE 12–XXIV: PARAFFIN WAX WEIGHT FRACTIONS WERE OBTAINED FROM NIST. THE ATOM DENSITIES WERE THEN MODIFIED FOR ISOTOPIC ABUNDANCE FOR NEUTRON MODELS.	139
TABLE 12–XXV: POLYETHYLENE WEIGHT FRACTIONS WERE OBTAINED FROM NIST. THE ATOM DENSITIES WERE THEN MODIFIED FOR ISOTOPIC ABUNDANCE FOR NEUTRON MODELS.	140
TABLE 12–XXVI: THESE ATOM DENSITIES ARE BASED ON THE 14 G BEING THE MASS OF AmO_2 WEIGHED OUT AND MIXED WITH 57.6 G OF BE POWDER. THE DENSITY IS BASED UPON THE MASS FRACTIONS AND COMPONENT DENSITIES USING AN ALLOY DENSITY EQUATION. OTHER ATOM DENSITIES WERE CALCULATED FOR A COMPARATIVE STUDY BASED ON DIFFERENT ASSUMPTIONS REGARDING THE SOURCE.	140
TABLE 12–XXVII: THESE ^3He ATOM DENSITIES ARE BASED UPON THE ASSUMPTION THAT CO_2 IS 2% OF THE GAS. THIS IS THE UPPER BOUND OF CO_2 CONCENTRATION ACCORDING TO GE REUTER STOKES.	140
TABLE 12–XXVIII: MODIFIED MASS DENSITY URANIUM DIOXIDE ATOM DENSITIES FROM THE SCALE STANDARD ATOM DENSITY TABLES.	144
TABLE 12–XXIX: REGULAR CONCRETE ATOM DENSITIES FROM STANDARD COMPOSITION.	144
TABLE 12–XXX: BORATED POLYETHYLENE ATOM DENSITIES CALCULATED FROM MANUFACTURER PROVIDED DENSITY AND ABUNDANCES.	145
TABLE 12–XXXI: TUNGSTEN CARBIDE ATOM DENSITIES CALCULATED FROM MANUFACTURER PROVIDED DENSITY AND ABUNDANCES.	145
TABLE 12–XXXII: STAINLESS STEEL 304 ATOM DENSITIES FROM STANDARD COMPOSITION.	145
TABLE 12–XXXIII: ALUMINUM ATOM DENSITIES FROM STANDARD COMPOSITION.	145
TABLE 12–XXXIV: SODIUM IODIDE ATOM DENSITIES CALCULATED FROM INFORMATION PROVIDED BY THE MANUFACTURER.	145
TABLE 12–XXXV: MU METAL ATOM DENSITIES DETERMINED FROM WEIGHT FRACTIONS GIVEN BY WWW.MUMETAL.COM/MUMETAL-SPECIFICATIONS.PHP	146
TABLE 12–XXXVI: ARGON GAS ATOM DENSITIES FROM STANDARD COMPOSITION.	146
TABLE 12–XXXVII: DRY AIR ATOM DENSITIES FROM STANDARD COMPOSITION.	146
TABLE 12–XXXVIII: PLUTONIUM DIOXIDE ATOM DENSITIES FROM STANDARD COMPOSITION MODIFIED FOR ISOTOPIC ABUNDANCE.	147
TABLE 12–XXXIX: REGULAR CONCRETE ATOM DENSITIES FROM STANDARD COMPOSITION MODIFIED FOR ISOTOPIC ABUNDANCE.	147
TABLE 12–XL: BORATED POLYETHYLENE ATOM DENSITIES CALCULATED FROM MEASURED DENSITY AND MODIFIED FOR ISOTOPIC ABUNDANCES.	147
TABLE 12–XLI: TUNGSTEN CARBIDE ATOM DENSITIES CALCULATED FROM MEASURED DENSITY AND MODIFIED FOR ISOTOPIC ABUNDANCES.	147
TABLE 12–XLII: STAINLESS STEEL 304 ATOM DENSITIES FROM STANDARD COMPOSITION MODIFIED FOR ISOTOPIC ABUNDANCE.	148
TABLE 12–XLIII: ^3He ATOM DENSITIES BASED UPON MANUFACTURER PROVIDED DATA AND MODIFIED FOR ISOTOPIC ABUNDANCES.	149
TABLE 12–XLIV: DRY AIR ATOM DENSITIES FROM STANDARD COMPOSITION MODIFIED FOR ISOTOPIC ABUNDANCE.	149
TABLE 12–XLV: ARGON ATOM DENSITIES FROM STANDARD COMPOSITION MODIFIED FOR ISOTOPIC ABUNDANCE.	149

TABLE 13–I: CONCRETE MADE IN-HOUSE AT ISU FOR SHIELDING MATERIAL.	150
TABLE 13–II: MASS, DIMENSIONS, AND DENSITY OF THE CONCRETE BLOCKS MADE IN-HOUSE FOR SHIELDING.....	150
TABLE 13–III: STAINLESS STEEL PROPERTIES	151
TABLE 20–I A LIST OF SCALE MODULES AND SEQUENCES CAPABLE OF PARALLEL PROCESSING AFTER BUILDING WITH MPI.	242
TABLE 20–II SCALE SUPPORTED OPERATING SYSTEMS.....	242

List of Equations

EQUATION 2-1: RELATIONSHIP OF TIME, EXPOSURE RATE, AND EXPOSURE TO A RADIATION SOURCE.	3
EQUATION 2-2: RELATIONSHIP BETWEEN EXPOSURE AT TWO DISTANCES FROM A RADIATION SOURCE.	3
EQUATION 2-3: THE RELATIONSHIP OF EXPOSURE THROUGH A SHIELD OF A GIVEN MATERIAL AND THICKNESS, INCLUDING BUILDUP FOR THICK SHIELD, FOR GAMMA-RAYS.	4
EQUATION 2-4: THE RELATIONSHIP OF EXPOSURE THROUGH A SHIELD OF A GIVEN MATERIAL AND THICKNESS FOR NEUTRONS.	4
EQUATION 2-5: PHOTOELECTRON ENERGY RELATED TO GAMMA-RAY ENERGY AND ELECTRON BINDING ENERGY.	5
EQUATION 2-6: PROBABILITY OF PHOTOELECTRIC EFFECT WITH RESPECT TO ATOMIC NUMBER, Z , AND GAMMA-RAY ENERGY, E_γ .	5
EQUATION 2-7: ENERGY OF THE SCATTERED GAMMA-RAY FROM A COMPTON SCATTERING EVENT.	7
EQUATION 2-8: KLEIN-NISHINA FORMULA FOR DIFFERENTIAL SCATTERING CROSS SECTION IN COMPTON SCATTERING.	7
EQUATION 2-9: PROBABILITY RELATIONSHIP FOR PAIR PRODUCTION AS RELATED TO THE ATOMIC NUMBER, Z .	10
EQUATION 2-10: FAST NEUTRON ENERGY RELATIONSHIP FOLLOWING AN ELASTIC SCATTER.	12
EQUATION 2-11: RECOIL NUCLEUS ENERGY FROM ELASTIC SCATTERING OF A FAST NEUTRON.	12
EQUATION 2-12: EXAMPLE EQUATION OF RADIATIVE CAPTURE.	13
EQUATION 2-13: EXAMPLE EQUATION OF A FISSION PROCESS.	13
EQUATION 2-14: REACTION EQUATION OF BORON-10 WITH A NEUTRON.	14
EQUATION 2-15: REACTION EQUATION OF HELIUM-3 WITH A NEUTRON.	14
EQUATION 7-1: DATA DISTRIBUTION FUNCTION.	56
EQUATION 7-2: THE PROBABILITY THAT A MEASURED VALUE WILL FALL WITHIN A DISTRIBUTION BASED ON THE MEAN OF THE DATA.	56
EQUATION 7-3: METHOD USED TO CALCULATE CHI SQUARED.	58
EQUATION 7-4: QUADRATURE OF ERRORS.	62
EQUATION 7-5: GAUSSIAN STATISTICAL ERROR RELATIONSHIP TO COUNTS COLLECTED ON A COUNTING SYSTEM.	63
EQUATION 7-6: UNIT ANALYSIS OF A MODIFIED F4 TALLY.	64
EQUATION 7-7: GAUSSIAN ENERGY BROADENING COEFFICIENT EQUATION.	66
EQUATION 7-8: MATHEMATICAL DEFINITION OF THE ANGLE OF DIVERGENCE WITH RESPECT TO THE LENGTH AND DIAMETER OF THE COLLIMATOR TUBE.	77
EQUATION 7-9: ^3He -NEUTRON REACTION.	85
EQUATION 12-1: THE FUNDAMENTAL EQUATION FOR ATOM DENSITY CALCULATIONS.	140
EQUATION 12-2: CONVERSION APPLIED TO AVOGADRO'S NUMBER TO OBTAIN PROPER UNITS FOR USE IN MONTE CARLO CODES.	141
EQUATION 12-3: EXAMPLE CALCULATION OF ^3He ATOM DENSITY IN THE NEUTRON PROPORTIONAL COUNTER DETECTOR.	141

EQUATION 12-4: ATOM DENSITY EQUATION USED WHEN WEIGHT PERCENT OF INDIVIDUAL COMPONENTS ARE KNOWN.	141
EQUATION 12-5: EQUATION FOR CALCULATING WEIGHT PERCENT OF A MOLECULE OR ALLOY....	142
EQUATION 12-6: EXAMPLE CALCULATION OF THE HYDROGEN AND CARBON ATOM DENSITIES IN PARAFFIN WAX.	143
EQUATION 12-7: ATOM DENSITY EQUATION WHEN CONSIDERING ISOTOPIC ABUNDANCE.	143
EQUATION 12-8: EXAMPLE OF ATOM DENSITY CALCULATION CONSIDERING ISOTOPIC ABUNDANCE OF BORON IN BORATED POLYETHYLENE.	144
EQUATION 14-1: DECAY EQUATION FOR DETERMINING CURRENT ACTIVITY.	154
EQUATION 14-2: CALCULATION OF CURRENT GAMMA EMISSION RATE FROM THE ^{137}Cs SOURCE.	154
EQUATION 14-3: CALCULATION OF THE CURRENT NEUTRON EMISSION RATE FROM THE $^{241}\text{Am/Be}$ SOURCE.	159
EQUATION 16-1: LINEAR ATTENUATION CALCULATED FROM MASS ATTENUATION AND DENSITY	168
EQUATION 16-2: EQUATION FOR CALCULATING FLUX AT A DISTANCE FROM THE SOURCE THROUGH A MATERIAL.	168
EQUATION 16-3: EQUATION FOR CALCULATING PARTICLE FLUENCE RATE OR PARTICLE FLUX DENSITY.	169
EQUATION 16-4: EQUATION FOR CALCULATING THE TOTAL PARTICLE FLUENCE RATE.	169

List of Units, Acronyms, and Symbols

Units			
b	barn	lf	linear foot
Bq	Becquerel	m-	milli-
c-	centi-	M-	mega-
Ci	Curie	μ-	micro-
eV	electron volt	m	meter
ft	foot	mt	metric ton
g	gram	rad	radiation absorbed dose
hr	hour	rem	Röntgen equivalent man
in	inch	s	second
k-	kilo-	V	volt
l	liter		
Acronyms			
3-D	three dimensional	ITER	The way
AGN	Aerojet General Nucleonics	IVNAA	In-vivo neutron activation analysis
BP	borated polyethylene	IVVS	In vessel viewing system
C	concrete	JENDL	Japanese evaluated nuclear data library
C/E	calculated to experimental ratio	MAVRIC	Monaco with automated variance reduction using importance calculation
C/H	calculated to hand calc ratio	MC	Monte Carlo
CADIS	consistent adjoint driven importance sampling	MCA	multi-channel analyzer
CE	continuous energy	MCNP	Monte Carlo N-Particle
cps	counts per second	MG	multi group
E	MCNP energy bin tally modifier	NCIA	MCNP neutron capture ion algorithm
ENDF	evaluated nuclear data file	NIM	nuclear instrument module
F4	MCNP track length estimator tally	NIST	National Institute of Science and Technology
F6	MCNP energy deposition tally	ORIGEN	Oak Ridge isotope generation
F8	MCNP pulse height tally	ORNL	Oak Ridge National Laboratory
FF	fission fragment	PHL	MCNP pulse height light tally modifier
FLUKA	Fluktuierende Kaskade	PHYS	MCNP physics modifier
FM	MCNP tally multiplier	PMT	photomultiplier tube
FT	MCNP special tally modifier	PNNL	Pacific Northwest National Laboratory
FW-CADIS	forward weighted CADIS	PVC	polyvinyl chloride

FWHM	full width half maximum	RHH	Radiological Health Handbook
GEB	Gaussian energy broadening	RNSD	Reactor and Nuclear Support division
GM	Geiger-Mueller	SCA	single channel analyzer
HPGE	high purity germanium detector	SD	MCNP segment divisor tally modifier
HPRH	Health Physics and Radiological Health	SS	stainless steel
ICH&CD	Ion cyclotron heating & current drive	UHMW	ultra-high molecular weight polyethylene
ISU	Idaho State University	WC	tungsten carbide
Symbols			
Superscripts			
n	variable number		
Subscripts			
γ	gamma	e^-	electron
o	initial	n	variable number
a	air	s	shield
b	binding energy	tot	total
Mathematical			
α	alpha particle	m	mass of incident neutron
γ	gamma-ray	m_0	rest mass of an electron
θ	angle	M	mass of scattered nucleus
κ	pair production probability	n	neutron
μ	γ -ray attenuation coefficient	N	number of measurements
ν	frequency	p	proton; photon; particle
ρ	mass density	p_0	critical values for χ^2
σ	microscopic cross section; mean population standard deviation; Compton scattering probability	$P(E,Z)$	complex function of energy and atomic number
Σ	macroscopic cross section; summation	$P(x)$	probability distribution function
τ	photoelectric probability	r_0	classical radius of an electron
$\dot{\phi}$	particle fluence rate	r	radius
χ^2	Pearson's chi-squared test	R^2	coefficient of determination
A	activity	s	mean sample standard deviation
B	build up factor	sp	source particle
C	constant	t	time
c	speed of light	w	Monte Carlo weight
d	distance; diameter	\bar{x}	mean value
e	electron	x	length, thickness, variable
E	energy	\dot{X}	exposure rate

$F(x)$	data distribution function	X	exposure
h	Planks constant	y	variable
l	length	Z	atomic number
Elemental			
Al	Aluminum	He	Helium
Am	Americium	I	Iodine
B	Boron	Li	Lithium
Ba	Barium	O	Oxygen
Be	Beryllium	Pu	Plutonium
C	Carbon	Po	Polonium
Cf	Californium	K	Potassium
Cl	Chlorine	Si	Silicon
Co	Cobalt	Na	Sodium
Cs	Cesium	Tl	Thallium
Eu	Europium	W	Tungsten
F	Fluorine	U	Uranium
H	Hydrogen		

Optimization of Neutron and Gamma Ray Layered Shielding for Hot Cells Containing Used Nuclear Fuel

Dissertation Abstract—Idaho State University (2018)

Traditional thinking for the construction of hot cells where used nuclear fuel is handled simply consists of 4 – 8 foot thick concrete walls to provide the necessary shielding to protect workers. This work considers alternative materials for the construction of the walls and shielding for such facilities in an effort to reduce the thickness of the walls yet afford the same protection as the traditional walls. The materials selected were tungsten carbide and borated polyethylene (5% boron, high density polyethylene 1.4 g/cm³).

Experiments were designed to test the alternative materials, along with concrete and stainless steel, for shielding against gamma-rays and neutrons. The experiments were modeled in MCNP and the data were compared to the MCNP results. There was excellent correlation between the gamma-ray results with computed to experimental ratios of near unity for all shielding setups. There was good correlation with the neutron results with ratios ranging from unity to 1.17. These results allow for modelling to be used to determine the optimal thickness of each material in the shield.

Using MatLab to generate and analyze results the optimal thickness of each alternative materials was found. The concrete and stainless steel thicknesses were held constant at 30 cm and 1.27 cm. The optimal thickness of tungsten carbide was found to be 11 cm and the optimal thickness of the borated polyethylene was found to be 19 cm. The total thickness of the alternative shield is 61 cm which is half of a four foot (122 cm) thick concrete wall.

Key Words: Radiation Shielding, Hot Cell, Pyroprocessing, Gamma-Ray, Neutron, MCNP, SCALE, Tungsten Carbide, Borated Polyethylene

1 Introduction

In a world where radioactive materials and nuclear power exist, shielding will be used. Shielding is ubiquitous because of its inherent properties providing a way to create a safe work environment in the presence of ionizing radiation. One of the most common shielding materials is concrete. Concrete is used because of its abundant availability and ease of use to form structures. Facilities working with used nuclear fuel are no exception.

Many facilities dealing with used nuclear fuel, such as a pyro-processing facility performing reprocessing functions, have specialized rooms for handling and processing the used nuclear fuel. These rooms are often referred to as “hot cells”. These rooms are designed to protect workers from the radiations emitted from the used nuclear fuel as well as provide the functional capabilities to perform the necessary work on the nuclear fuel. A typical hot cell will have walls, floor, and ceiling constructed of concrete. The thickness of the floor will be thick enough to structurally support the weight of machinery and materials used in the room. The walls and ceiling will be thick enough to provide, at least, the commensurate level of protection promulgated in regulatory guidelines. Design and construction practices at these facilities has always been centered on determining how much concrete to use to provide that level of protection. This leads to the walls being between one and three meters thick ($\sim 3 - 8$ ft) and ceilings up to 1.5 meters thick (~ 5 ft).

Though shielding materials [1], [2], [11], [12], [3]–[10], including variations to concrete [13]–[23], and shielding designs [24]–[33] have been studied extensively for specific, narrow focused uses, consideration of materials other than concrete in hot cell facility wall and ceiling designs have not been studied. The traditional practice of using concrete, with an attitude of “just add more,” has prevailed from the beginning in the design of these facilities.

2 Radiation: Principles and Interactions

Before discussing the research experiments and simulations it is worthwhile to briefly discuss topics related to radiation to provide a basis of understanding to all who may read this work. This chapter will cover a little about the basic principles of radiation protection and how radiation, specifically gamma-rays and neutrons, interact with matter. These topics are important to this work because shielding is a prominent method of protection from radiation. Also, the shielding is made up of matter and understanding the basics of how radiation interacts with matter helps one to understand how it affords protection. These topics are well understood and discussed in introductory textbooks for nuclear engineering and health physics as well as radiation detection textbooks, such as [34]–[36].

2.1 Radiation Protection Principles

The primary principles of radiation protection are time, distance, and shielding. Each plays a role in how it affords protection to those working with radioactive materials or may be exposed to radiation. A short discussion of each of these principles and how they provide protection is provided hereafter.

In this section the term exposure is used. In the fields of nuclear science exposure has a very specific meaning related to the amount of energy deposited into a given mass of air. Exposure, as used in this section, is a generic term for how much radiation interacts with an individual. The various specific terms for dose, dose rate, exposure, exposure rate, etc. may be substituted into the equations in place of the generic exposure term.

The protection principle of time is the least effective at providing protection. This is because time, t , has a linear relationship between exposure rate, \dot{X} , and exposure, X .

$$X = \dot{X} \cdot t$$

Equation 2-1: Relationship of time, exposure rate, and exposure to a radiation source.

For example, if an individual decides to work with radiation, but does not have a plan, the work may take longer than if a plan were devised. Assume the case without a plan takes twice as long as the planned case. The individual would receive twice the exposure in the unplanned work, as compared to the planned work

Distance, d , provides better protection than time due to an inverse squared relationship between exposure (or exposure rate) and distance.

$$\frac{X_1}{d_1^2} = \frac{X_2}{d_2^2}$$

Equation 2-2: Relationship between exposure at two distances from a radiation source.

A practical example to demonstrate this principle is the use of utensils to assist in moving or handling a radioactive source. Worker A uses tweezers to handle the source, holding the source one foot away. Worker B uses a gripper and holds the source three feet (91 cm) away and spends the same amount of time with the source as Worker A. Worker A would receive an exposure nine times the exposure of Worker B. (NOTE: This example applies well to a point source, but not to a line or area source.)

Shielding affords the best protection from radiation because of an exponential relationship between exposure (or exposure rate) from one side of the shield to the next. The effectiveness of the shield is dependent on the energy, E , of the radiation, the shielding thickness, x , as well as the linear attenuation coefficient, μ , and a buildup factor, B , for gamma-rays or the macroscopic cross section, Σ , for neutrons. The linear attenuation coefficient and macroscopic cross section are a measure of a materials ability to reduce the energy of the radiation through scattering and remove

radiation through absorption. The mathematical representation of this process for gamma-rays is provided in Equation 2-3 and for neutrons in Equation 2-4.

$$X_2(E) = B \cdot X_1(E) \cdot e^{-\mu \cdot x}$$

Equation 2-3: The relationship of exposure through a shield of a given material and thickness, including buildup for thick shield, for gamma-rays.

$$X_2(E) = X_1(E) \cdot e^{-\Sigma \cdot x}$$

Equation 2-4: The relationship of exposure through a shield of a given material and thickness for neutrons.

Worker A performs a procedure with a source emitting 500 keV gamma-rays. The worker does not use any shielding for the work and spends 5 minutes accomplishing the task. Worker B places a 1.26 cm lead shield then performs the same task in the same amount of time. Worker A receives a dose 10 times the dose of Worker B.

2.2 Radiation Interactions with Matter

Interactions with matter primarily fall into scattering or absorbing events. There are nuances between how the different types of radiation interact. This section will briefly discuss these nuances to provide a basic understanding to the reader.

For the purpose of this work, discussion is constrained to gamma-ray and neutron interactions with matter. These two particle types are of the greatest concern when contemplating a shield design for a facility handling used nuclear fuel because of their ability to penetrate deeply through matter. In general, neither alpha, nor beta, particles produce health hazards beyond the shield created to protect for gamma and neutron radiations.

2.2.1 Gamma-ray Interactions with Matter

There are three primary interactions when considering gamma-rays. These interactions are the photoelectric effect, Compton scattering, and pair production, see Figure 2-1. Each of these

interactions plays a part in the attenuation of the rays as they move through matter. They are also responsible for the signal produced in the detector.

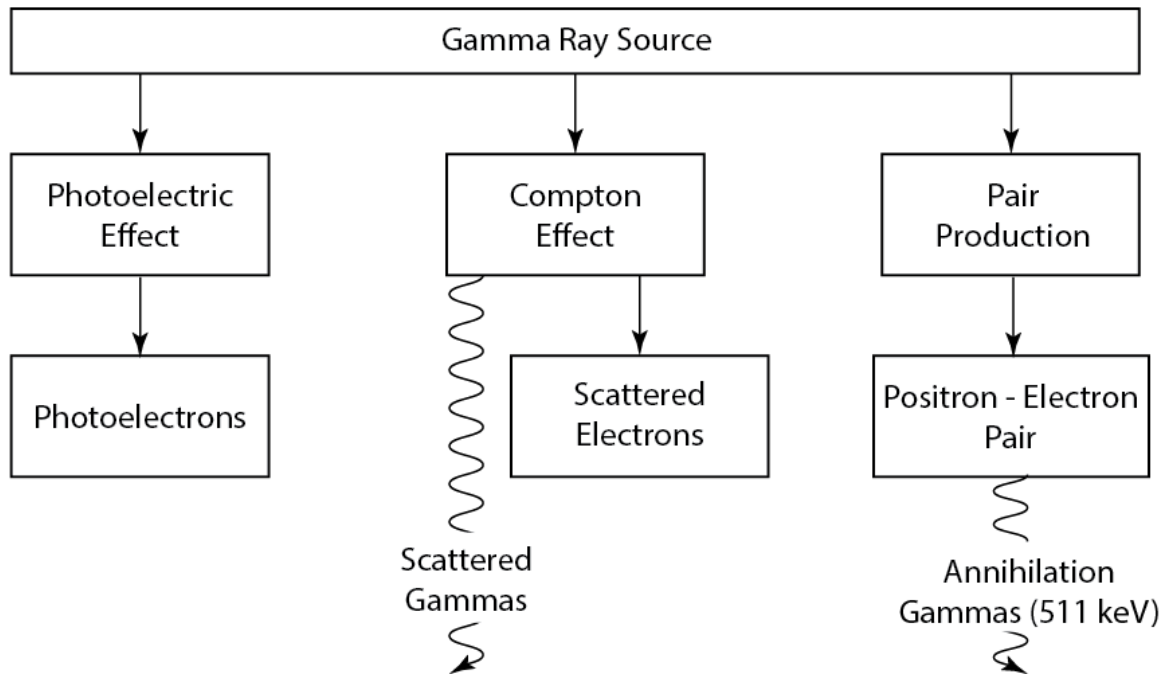


Figure 2-1 Interactions of a source gamma-rays (adaptation from Course Notes by Jack Courtney [37]).

The photoelectric effect is an absorption process where the photon is absorbed by an atom and an electron is ejected from the inner shells. The energy of the electron, E_{e-} , is the energy of the absorbed photon, $h\nu$, minus the electron binding energy, E_b , for the electron ejected.

$$E_{e-} = h\nu - E_b$$

Equation 2-5: Photoelectron energy related to gamma-ray energy and electron binding energy.

This effect occurs more prominently at lower gamma-ray energies. It is also more probable for atoms with a higher atomic number, or higher Z materials. The probability for the photoelectric effect, τ , may be approximated by the following relationship.

$$\tau \cong C \cdot \frac{Z^n}{E_\gamma^{3.5}}$$

Equation 2-6: Probability of photoelectric effect with respect to atomic number, Z , and gamma-ray energy, E_γ .

where C is a constant and E_γ is the gamma-ray energy. The contribution from the photoelectric effect to the total attenuation is shown in Figure 2-5.

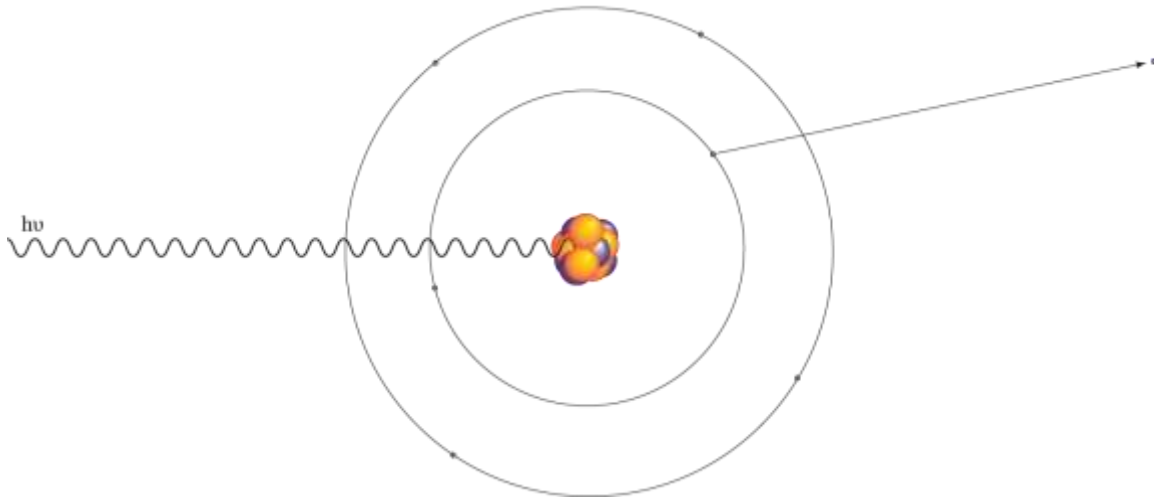


Figure 2-2 The photoelectric effect.

Following photoelectron ejection an inner shell vacancy is created leaving the atom in an excited state. The atom relaxes to the ground state by an outer shell electron filling the inner shell vacancy. As the electron relaxes to fill this vacancy a secondary release of energy occurs by emitting a characteristic x-ray or an auger electron. If a characteristic x-ray is emitted it will have the same energy as the difference in energy of the inner shell and the outer shell. If an auger electron is emitted it will have a kinetic energy of the energy difference between the inner shell and the outer shell minus the binding energy of the electron ejected. The primary processes of the photoelectric effect, absorption of the gamma-ray and ejection of the photoelectron, are shown in Figure 2-2.

Compton scattering is a process where a gamma-ray interacts with the electrons of an atom imparting a portion of its energy to an electron. Sufficient energy is given to the electron to become a recoil electron and is ejected from the atom. The gamma-ray is redirected in a direction different from the original direction at an angle, θ . This process is shown in Figure 2-3.

The energy of the scattered photon is related to θ and the original photon energy by

$$hv' = \frac{hv}{1 + \frac{hv}{m_0c^2}(1 - \cos\theta)}$$

Equation 2-7: Energy of the scattered gamma-ray from a Compton scattering event.

where hv is the original gamma-ray energy, hv' is the scattered gamma-ray energy, and m_0c^2 is the rest-mass energy of an electron (0.511 MeV). The distribution of the scattering angle, θ , is described by the *Klein-Nishina formula* providing the differential scattering cross section as

$$\frac{d\sigma}{d\Omega} = Zr_0^2 \left(\frac{1}{1 + \frac{hv}{m_0c^2}(1 - \cos\theta)} \right)^2 \left(\frac{1 + \cos^2\theta}{2} \right) \left(1 + \frac{\left(\frac{hv}{m_0c^2} \right)^2 (1 - \cos\theta)^2}{(1 + \cos^2\theta) \left[1 + \frac{hv}{m_0c^2}(1 - \cos\theta) \right]} \right)$$

Equation 2-8: Klein-Nishina formula for differential scattering cross section in Compton scattering.

where Z is the atomic number and r_0 is the classical electron radius.

The Compton scattering contribution to total attenuation probability is shown, in general, in Figure 2-5. The probability of Compton scattering, σ , covers a wide range of energies, but is most probable in the mid-range of energies. The probability is dependent on how many electrons are available as a scattering point and increases linearly with respect to the atomic number, Z , of the absorbing material.

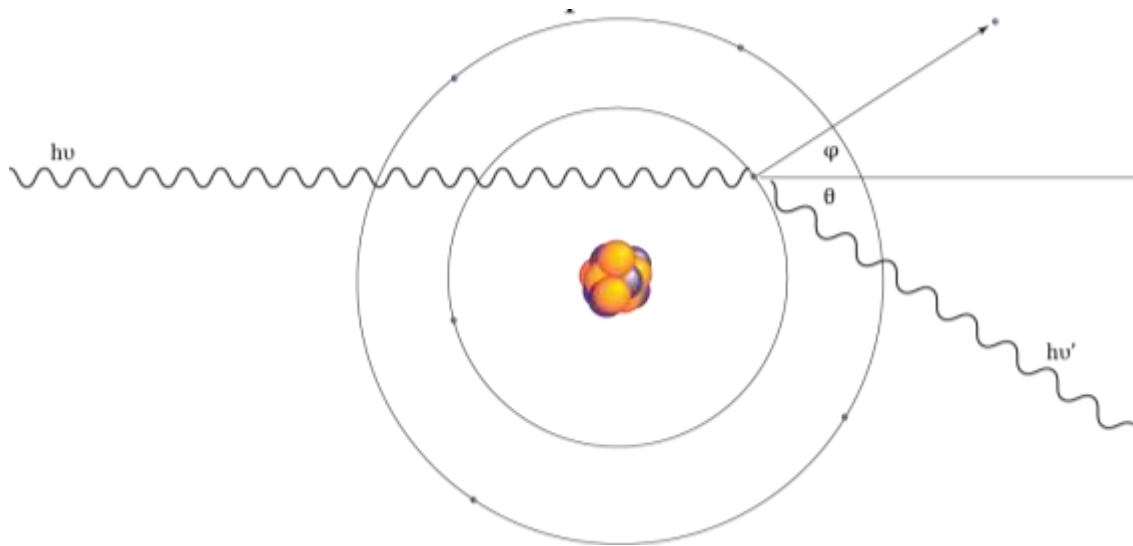


Figure 2-3 Compton scattering.

Pair production is the third major component to attenuation we will consider. Unlike the other two effects, pair production has a minimum energy requirement below which it cannot occur. The gamma-ray must have at least this minimum energy in order for pair production to occur, 1.022 MeV, or twice the rest-mass of an electron. Pair production may occur in the nuclear field near the nucleus of an atom or in the electron field near an electron. Pair production occurring in the nuclear field is much more probable. When pair production occurs, the photon vanishes and two particles, an electron and positron, are formed. Any energy above the minimum is distributed as kinetic energy to the two particles. The electron becomes a free electron. The positron will annihilate when it loses its kinetic energy and comes in contact with an electron. When annihilation occurs, two 0.511 MeV photons are created and will attenuate further through processes previously discussed. The basic pair production process is shown in Figure 2-4.

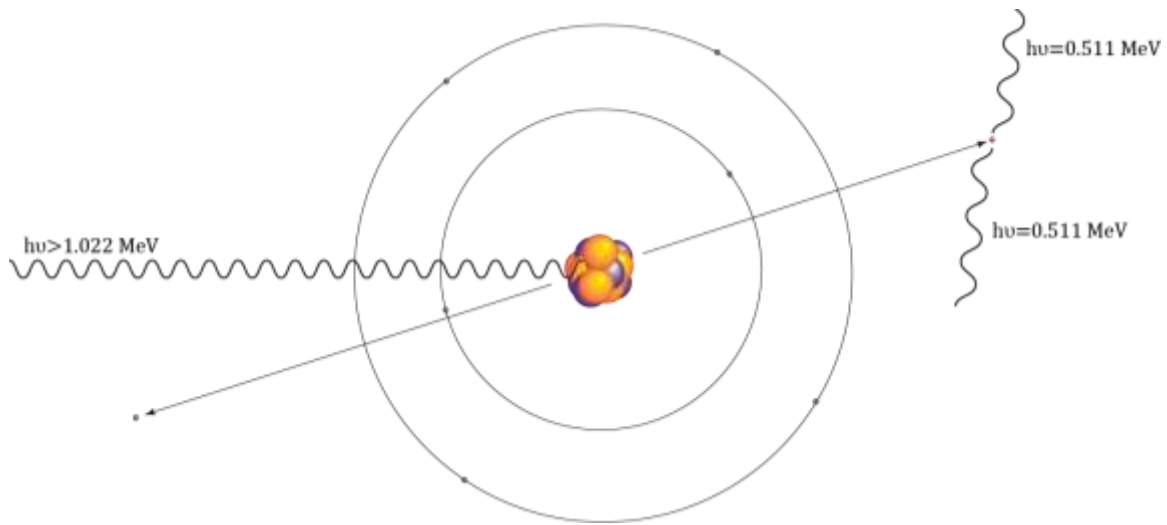


Figure 2-4 Pair Production as may occur near a nuclear field.

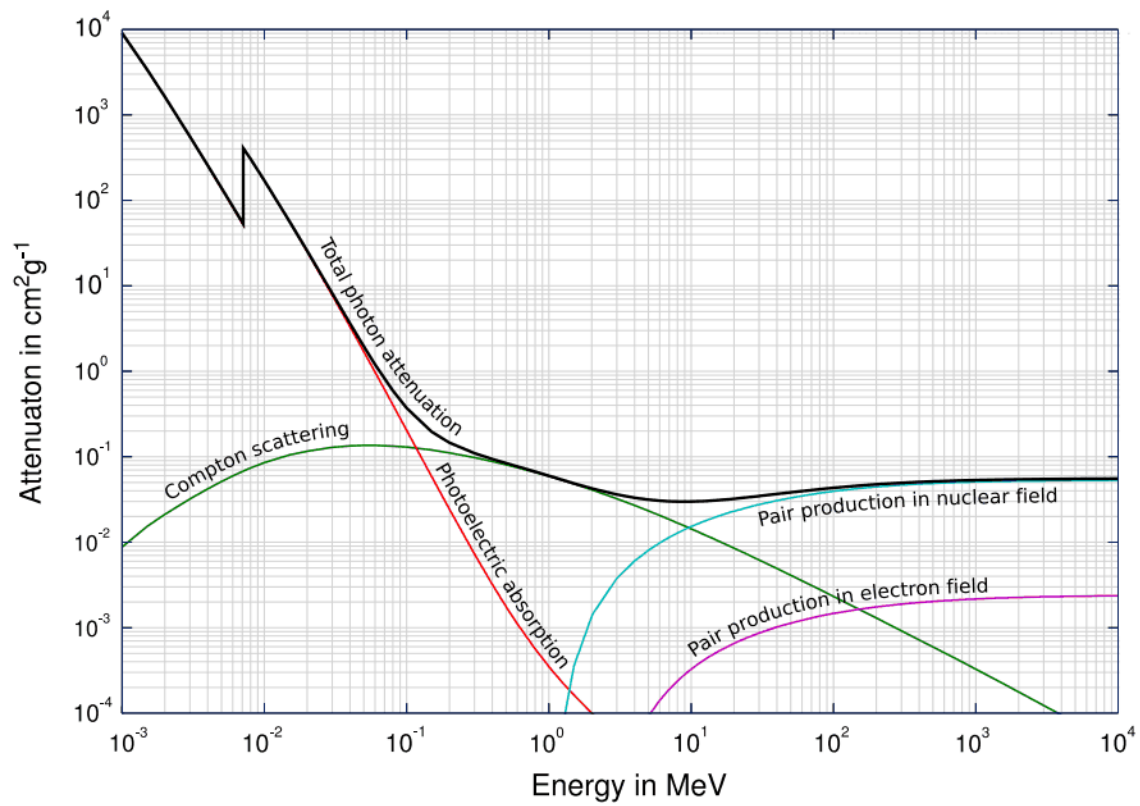


Figure 2-5 Attenuation probability of the various photon interactions to and their contributions to total attenuation probability. SOURCE: Wikimedia Commons.

The probability of occurrence does not have a simple expression to describe it. The relative probability, κ , from one material to another may be correlated to the square of the atomic number,

Z^2 , see Equation 2-9. The contribution of pair productions to the total attenuation is shown in Figure 2-5.

$$\kappa = Cr_0^2 Z^2 P(E, Z)$$

Equation 2-9: Probability relationship for pair production as related to the atomic number, Z.

where C is a constant, r_0 is the classical radius of an electron, Z is the atomic number, and $P(E, Z)$ is a function dependent on energy and atomic number.

2.2.2 Neutron Interactions with Matter

Neutrons also have three primary interactions of concern. Those interactions are absorption, elastic scattering, and inelastic scattering, see Figure 2-6. The probability of each is isotope dependent and neutron energy dependent. This probability is referred to as the cross section and can be described as the macroscopic, Σ , or microscopic, σ , cross section, depending on the units (cm^{-1} or barns) you desire and the particular use. Cross section plots are provided in microscopic cross sections and tables may be in either micro- or macroscopic.

As noted previously scattering of neutrons comes in two flavors, inelastic and elastic. Both act to reduce the energy of, or moderate, the neutron, but through slightly different mechanisms. In inelastic scattering the neutron interacts with the target nucleus and imparts a portion of energy to the atom, placing the atom into an excited state, and is subsequently redirected from its original path. The excited atom then emits a recoil gamma-ray. The nucleus also undergoes a recoil with a small amount of kinetic energy. This process is more probable for high energy, or fast, neutrons and is depicted in Figure 2-7.

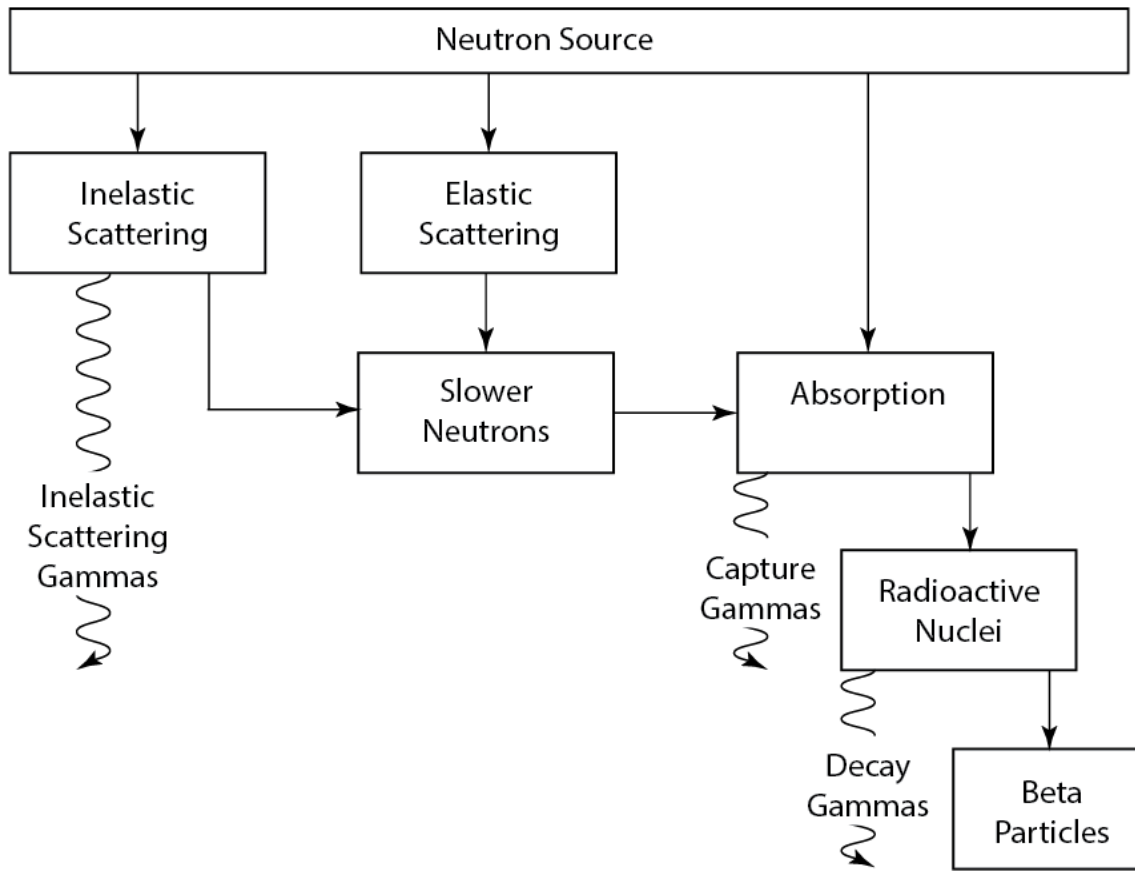


Figure 2-6 Interactions of source neutrons (adaptation from [37]).

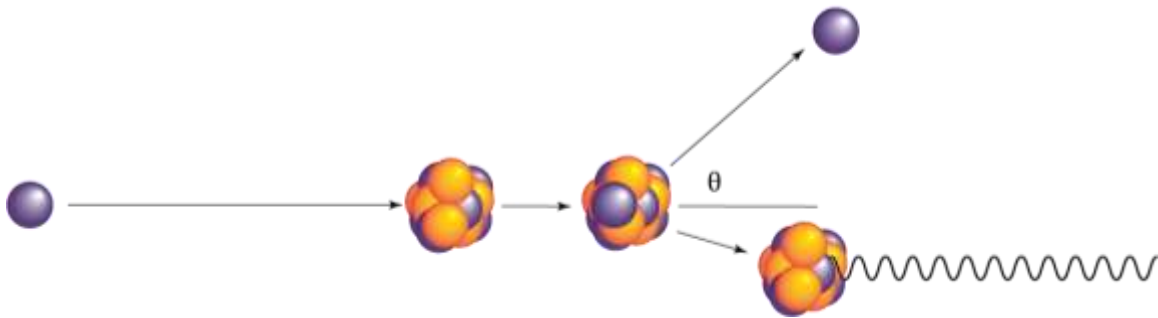


Figure 2-7 Inelastic neutron scattering.

Elastic scattering occurs when a neutron interacts with a nucleus and appears to “bounce off” without imparting any energy to the nucleus. At low energies the neutron is redirected and the atom remains unperturbed while at high neutron energies the atom may recoil. This type of scattering is more probable at low neutron energies and is part of the process for thermal equilibration of neutrons in a medium. However, elastic scattering is also appreciably probable for

fast neutrons and is an important part of moderating a neutron to thermal energy (0.025 eV). Elastic scattering is not a useful process for detecting neutrons at low neutron energies but may work well at high energies as a recoil nucleus is created and may be detected. Elastic scattering of a neutron is depicted in Figure 2-8.

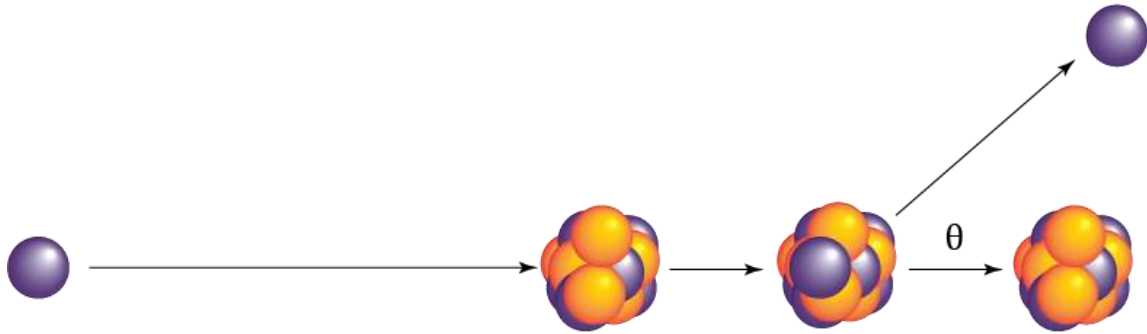


Figure 2-8 Elastic neutron scattering.

The relationship of neutron energy before and after a head-on elastic collision for fast neutrons is

$$E = E_0 \left(\frac{M - m}{M + m} \right)^2$$

Equation 2-10: Fast neutron energy relationship following an elastic scatter.

where E_0 is the incident neutron energy, M is the mass of the scattering nucleus, and m is the mass of the incident neutron.

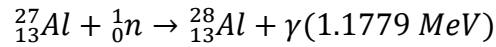
It follows that the nucleus of such a collision will gain some kinetic energy. The energy imparted to the nucleus is

$$E_0 - E = E_0 \left[1 - \left(\frac{M - m}{M + m} \right)^2 \right]$$

Equation 2-11: Recoil nucleus energy from elastic scattering of a fast neutron.

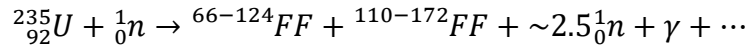
Neutron absorption is the process of a neutron interacting with a nucleus and remaining a part of the atom, rather than being re-emitted or redirected. When a neutron is absorbed there are numerous processes that may occur. Figure 2-9 depicts three processes, two of these are specific

processes and one is a general process describing many possibilities. The specific processes shown are 1) radiative capture where a neutron is absorbed and followed by emission of a capture gamma-ray and 2) fission where a neutron is absorbed followed by the splitting of the atom and the emission of particles and gamma-rays. An example of radiative capture is aluminum. The expression of this process is given in Equation 2-12.



Equation 2-12: Example equation of radiative capture.

An example of fission is given in Equation 2-13.



Equation 2-13: Example equation of a fission process.

where *FF* is a fission fragment with a range of atomic masses indicated superscript to the left.

In terms of usefulness for detection of neutrons radiative capture is not desirable because gamma-rays are not as easily detected as charged particles. Fission is a very useful process for detecting neutrons because the process produces two very large charged particles and possibly many smaller charged particles.

The general process shown in Figure 2-9 is a neutron-induced reaction. A neutron-induced reaction begins with the absorption of a neutron by an atom and then a myriad of resultant products may occur depending on the atom. Some of the more common neutron-induced reactions are (n, α), (n, p), and (n, ${}^3\text{H}$). Many times, a decay gamma-ray will be emitted in conjunction with these reactions. Two examples of neutron-induced reactions, which are also very important detection reactions, are shown in Equation 2-14 and Equation 2-15.

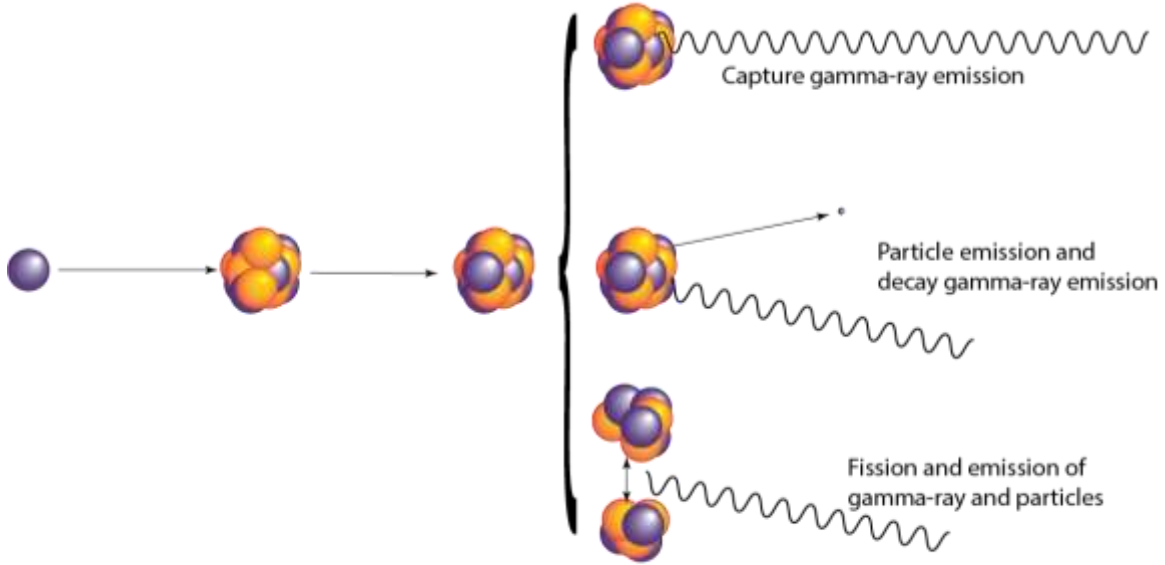
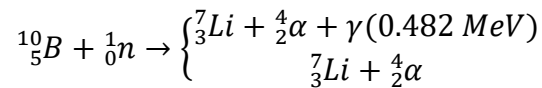
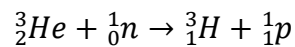


Figure 2-9 Neutron absorption.

The ^3He reaction of Equation 2-15 is the premise for the detector used in the neutron experiments of this research. The detector uses a mixture of ^3He and carbon dioxide (CO_2) as the detection medium. A potential is placed across the anode and cathode to draw the charged particles, proton and triton, to induce a current measured by the detection system.



Equation 2-14: Reaction equation of boron-10 with a neutron.



Equation 2-15: Reaction equation of helium-3 with a neutron.

As mentioned earlier, the probability of a neutron interaction is referred to as cross section. The absorption cross section for fast neutrons in most materials is relatively constant and is not very probable. In many materials the absorption cross section exhibits a unique characteristic at low energies. The cross section becomes proportional to the reciprocal of the square root of the neutron kinetic energy, or the reciprocal of the velocity of the neutron. These features are clearly seen in the cross section plot for ^3He shown in Figure 2-10.

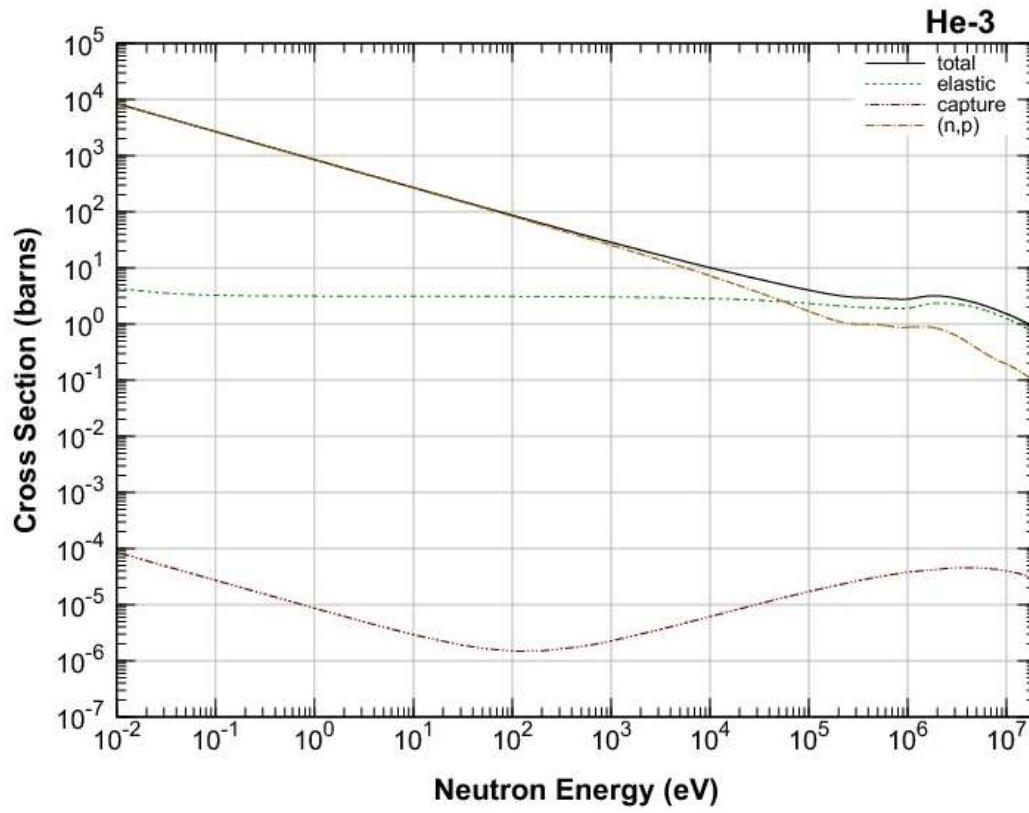


Figure 2-10: Neutron cross section plot of various interactions and the total cross section for ^3He . Plot is courtesy of Japan Atomic Energy Agency Nuclear Data Center, from JENDL-4.0 [38].

3 Shielding

The ideal shielding material would stop all radiation types, is easy to construct into any shape, and is inexpensive. Concrete is sometimes viewed as an ideal shielding material because it fits the description well, but not perfectly. Concrete can be formed into just about any shape and it is relatively inexpensive. Concrete is not the most effective or efficient material to use to stop all radiation types. It does not take much to stop alpha or beta particles, but it may require a fair amount to stop gamma-rays or neutrons. A frequent thought to meet regulatory requirements is, “just add more” concrete to meet the required limit.

3.1 Shielding Materials and Radiation Type

To design an ideal shield a priori knowledge of all radiation types emitted, energies of the radiations emitted, and the interaction probabilities of each radiation type with respect to energy with each isotope in the shielding material is required. No such shield exists. However, using such knowledge allows for the development of adequate shields.

If shielding is to be used, then consideration of radiation type is essential. Materials capable of shielding gamma rays effectively may do very little to stop neutrons and vice-versa. In general, good gamma-ray shielding materials are dense, where higher density materials perform better. Examples of common gamma shielding materials are concrete, steel, lead, uranium, and tungsten. Neutron shielding materials come in two types, those generally contain high atom fractions of hydrogen or carbon for scattering, such as plastics, wax, water, or graphite, and those with large neutron absorption cross sections at lower energies, such as boron, lithium, and cadmium. Frequently neutron shields will make use of both types of materials mixing them to make a shield that will moderate and absorb neutrons. Examples of such materials are borated polyethylene, boron carbide, and borated aluminum (Boral®).

Further consideration must be taken for the types of interactions and how secondary radiation must be shielded. This is more important for neutron shields since some of the interactions emit gamma-rays. As noted in Equation 2-14 there is a probability that a gamma-ray will be emitted after absorption of the neutron. If this occurs in borated polyethylene it will do little to stop the gamma-ray and additional shielding material should be considered for placement on the side opposite the source to stop the gamma-rays produced.

The source term for the optimization study mimics used nuclear fuel. The shield must be interrogated using both gamma-rays and neutrons because they are deep penetrators of material. From a safety standpoint the gamma-ray component dominates the day to day operations. The neutron component dominates the safety requirements only when a criticality accident occurs. Because gamma rays and neutrons are intrinsic hazards when handling used nuclear fuel, the shield in this study will incorporate materials to attenuate and absorb both.

3.2 Shielding Optimization Studies

Monte Carlo (MC) modelled shielding optimization studies are common for specific facilities, detector arrangements, or specific problems. ITER (meaning “the way” in Latin) is the world’s largest fusion project and is one of the specific facilities extensively studied. The proposed In-Vessel Viewing System (IVVS) units were recently modeled to optimize shielding components associated with the systems probe [32]. The ITER IVVS Monte Carlo N-Particle (MCNP) study concluded the addition of several shielding components were required to reduce dose rates to acceptable levels within the unit. Another study modeled for ITER looked at optimizing the shielding to reduce shutdown dose rates in the Ion Cyclotron Heating and Current Drive (ICH&CD) system port [33]. The ITER ICH&CD MCNP study concluded modifications to a few shielding components were required to reduce dose rates to acceptable safety levels. An MC study

optimizing shielding of the vault around a general cyclotron facility associated with hospitals was performed using the code FLUKA (FLUKA) [29]. Dose rates were compared to experimental results measured at corresponding cyclotrons. The study found corroboration between the simulated and experimental data. MC has been used to optimize the shielding, moderator, collimator and detector design for radiation portal monitors [28]. The FLUKA MCNP study concluded that specific placement of a collimated layer of polyethylene and a moderator layer of polyethylene on the front of the portal monitor, as well as borated polyethylene on the back of the monitor as a shield, afforded significant improvement in the radiation portal monitor response. Monte Carlo has been used in optimization studies of concrete as a gamma and neutron shield [26] using MCNP5 and to improve neutron shielding properties of various concretes using MCNPX and a code developed by the authors named SPOT [22]. In the Calzada et al. [26] study new additives, a mixture of polyethylene, boron carbide and steel, to concrete were optimized to improve shielding at the ANTERES facility and found the optimized volume fraction of polyethylene and steel for the concrete mixture. In the Piotrowski et. al. study different compressive strengths of ordinary and barite concrete were investigated for neutron attenuation properties. Piotrowski et al. [22] found that higher compressive strength of concrete correlates to higher neutron attenuation, however specific use of barite aggregate to improve neutron shielding properties over ordinary concrete was inconclusive. In an MC (MCNP-4C) shielding optimization study for an in-vivo neutron activation analysis (IVNAA) setup [6], Moghaddam et al. found the use of boron carbide, to shield neutrons, and bismuth, to shield gamma rays, performed better than other boron and lithium containing materials to optimize the prompt gamma spectrum from the IVNAA.

3.3 Shielding in Layers

The concept of layering shielding materials is not new. Neutron shields rely on material layers. A common layering technique for neutron shielding consists of a moderator inside an absorber surrounded by a gamma attenuator (e.g. polyethylene, cadmium, lead). Greene, et al. [39] conducted experiments using a collimated 14 MeV source placing layers of steel, polyethylene, and boron in the beam as attenuators to discover if layering improves shielding effectiveness. These materials were layered in order of steel; steel and polyethylene; and steel, polyethylene, and boron. The thickness of each layer was varied maintaining a constant total thickness. Greene et al. found an optimum attenuation is reached when some polyethylene is layered with about 3 times as much steel and that boron, added to the polyethylene, further improves attenuation. Maruyama, et al. [40] expanded the experimental study of Greene by introducing additional materials, repeating layers, and varying the thickness of each material in the layers. In addition to steel and polyethylene, Maruyama used borated wood and borated paraffin. The source was a 15 MeV collimated neutron source. The results indicate repeatedly layering the materials improves the shield over a single layering of the materials. In a more recent MC study Whetstone, et al. expanded the materials used to make a layered collimator for a 14 MeV isotropic neutron source [41]. This differs slightly from the Greene and Maruyama study as they were studying materials to place in the beam as attenuators, whereas Whetstone is looking at materials to improve the collimator around the neutron source. These materials included polyethylene, borated polyethylene, water, bismuth, steel, nickel, INCONEL® alloy 600, tungsten, and depleted uranium. They concluded several layers of polyethylene and steel were the most effective at collimating the source by reducing neutron leakage out the sides and back of the collimator.

3.4 Hot Cell Shielding

Traditionally hot cell, and other nuclear facility, shielding consists of thick walls, typically four to five feet (1.2 - 1.5 m), of concrete. Concrete, historically, has been inexpensive and is versatile in construction because it can be poured into forms to make it the shape and thickness needed. This process has, historically, been accomplished by placing rebar for structural integrity followed by pouring the concrete into forms.

Cement is mixed with aggregates, like sand or gravel, and sometimes it is mixed with specialized aggregates to increase the density for improved gamma-ray shielding properties, such as iron filings, magnetite, or barite, ores rich in iron [13]. Sometimes special materials are mixed in to the cement, such as boron or plastics, to improve neutron shielding properties. Many studies have been performed on cement with different additives to determine the shielding and physical properties. Studies of various aggregates include those of Akkurt [14], Bashter[15], Korkut[18], Makarious [19], Okuno [20], and Oto [21] each showing the various aggregates improve the density and shielding properties for either gamma-rays or neutrons. Another study by Gallego investigated boron additives for improved neutron shielding [17]. These additives did improve the shielding in terms of neutron attenuation. However, the density and structural aspects of the concrete were diminished. In an effort to better understand how shielding properties are effected by moisture content a study was undertaken [23] wherein the conclusion was for each 1% increase in moisture content a 10% increase in thermalization of neutrons occurred. Both of Piotrowski's studies, [22] and [23], looked at different additives and how they affect the neutron shielding properties.

3.5 Concrete: Then and Now

As stated in the previous section concrete has historically been used in building by placing rebar and forms to shape and provide strength to the finished structure. Modern techniques are moving away from using rebar as the structure for form filling. These newer techniques either use a precast method for components, which may be prestressed, or use onsite pouring and prestressing.

Prestressing of concrete occurs by one of two methods: pre-tensioning or post-tensioning. Pre-tensioning is accomplished by placing tendons from anchors outside the casting area or by use of a frame. The tendons are stretched followed by concrete casting over the stressed tendons. After the concrete has set and has bonded to the stretched tendons the pressure is released from the anchors or frame transferring the stress to the concrete. This process is depicted in Figure 3-1. Post-tensioning requires the placement of conduits, sleeves, or greased tendons throughout the area followed by running tendons through the conduits or sleeves to anchors (see Figure 3-2 for an image of an anchor). The concrete is poured and cured then the tendons are stretched by jacks to apply stress to the concrete. The force applied to the tendons in both methods are thousands to millions of pounds, depending on the application of construction.

Precast concrete is convenient because components are ordered and formed prior to construction. Precast components are prestressed during the fabrication to make them strong. The components are shipped in and tied together. They come in a wide variety of shapes and thicknesses.

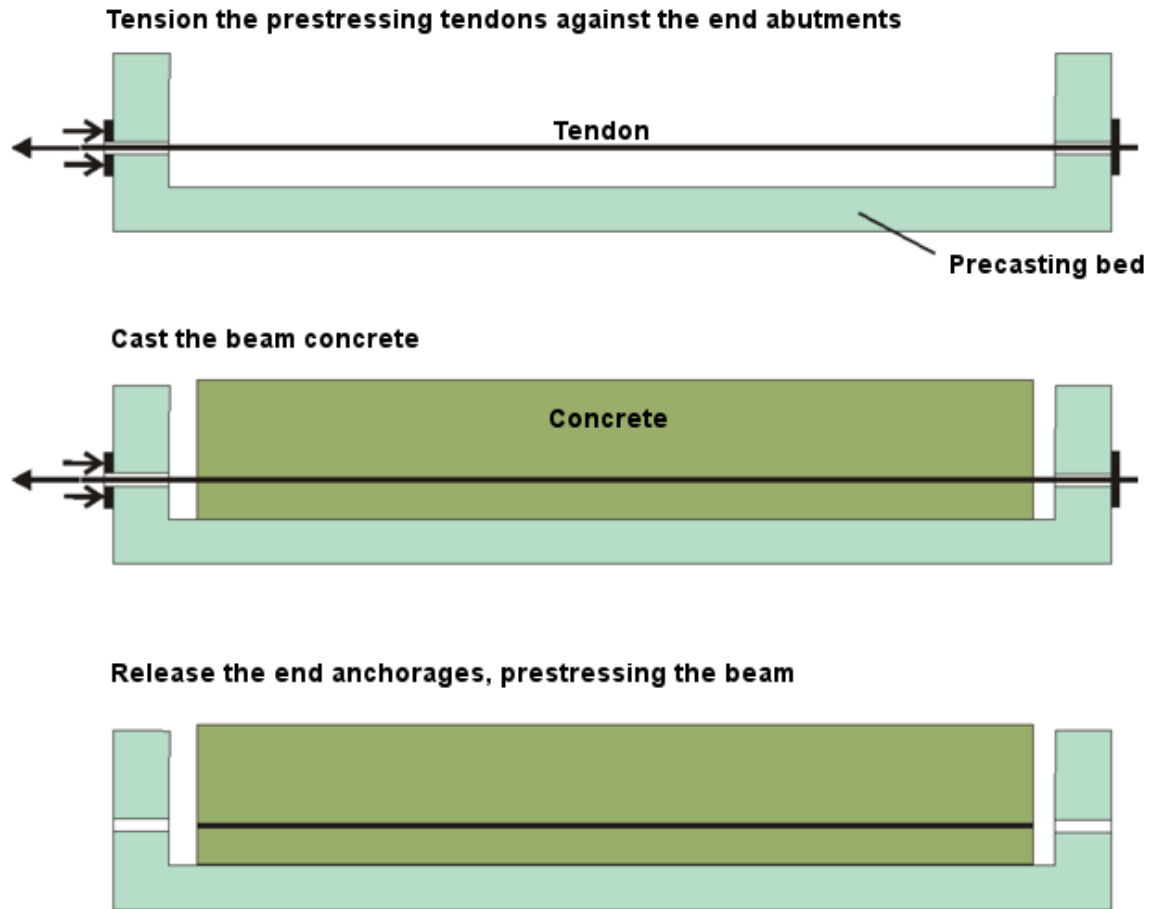


Figure 3-1 Pre-tensioning method to prestress concrete. Image from Wikipedia.

The nuclear industry has made use of these newer construction techniques when building the containment vessels for nuclear reactors. Fort Saint Vrain was the first nuclear reactor to use prestressed concrete in its construction. However, prestressed concrete has not been used in hot cell/reprocessing facility construction. It is in the interest of the nuclear industry to look further at new shielding methods that will complement the newer concrete construction techniques.



Figure 3-2 Post-tensioning multi-tendon anchor for prestressing concrete. Image from Wikipedia.

4 Computation and Simulation

There are two primary methods used to computationally solve particle transport problems in nuclear sciences. One primary method for solving particle transport problems is finding solutions to the diffusion theory approximation of the Boltzmann equation. Boltzmann equation solutions are deterministic methods which include the use of discrete ordinates, discretization, and others to find a suitable solution. The other primary method for solving particle transport problems is to use the power of iterative sampling based upon natural or assumed probability density functions for random processes. The method is called Monte Carlo. The Monte Carlo method was used for simulation of experimental problems in this work and will be discussed in further detail.

4.1 Monte Carlo

Monte Carlo is based around a random (or pseudo-random) number generator. The random numbers are used to pick the process that will occur based upon the probability density function for an action. The simulation is designed with a given geometry, source, materials, and tallies. Many other parameters may be introduced to improve the mean value or statistical error of the mean value tallied. Parameters to improve the mean value may include changes to the probability density functions associated with physics occurring with the particle. Parameters used to improve the error of the mean value are variance reduction techniques such as the use of particle importance and weight, cut-off values, etc.

A very basic example of an analog Monte Carlo neutron problem is presented in Figure 4-1. This problem represents the full life of a neutron through a set of decisions where the answers are determined by random numbers generated by the program. When the neutron is born random numbers determine the starting location, energy and direction of the neutron. Then another set of random numbers determines how far the neutron travels. If the neutron travels far enough to “leak”

out of the defined geometry then the process begins again with a new neutron. If a collision occurs random numbers are used to determine what kind of collision. If capture occurs then a new neutron begins. If fission occurs, then random numbers determine how many fission neutrons are created and run later. If scatter occurs then random numbers determine the new direction, energy, and path length of the neutron in a loop until one of the other options occurs.

A Fission Neutron Problem Using Analog Monte Carlo

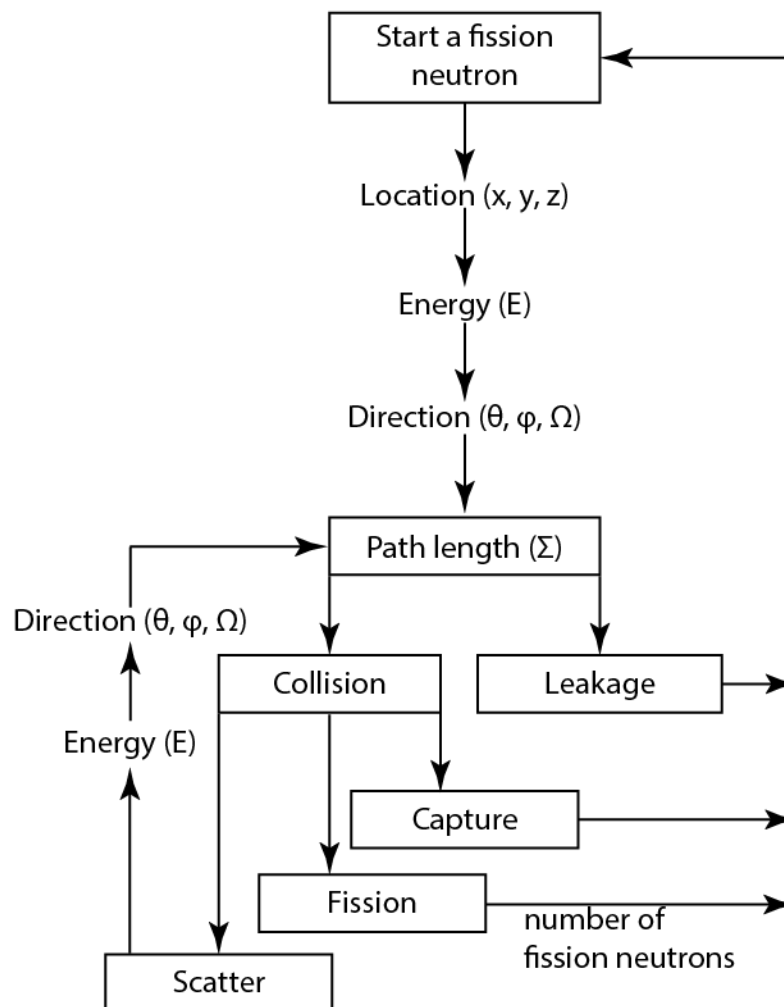


Figure 4-1 The basic process of analog Monte Carlo for the life of a neutron and the selection of random numbers to describe its life. Diagram adapted from MCNP lecture notes by Dr. Chad Pope.

Two Monte Carlo codes were considered for this work: MCNP and SCALE (NOTE: SCALE is not an acronym, as per the creators at Oak Ridge, TN). Both were used in the preliminary studies

comparing simulation results to point kernel hand calculations and MCNP was used for the simulations of experimental results and for the optimizations.

4.1.1 Monte Carlo N-Particle (MCNP)

“MCNP6™ is a general purpose, continuous-energy, generalized-geometry, time-dependent, MC radiation-transport code designed to track many particle types over broad ranges of energies.” [42] “MCNP can be used for neutron, photon, electron, or coupled neutron/photon/electron transport, including the capability to calculate eigenvalues for critical systems.” [43] It uses pointwise cross section data accounting for all reaction types for neutrons as well as incoherent and coherent scattering for photons.

MCNP version 6.1.0 was used. Example input files are provided in Appendix F: Monte Carlo Neutron Particle (MCNP) Input Files.

4.1.2 SCALE

The SCALE Code System is a widely-used modeling and simulation suite for nuclear safety analysis and design that is developed, maintained, tested, and managed by the Reactor and Nuclear Systems Division (RNSD) of Oak Ridge National Laboratory (ORNL). SCALE provides a comprehensive, verified and validated, user-friendly tool set for criticality safety, reactor and lattice physics, radiation shielding, spent fuel and radioactive source term characterization, and sensitivity and uncertainty analysis. Since 1980, regulators, licensees, and research institutions around the world have used SCALE for safety analysis and design. SCALE provides an integrated framework with dozens of computational modules including three deterministic and three Monte Carlo radiation transport solvers that are selected based on the desired solution strategy. SCALE includes current nuclear data libraries and problem-dependent processing tools for continuous-energy (CE) and multigroup (MG) neutronics and coupled neutron-gamma calculations, as well

as activation, depletion, and decay calculations. SCALE includes unique capabilities for automated variance reduction for shielding calculations, as well as sensitivity and uncertainty analysis. [44]

Monaco with Automated Variance Reduction using Importance Calculations (MAVRIC) is a sequence within the SCALE code system used “to apply the multigroup and continuous energy fixed-source MC code Monaco to solve problems too challenging for standard, unbiased MC methods” [44]. MAVRIC uses a variance reduction methodology based upon Consistent Adjoint Driven Importance Sampling (CADIS), which creates an importance map and a biased source. MAVRIC creates the problem dependent cross section data then uses Denovo, a coarse mesh 3D discrete ordinates transport calculation, to determine the adjoint flux. These are used to optimize the shielding calculation within Monaco. If multiple tally locations are used, then a secondary Denovo calculation is run in the Forward-Weighted CADIS (FW-CADIS) method, optimizing the Monaco calculation to provide uniform uncertainties for the various tally locations.

SCALE version 6.2.2 was used. Example input files are provided in Appendix H: SCALE Input Files.

4.2 Variance Reduction

Deep penetration shielding problems are not feasible with analog “brute force” in MC calculations. Simply throwing more particles at the problem is not practical as most, if not all, of the particles are attenuated before reaching the tally detector. This is the case for the optimization problem because the shielding is thick ($\sim 0.75 - 2.5$ m). Application of variance reduction methods are required to achieve results and to achieve these results within a reasonable amount of time. Several variance reduction techniques in MCNP were tested in the point kernel simulations. These methods are discussed in the following section and the basis of the information comes from [42].

4.2.1 MCNP Variance Reduction Methods

MCNP has two variance reduction techniques that are always applied, unless the user turns them off. These two are implicit capture and particle weight control. In analog MC the capture of a particle eliminates it and another particle is started. This may be seen as a waste of particles and computer time. Implicit capture allows for the particle to undergo a scattering event instead of capture. The particle weight is modified by the scattering probability.

Within a simulation the statistical weight of a particle changes based on particle interactions experienced, variance reduction techniques applied, tally specifications, etc. Weight control is an important feature when conducting simulations, especially when using variance reduction methods. During the simulation, the statistical weight of particles is adjusted throughout the phase space of the problem. Some particles may have their weight reduced to minute fractions and they do not contribute much to the tally. Using weight cut-off allows the simulation to play Russian roulette with particles when the weight of the particle drops below the specified value. If the particle survives, additional weight is given to the particle.

Other standard variance reduction techniques available, but must be turned on, within MCNP are: cell importance, weight windows (cell or mesh based) with energy and time upper and lower limits, energy splitting with roulette, time splitting with roulette, exponential transform, forced collisions, deterministic transport spheres, as well as source, bremsstrahlung, photon-production and secondary particle biasing, and photon weighting. Of the listed variance reduction methods, cell importance and weight windows are briefly described in Sections 4.2.1.1 and 4.2.1.2, respectively. It was determined these two would suffice for the optimization simulations. These

methods were chosen from comparison of results from the point kernel hand calculation simulations using variance reduction to the hand calculations.

Another useful cut-off is the energy cut-off. A card may be added to define the energy below which particles are terminated. Caution must be given when using this cut-off, as important particles may inadvertently be eliminated. The problem should be run without energy cut-off to determine the contribution of particles below the desired cut-off energy. Once it is determined few particles contribute, then the energy cut-off card may be added with more confidence.

4.2.1.1 Cell Importance

Cell importance is a required feature for the input of each cell in the geometry. The value of the importance is used to perform particle splitting or roulette based on the boundaries of each cell. If the importance of each cell is unity, then no splitting or roulette occurs to particles as they cross geometric boundaries defined by the cells in the problem. If the importance from one cell to the next is not equivalent then either particle splitting or roulette occurs as the particles cross the cell boundaries. For example, define two cells A and B and set the importance of cell A to x and the importance of cell B to y , where y is greater than x ($y > x$). If particles cross the boundary between A and B traveling from A to B then the particles are split with a ratio of y divided by x (y/x) and a new weight is assigned. If the old weight is w , the new weight is w times x divided by y ($w * x/y$). If particles travel the opposite direction, from B to A, then Russian roulette is played with a survival rate of x divided by y (x/y). If the particle survives the weight is adjusted so the new weight is w times y divided by x ($w * y/x$).

This technique works well when a highly attenuating shield is divided into many cells and importance is increased in the direction from the source to the detector. The thickness of the cell divisions should be between one and ten mean free path lengths for the particle. The importance

should be set to a multiple between two and four from the previous cell in the shield. Doing this allows particles to pass all the way through the shield keeping the population nearly constant. Particle weights will be very small by the time they reach the other side of the shield. Regardless, particles will make it to the detector region and contribute to the tally.

4.2.1.2 Weight Windows

Weight windows are a method of weight control. This method is more thorough than a simple weight cut-off, as defined earlier. Weight windows applies an upper and lower limit to the particle weights. When particles enter the region of interest, either cell or mesh based, the weight is compared to the upper and lower limits. If the particle has a weight within the window, nothing occurs. If the particle has weight greater than the upper limit, the particle is split in to two or more particles so the weight of each is within the upper and lower bounds. If the particle has less weight than the lower limit Russian roulette is played on the particle adjusting the weight to be within the upper and lower limit if the particle survives.

Weight windows may be defined by a weight windows parameter card or created using a weight windows generator. Use of the parameter card requires the weight windows to be cell based. Use of the weight windows generator may make use of either cells or use a superimposed mesh. Other options include adding energy or time dependence to the window. Also, the location of where the window is applied may be defined to include at the point of an interaction within the cell or mesh, at the boundary of a cell or mesh, or both at the point of interaction and the boundary.

Weight windows are very useful for maintaining a more stable weight distribution for the particles tallied. Without weight windows the distribution of particle weight may be very large and increase the time for the problem to converge.

5 Discussion

5.1 Shielding Material Selection

Two different material selections occurred during this work. The first was for the point kernel comparisons and the second was for the experiments and optimization calculations.

The decision of what materials to use in the point kernel problem was kept relatively simple. Concrete is a constant material throughout the whole work and was selected. In wanting to keep good left and right boundaries on the work only three more materials were selected for this problem. The material selection was based upon density, one low, one medium, and one high. These correspond to aluminum, iron, and lead. These materials are common to shielding and have well documented values for mass attenuation and linear attenuation coefficients allowing for ease of calculations.

The initial net thrown for materials to use in the experimental shielding was wide. Possible shielding materials considered for gamma-ray attenuation were tungsten, tungsten carbide, depleted uranium, concrete, and stainless steel. Those considered for neutron moderation and attenuation were borated polyethylene, lithiated polyethylene, boron carbide, Boral®, and Bakelite®, for neutron. Other, less likely, candidates found in the literature are more exotic such as epoxy resins [5], ceramics [2], metathesis-polymers [7], lead and bismuth-lead borate glasses [10], and ultra-high molecular weight polyethylene samarium oxide composites [12]. However, consideration for time and financial constraints must also be entertained, and so we limit the options to the better suited materials. The selected materials were concrete, stainless steel, tungsten carbide, and borated polyethylene.

Ordinary concrete is useful for both gamma-ray and neutron shielding. Concrete is beneficial from both a shielding and construction perspective. It is one of the most common building materials and may be pre-formed to shapes and thicknesses desired for construction. It has a density of approximately 2.3 g/cm^3 making it somewhat useful for attenuating gammas. It contains substances useful for stopping and scattering neutrons. Precast thicknesses, ranging from 3 – 12 inches (7.62 – 30.48 cm) could be purchased when applying the shielding techniques studied. The actual concrete used in experiments were made in-house. Four blocks were cast with dimensions of 10.16 cm x 10.16 cm x 7.62 cm (nominal). Though all blocks were considered for experimental use, only one was used, block labeled #2. Actual dimensions were measured using a caliper with precision of $\pm 0.001 \text{ cm}$ and three measurements were averaged for each side. The averaged measured results were 10.298 cm x 10.622 cm x 7.811 cm $\pm 0.006 \text{ cm}$ on each side. The mass was measured on a scale with a precision of $\pm 0.5 \text{ g}$ to be 2004.6 g. The density was calculated to be $2.3462 \pm 0.0006 \text{ g/cm}^3$.

Tungsten carbide [WC] is mostly useful for gamma-ray shielding but has some usefulness for neutron shielding. This material is the primary component for gamma-ray attenuation with a nominal density of, 15.6 g/cm^3 . It will play a small roll in neutron scattering and attenuation because of the presence of the carbon atoms in a one to one ratio with the tungsten. Tungsten carbide can be purchased in plates with thicknesses ranging from 5 – 80 mm and lengths and widths of plates ranging between 10 – 300 mm. Eight plates were purchased from H. B. Carbide. The nominal dimensions and density stated by the company were 10.16 cm x 10.16 cm x 0.3175 cm and 14.93 g/cm^3 . One specific plate was selected for use and measurements made to obtain specific dimensions and density. The measured dimensions were 10.329 cm x 10.331 cm x

0.394 cm \pm 0.006 cm. The mass was measured as 624.0 \pm 0.5 g. The density was calculated to be 14.842 \pm 0.0248 g/cm³.

Stainless steel is useful for gamma-ray shielding. Though the stainless steel will provide some shielding, this is not its primary function. Stainless steel is present because it is used to seal the interior of the hot cell providing the ability to maintain an inert atmosphere. It was used in both experiments and models because of its required presence in the context of the study. Its density is nominally given as 8.0 g/cm³. The thickness of the stainless steel liner is typically 0.5 inch (1.27 cm). Four stainless steel 304 sheets with dimensions of 15.24 cm x 15.24 cm x 0.3048 cm were purchased from McMaster Carr. They were cut down to 10.16 cm x 10.16 cm x 0.3175 cm to match the size of the tungsten carbide. One sheet was selected for experiments and the actual dimensions were measured as 10.511 cm x 10.515 cm x 0.302 cm \pm 0.006 cm. The mass was measured as 265.0 \pm 0.5 g. The density was calculated to be 7.9394 \pm 0.021334 g/cm³.

Borated polyethylene [(CH₂)_n, B] is useful for neutron shielding. Polyethylene has high hydrogen and carbon content making it excellent at slowing and scattering neutrons and suitable as a neutron shield. Addition of boron increases the attenuation of the slowed neutrons through the material making it an even better shield. The density typically ranges from 1.1 – 1.6 g/cm³ but is dependent on the load of boron and the density of the polyethylene. Boron may be loaded from 0.5 – 30 weight percent. Borated polyethylene can be purchased in lengths and widths ranging from 24 – 96 inches (60.96 – 243.84 cm) and thicknesses of 1, 2, or 4 inches (2.54, 5.08, or 10.16 cm), depending on boron concentration. A 24 x 24 x 1 inch (60.96 x 60.96 x 2.54 cm) slab of type 207 self-extinguishing borated polyethylene was purchased from Shieldwerx. From this slab five blocks were cut with nominal dimensions of 10.16 cm x 10.16 cm x 2.54 cm. One block was selected for experimentation from the batch. The measured dimensions were 10.260 cm x

10.229 cm x 2.533 cm \pm 0.006 cm. The mass was measured as 393.0 \pm 0.5 g. The density was calculated to be 1.4783 \pm 0.0019 g/cm³.

Material information for the concrete and each of the purchased materials may be found in Appendix B: Shielding Material Information.

5.2 Radionuclide Source Selection

Selection of the radionuclide sources are broken into two categories and additional subcategories for each category. The categories are experimental and simulation. The subcategories are based on radiation types.

Selection of the radiation sources began with consideration of the final component of the research, the optimization of the shield for hot cells containing used nuclear fuel. Because used nuclear fuel is the source in the optimization knowledge of the radiation types and approximate energy spectra of the radiations emitted are also known. The source radiation types will be limited to gamma-rays and neutrons because the problem is a deep penetration shielding problem and alpha and beta particles provide a negligible contribution to radiation hazards to the worker side of the shield.

Source definitions in the models were determined by the stage of the research: simulations of the point kernel hand calculations, experimental simulations, and optimization simulations. The source for simulating the point kernel hand calculations needed to be a simple source because it is easiest to calculate the point kernel values with a monoenergetic gamma-ray that is given in the linear attenuation coefficient tables. The source, for both hand calculation and the model, was a point, monoenergetic gamma-ray with energy of 1 MeV. This energy alleviated the need to extrapolate between energies on the attenuation coefficient tables during the hand calculations.

The radiation sources for the experimental simulations were solely based upon the selected radioisotopes used in the experiments. The gamma-ray experimental source was modeled to have an energy of 0.662 MeV, as is emitted from a ^{137}Cs source. The dimensions, mass density, and atom densities were obtained/calculated from manufacturer provided specifications, see Section 14.2 ^{137}Cs Certificate. The neutron experimental source was modeled as AmO_2/Be (more commonly referred to as AmBe). The dimensions were obtained from manufacturer specifications, see Section 14.3 AmBe Certificate. However, a parametric study of the mass density and atom densities was required to provide the best model since there are several unknowns about the way the source was manufactured. Much effort was used to obtain more information about the source, but the company has restructured many times and the information is lost to time. The specifications provided in Section 14.3 AmBe Certificate are all that remain. A series of models were created, using best guesses, to provide the best source geometry in the simulations to match experiment results. The energy spectrum used in the source definition was based upon the ISO 8529-2 recommended spectrum as seen in Figure 5-1.

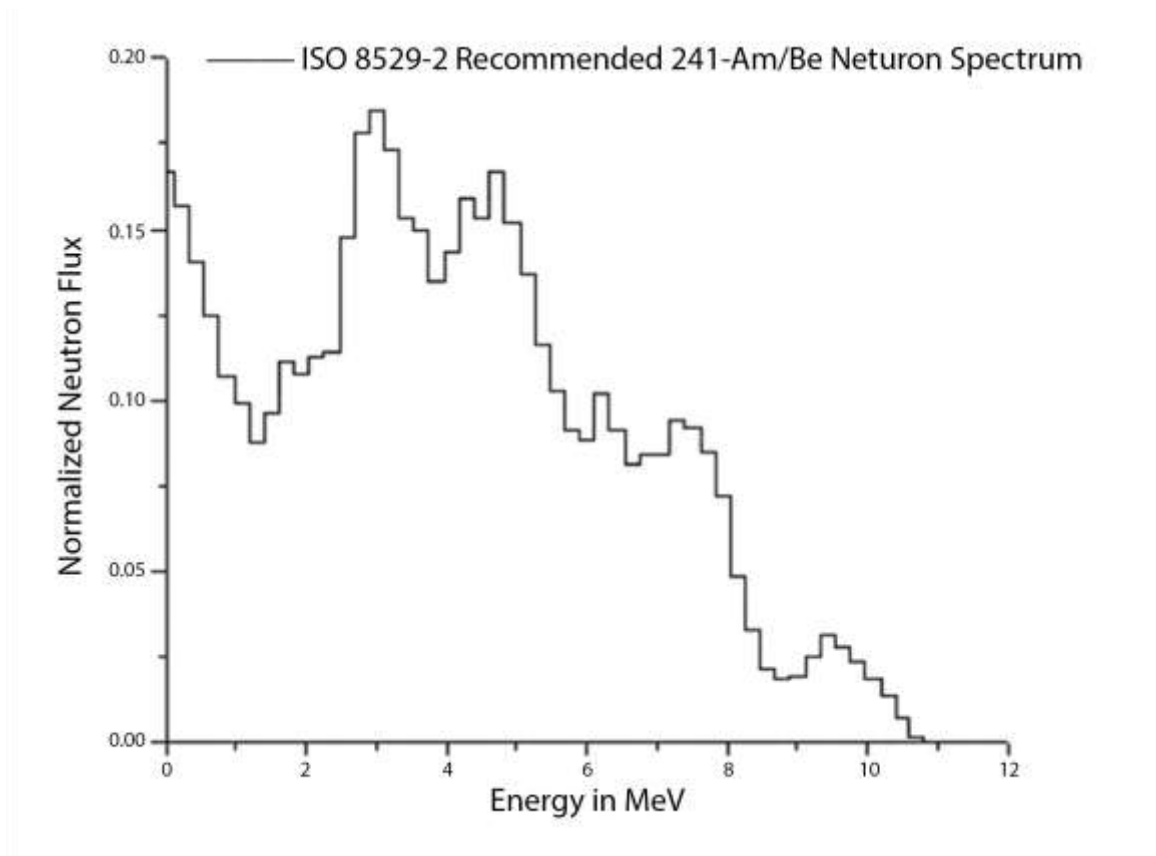


Figure 5-1 Recommended energy spectrum from an $^{241}\text{AmBe}$ neutron source used in experimental models [45].

The gamma-ray source in the optimization models has a dimensional geometry consistent with a Westinghouse 17x17 fuel assembly. The uranium dioxide (UO_2) atom densities, see Appendix 12.3, were modified from the standard composition listed in the Compendium of Material Composition Data for Radiation Transport Modeling (PNNL Compendium) [46] to be homogenized over the whole volume of the fuel assembly. This altered the mass density from 10.96 g/cm^3 to 5.485 g/cm^3 . The gamma-ray energy spectra, shown in Figure 5-2, were calculated using the Oak Ridge Isotope Generation (ORIGEN) code, a module in the SCALE code system, as part of a previous work [47].

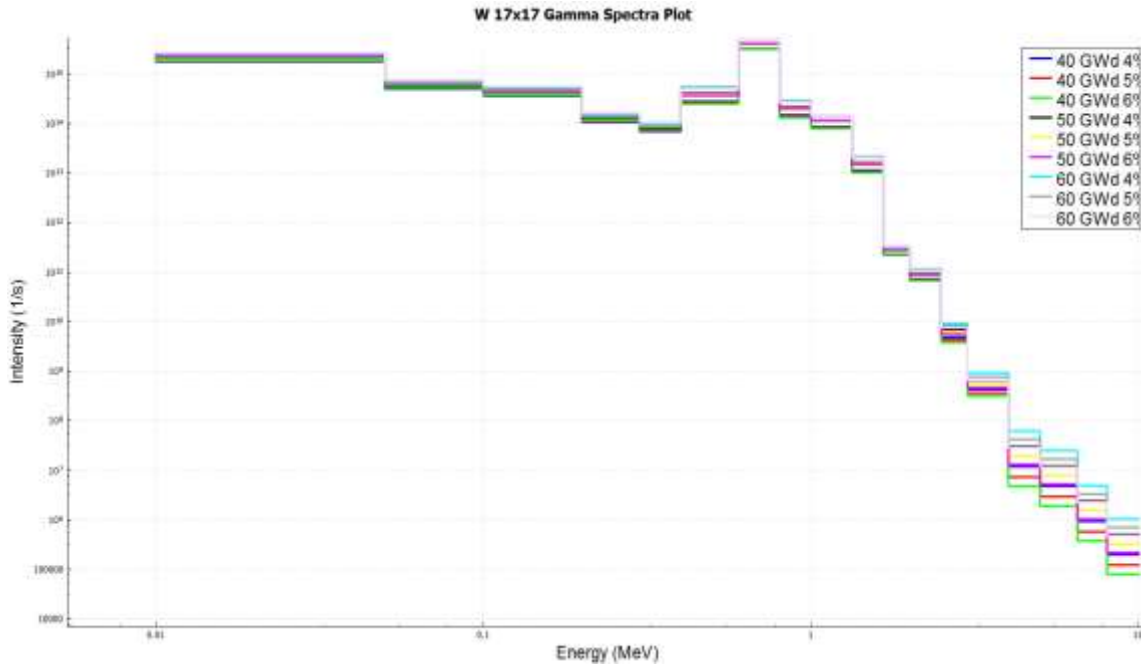


Figure 5-2 Gamma-ray spectrum estimated by ORIGIN/SCALE for a Westinghouse 17x17 fuel assembly with various burnup and initial enrichment.

The neutron source for the shielding optimization models was a sphere of plutonium oxide (PuO_2). Plutonium was selected because there is sufficient mass of Pu to create a criticality, if the geometry were correct. There is not enough ^{235}U , in the absence of moderator, to create a criticality. The atom densities for these models were defined as plutonium dioxide in the PNNL Compendium [46]. The atom densities are listed in Appendix 12.3.2. The size of the sphere was determined by using the ORIGIN calculated mass of all Pu created through depletion and then adjusting for density and mass differences of metal Pu and PuO_2 . The energy spectrum selected was the Watt fission spectrum for Pu, as shown by the blue line in Figure 5-3.

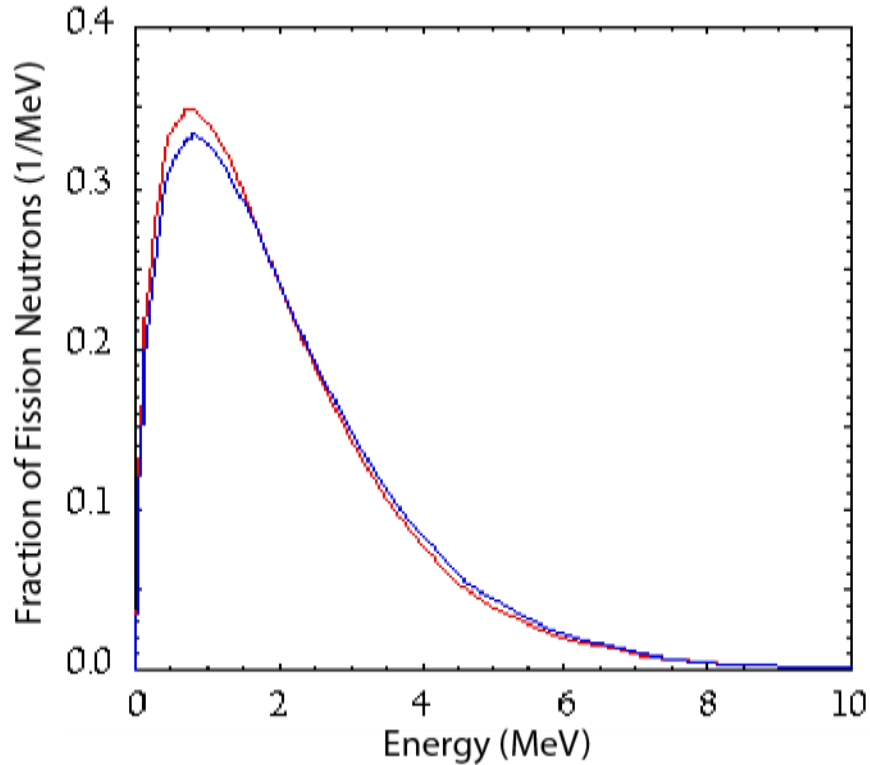


Figure 5-3 Fission neutron spectrum approximated by the Watt distribution for ^{235}U (red line) and ^{239}Pu (blue line). (image from <http://neutron.kth.se/courses/transmutation/Spectra/Spectra.html>)

Selection of which radionuclide sources used for experimental portion of the research was driven by two factors: what radionuclide sources presently exist in the inventory at Idaho State University (ISU) and what sources from the inventory provide a reasonable estimate of the desired spectrum and radiation type relative to used nuclear fuel.

The radionuclide ^{137}Cs was selected for the gamma-ray experiments. It has a gamma-ray emission of 0.66175 MeV. When compared to the spectrum of the fuel assembly gamma-ray emission, Figure 5-2, this value is close to the peak value and the mean. Having a monoenergetic gamma-ray source would also be easier to simulate.

ISU had several ^{137}Cs sources in inventory ranging from 1 μCi to 20 Ci ($0.37 - 7.4 \times 10^5$ MBq). Initially, the shielding material was interrogated with a 1 Ci (3.7×10^4 MBq) source. There were two problems with using this source. It was in a small room with a 20 Ci (7.4×10^5 MBq) source.

Having both sources in such a small space created a high background region. The detector was too sensitive to handle this level of background and results were tenuous. Later a 1 mCi (37 MBq) source was selected for use in the ISU Reactor Laboratory, a large room, with little background.

For the neutron experiments source options were limited to a 50 Ci (1.85×10^6 MBq) AmBe source and a 100 mCi (3.7×10^3 MBq) ^{252}Cf source. With a half-life of 2.646 years the ^{252}Cf source was sufficiently old, certificate date of 24 June 1993, that it would not provide sufficient neutron flux to perform the experiments. The 50 Ci (1.85×10^6 MBq) AmBe source has a half-life of 432.7 years. It is still approximately 50 Ci (1.85×10^6 MBq), even after being manufactured on 25 August 1965, and provides significant neutron flux for the experiments.

Radiation source certificates are located in Appendix C: Current Source Strengths and Source Certificates.

5.3 Radiation Detector Selection

Similar to selecting sources for the experiments, selecting detectors came from what was available, which limits the types for use. Discussion of detector selection will be based upon radiation type. Two detectors were required to complete the experiments because we needed one to detect the gamma-rays emitted by the ^{137}Cs source and one to detect the neutrons emitted by the AmBe source.

Readily available options for gamma-ray detection were limited to sodium iodide (NaI) scintillation detectors, both 2 in x 2 in and 3 in x 3 in, a Geiger-Meuller (GM) detector, and a high purity germanium (HPGE) detector. A detailed list of all of the different gamma-ray detectors available is shared in Table 5–I. Neither of GM nor the HPGE were feasible due to mass and size of the inherent shielding associated with the detectors. Other detectors may have been available

upon request or searching, but NaI detectors would work well for the planned experiments, especially after reducing to a 1 mCi 3.7×10^3 MBq) gamma-ray source.

Initially a 3 in x 3 in NaI detector was selected, but during preliminary tests, such as calibration and counting tests, it exhibited problems. Spectra were distorted and incorrect even after calibration. A 2 in x 2 in NaI was then selected and tested with good results. Instrumentation information and data for the calibration and counting tests are provided in Chapter 7 Shielding Experiment and Simulation.

Table 5-I: Gamma-ray detector options.

Manufacturer	Model	Type	Other
Bicron	2M2/2PLP, 2M2-X, and 2M2/2	NaI(Tl)	2x2
Bicron	3M3/3P-X	NaI(Tl)	3x3
Measurements Inc	2M2-X	NaI(Tl)	2x2
Quartz and Silice	44S5I	NaI(Tl)	1.5x1.5
Quartz and Silice	76S76	NaI(Tl)	3x3
Ludlum	180-8	GM	
Ortec		HPGE	

Three types of neutron detectors were available, helium-3 (^3He), boron-10 lined (^{10}B), and boron trifluoride (BF_3). A detailed list of all of the available neutron detectors is shared in Table 5-II. All three are proportional gas counters and all three would work well. However, the ^3He detectors are more sensitive to neutrons and slightly less sensitive to gamma-rays, allowing for better discrimination in the two signals. Instrumentation information and data from tests are provided in Chapter 7 Shielding Experiment and Simulation.

Table 5-II: Neutron detector options.

Manufacturer	Model	Type	Other
Reuter Stokes	RS-P4-0812-217	^3He	
	RS-P4-0406-212	^3He	
	RS-B1-0936-213	^{10}B lined	
	RSN-28A-MG	BF_3	Modern equivalent RS-P1-1609-101
	RSN-44A-MG	BF_3	Modern equivalent RS-P1-1613-144
	RSN-127A	^{10}B lined	Modern equivalent RS-P7-0805-127
Nancy Wood Counter Lab	1750-2050	BF_3	ca. 1950s
	G-10-121A	BF_3	ca. 1960s

6 Point Kernel (Hand and Simulation Calculations)

To gain confidence in and assist in selecting the primary Monte Carlo code for use in this research a basic comparison was designed. This comparison utilized well understood point kernel approximations to estimate the fluence rate and Monte Carlo codes, MCNP and SCALE/MAVRIC, to determine the fluence rate based upon the same geometry. Results from the point kernel approximations were compared to results from both MCNP and SCALE/MAVRIC.

6.1 Design

The geometry, source, shielding materials, and distances were all selected to simplify the point kernel calculation as much as possible. The geometry was selected as a sphere of shielding material to house a point, isotropic, monoenergetic, constant activity source. The source was placed at the exact center of the spherical shield. The detector was considered a point detector held a constant distance from the source and an atmosphere of air was assumed to be surrounding the whole system. A diagram of this geometry is shown in Figure 6-1 Diagram of the point kernel experiments.

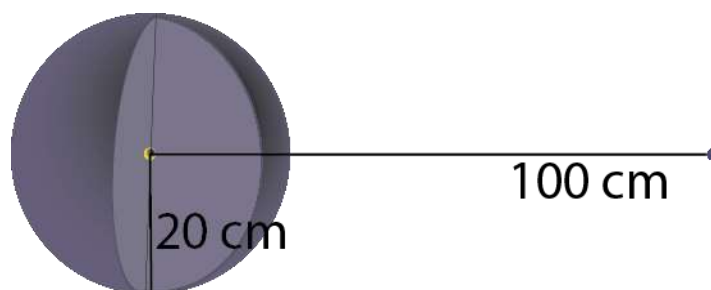


Figure 6-1 Diagram of the point kernel experiments.

Four shielding materials were selected for comparison between point kernel and MC calculations. The materials were aluminum, iron, lead, and concrete. Aluminum, iron, and lead were selected for their variations in density; low, medium, and high, respectively. Each of these

was assumed to be a pure, elemental form of the shield. Concrete was selected because it is ubiquitous as a building material and a shielding material in facility structures.

Another aspect of this preliminary comparison was to test and decide which variance reduction techniques to use in later parts of this work. Within the MCNP testing not only was the standard survival biasing with weight cutoff applied, other techniques investigated were the use of importance splitting/roulette, energy splitting/roulette, mesh-based weight windows generation, exponential transform, and power source biasing. Cell based importance splitting/roulette was selected based upon ease and closeness of results. Within SCALE source and response biasing were applied. However, because MCNP has a more versatile set of tally detectors for this type of simulation and the user is more familiar with MCNP, SCALE was not used in later computations.

6.2 Results and Analysis

To calculate the particle fluence rate, comparable to the uncollided flux in MCNP, and the total particle fluence rate, comparable to the total flux in MCNP, at the detector one needs the activity of the source (A), energy of the source emission (E_γ), shield radius (r), density of the shield (ρ_s), distance to the detector (d), the density of air (ρ_a), the mass attenuation coefficient for the shielding material (μ/ρ_s) and air (μ/ρ_a) at the gamma energy, and the build-up factor (B). Because there is some variance in mass attenuation coefficients values were selected from a variety of sources to develop potential ranges of answers: Health Physics and Radiological Health (HPRH), National Institute of Standards and Technology (NIST), Radiological Health Handbook (RHH), Fundamentals of Nuclear Science and Engineering (Shultis), and Introduction to Nuclear Engineering (Lamarsh) [36], [48]–[51]. For similar reasons the build-up factors were determined from two references: HPRH and Lamarsh [36], [48]. The densities were consistent from one source

to the next and were selected from HPRH [48]. The source properties, material densities, and geometry specifications are provided in Table 6–I.

Table 6–I: Point kernel source properties, material densities, and geometry specifications.

Property	Magnitude	Units	Density	Magnitude (g/cm ³)
Source activity (<i>A</i>)	1.0	Ci	Aluminum	2.702
Gamma-ray energy (<i>E_γ</i>)	1.0	MeV	Iron	7.874
Shield radius (<i>r</i>)	20	cm	Lead	11.350
Detector distance (<i>d</i>)	100	cm	Concrete	2.300
			Air	1.205x10 ⁻³

The mass attenuation coefficients and build-up factors utilized in the calculations for each material are shared in Table 6–II.

Table 6–II: Material mass attenuation coefficients and build-up factors.

Mass Attenuation Coefficients (cm ² /g)					
Material	HPRH	NIST	RHH	Shultis	Lamarsh
Aluminum	6.146 x10 ⁻²	6.146 x10 ⁻²	6.130 x10 ⁻²	N/A	6.140 x10 ⁻²
Iron	5.995 x10 ⁻²	5.995 x10 ⁻²	5.990 x10 ⁻²	5.951 x10 ⁻²	5.950 x10 ⁻²
Lead	7.102 x10 ⁻²	7.102 x10 ⁻²	7.080 x10 ⁻²	6.803 x10 ⁻²	6.840 x10 ⁻²
Concrete	6.495 x10 ⁻²	6.495 x10 ⁻²	6.370 x10 ⁻²	6.369 x10 ⁻²	6.350 x10 ⁻²
Air	6.358x10 ⁻²	6.358 x10 ⁻²	6.360 x10 ⁻²	6.353 x10 ⁻²	6.360 x10 ⁻²
Build-up Factors					
Aluminum	8.7444	-	-	-	9.095
Iron	23.7092	-	-	-	24.38
Lead	5.08304	-	-	-	5.621
Concrete	7.4323	-	-	-	N/A

An example of the particle fluence rate and total particle fluence rate calculations for aluminum is shown in Appendix E: Point Kernel Hand Calculation Example. A summary of the calculated values for particle fluence rate and total particle fluence rate using the coefficients and factors from HPRH are shared in Table 6–III.

The MCNP and SCALE models were created based upon the geometry described above. Two different detectors were used in the MCNP model for comparison and to obtain both the total and

uncollided particle flux. The detectors were a particle track length estimator, F4 type, and a next event point detector, F5 type. An example MCNP input file is shared in Appendix F: Monte Carlo Neutron Particle (MCNP) Input Files. The SCALE model only used a point detector similar to the MCNP F5 type. An example of the SCALE input file is given in Appendix H: SCALE Input Files.

Results for MCNP and SCALE simulation for aluminum, iron, lead, and concrete are shown in Table 6–III. A ratio of the computed value to hand calculated value (C/H) is provided to assist in evaluation of the results. This C/H allows the reader to see how close the computed values are to the hand calculated values; ideally the ratio would be unity. The MCNP results shown made use of cell importance values for particle splitting and Russian roulette as a variance reduction technique, especially needed for the lead shield. The SCALE results made use of a variance reduction technique to determine the importance function for each voxel of a mesh placed over the space in the problem. The MCNP results for the particle fluence rate were quite good, with the largest variance from the hand calculations being for lead when compared to the hand calculation using the parameters from HPRH. Despite the variance from the HPRH in the lead values the results are still bounded by the hand calculations when considering parameters from the other references. The results for the SCALE simulation were not as close as desired for the particle fluence rate. When comparing the total particle fluence rate, SCALE fared quite well for aluminum and concrete, but not so well for iron and lead. MCNP results tended to be more reliable.

These results indicated the codes were capable of providing reasonable results relative to hand calculated estimates and thus should provide good estimates of the experiments, though MCNP seems to provide a better estimate for the types of simulations being performed. The next step was to devise experiments for testing the shielding materials and then modeling these experiments in MCNP.

Table 6–III: Table of computed and simulated values for the contrived shielding problem having a 1 MeV photon source at the center of a 20 cm spherical shield with the detector 100 cm away.

$\gamma/s \cdot cm^2$	Aluminum ($\pm \% \sigma$)	C/H	Iron ($\pm \% \sigma$)	C/H
$\dot{\Phi}$ (HPRH)	1.057×10^4		2.324×10^1	
$\dot{\Phi}$ (MCNP, F5)	1.0747×10^4 (0.01)	1.02	2.45129×10^1 (0.02)	1.05
$\dot{\Phi}$ (SCALE)	1.22763×10^4 (5×10^{-7})	1.16	$3.65950 \times 10^1 \pm (6 \times 10^{-7})$	1.57
$\dot{\Phi}_{tot}$ (HPRH)	9.482×10^4		6.276×10^2	
$\dot{\Phi}_{tot}$ (MCNP, F4)	8.75420×10^4 (0.91)	0.92	4.98272×10^2 (1.55)	0.79
$\dot{\Phi}_{tot}$ (MCNP, F5)	8.81784×10^4 (0.01)	0.93	5.01757×10^2 (0.04)	0.80
$\dot{\Phi}_{tot}$ (SCALE)	9.39376×10^4 (0.009)	0.99	7.05001×10^2 (0.05)	1.12

$\gamma/s \cdot cm^2$	Lead ($\pm \% \sigma$)	C/H	Concrete ($\pm \% \sigma$)	C/H
$\dot{\Phi}$ (HPRH)	2.916×10^{-2}		1.475×10^4	
$\dot{\Phi}$ (MCNP, F5)	3.42775×10^{-2} (0.03)	1.18	1.55555×10^4 (0.00)	1.05
$\dot{\Phi}$ (SCALE)	1.0989×10^{-1} (7×10^{-7})	3.77	1.75821×10^4 (6×10^{-7})	1.19
$\dot{\Phi}_{tot}$ (HPRH)	1.751×10^{-1}		1.113×10^5	
$\dot{\Phi}_{tot}$ (MCNP, F4)	2.80519×10^{-1} (3.60)	1.60	1.12422×10^5 (0.17)	1.01
$\dot{\Phi}_{tot}$ (MCNP, F5)	2.73419×10^{-1} (0.17)	1.56	1.12638×10^5 (0.01)	1.01
$\dot{\Phi}_{tot}$ (SCALE)	8.93024×10^{-1} (0.38)	5.10	1.18849×10^5 (0.007)	1.07

7 Shielding Experiment and Simulation

7.1 Experimental Design

The design of an experiment is crucial to the success of the research. Thought needs to be given to each of the details involved in the design and how to obtain the desired information. Neglecting details or insufficient pre-investigation can lead to poor results or delays in obtaining successful results due to the need to redesign the experiments. However, nothing can replace experience and hindsight. While working on the experiment new information or experience may be acquired causing a shift in how the experiment is performed or what data needs to be collected.

In any shielding experiment the base design includes three components: a radioactive source, a shield, and a radiation detector. These experiments are no different, in that they contain these three main components. It is in the details where experiments diverge. In the following sections the details of the experiments are provided, along with results obtained from these experiments. Analysis of these data are also provided.

7.2 Gamma-Ray Experiment

7.2.1 The First Attempt

Initially a nominally 1 Ci (3.7×10^4 MBq) ^{137}Cs source was used in conjunction with a 3 in x 3 in NaI(Tl) scintillation detector. The activity of the source was calculated to be 276 mCi (1.021×10^3 MBq) on 20 Sept 2017. The detector was attached to a standard photo-multiplier (PM) Base with Preamplifier. The preamplifier was routed to a standard set of NIM equipment and a multi-channel analyzer (MCA) for data collection. Source, detector, and equipment data details are provided in Table 7–I. In the “Date/Notes” column of Table 7–I the term “Rev” refers to the revision number of the piece of equipment, indicating some modification was made to this version as compared to previous versions.

The source was fixed in a location and shielding materials, detector, and data collection equipment were brought to the source. The source was located in a vault type room with concrete walls, floor, and ceiling. The vault was approximately ten feet (3 m) long, six feet (1.8 m) wide, and eight feet (2.4 m) high. A second, larger source (20 Ci (7.4×10^5 MBq) J L Shepherd Irradiator, Model 81-8, assay date 25 June 1984, current activity 9.35 Ci (3.4595×10^5 MBq)) was located in the same vault.

Table 7-1: Source, detector, and equipment data from initial gamma-ray experimental set-up.

Make	Model	Serial	Date/Notes
Source Information			
J L Shepherd Calibrator	28-6A	587	22 Nov 1966
Detector Information			
Quartz & Silice	PM8054-864/5	N:E.190	Type 76S76
Ortec PM Base and Preamplifier	276		
NIM and MCA Information			
Canberra NIM Bin	2100		
Canberra NIM Power	AEC320-9B	9007091	
Ortec Single Channel Analyzer		699S	Rev. 8
Canberra Amplifier	2012	11811074	
Ortec Timer/Counter	871	08028817	Rev. E
Canberra High Voltage Power Supply	3002	4814932	
Ortec ADCAM Multi-Channel Buffer	926	10256522	Rev. F
AMP ADCAM cable	DPM-USB	10264156	Rev. E
Dell Optiplex computer	780		

Prior to data collection the instrument parameters were set by performing system checks and calibrations. A set of check sources were used to aid in these preliminary tests to determine instrument settings and to calibrate the multi-channel analyzing system. The isotopes used were ^{133}Ba , ^{137}Cs , and ^{60}Co (each approximately 1 μCi (0.037 MBq)). These sources provide a wide range of gamma-ray energies to allow for good calibration of a scintillation detector using the MCA. The ^{137}Cs spectrum from the calibration is shown in Figure 7-1.

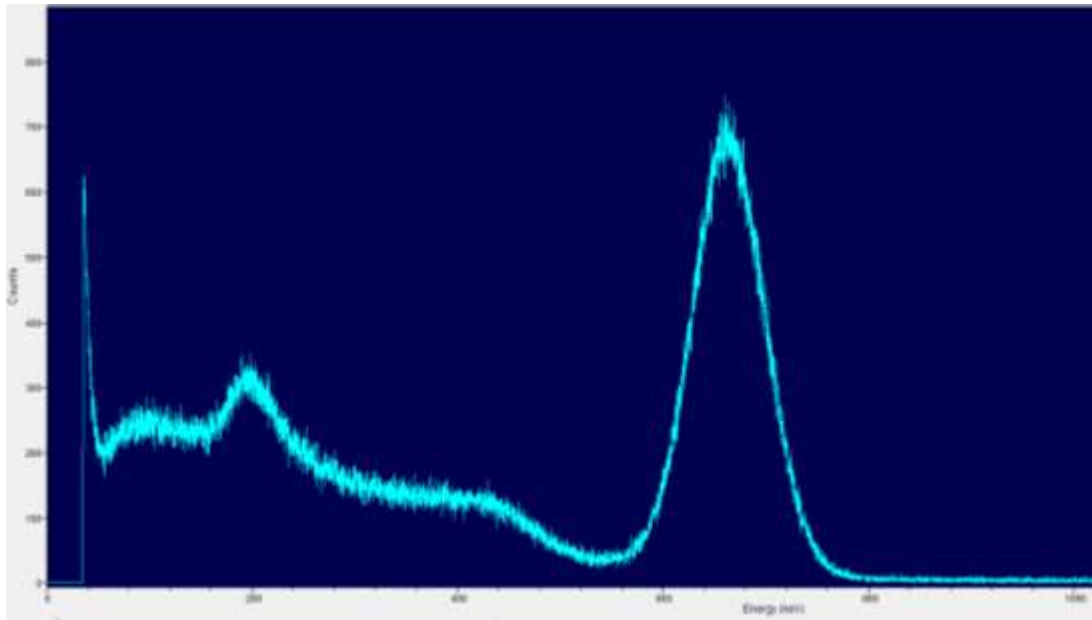


Figure 7-1 Spectrum from the ^{137}Cs calibration source.

The instrument settings were determined to be as follows:

1. High Voltage, 900 V.
2. Amplifier
 - a. Course Gain, 64.
 - b. Fine Gain, 9.40.
3. Single Channel Analyzer
 - a. Window/Upper Level, 10.0
 - b. Lower Level, 2.8.
 - c. Toggle set to window
4. Multi-channel Buffer
 - a. Gate, off.
 - b. Conversion gain, 8192.

Three sets of experimental data collection were attempted for this set-up. A bracket was created to hold the shielding material in front of the calibrator window. This bracket could hold multiple

blocks of each material. The detector was placed approximately 15 inches (38.1 cm) from the front outer surface of the calibrator window for two of the data collections and 83.75 inches (2.13 m) for the third. It was aligned axially to point directly at the source, see Figure 7-2. Count were taken for 300 seconds on both the timer/counter and the MCA for each run.

During the first data collection of this set up, two blocks of each shielding material were placed into the bracket making the shield $\frac{1}{4}$ inch (0.635 cm) stainless steel, $\frac{1}{4}$ inch (0.635 cm) tungsten carbide, 2 inches (5.08 cm) borated polyethylene, and 6 inches (15.24 cm) concrete. The second and third data collections contained only one block of each material. Stainless steel was always closest to the source, while the other three materials were rotated through order. This was done to see if the material order had any effect of the efficiency of the shield.

The following two figures, Figure 7-3 and Figure 7-4, are the spectra from data collection with the detector at 15 inches (38.1 cm) and the order of shielding material is stainless steel (SS), borated polyethylene (BP), tungsten carbide (WC), and concrete (C), or in condensed notation SSBPWCC. The first is with two layers of each material while the second is of one layer each.

With two blocks of each shielding material the range of total counts were from 214,345 to 239,603. This count rate is still within the ability of the detector, but the spectrum is not as expected. Similarly, with one block each the spectrum did not come out as expected. The total counts ranged from 1,156,113 to 1,251,557, which corresponds to a count rate of nearly 4000 count/sec (cps).

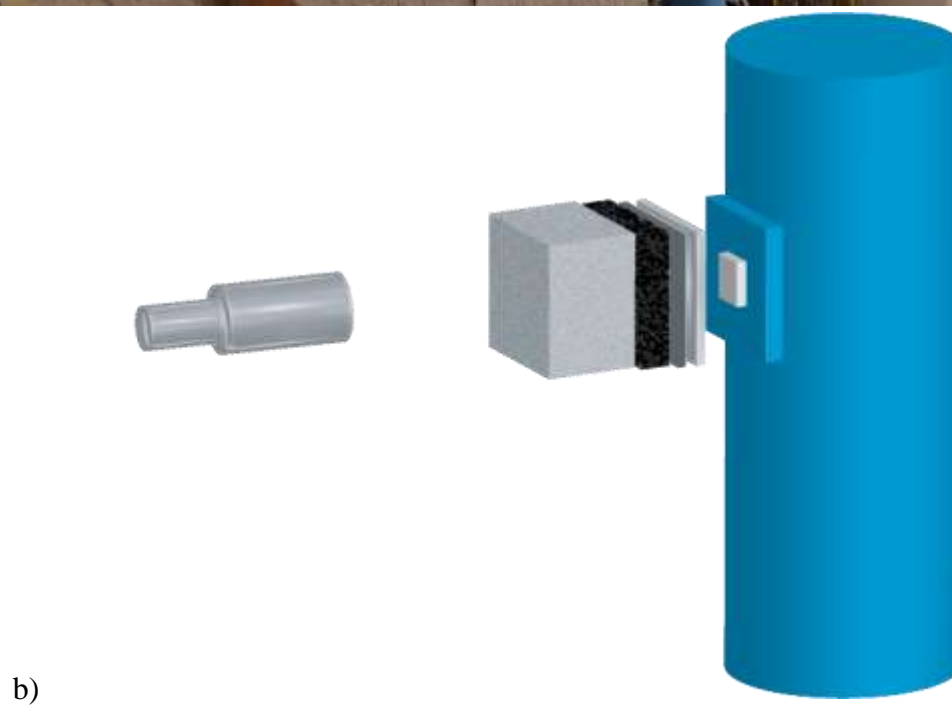


Figure 7-2 a) Photograph of and b) drawing of the set up for the J L Shepherd 1 Ci (3.7×10^4 MBq) calibrator showing a single layer of each material and the 3x3 NaI detector.

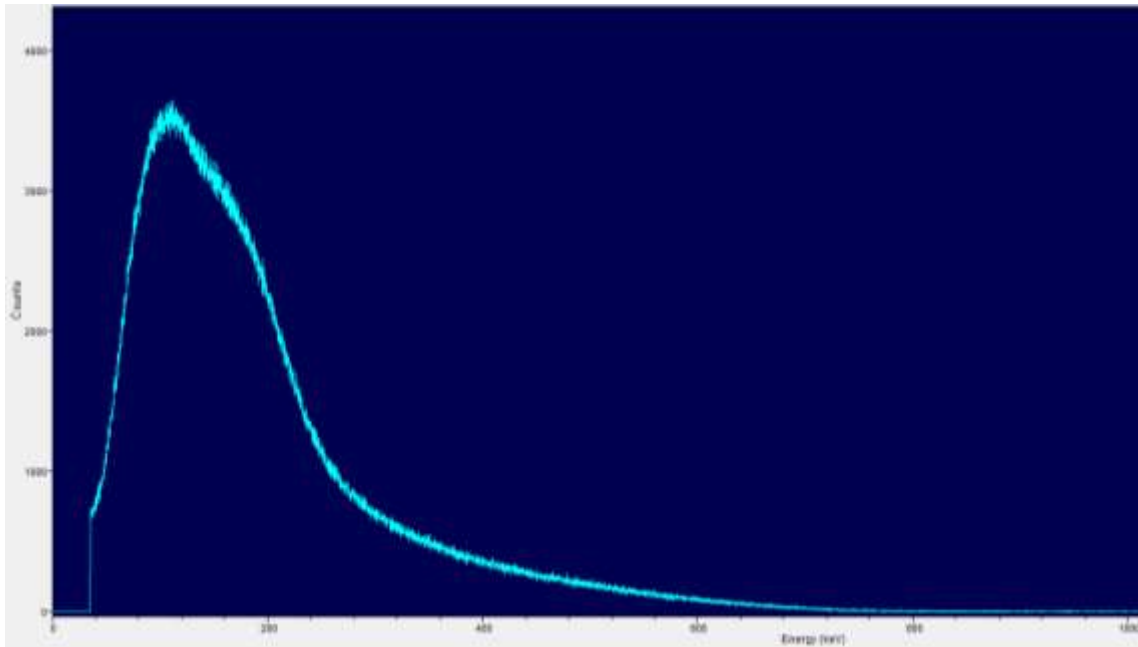


Figure 7-3 Spectrum obtained from 1 Ci (3.7×10^4 MBq) ^{137}Cs on a Q&S 3x3 NaI detector having two layers of each shielding material between source and detector.

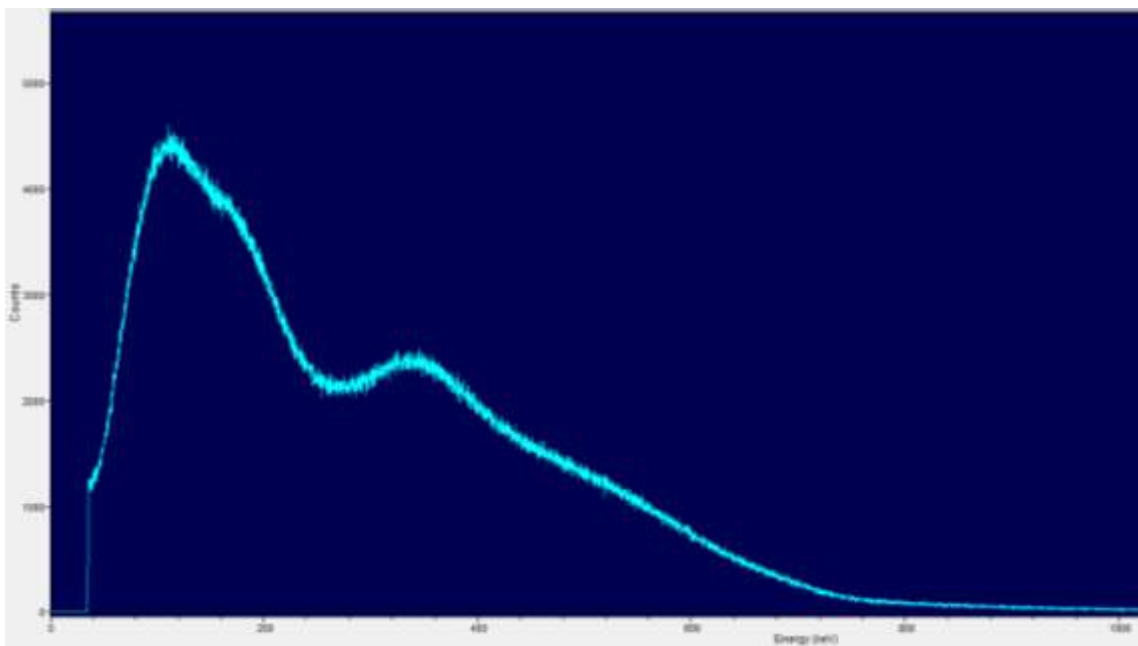


Figure 7-4 Spectrum obtained from 1 Ci (3.7×10^4 MBq) ^{137}Cs and Q&S 3x3 NaI detector with one layer of shielding material between source and detector.

The expected spectrum would have a relatively flat region from the lowest energy at about 40 keV up to about 475 keV where the Compton edge will drop off. This flat region may have a backscatter peak around 200 keV. There should be a distinct full energy peak at 661 keV. None of

these features are present leading to a faulty system or poor set up due to overwhelming intensity of radiation, though the calibration spectrum indicates a good detector. However, detectors can go bad or get damaged during use.

The spectra taken with the detector placed at 83.75 inches (2.13 m) from the source were similar to the spectra above. Because of the peculiar nature of the spectra taken during experiments a background was taken as well, see Figure 7-5. In this spectrum you can clearly see a full

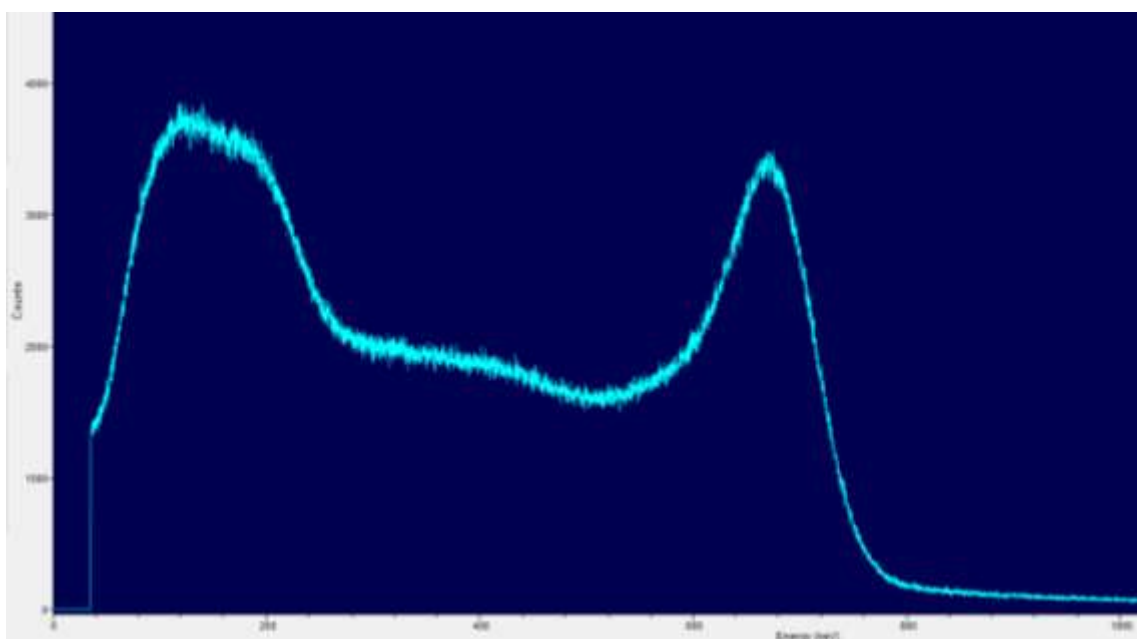


Figure 7-5 Background spectrum taken in the vault containing the J L Shepherd calibrator and irradiator using the Q&S 3x3 NaI detector.

energy peak at the expected location, except both sources were closed and secured. This means there is a large background of 661 keV gamma-rays in the area. A high background is detrimental to experiments. At this point a decision was made to abandon these sources for a smaller one and to set up in a lower background location. A change of detectors was also being considered. After another calibration was attempted on the Quartz and Silice 3x3 NaI detector affording poor spectra the choice was made to switch to another detector.

7.2.2 The Second Attempt

Due to the change in the location of the experiment and the decision to use a new detector most of the equipment changed from the first attempt. The equipment used in the second iteration is documented in Table 7-II.

Table 7-II: Source, detector, and equipment data for the gamma-ray experimental set-up providing results used in this work.

Make	Model	Serial	Date/Notes
Source Information			
Eckert & Ziegler	193	N3-540	1 Mar 2016
Detector Information			
Bicron NaI 2x2	2M2/2	BM-689	
Ortec PM Base and Preamplifier	276	10253417	Rev. K
NIM and MCA Information			
Ortec NIM Bin	4001/4002D	10323645	Rev. A
Ortec 160W NIM Power Supply	4002D	10309513	Rev. Y
Ortec Single Channel Analyzer (SCA)	550A	816	
Ortec Spectroscopy Amplifier	672	0808897	Rev. U
EG&G Ortec Timer/Counter	871	453	Rev. 07
Otec High Voltage Power Supply	556	14328996	Rev. R
Amtek Ortec MCA	Easy-MCA-8k	10243286	Rev. D
Tektronix Oscilloscope	TDS 3032B	B012822	
Dell w/ Windows 7			

The set-up of the system used in this iteration of experiments was similar to the previous set up and can be seen in Figure 7-6. Prior to use, a calibration of the new instrumentation and detector was performed using ^{133}Ba and ^{137}Cs check source. This allowed for good calibration of the low and mid-range energies. The spectrum is provided in Figure 7-7.

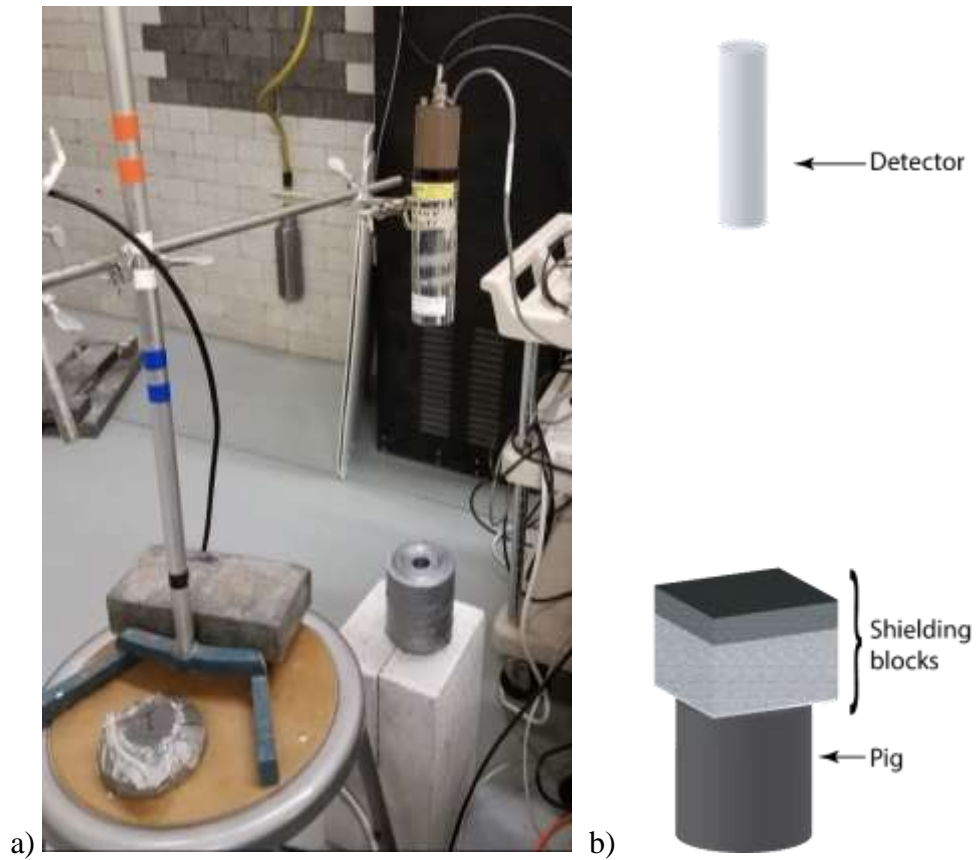


Figure 7-6 a) A photograph of the detector to pig set up used. b) shows a drawing of the same set-up but including shielding blocks.

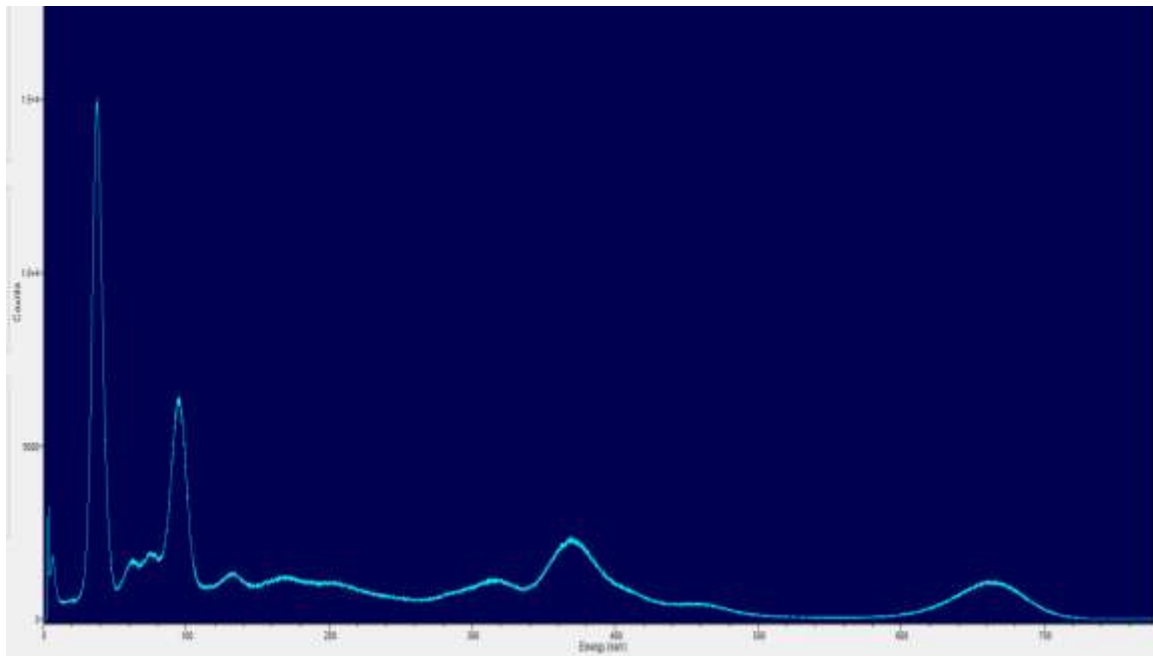


Figure 7-7 Calibration spectrum for the Bicorn 2x2 NaI detector using ^{133}Ba and ^{137}Cs sources.

7.2.2.1 Counting System Checks

In addition to calibration, a counting system check was performed to determine if the counting equipment was working optimally and not introducing a systematic bias into the counts. There are multiple checks that one can make of the data to determine if the counting system is working well. One check for data and system “goodness” is comparing a data distribution function, $F(x)$, to a probability distribution function, $P(x)$. Another check for the system and data “goodness” is to calculate chi squared, χ^2 , and compare this value to upper and lower critical values determined by the degrees of freedom for χ^2 .

The check was completed for a set of data taken as 40 one minute readings. The results for this check are shared in Table 7–III. The mean, \bar{x} , and standard deviation, s , were calculated for the data set. The data was processed into a frequency of a reading per bin and then calculating the data distribution function, $F(x)$, according to Equation 7-1.

$$F(x) = \frac{\text{occurrences of the value of } x}{N}$$

Equation 7-1: Data distribution function.

where N is the number of measurements.

The probability distribution function is based on the Gaussian statistical nature of the data when sufficient data are collected and the mean is large (typically for $\bar{x} > 20$). If the mean is small ($\bar{x} \leq 20$) then a Poisson distribution would be used. The equation to describe the Gaussian probability distribution function, $P(x)$, is:

$$P(x) = \frac{1}{\sqrt{2\pi\bar{x}}} e^{\frac{-(x-\bar{x})^2}{2\bar{x}}}$$

Equation 7-2: The probability that a measured value will fall within a distribution based on the mean of the data.

where x are the integers between and including the minimum and maximum measured values of x and \bar{x} is the mean of the data set.

Table 7–III: Raw data for the counting system check.

Count #	x	Count #	x	Count #	x	Count #	x
1	23010	11	22612	21	22962	31	22867
2	22490	12	22676	22	22962	32	22539
3	22638	13	22627	23	22787	33	22688
4	22757	14	22669	24	22597	34	22651
5	22688	15	22888	25	22387	35	22518
6	22612	16	22584	26	22846	36	22768
7	22657	17	22820	27	22829	37	22665
8	22818	18	22752	28	22441	38	22897
9	22480	19	22686	29	22744	39	22949
10	22554	20	22804	30	22821	40	22662
\bar{x}	22710	s^2	151.98				

The frequency of each measurement within a bin and data distribution function for each bin are found in Table 7–IV. The probability distribution function was calculated according to Equation 7-2, where $22,387 \leq x \leq 23,010$ and $\bar{x} = 22,710$, but the values are not tabulated. Figure 7-8 shows the data distribution function and probability distribution function plotted together as a histogram and scatter plot for comparison. This comparison is a qualitative one. The two distributions have similar shape, which is a good indication, though the amplitudes differ, requiring further analysis for “goodness”.

Since another test of “goodness” is required, a χ^2 test was completed. The value of χ^2 , shown in Table 7–IV, was calculated based upon Equation 7-3. This value was compared to the upper and lower critical values, $p(0.9)$ and $p(0.1)$, also in Table 7–IV, for a degree of freedom = 39. When used as a “goodness” fit the calculated χ^2 value should fall between the upper and lower critical values to indicate a proper distribution of data, which it does fall between the critical values.

$$\chi^2 = \frac{(N - 1)s^2}{\bar{x}}$$

Equation 7-3: Method used to calculate chi squared.

Table 7-IV: Frequency and probability data. NIST tables reference:
<https://www.itl.nist.gov/div898/handbook/eda/section3/eda3674.htm>

Bin	Frequency	F(x)	chi ²
22405	1	0.025	39.66473
22455	2	0.05	p(0.9), from NIST tables
22505	2	0.05	50.660
22555	2	0.05	p(0.1), from NIST tables
22605	5	0.125	28.196
22655	6	0.15	Degrees of Freedom
22705	3	0.075	39
22755	4	0.1	
22805	6	0.15	
22855	2	0.05	
22905	1	0.025	
22955	2	0.05	
23005	1	0.025	

A secondary check of the counting system included use of the SCA to create a pulse height spectrum. This is a good way to check your system to see if you can replicate a spectrum like you would expect to see using an MCA. The counter timer was set to take one minute counts. The data are shared in Table 7-V and the spectrum generated by this method is shown in Figure 7-9. The amplifier settings were:

1. High Voltage, 900 V.
2. Amplifier
 - a. Course Gain, 100.
 - b. Fine Gain, 14.5.
 - c. Shaping Time, 0.5 μ s.
3. Single Channel Analyzer
 - a. Window, 200 mV.

- b. Lower Level, started at 0 and incremented up to 10.
- c. Toggle set to window.

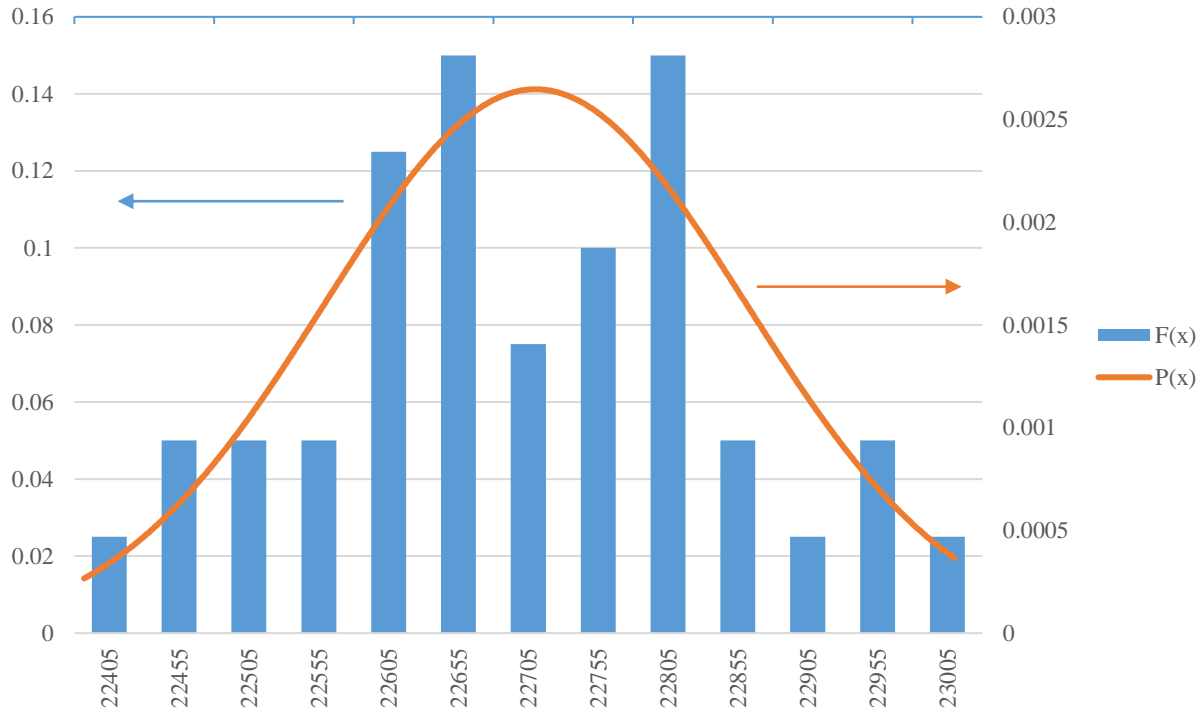


Figure 7-8 Histogram of counting system check data frequency, $F(e)$, and plot of counting system check probability, $P(e)$.

The pulse height spectrum shows all of the main features expected. It shows the full energy peak representing the 661.7 keV emission at approximately 9000 mV. It shows the Compton edge and the backscatter peak at the appropriate relative position with respect to the full energy peak, where the relation between keV and mV is approximately 0.073 keV/mV.

Analysis of the results from the system check indicate that the system is working well, the system is not introducing systematic errors or biases to the results, and the results are Gaussian in nature. These conclusions are based upon the result of χ^2 being between the two values of $p(0.9)$ and $p(0.1)$ and upon the SCA generated spectrum matching expectation.

Table 7–V: Pulse height spectrum data.

Lower Limit (mV)	Counts	Lower Limit (mV)	Counts	Lower Limit (mV)	Counts	Lower Limit (mV)	Counts
0	128082	2600	4459	5200	3165	7800	1072
200	2060	2800	5085	5400	3272	8000	1416
400	2341	3000	4669	5600	3262	8200	2383
600	2764	3200	4204	5800	3351	8400	4114
800	2909	3400	3854	6000	3281	8600	6607
1000	2951	3600	3669	6200	2941	8800	10380
1200	3565	3800	3519	6400	2685	9000	13400
1400	3102	4000	3321	6600	1874	9200	14327
1600	2915	4200	3186	6800	1519	9400	10494
1800	3104	4400	3224	7000	1171	9600	5735
2000	3220	4600	3124	7200	1025	9800	2106
2200	3268	4800	3206	7400	955	10000	911
2400	3605	5000	3277	7600	902		

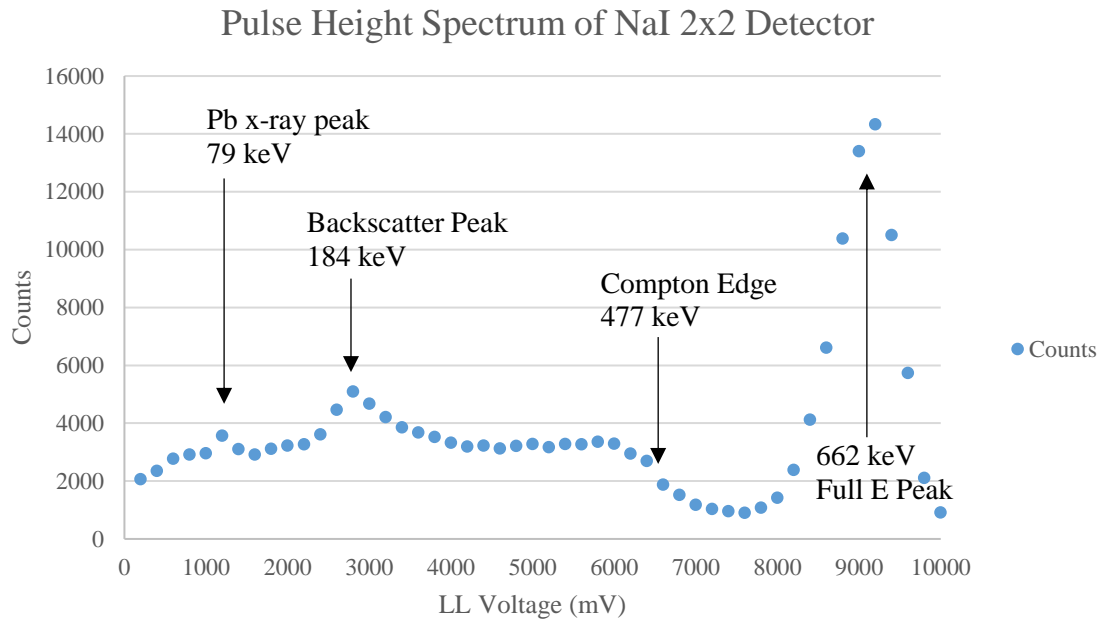


Figure 7-9 Pulse height spectrum obtained using a Bicron 2x2 NaI detector and a ^{137}Cs source.

7.2.2.2 Experimental Results

The signal pulses created by gamma-ray interactions in the NaI(Tl) scintillator and amplified by the photomultiplier tube were shaped and amplified by the preamplifier and then further

amplified by a spectroscopy amplifier. Following the amplifier, the signal was split. One side of the split used a single-channel analyzer to set a lower pulse height limit to eliminate electronic noise prior to being counted by the counter timer. The other side of the split made use of a multi-channel analyzer (MCA) to set a lower limit on pulse height, bin the pulses by height, and count the total number of pulses. The counter timer and the MCA were both set to collect counts for 300 seconds. The lower level was set to 200 mV on the MCA and 0.25 V on the SCA. The spectroscopy amplifier course gain was set to 100, the fine gain to 14.50 and the shaping set to 0.5 μ s. Both sets of data are reported in Table 7–VI, but the MCA data is considered more accurate, precise, and reliable and will be used in the final analysis.

Table 7–VI Gamma-ray data.

Shielding Setup	Counter Timer total counts	Counter Timer counts/second	MCA total counts	MCA counts/second
No shielding	5449626	18165	5910050	19700
SS	4620398	15401	4945240	16484
BP	4145676	13819	4403740	14679
C	1631066	5437	1666050	5554
WC	3139688	10466	3283930	10946
SSBPCWC	677797	2259	682552	2275
SSBPWCC	708624	2362	713971	2380
SSCBPWC	658869	2196	663627	2212
SSWCBCP	668277	2228	672951	2243
SSWCBPC	706254	2354	711362	2371
SSWCCBP	696831	2323	701957	2340

The following abbreviations for shielding materials will be used throughout the experimental and simulation reports: SS = stainless steel (0.3175 cm nominal thickness), BP = borated polyethylene (2.54 cm nominal thickness), C = concrete (7.62 cm nominal thickness), WC = tungsten carbide (0.3175 cm nominal thickness). Variations to the nominal thickness will be discussed in 7.3.3 Geometry Refinements.

Each of the MCA data collections was accompanied by a spectrum. A typical spectrum for the shielded versions of the experiment is shown in Figure 7-10.

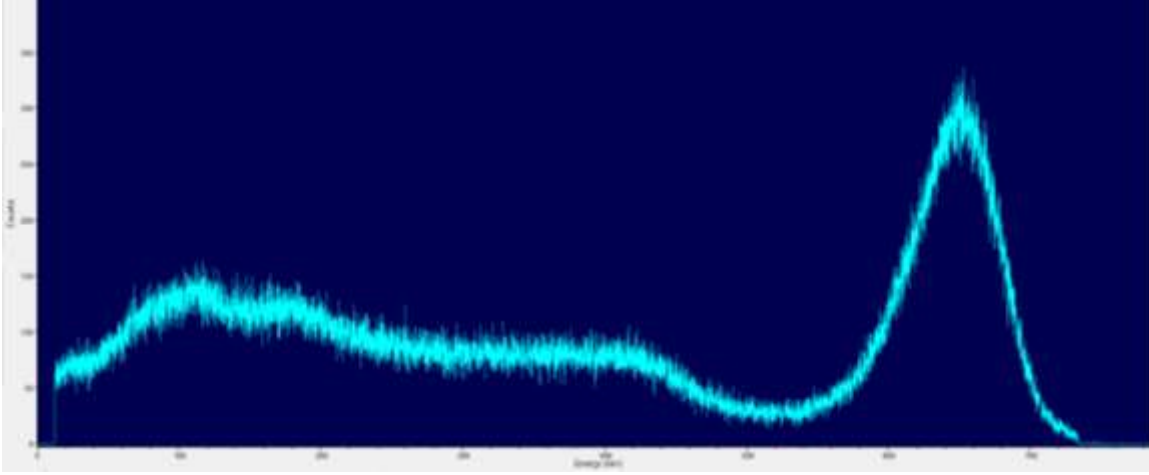


Figure 7-10 Spectrum collected for the experimental run with a shielding configuration of SSWCBPC.

7.2.2.3 Error Analysis

With any experiment comes error. For the gamma-ray experiments two primary errors were considered, counting statistical errors and source strength error. Because a counting system is used to collect the data counting statistical errors must be accounted. The source strength is used as a conversion factor for the comparison of experimental data to the simulation data and thus must be incorporated into the errors accounted. The method for error accounting in this work is the quadrature method, see Equation 7-4.

$$\sigma_{tot} = \sqrt{\sum_i \sigma_i^2}$$

Equation 7-4: Quadrature of errors.

The source strength error was given as a percent of activity error, $\pm 15\%$. All of the other errors will be converted to percent (or relative) prior to the quadrature calculation.

For data conforming to a Gaussian nature, as the counting data does, the statistical error is related to the counts by the following relationship

$$\sigma = \sqrt{N}$$

Equation 7-5: Gaussian statistical error relationship to counts collected on a counting system.

where N is the number of counts collected. To convert the data to counts per second the data is divided by a constant, time, with units in seconds, to obtain a unit of counts. To account for this in the counting statistical error you simply divide the error calculated in Equation 7-4 by the same constant.

Table 7–VII: Experimental error accounting for gamma-ray experiments.

Shielding setup	$\pm\sigma_i$ of MCA (counts)	$\pm\sigma_i$ of MCA (cps)	% error of MCA (cps)	% error of source strength	Experimental cps (\pm % σ_{tot})
No shield	2431	8.10	0.0411	15	19700 (15)
SS	2224	7.41	0.0450	15	16484 (15)
BP	2098	7.00	0.0476	15	14679 (15)
C	1291	4.30	0.0775	15	5554 (15)
WC	1812	6.04	0.0552	15	10946 (15)
SSBPCWC	826	2.75	0.1210	15	2275 (15)
SSBPWCC	845	2.82	0.1183	15	2380 (15)
SSCBPWC	815	2.72	0.1228	15	2212 (15)
SSCWCBP	820	2.73	0.1219	15	2243 (15)
SSWCBPC	843	2.81	0.1186	15	2371 (15)
SSWCCBP	838	2.79	0.1194	15	2340 (15)

7.3 Gamma-Ray Simulation

Monte Carlo N-Particle (MCNP) version 6.1.0 was used to perform the simulations. Once, a professor said, “if you treat MCNP like a black box it will give you exactly what you asked for, regardless if it is correct”. Another said, “if you put junk in, you get junk out”. This work generated a great appreciation for these statements.

Each card added to an input file turns into an area of great importance when designing the input file for MCNP so you do not put junk in and get junk out. For this work three specific cards in the input files were major areas of interest, because they required multiple iterations to achieve convergence of the experimental and simulation answers. These cards were tally selection, atom

densities, and geometry specifications. Refining each of these, to provide the closest replication of the real experiment, was a significant challenge.

7.3.1 Tally Selection

When one first learns to use MCNP it is believed that selection of one of the simple, general tallies will suffice and provide the perfect answer the first time run. No! This is not true although it is sometimes promoted in courses by use of over-simplified or contrived examples necessary for demonstrating how to use MCNP. Selection of the tally to properly reflect a real detector or to simulate a real experimental measurement is complex and requires the use of many add on components such as multiplier cards, etc.

At first, a simple track-length estimator, F4 tally was chosen and found to be lacking. It was not possible to apply the necessary conversion factors to obtain counts per second to replicate the detector. The next attempt made use of modifiers, FM and SD, to the F4 tally. This was more reasonable, because doing unit conversions could get you to counts per second, see Equation 7-6.

$$cps \left[\frac{p}{s} \right] = flux \left[\frac{p}{cm^2 \cdot sp} \right] \times vol[cm^3] \times atom\ density \left[\frac{atom}{b \cdot cm} \right] \times cross\ section \left[\frac{b}{atom} \right] \\ \times activity \left[\frac{sp}{s} \right]$$

Equation 7-6: Unit analysis of a modified F4 tally.

where p is particle, s is seconds, sp is source particle, and b is barn.

The tally card would be entered as:

```
F4:p cell #
FM4 -1 (material number) (reaction #)
SD4 1
```

The FM card multiplies the F4 tally by the atom density (when the first entry is -1) and the cross section (in this work the reaction number was -5 for total photon cross section) for the

material indicated by the material number and the SD card effectively multiplies the F4 tally by the volume of the cell selected by changing that volume to unity. The only number needed for post processing is the activity. This tally provided answers that were close to those of the experiments, but about a factor of 2.7 too high.

The thought that a scintillating detector being binned into pulse height by an MCA led to the subsequent selection of the pulse-height tally, F8. Again, just a simple F8 tally for photons was not sufficient and provided similar results to the F4 tally for photons. Several different iterations were attempted, including use of the special treatments cards of Gaussian Energy Broadening, GEB and Pulse-height light tally with anticoincidence, PHL. Additional insight was afforded through MCNP help to adjust the mode card to include electrons, e, and not just photons, p. The PHL option allows for the use of F6 tallies to assist in the determination of the tally as well as a special treatment by specifying NAI-1 to incorporate well known characteristics of a NaI(Tl) detector [52].

The final version of the F8 tally, that afforded the same answers as the experimental results, was similar to:

```
F8:e cell #  
E8 0 1e-5 0.015 255I 0.745  
FT8 GEB a b c &  
PHL 1 6 1 NAI-1  
F6:e cell #
```

The e means electrons were added to the mode card. The E8 card creates energy bins for the tallies to be divided into. The special treatment, FT8, card GEB gives coefficients for energy broadening applied to the tally after a specific particle tally is complete. This broadening allows for simulation of the broadening of a full energy peak and other features of the spectrum representing the finite resolution of the detector. Otherwise the full energy peak would be mono-

energetic, which is not realistic. The GEB coefficients a, b, and c are detector dependent and should be determined for the actual detector used. The PHL card allows the user to select multiple factors that affect the detector output. In this case the first 1 indicates only one factor will be considered. The 6 indicates the use of an energy deposition tally, F6, for electrons in the cell selected. The NAI-1 applies well understood and well characterized sodium iodide detector treatments to the tally.

The GEB coefficients required the taking of data using the detector from the experiments. The data needed was the energy of a full energy peak and the corresponding full width half maximum (FWHM) for each full energy peak. Then least squares fitting to the function found in the MCNP manual [42] and in Equation 7-7 provides the coefficients.

$$FWHM = a + b(E + cE^2)$$

Equation 7-7: Gaussian energy broadening coefficient equation.

where E is the peak energy in MeV. The data pairs of energy and FWHM are provided in Table 7–VIII, as well as the solved coefficients. A mix of sources were used to obtain these data: ^{22}Na , ^{60}Co , ^{137}Cs , mixed $^{152, 154, 155}\text{Eu}$, and ^{133}Ba .

Table 7–VIII: Data for GEB coefficient calculation.

GEB coefficient data								
Actual peak	1.3203	1.2529	1.1713	0.6686	0.5188	0.3701	0.1372	0.0933
True peak	1.3325	1.2745	1.1732	0.6617	0.5110	0.3560	0.1231	0.0865
FWHM	0.0990	0.0907	0.1059	0.0578	0.0524	0.0470	0.0196	0.0127
a	-0.0141448		b	0.0897491		c	0.191194	

7.3.2 Atom Densities

Changes to atom densities of materials used in the geometry can have profound effects on the results of the tallies. Initially, generalized atom densities from sources such as the PNNL Compendium [46] were used for almost all materials. It became clear that these would not work

for all materials. In particular the atom densities for the source material, the shielding materials, and the detector materials needed to be specific to the actual items used. All atom densities used in the final versions of the input files are tabulated in Appendix A: Atom Densities.

The atom densities for the source material started with the assumption it was CsCl powder with a density of 3.99 g/cm^3 . Further investigation through discussion with the source manufacturer revealed the source material was CsCl in a porous glass. The exact composition of the porous glass is proprietary information and was not given by the manufacturer, however the density of the glass was given as 1.5 g/cm^3 . A composition of general porous glass was obtained online (SiO_2 75%, B_2O_3 21.5%, Na_2O 3%, and K_2O 0.5%). The final atom density was developed using this new mass density, the general porous glass composition, and activity information for the CsCl composition.

The atom density for the detector was originally just sodium and iodine, NaI, as given in the PNNL Compendium. This is a good starting point, but the NaI is typically doped with a small quantity of thallium, Tl, for better light production efficiency and reducing self-absorption of the light emitted. Typical quantities of thallium added were obtained online from a general search for detector materials. The mass density was not changed from 3.67 g/cm^3 , but thallium was added to the mix. Also, the materials used in defining the detector housing was modified to include a vacuum for the photomultiplier tube (PMT) area and mu metal surrounding the PMT.

The atom densities for the stainless steel, borated polyethylene, and tungsten carbide were initially developed from general information about the density and composition provided by the manufacturer about each product. The concrete was taken to be regular concrete from the PNNL Compendium. It was determined these would need to be modified. More detailed information about the composition of stainless steel, borated polyethylene, and tungsten carbide were sought

from the manufacturers, to include elements down to 1% of the total composition, and lower, if available or provided. The atomic composition of the concrete was still assumed to be consistent with those listed in the PNNL Compendium. Mass densities were measured for each of the four materials by measuring the volumetric dimensions and the mass. These newly calculated mass densities were used in lieu of the generally provided mass densities in determining the material atom densities.

7.3.3 Geometry Refinements

Three significant geometric definitions changed from beginning to end. Just like in the atom density modifications, these changes involve the source, the shielding, and the detector. These also made notable changes to the results, honing the answer closer to the experimental results.

The active volume of the source was originally assumed to be a particular volume based upon the activity, specific activity, and mass density of CsCl. Later the volume was modified based upon further information provided by the manufacturer. The specific dimensions of the source were provided as a cylinder with diameter of 0.125 inch (0.3175 cm) (given in manufacturer literature) and a height of 0.090 inch (0.2286 cm) (provided by communication with the manufacturer).

The detector was originally designed as a cylinder of NaI with a diameter of 2 inches (5.08 cm) and a height of 2 inches (5.08 cm). This was a good first estimate but needed to be refined. As stated in the atom density sections the detector was defined as a more detailed object. A vacuum cylinder was added behind the NaI cylinder and then an aluminum housing was added like a cup around the NaI and an inverted cup of mu metal, a special alloy that inhibits transmission of electro-magnetic radiation, was added around the vacuum. The differences can be seen in Figure 7-11.

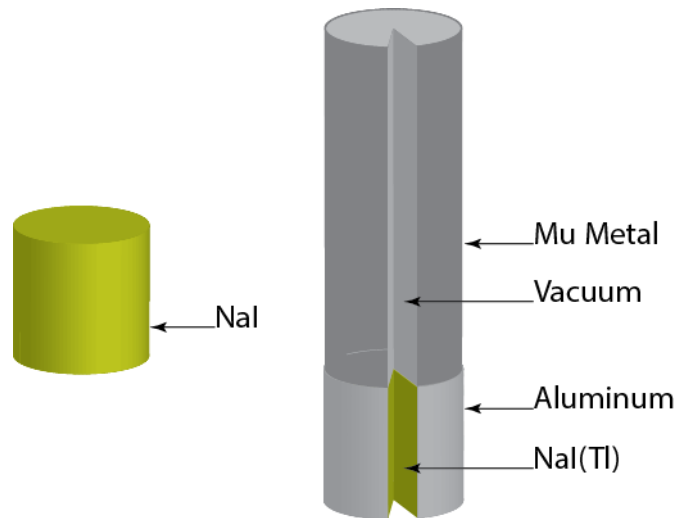


Figure 7-11 Changes to the geometric and material descriptions of the detector from beginning to end. A cut away from the full detector is provided for identification of internal parts.

The thickness dimension of each shielding material was originally based upon the nominal thickness provided by the manufacturer for stainless steel ($1/8^{\text{th}}$ inch, 0.3175 cm), borated polyethylene (1 inch, 2.54 cm), and tungsten carbide ($1/8^{\text{th}}$ inch, 0.3175 cm). The concrete was input at the design thickness (3 inches, 7.62 cm). When obtaining the mass density for new atom density calculations the variations in dimensions were noted and alterations were made to the input files. The measured thicknesses were SS = 0.302 cm, BP = 2.533 cm, C = 7.811 cm, and WC = 0.394 cm. These alterations, like the others, made slight changes to the overall result but the cumulative result of the changes brought all simulations into the desired tolerance (within 5%), with respect to experimental results.

7.3.4 Simulation Results with Comparison to Experimental Results

Two tally results were collected for each set up of the gamma-ray experiment, an F8 and an F4 as described in Section 7.3.1. The tally results were then multiplied by the source strength to obtain the proper units, counts per second, for comparison to the experimental results. The relative errors determined by MCNP were multiplied by the tally value and the source strength to give the standard deviation of the tally in counts per second. The source strength was 30,282,852 Bq on the

date of experimentation. The F4 tallies were obtained for comparison and for potential use in the optimization due to limited variance reduction capabilities when using an F8 with PHL.

The computed to experimental ratio, C/E, was selected as the figure of merit for comparison of data computed and collected for this work. Ideally all of these values would be unity, though unrealistic. An acceptable range of values was determined to be $0.95 \leq C/E \leq 1.05$. Recall MCA values are used in these ratio calculations.

The F8 and F4 tally results along with associated errors and the C/E ratios are shared in Table 7–IX and Table 7–X, respectively. The F8 tallies all afforded C/E within the acceptable range. The F4 tally results all had C/E ratios more than $2.5\times$ the desired range. This is expected due to the differences in the way the tallies are accounted. The F4 tally counts tracks of particles passing through the volume given as the detector while the F8 tally counts energy deposited by particle interactions within the volume. This would be similar to a real detector. For example, a photon may traverse the detector volume and not interact and does not deposit any energy. This photon would be counted in the F4 tally, but not the F8 tally.

The experimental and simulation results were plotted together with associated errors. This plot is shown in Figure 7-12. As can be seen the data follow each other and are within the calculated uncertainties.

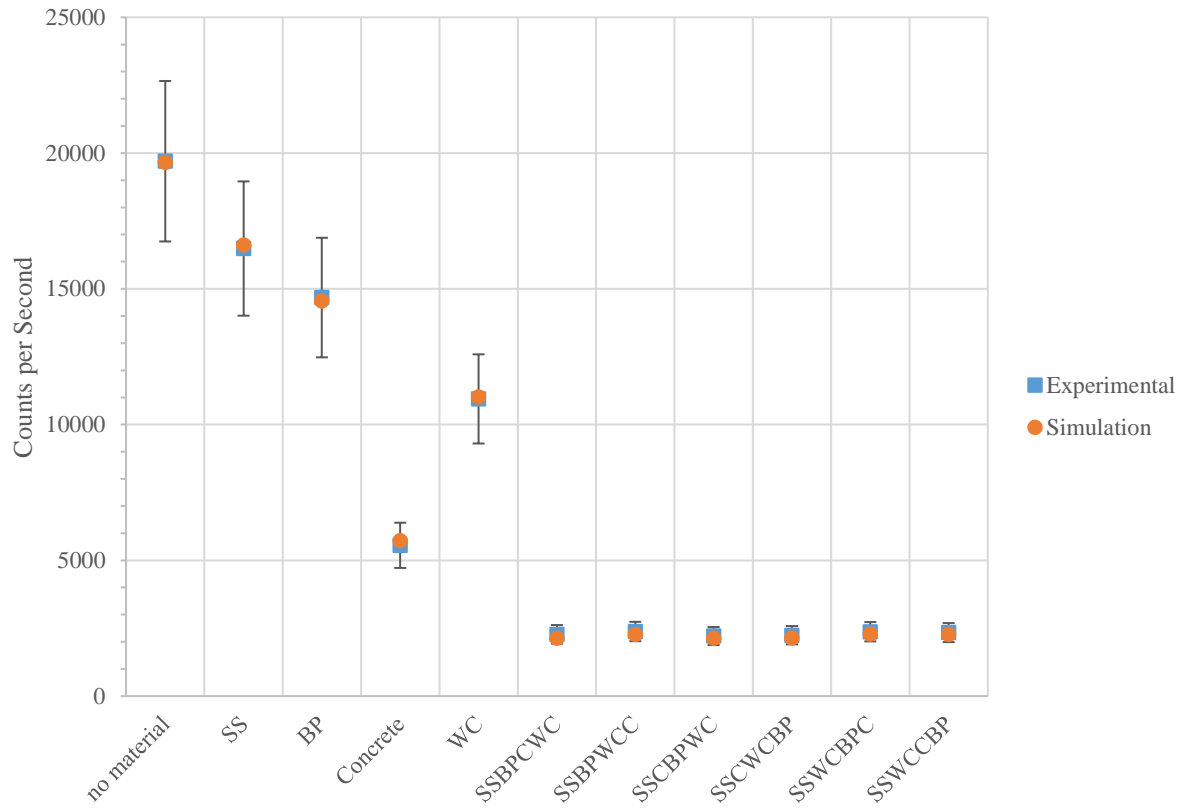


Figure 7-12 Plot of gamma-ray experimental and simulation results with associated errors.

Table 7-IX: MCNP F8 tally data with calculated values for comparison to experimental. Computed to experimental ratios are also tabulated.

Shielding Setup	F8:e GEB&PHL	$\pm\sigma$ of F8:e	Counts per Second	$\pm\sigma$ of CPS	C/E
No shielding	6.4915×10^{-4}	7.7898×10^{-7}	19658	23.6	0.9979
SS	5.4879×10^{-4}	7.1343×10^{-7}	16619	21.6	1.0082
BP	4.8078×10^{-4}	6.7309×10^{-7}	14559	20.4	0.9918
C	1.8912×10^{-4}	4.3498×10^{-7}	5727	13.2	1.0312
WC	3.6389×10^{-4}	6.1861×10^{-7}	11020	18.7	1.0067
SSBPCWC	7.0349×10^{-5}	2.6733×10^{-7}	2130	8.1	0.9364
SSBPWCC	7.5186×10^{-5}	2.7067×10^{-7}	2277	8.2	0.9567
SSCBPWC	7.0310×10^{-5}	2.6718×10^{-7}	2129	8.1	0.9625
SSWCBCP	7.0959×10^{-5}	2.6964×10^{-7}	2249	8.2	0.9579
SSWCBPC	7.5334×10^{-5}	2.7120×10^{-7}	2281	8.2	0.9621
SSWCCBP	7.5148×10^{-5}	2.7053×10^{-7}	2276	8.2	0.9726

Table 7-X: MCNP F4 tally data with calculated values for comparison to experimental. Computed to experimental ratios are also tabulated.

Shielding Setup	F4:p FM&SD	$\pm\sigma$ of F4:p	Counts per Second	$\pm\sigma$ of CPS	C/E
No shielding	1.7342×10^{-3}	2.4279×10^{-6}	52516	73.5	2.6658
SS	1.4679×10^{-3}	2.2019×10^{-6}	44452	66.7	2.6967
BP	1.2852×10^{-3}	2.0563×10^{-6}	38920	62.3	2.6514
C	5.0231×10^{-4}	1.2558×10^{-6}	15211	38.0	2.7391
WC	9.7720×10^{-4}	1.7590×10^{-6}	29592	53.3	2.7034
SSBPCWC	1.8891×10^{-4}	7.7453×10^{-7}	5721	23.4	2.5144
SSBPWCC	1.9883×10^{-4}	7.9532×10^{-7}	6021	24.1	2.5300
SSCBPWC	1.8874×10^{-4}	7.7383×10^{-7}	5716	23.4	2.5838
SSWCBCP	1.8994×10^{-4}	7.7875×10^{-7}	5752	23.6	2.5642
SSWCBPC	1.9927×10^{-4}	7.9708×10^{-7}	6034	24.1	2.5449
SSWCCBP	1.9908×10^{-4}	7.9632×10^{-7}	6029	24.1	2.5765

Two different mesh tallies were also taken on a limited number of simulations. The limited number was due to computing time limitations. One mesh tally was a track length estimator, F4, to see the distribution of photons throughout the geometry. The other mesh tally was the track length estimator, F4, modified for reaction rate for total cross section, however the volume modifier was not allowed to be applied. The tally forms were:

```
FMESH4:p GEOM=xyz ORIGIN=coordinate of the bottom, back, left most position
  IMESH x IINTS x'
  JMESH y JINTS y'
  KMESH z KINTS z'
```

And

```
FMESH4:p GEOM=xyz ORIGIN=coordinate of the bottom, back, left most position
  IMESH x IINTS x'
  JMESH y JINTS y'
  KMESH z KINTS z'
```

FM4 -1 0 -5 (where -1 multiplies by atom density, 0 select the material of the current cell, and -5 applies the total cross section for photons)

Plots of each of these mesh tallies, and a close up of the source and detector, are shared in Figure 7-13 and Figure 7-14. The false color scaling is provided to give a relative scale.

Energy bins were included in the pulse-height, F8, tallies. This allows for the building of a spectrum from the calculated tallies. Two plots are provided for comparisons. The first is experimental compared to simulation for the no shielding set up. The second is for a shielded configuration of SSCBPWC. These are shown in Figure 7-15 and Figure 7-16. There is fairly close agreement between the spectra. It is possible the variations are due to the GEB values being determined with different amplifier settings. Amplifier settings were different between experiments and GEB data collection because higher energy peaks, > 1 MeV, needed to be measured to obtain appropriate GEB values while experiments only needed to see up to 0.8 MeV.

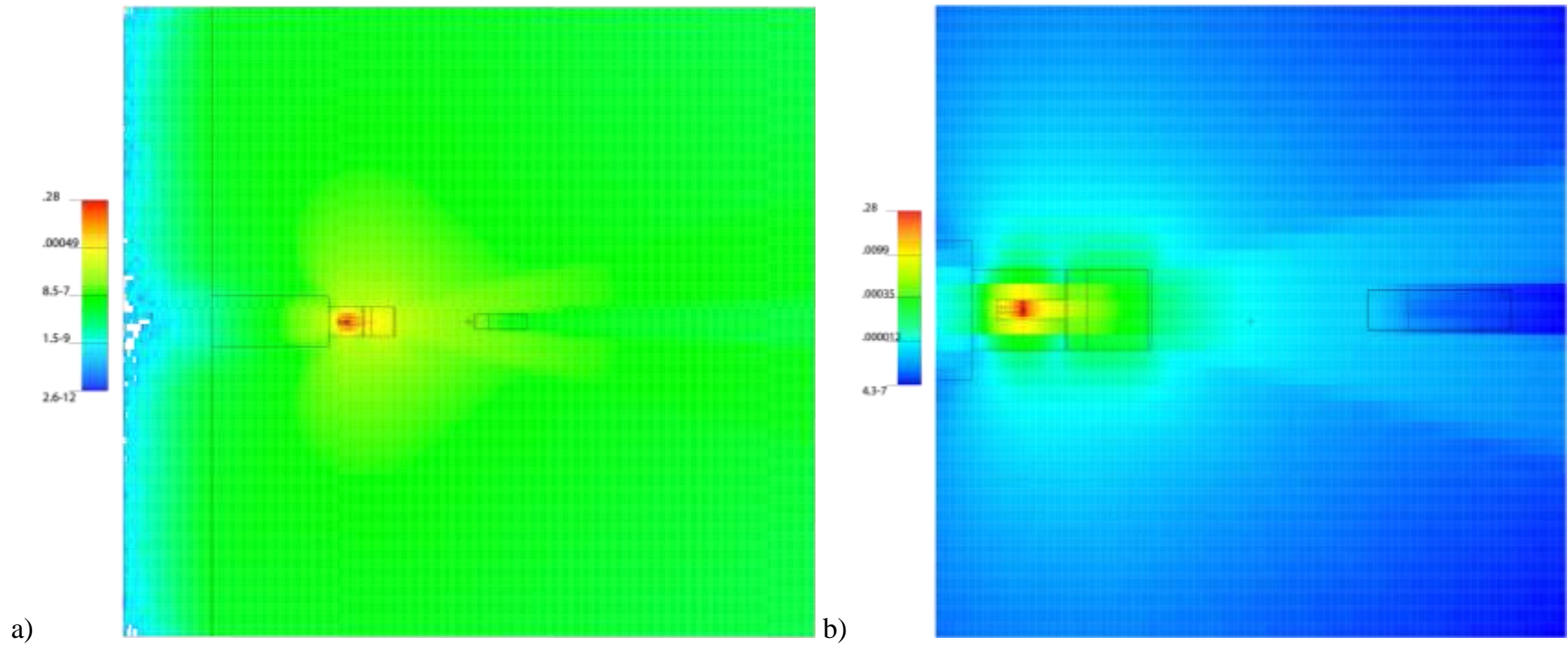


Figure 7-13 a) Track length estimator, F4 tally of the geometry indicating the relative flux of photons. b) Zoom of the source, shielding, and detector region of the problem for the F4 tally showing relative flux of photons throughout the problem.

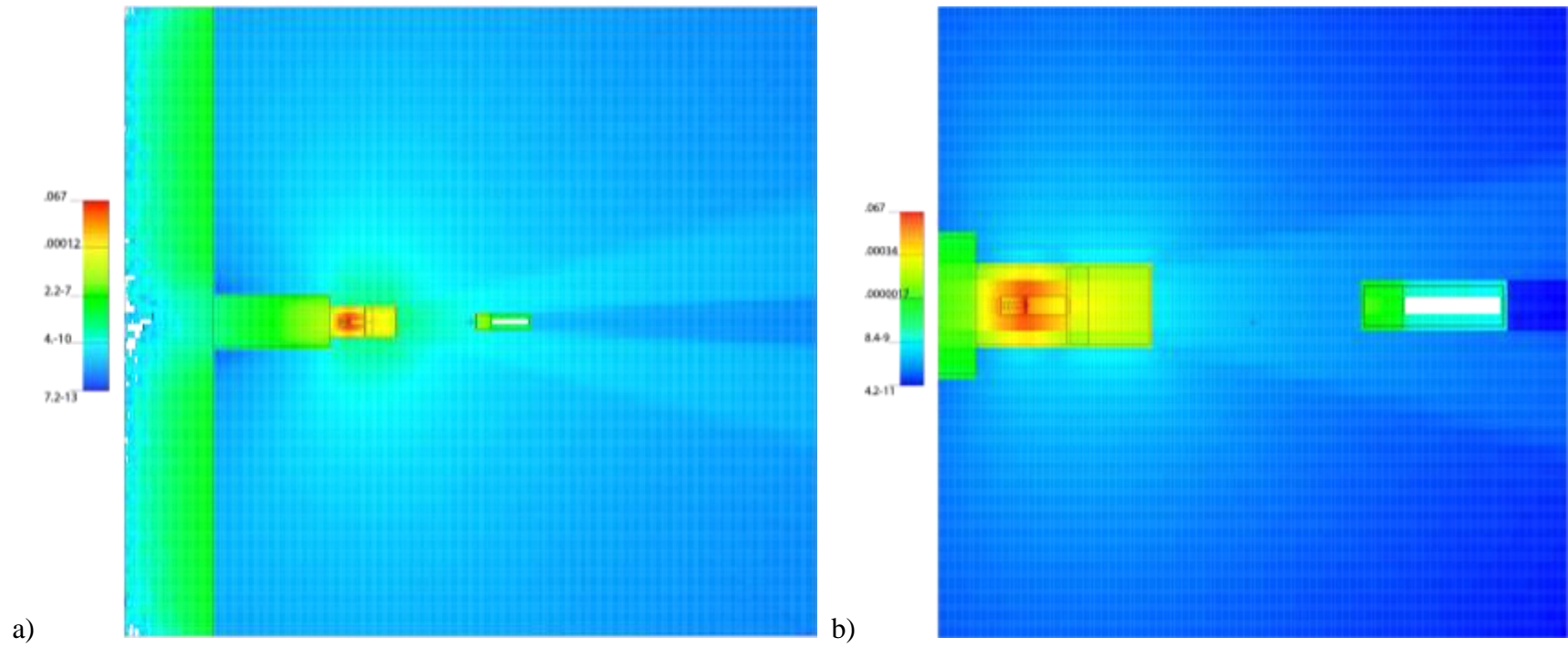


Figure 7-14 a) A modified track length estimator, F4, tally showing the relative interaction rate for photons throughout the geometry. b) A close up of the source, shielding, detector region of the modified track length estimator indicating relative photon interaction rate.

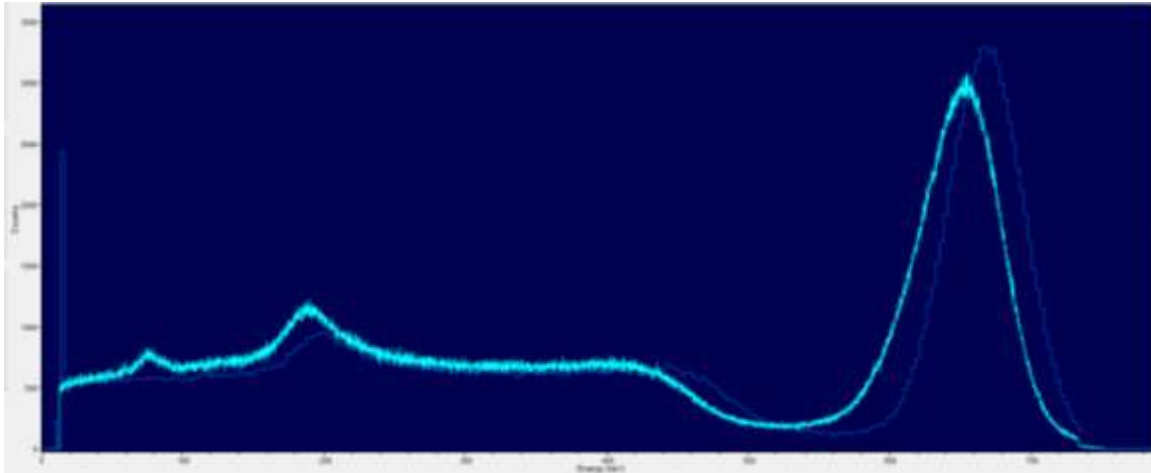


Figure 7-15 Comparison of the experimental and simulated spectra for a no shield configuration of the experiment.

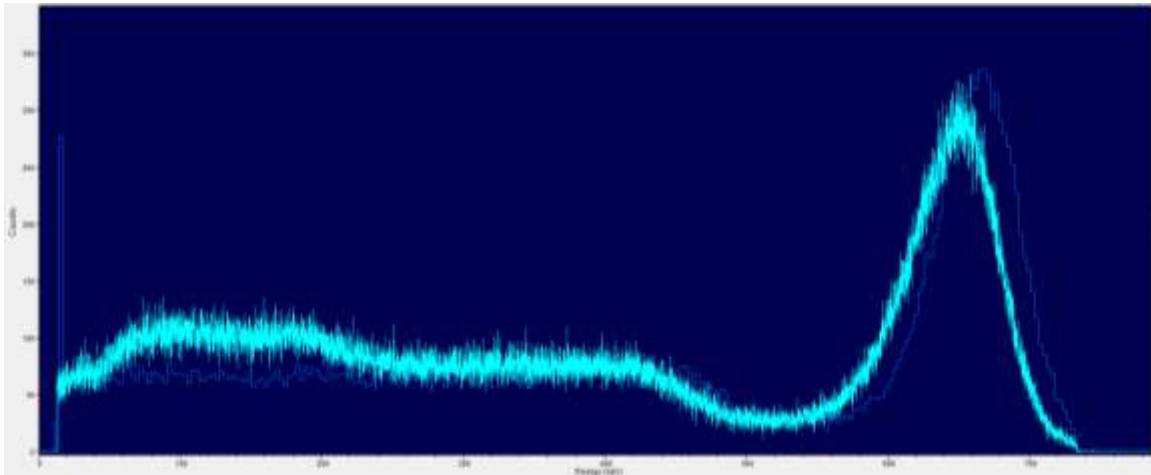


Figure 7-16 Comparison of the experimental and simulated spectra for the SSCBPWC shielded configuration of the experiment.

7.4 Neutron Experiment

Though a criticality accident occurring in the hot cell is nearly negligible, it is still a possibility so neutron experiments are needed to approximate the effectiveness of the shielding materials because the result of a criticality is extremely severe socially, politically, and even possibly physically. This hazard is the lesser hazard when compared to the day to day hazard presented by the presence of gamma-rays. It is still necessary to include this component of the study for proper analysis of the shielding capabilities of the materials, because such an event is possible, however improbable.

7.4.1 Collimator/Storage Drum

The neutron source had an additional aluminum container placed around the manufacturer's lead and stainless steel containment. This container was posing an additional health hazard due to activation of the aluminum. It needed to be removed. Also, the source was being stored in a pit in the floor with no storage drum. A method for housing the source outside of the pit was needed to perform the experiments and to collimate the neutrons into a beam, rather than an isotropic source.

To aid in satisfying all of the needs for the research a drum was designed with a dual purpose for storage and to act as a collimator. A special PVC cradle was created to hold the source as a replacement for the aluminum container.

7.4.1.1 Design

When designing a device that will operate as a collimator and as a storage device it must meet the requirements for both purposes. The design criterion for a collimator is the desired angle of divergence, θ . The design criterion for a storage drum is the regulatory dose rate at a specified distance.

The angle of divergence, θ , is found through trigonometry. Knowing the length and the diameter of the collimator tube allows one to define this angle. Figure 7-17 diagrams how this looks. Equation 7-8 provides the mathematical means for determining the angle.

$$\theta = \tan^{-1} \left(\frac{d}{l} \right)$$

Equation 7-8: Mathematical definition of the angle of divergence with respect to the length and diameter of the collimator tube.

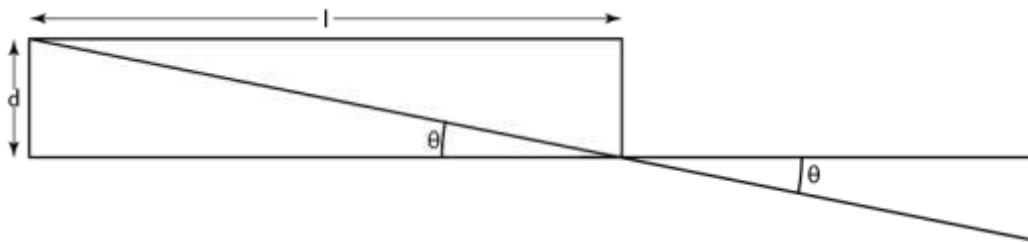


Figure 7-17 Diagram depicting how the angle of divergence of a collimator is determined from the length and diameter of a tube.

For this work the desired angle of divergence needed to be less than 5° . Several l/d combinations were pre-calculated and are tabulated in Table 7–XI.

Table 7–XI: Relationship between length to diameter ratio and divergence angle.

Divergence Angle Relationships				
l/d	5	10	15	20
θ	11.31	5.71	3.81	2.86

Since the Idaho State University Nuclear Reactor Laboratory is a restricted access area containing radioactive material and requiring dosimetry the dose rate limits are not as stringent as if it were being stored in a non-restricted area. The reactor manager desired a dose rate of 2 mrem/hr at 30 cm from the surface of the drum. The contact dose rate for the AmBe source is given as 1.18 mrad/hr neutron and 18 mrad/hr gamma-ray by the manufacturer. To convert this to mrem we assume a quality factor of 3 for the neutrons and 1 for gamma-ray. This gives a dose rate of 3.54 mrem/hr neutron and 18 mrem/hr gamma-ray. The drum contains paraffin wax as the fill having a 25.4 cm minimum pathlength and the drum is steel with a thickness of 0.15 cm. Paraffin wax has a 6.6 cm half value layer for a PoBe neutron spectrum, which is quite similar to the AmBe spectrum, making it a fair assumption. This would reduce the neutron dose rate to about 0.25 mrem/hr. Using point kernel technique, the mass attenuation coefficients (paraffin = 0.197 cm/g, steel = 1.205 cm/g for the primary emitted from ^{241}Am at 59 keV), mass densities (paraffin = 0.92 g/cm³, steel = 8.03 g/cm³), and thicknesses of the paraffin and steel the dose rate

of gamma-rays reduces to about 0.04 mrem/hr. The total dose rate at the surface of the drum would be 0.29 mrem/hr meeting the requirements.

7.4.1.2 Construction

The materials purchased for the making of the collimator/storage drum and the source cradle were a 55 gallon (208.2 l) drum (New Pig, DRM837), 420 pounds (190.5 kg) of paraffin wax (Lone Star Candle Supply, 2281), 2.5 inch (6.35 cm) schedule 40 PVC pipe, 1.5 inch (3.81 cm) schedule 40 PVC pipe, 2.5 inch (6.35 cm) PVC cap, 1.5 inch (3.81 cm) PVC cap, 1.5 inch (3.81 cm) PVC threaded adapter, and 1.5 inch (3.81 cm) PVC threaded plug. Two items were manufactured by Gemstate Machining. These were a 1 inch (2.54 cm) diameter rod made of ultra-high molecular weight (UHMW) polyethylene and a UHMW polyethylene cylinder with an outer diameter snug to the inner diameter of the 2.5 inch (6.35 cm) PVC pipe and an inner diameter snug fit to the 1 inch (2.54 cm) UHMW polyethylene rod. Both the hollow cylinder and the rod were 22 inches (55.88 cm) in length.

Making the collimator began by setting the drum up on three pillars of blocks so it sat over a propane burner used for turkey fryers. The paraffin wax came in 10 pound (4.54 kg) blocks and several were placed in the bottom of the drum to melt. The heat was kept low, but high enough to melt the wax without burning/scorching. The plan included placement of a 10 inch (25.4 cm) long piece of 2.5 inch (6.35 cm) PVC tube in the bottom center of the drum as a stabilizer, but this was not placed as planned. Paraffin was added continually throughout the process to fill the drum. The main tube was cut to a length of 24 inches (60.96 cm) out of 2.5 inch (6.35 cm) PVC pipe. A cap was placed on the bottom end to keep it from filling with wax and it was suspended in the center of the drum with a hoist approximately 25.4 cm above the bottom of the drum. Paraffin wax was continually added until the drum was filled. The main tube was counter-weighted to prevent

buoyant floating. Additional weights were placed upon rods to hold the tube against floating. A 0.5 inch (1.27 cm) spacer was placed between the tube and the rods to allow for some space above the tube for the lid. Once the drum was filled with meted wax the heat was removed. A blanket was placed around the drum to slow the cooling process in an effort to minimize the contraction of wax as it cooled. Additional wax was melted and poured onto the top to fill in where the wax had contracted. Figure 7-18 is a diagram of the collimator. The color scheme is as follows: yellow = paraffin wax, light blue = PVC, orange = UHMW, grey = air, maroon = concrete, green = lead, blue = stainless steel, and purple = AmBe.

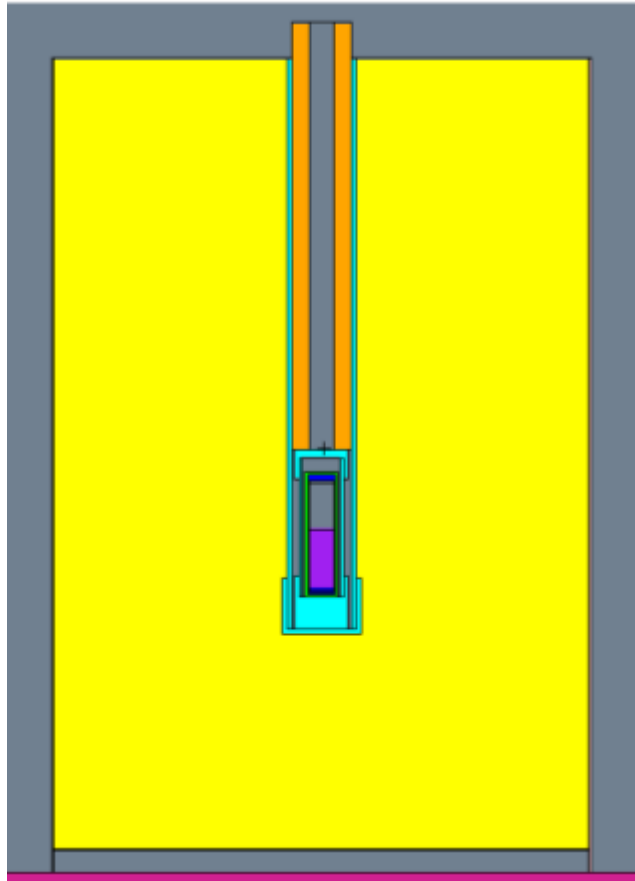


Figure 7-18: MCNP depiction of the collimator and source capsule containing the AmBe source.



Figure 7-19 The full drum while cooling with rods above for additional weighting.



Figure 7-20 Drum during cooling with weights and spacer to press the tube low enough for the lid.

After the drum was completed it was transported to the Nuclear Reactor Laboratory at Idaho State University, see Figure 7-21.

The replacement capsule to hold the source was made of PVC components. A 5 3/8 inch (13.6525 cm) piece of 1.5 inch (3.81 cm) PVC pipe was cut as the body of the capsule. A cap was sealed to one end of the pipe and a 1/4-20 tap hole was placed in the center of the cap. A coupler with an inner thread was placed on the opposite end of the pipe. A threaded plug was used to close the capsule. The choice to add the threaded plug was made to allow for easy removal of the source from the capsule for inspection, or other, purposes.



Figure 7-21 Transportation of the drum, approximately 500 pounds, to the university using an engine hoist.

7.4.2 The Equipment

Only three detector components differed between the gamma-ray and neutrons experiments. These were the detector, preamplifier, and the high voltage power supply. These three components are listed in Table 7–XII. The settings were altered on the equipment to be appropriate for the collection of signal produced by the ^3He detector.

The instrument settings were determined to be as follows:

1. High Voltage, 1000 V.
2. Spectroscopy Amplifier
 - a. Course Gain, 20.
 - b. Fine Gain, 10.0 (0.5 – 1.5 scale).
 - c. Shaping Time, 2 μ s
3. Multi-channel Buffer
 - a. Gate, off.
 - b. Conversion gain, 8192.

Table 7–XII: Neutron Experimental equipment list.

Make	Model	Serial	Date/Notes
Source Information			
Monsanto Research Corporation		MRC-N-SS-W-AmBe-262	25 Aug 1965
Detector Information			
Reuter Stokes He-3	RS-P4-0812-217	14K01RPL M6011	
EG&G Ortec Preamplifier	142 PC	Z498	Rev. 17
NIM and MCA Information			
Ortec NIM Bin	4001/4002D	10323645	Rev. A
Ortec 160W NIM Power Supply	4002D	10309513	Rev. Y
Ortec Single Channel Analyzer (SCA)	550A	816	
Ortec Spectroscopy Amplifier	672	0808897	Rev. U
EG&G Ortec Timer/Counter	871	453	Rev. 07
Otec High Voltage Power Supply	556	14328185	Rev. R
Amtek Ortec MCA	Easy-MCA-8k	10243286	Rev. D
Tektronix Oscilloscope	TDS 3032B	B012822	
Dell w/ Windows 7			

An image of the set-up and a depiction of the set-up are shared in Figure 7-22.

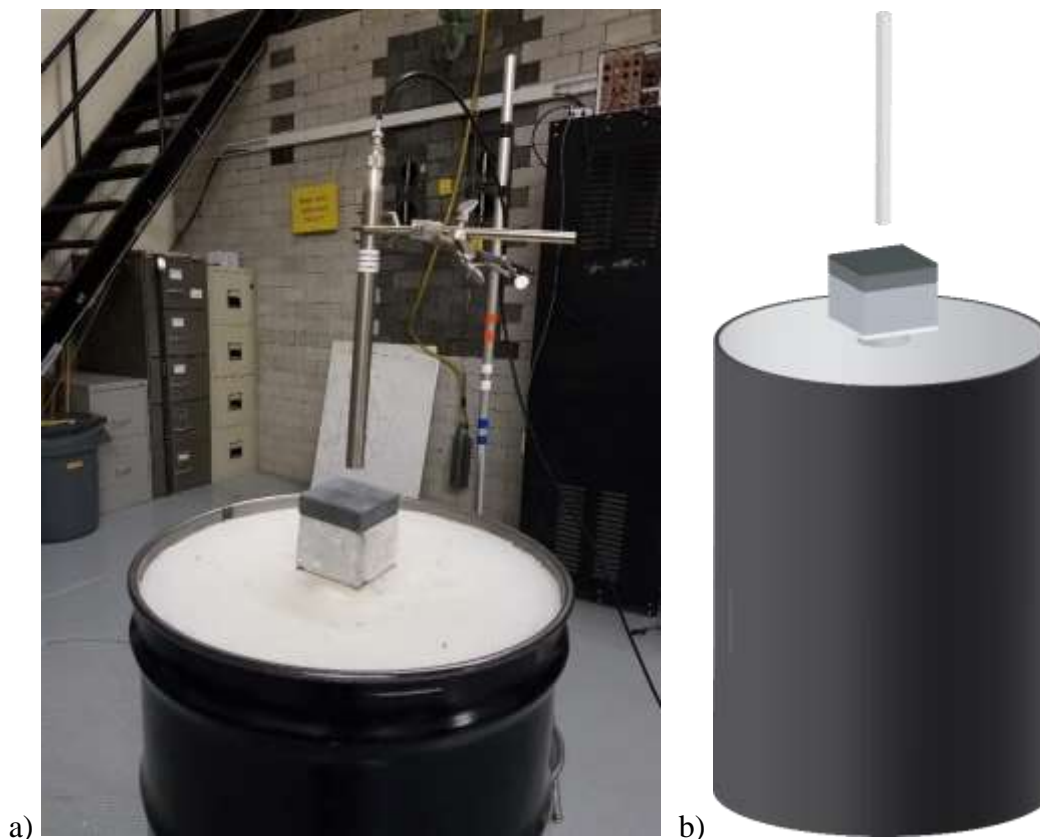
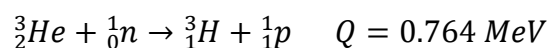


Figure 7-22 a) Photograph of the set-up with shielding in place. b) Depiction of the set-up with shielding in place.

7.4.2.1 Counting System Checks

Because most of the components are the same, a more simplified test of the system was made. This test included the creation of a spectrum using the SCA to show the full energy peak and wall effects of the $^3\text{He} + n$ reaction, as noted in Equation 7-9. The wall effects occur at 191 keV and 573 keV for the triton and proton, respectively. The full energy peak occurs at 764 keV, the sum of the energy from the two particles.



Equation 7-9: ^3He -neutron reaction.

The SCA lower level setting was started at 250 mV with a window of 250 mV. Counts were taken for 1 minute on the counter/timer. The amplifier settings were the same as listed above. The

spectrum created by this method is shown in Figure 7-23 Counting system spectrum generated by SCA windows of 250 mV width..

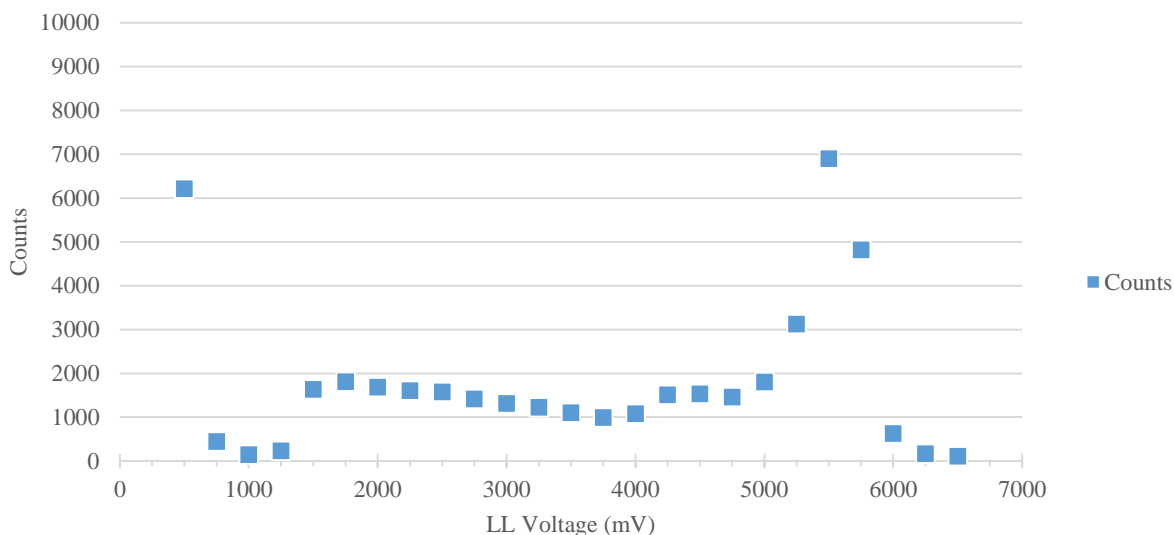


Figure 7-23 Counting system spectrum generated by SCA windows of 250 mV width.

As seen in the generated spectrum, two wall edges and a full energy peak exist. The first wall effect falls between 1250 and 1500 mV and the second between 4000 and 4250 mV and the full energy peak at 5500 mV. This gives a 0.135 keV/mV ratio. This would correspond to a wall edges of 189 keV at 1400 mV and 573 keV at 4250 mV.

7.4.3 Results

Signal pulses are generated by the reaction of ^3He and neutrons as described earlier in Equation 7-9. The induced pulse created by the motion of the ions and electrons to their respective electrode in the detector. The preamplifier shapes the pulse and the spectroscopy amplifier multiplies the signal for counting. The signal was split to both an MCA and SCA. The MCA was set to bin the pulses into 8192 bins with a lower limit (cut off) set to channel 1200 (130 keV). The SCA lower limit was set to 1.2 mV without an upper limit. Count times were set to 20 minutes. Both sets of data are reported in Table 7–XIII: Neutron data., but the MCA data is considered more accurate,

precise, and reliable and will be used in the final analysis. The MCA is considered more accurate, precise and reliable because several human errors are removed by integrating operations and functions into the MCA. For example, digital settings for pulse height windows on the MCA is more accurate than using the human eye to set them on the SCA.

As a reminder, the following abbreviations for shielding materials will be used throughout the experimental and simulation reports: SS = stainless steel (0.3175 cm nominal thickness), BP = borated polyethylene (2.54 cm nominal thickness), C = concrete (7.62 cm nominal thickness), WC = tungsten carbide (0.3175 cm nominal thickness).

Table 7–XIII: Neutron data.

Shielding Setup	Counter Timer total counts	Counter Timer counts/second	MCA total counts	MCA counts/second
No shielding	458220	382	455057	379
SS	445699	371	442650	369
BP	414565	345	412501	344
C	408513	340	406734	339
WC	446631	372	443831	370
SSBPCWC	392799	327	391625	326
SSBPWCC	395852	330	394717	329
SSCBPWC	396662	331	395542	330
SSCWCBP	388092	323	386973	322
SSWCBPC	395696	330	394486	329
SSWCCBP	387111	323	386007	322

A typical spectrum collected by the set-up is presented in Figure 7-24.

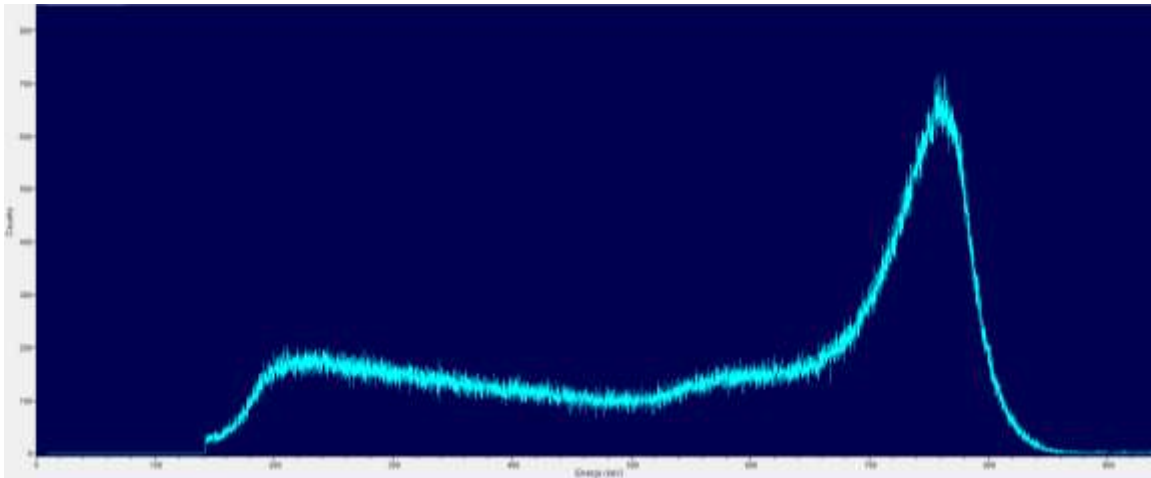


Figure 7-24 Spectrum of the neutron experiment with shielding configuration of SSCBPWC. It is representative of the shielded configurations.

7.4.4 Error Analysis

Similar to the gamma-ray experiments, an error analysis was performed on various aspects of the experiment. There are several more errors considered for the neutron experiments as compared to the gamma-ray experiments. These include source strength, source composition, source to detector distance, axial alignment of detector, and detector composition. Relative errors for these were either assumed, calculated or found through simulations. These errors are tabulated in Table 7–XIV.

The first error listed in Table 7–XIV is the statistical error due to the counting system. This error is always accounted for when using counting systems. It accounts for the Gaussian nature of radioactive material decay and counting.

The error in modern source strength is often quoted as $\pm 15\%$. Since there is no statement on the source certificate regarding the possible error in source strength, an assumption of $\pm 18\%$ is made. The addition to the error over modern sources is a valid assumption, and conservative, considering manufacturing practices and regulations from 1965 compared to today. An effort was made to learn more about the source from the manufacturer. The manufacturer was restructured

and sold several times since the source was made and no additional documentation exists, beyond the source certificate, on the practice of the company and how these sources were made at that time.

The exact distance between the source and detector is unknown but was estimated by measuring the distance from the top of the source capsule to the bottom of the detector and assuming the remaining distance from the top of the source capsule to the source material based upon calculations of the source material volume within the source capsule. There are two components to this error. One comes from the error in measurement by ruler. The second comes from actual position of the source material relative to the detector position. The first, error in ruler measurement, was calculated to be $\pm 0.03\%$. The second was simulated using the final geometry to find the error based upon uncertainty in the exact location of the source material. It simulation allowed for a discrepancy of ± 2.5 cm in the placement of the source material. This lent to an error of $\pm 2.995\%$ from the expected location.

The source composition is somewhat in question because the source certificate states, “Am = 14.0 g”. Is this the mass of americium in the americium oxide or is it the mass of americium oxide (the common material used to make these types of sources at the time it was made)? Likewise, the mass of the beryllium is stated as “Be = 57.6 g”. Is this the mass of Be in BeO or the mass of BeO (as with the Am, the beryllium is an oxide)? Simulations were performed to determine the magnitude of error caused by these uncertainties in mass measurements. The error was found to be $\pm 0.856\%$.

Alignment of the detector over the collimator was performed visually from two positions 90° apart. It is possible the detector was not exactly aligned centered over the collimator. Some variation of axial offset may exist and is assumed to be no more than 0.5 inch (1.27 cm) off-center

because of the two-position visual alignment. Simulations were conducted at 0.25 inch (0.635 cm) and 0.5 inch (1.27 cm) off axis to determine the relative error from the expected value. The error was determined to be $\pm 0.845\%$.

The detector consists of two gasses, ^3He and CO_2 . The exact composition of CO_2 is proprietary and is not known, though the manufacturer stated it is “less than 2% of the mixture”. The standard, or actual, concentration is assumed to be 2% CO_2 for all simulations. However, since this may not be true simulations varying the weight percent of CO_2 (2.0%, 1.5%, 1.0%, and 0.5%) were performed to determine the effect of the composition changes. It is assumed the minimum concentration would be 1% which would afford an error of $\pm 13.615\%$.

Solving for the experimental errors shows that neutron experiments have significant uncertainties in the detector responses obtained. Some of the uncertainties are relatively negligible and could be eliminated from consideration but others have appreciable magnitude and must be maintained, such as the error in the source strength, source location, and detector composition. All errors discussed were kept in the calculation of the total experimental error for this work.

Table 7–XIV: Experimental relative error analysis for neutron experiments.

Shielding setup	$\pm\sigma_i$ MCA (counts)	$\pm\sigma_i$ MCA (cps)	MCA error (%)	Source strength error (%)	Source to detector distance error (%)	Source material location error (%)	Source composition error (%)
No shield	677	0.56	0.1482	18	0.03209	2.995	0.856
SS	668	0.55	0.1503	18	0.03209	2.995	0.856
BP	644	0.54	0.1557	18	0.03209	2.995	0.856
C	639	0.53	0.1568	18	0.03209	2.995	0.856
WC	668	0.56	0.1501	18	0.03209	2.995	0.856
SSBPCWC	627	0.52	0.1598	18	0.03209	2.995	0.856
SSBPWCC	629	0.52	0.1592	18	0.03209	2.995	0.856
SSCBPWC	630	0.52	0.1590	18	0.03209	2.995	0.856
SSCWCBP	623	0.52	0.1608	18	0.03209	2.995	0.856
SSWCBPC	629	0.52	0.1592	18	0.03209	2.995	0.856
SSWCCBP	622	0.52	0.1610	18	0.03209	2.995	0.856

Shielding setup	Detector axial alignment error (%)	Detector composition error (%)	Experimental cps ($\pm\sigma_{\text{tot}}$ %)
No shield	0.845	13.615	379 (22.8)
SS	0.845	13.615	369 (22.8)
BP	0.845	13.615	344 (22.8)
C	0.845	13.615	339 (22.8)
WC	0.845	13.615	370 (22.8)
SSBPCWC	0.845	13.615	326 (22.8)
SSBPWCC	0.845	13.615	329 (22.8)
SSCBPWC	0.845	13.615	330 (22.8)
SSCWCBP	0.845	13.615	322 (22.8)
SSWCBPC	0.845	13.615	329 (22.8)
SSWCCBP	0.845	13.615	322 (22.8)

7.5 Neutron Simulation

When starting the neutron simulations there was great hope that the lessons learned during the gamma-ray simulations would make the problem easier. There is some truth to this but there is much false with it as well. The truth comes in that the processes needed to refine the model with each iteration for improvement are similar. The falsehood is that quick convergence of accuracy will occur.

During the gamma-ray simulations initial work on the neutron simulations began. The first simulation to be tested was the unshielded setup. This setup was a simple source and detector placed in an atmosphere with no floor, walls, etc. added. The source geometry and collimator were quite detailed in this original setup with the source material filling the bottom half of the source container (light pink). The detector was a simple cylinder of pure ^3He , see Figure 7-25. The source was modeled in an older version of an open top cradle.

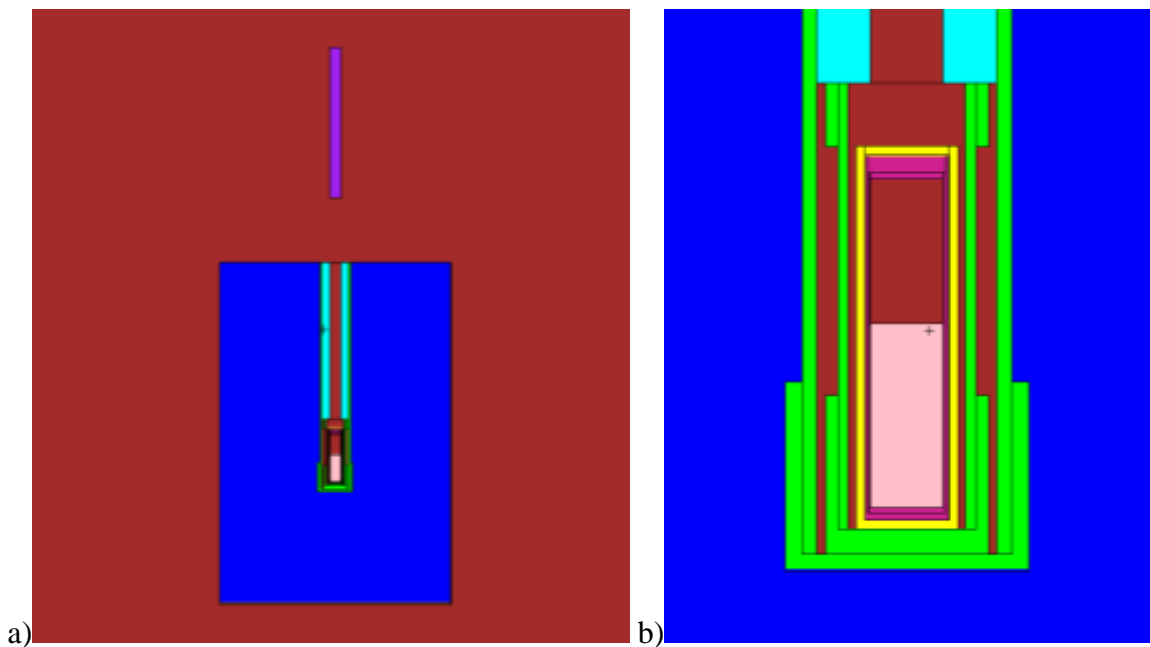


Figure 7-25 a) Depicts the source in the drum and the detector above in an air atmosphere. b) Shows a close up of the source to provide a view of the detail.

After running this first iteration of the unshielded setup it looked promising. The C/E ratio was approximately 1.0 as was desired. This lent to a confidence in the design that would be dispelled upon running the shielded versions where C/E ratios obtained were on the order of 0.45. Modifications to the input file were needed to improve the shielded C/E.

When considering modifications to the input file, lessons learned from the gamma-ray simulations afforded a wealth of help. The areas to focus were already defined as tally modification and selection, atom density improvements, and geometry refinements. When modifying atom densities, the main focus is three-fold, source, shielding, and detector. The geometry could lead anywhere from addition to more detail in the room to refining details of the collimator, etc.

7.5.1 Tally Selection

Knowledge that a ^3He detector is a proportional counter and can be operated as a pulse height detector aided in the selection of a pulse height, F8 tally. This F8 was quickly modeled after the gamma-ray experiments where the E card was used to create energy bins for obtaining spectra and an FT card was used, having the GEB and PHL cards to modify the pulse height data collection for a more realistic spectrum and counts result.

It was not clear how to obtain GEB values for a neutron detector since it is not readily known how to collect multiple full energy peaks of differing energy. The GEB values were obtained from an input file provided by another MCNP user on the MCNP Forum. The values provided afford an appropriate energy broadening when comparing experimental to simulated spectra, see Figure 7-26.

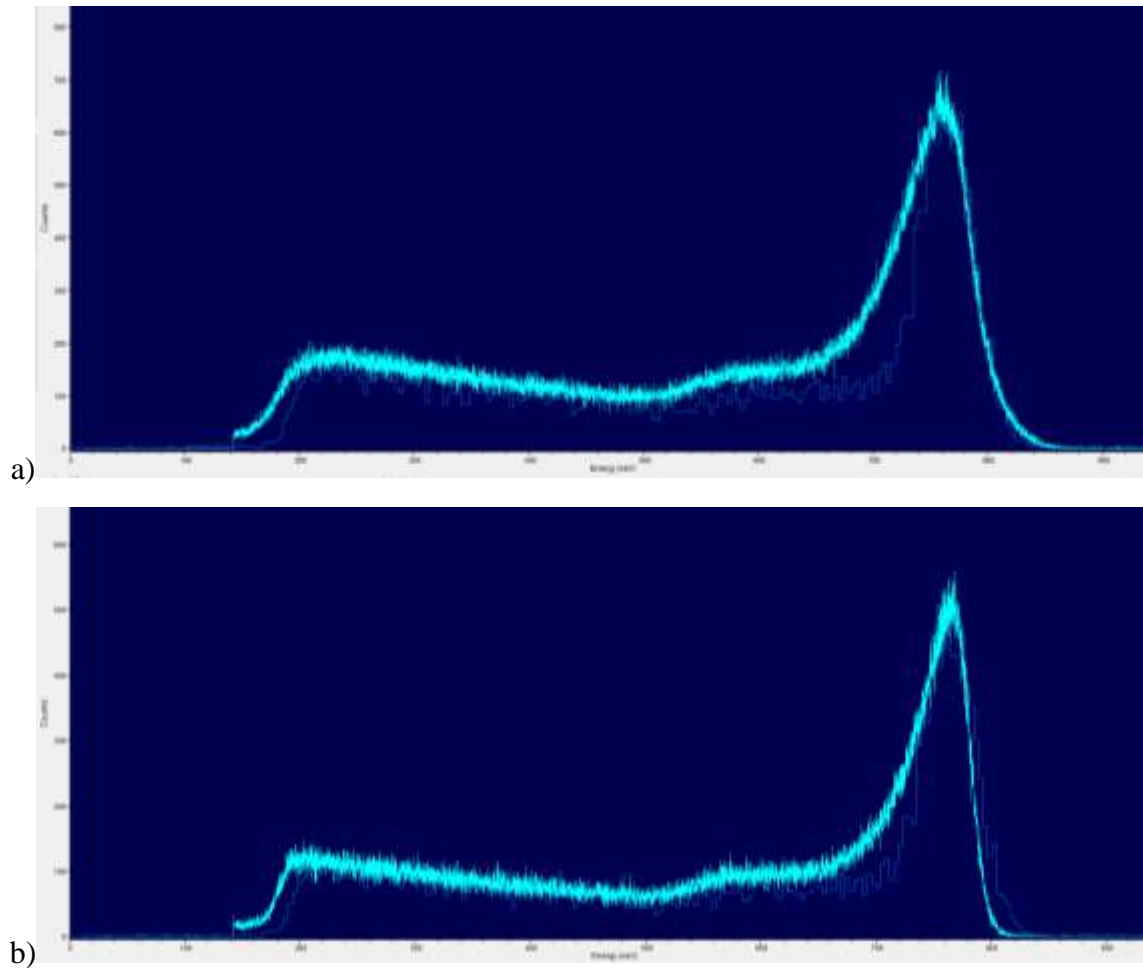


Figure 7-26 a) Comparison of experimental and simulated neutron/³He reaction spectrum for the unshielded setup and b) the SSCBPWC shielded setup.

The PHL card was slightly different from the PHL card used in the gamma-ray simulations. In the gamma-ray simulations only one additional particle was considered, electrons, since that is the only secondary particle generated. In a neutron-³He reaction there are two secondary particles of concern, proton and recoil ³H (triton) nucleus. Both need to be accounted for on the PHL card to properly represent the energy deposition into the ³He gas. Adding the proton and triton also requires the addition of PHYS cards for both, as well as making changes to the neutron physics by adding a PHYS:n card. The neutron physics are modified by turning on the Neutron Capture Ion Algorithm (NCIA). This algorithm makes more detailed analysis of the charged particles providing the correct energy distribution and correlated angular distribution. Without NCIA the secondary

particles are treated with standard physics model which may not provide the correct energy and angular distributions [52]. The final F8 tally looks something like:

```
F8:n cell #  
E8 0 1e-5 0.01 255I 1.0 2.0 10  
FT8 GEB a b c &  
PHL 2 6 1 16 1 HE3-1  
F6:h cell#  
F16:t cell #
```

where the GEB values are $a = 0.0$, $b = 0.06$, and $c = 0.0$.

A second tally was also considered for the detector region, a modified track length estimator, F4 with FM and SD cards. This was also made similarly to the F4/FM/SD tally of the gamma-ray simulation. The primary difference is the reaction number used on the FM card. For neutron reactions with ^3He reaction number 103, or the combination of 103:104, is used. Reaction number 103 is the proton recoil reaction and 104 is the triton recoil reaction. Each F4 tally with either 103 or 103:104 gives an answer statistically the same as the F8 tally described above. The tally form is:

```
F4:n cell#  
FM4 -1 (material number) (reaction number)  
SD4 1
```

As work progressed there seemed to be a bias in the results being provided by MCNP. In an effort to understand the bias in the results, additional tallies were used to learn more about how the neutrons were being transported throughout the geometry. It was believed neutrons were being scattered by the shielding material and return scatter from concrete structures was making a large contribution. Surface tallies, F2, were placed on the surfaces of the shielding material block and the surfaces of the detector with energy and cosine bins to understand the energy distribution/contribution and direction of travel of neutrons. The tallies on the detector surface

provided results as expected, that most of the neutrons entering the detector come from the flat surface closest to the source. The second highest contribution was from the cylindrical part of the cylinder. It also showed that higher energy neutrons tended to enter and leave the detector, while low energy neutrons tended to enter and contribute to the tally by interacting and not leaving the detector.

The last set of tallies used were mesh tallies similar to those used in the gamma-ray simulations. The mesh tally was used as both a track length estimator, fmesh4 and as the reaction rate estimator, the modified fmesh4 with and FM card. Images of the track length estimation mesh tally is shown in Figure 7-27 and the modified track length estimator for reaction rates is shown in Figure 7-28. The track length estimator mesh tally was written as:

```
FMESH4:n GEOM=xyz ORIGIN=-381 -281.94 -40
    IMESH 533.4 IINTS 1
    JMESH 632.46 JINTS 500
    KMESH 716.28 KINTS 500
```

and the modified track length estimator for reaction rate was written as:

```
FMESH14:n GEOM=xyz ORIGIN=-381 -281.94 -40
    IMESH 533.4 IINTS 1
    JMESH 632.46 JINTS 500
    KMESH 716.28 KINTS 500
FM14 -1 0 103
```

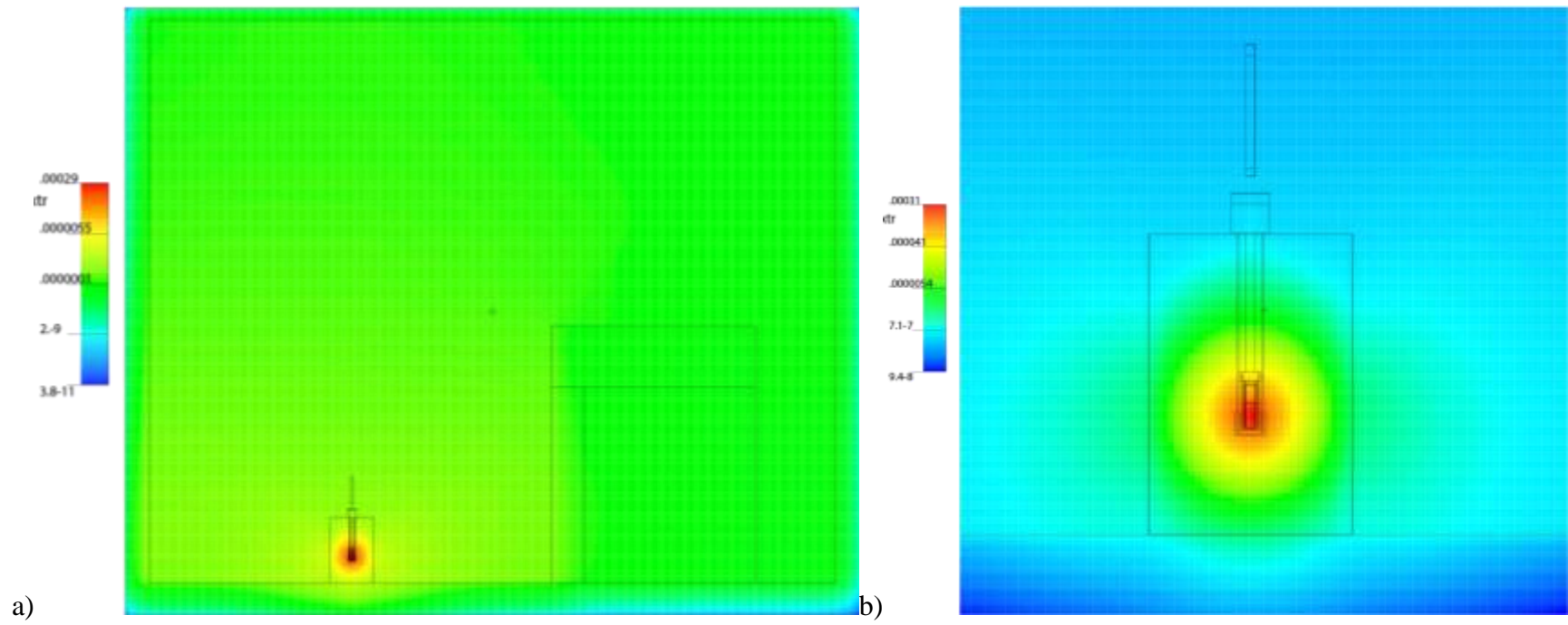


Figure 7-27 a) Track length estimator neutron tally for the whole geometry. b) zoom of the source and detector.

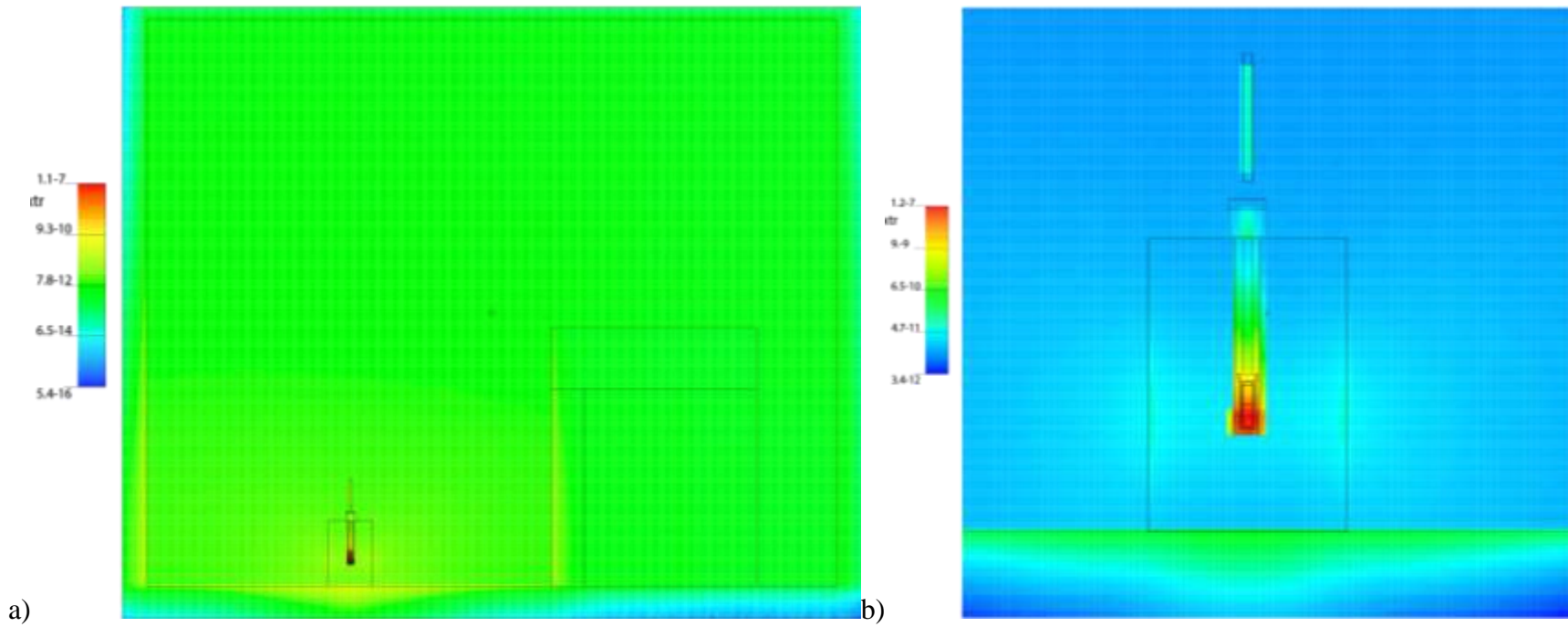


Figure 7-28 a) Modified track length estimator for neutron tally showing reaction rate for proton recoil across the whole geometry and b) zoom to the area around the source and detector.

7.5.2 Atom Densities

Atom densities went through several iterations for both improvement and error analysis of the problem. The three components of the problem considered the most important to atom density corrections were shielding materials, source material, and detector fill gas. Each of these is discussed in detail as to how changes were made for improvement and why alterations were made for error analysis.

The original atom densities used also relied heavily upon the option of built in natural abundances. When using this form not all of the most current cross sections were being called from the evaluated neutron data files (ENDF) (such as .50c and .70c instead of .80c). Once it was noticed various cross section versions were being used, atom densities were recalculated accounting for isotopic abundances using the Chart of the Nuclides [53] to assist in determining the abundances. This alteration made all of the cross sections come from the same set (.80c) in ENDF. This change was made in conjunction with a major geometric change and the effect of this individual change is unknown. However, the overall change in the results, caused by the geometry and atom density modification, was significant and will be discussed with the geometry alterations in Section 7.5.3.

7.5.2.1 *Shielding Materials*

Changes to the atom densities for shielding materials was solely for the improvement in data comparison to experimental. The original atom densities for the stainless steel (SS), borated polyethylene (BP), and tungsten carbide (WC) were based upon manufacturer specification sheets and for the concrete (C) it was based upon regular concrete in the PNNL compendium [46]. After further investigation with each manufacturer additional, low weight percent elements were added to the mix for SS, BP, and WC. All four materials had a further modification when the actual volume and mass of each block being used was measured to obtain the mass density. This new

mass density for each material was used in the atom density calculation to provide better results. The change to the atom density because of measured mass density was accompanied by slight changes to the geometry in shield block thicknesses. These changes made notable improvements to the simulation compared to the experimental by several percent change to the C/E ratio.

7.5.2.2 *Source Material*

The source certificate indicates the materials used were americium (Am) and beryllium (Be). It was assumed this meant the two masses indicated were the amount of metal blended together to create an alloy with a mass density near 7 g/cm^3 for the first round of input files. Investigation into the manufacturing process of AmBe sources revealed this was a poor assumption. These types of sources, especially when manufactured in the 1960s, was a mix of oxide powders. The manufacturer would measure out an amount of AmO_2 powder and an amount of BeO powder. These powders would be mixed and then pressed into a stainless steel capsule. There is no indication in the process whether the mass measured is the mass of the Am and Be component or the mass of AmO_2 powder and BeO powder. It would seem logical to assume it was the mass of powder. However, if it is the mass of Am in AmO_2 then the activity is closer to the stated activity based upon the specific activity of Am. No further information about the source is available because the manufacturer does not exist and no records are available from daughter entities. This uncertainty in the source composition required an iterative comparative study of changes to the atom densities based upon changes in the AmBe composition and mass densities of the source. The reasonable assumptions regarding the source are that the mass is either the mass of Am in the oxide or the mass of the oxide powder. The difference in these measurements lends to a difference of 2 g of Am or a 0.856% difference in the counts per second produced in simulations.

7.5.2.3 Detector Gas

The initial assumption was that the helium in the tube was pure ^3He and that the gas was 100% ^3He . The first part of this assumption was maintained throughout the simulations. The second part of the assumption was brought into question when an input file from an MCNP Forum user indicated a mix of helium and carbon dioxide (CO_2). The manufacturer of the ^3He detector was contacted to learn what the CO_2 content was in the detector. It was learned that the content of the CO_2 was less than 2 weight percent of the total gas and that the exact concentration is proprietary. Without knowing the exact concentration there is a fair amount of uncertainty in the possible measurements. This is because ^3He is very sensitive to neutron interaction. A change of 1% in the CO_2 concentration could significantly impact the detection of neutrons and also the answer given in simulations. Various concentrations of CO_2 content, from 0% - 2% in 0.5% increments, were simulated to determine the effect. The further from the expected CO_2 concentration the greater the variance as the concentration is decreased. If it is assumed that 2% is the given standard and comparison of lesser concentrations are made to this simulated value, then you obtain the data in Table 7–XV. The relative error caused by the concentration being at 1% instead of 2% was used in error estimations but 2% was used in all other calculations. When the CO_2 concentration is decreased the ^3He is increased because the total pressure remains constant. Because of this increase in ^3He one sees an increase in the tally because there are more ^3He atoms/vol to interact with.

Table 7–XV: Comparison of CO_2 concentration on the variance in the expected value.

CO_2 Concentration in Weight Percent	% Error from the Expected Value
2.0% (Expected)	0.00
1.5%	6.40
1.0%	13.62
0.5%	21.66

7.5.3 Geometry Refinements

The geometry was altered over time primarily to improve the C/E ratio between the simulations and the experiments. Geometry modifications occurred in three main iterations, the addition of floors, walls, and ceiling, the addition of inactive regions to the detector, and refinements to the drum/collimator to better match manufactured and measured values, which did not always agree for the drum. Each iteration afforded improvements to the C/E ratio.

7.5.3.1 Addition of Walls

The thought to add more to the geometry regarding structures in the room was the first to occur. This came from the understanding that neutrons scatter off of concrete and there were a lot of concrete surfaces in the room used for experiments. The first alteration was to add a 40 cm thick floor below the drum. This had a noticeable effect on the values causing a rise in both the unshielded and shielded setups. An interesting aspect of the addition of the floor was the addition closed the gap between the two setups. For example, the C/E for the unshielded raised from 1 to 1.15 and the shielded raised from 0.45 to 0.65.

The next step was to add walls and ceiling. This too raised the C/E of each and closed the gap a little more. The final addition was the concrete walls surrounding the AGN-201 nuclear reactor in the laboratory. These walls are slightly closer than any other walls. When all of the room structure was added to the geometry, the gap between unshielded and shielded setups was gone. However, the bias was large with a C/E ratio of approximately 1.7 for both setups.

Curiosity arose from this apparent closing of the gap between unshielded and shielded C/E results. Additional information was needed to help explain what was occurring. The addition of surface tallies with energy and cosine bins were added to two regions in the geometry to help provide the desired information, most of which was discussed in Section 7.5.1 Tally Selection.

These tallies provided insight into the scattering effects of the added walls, floor, and ceiling. It also increased confidence in the relative model because they showed what was expected, after considering the magnitude of neutron scattering occurring.

This bias spurred thought of what else may need to be considered for improvement. Two more thoughts came to mind regarding the geometry, the source position and perfecting the detector geometry. The source material does not fill the whole volume of the cavity in which it is placed. The question of orientation came to mind and the source was retrieved to inspect its orientation. The assumed orientation was opposite of what was real. A quick modification of the source location reduced the C/E from 1.7 to about 1.55.

7.5.3.2 *Detector Inactive Regions*

The second thought after addition of the floor, walls, and ceiling was detector geometry. Altering the detector geometry was a two-fold effort. The first was to bring C/E closer to unity while the other was an addition to the error analysis. The effort to bring the C/E closer to unity was the addition of inactive regions to the detector. The effort of adding to the error analysis was associated with axial alignment of the detector with respect to the collimator axis and was discussed earlier in Section 7.4.4.

The detector was originally designed as a cylinder of gas surrounded by a stainless steel can. The length and diameter were that of the physical dimensions of the real detector. Upon inspection of the design specifications for the detector, seen in Section 15.2, and after some assistance from the MCNP Forum, inactive regions were added to the two ends of the detector length, keeping the total length the same as the real detector, see Figure 7-29 a). Adding the inactive regions also corrected the active region length. The inactive regions were modeled as vacuum. Addition of the

inactive regions and correction of the active region length brought the C/E of each setup to approximately 1.5 – 1.55.

7.5.3.3 Drum/Collimator Refinements

Having a bias in the C/E ratio, being about 1.5, and not having experimental and simulation results within statistical error of each other is somewhat disconcerting to an experimenter. One last thought process raised doubt in the modeling of the drum/collimator dimensions. Another round of measurements made to the various components of the drum and collimator found several of the measurements were off slightly. The drum measurements were originally taken from the drum description as opposed to actual measurement of the drum. It was found the diameter and height were both not true to the description. Also, the length of the 2.5” PVC collimator tube was too short in the model. The cradle was still being modeled after the original open-topped design rather than the enclosed design having a screw cap for access to the source. The actual position of the source with respect to the floor was approximately the same, but there is an additional 5 cm of wax above the source. The collimator is slightly longer than previously modeled. All of these changes, including the air space beneath the drum due to a rim of metal at the bottom of the drum, were made to the model, see Figure 7-29 b). The C/E ratio for the unshielded setup returned to approximately unity and the shielded setups were approximately 1.17, see Table 7–XVI. This alteration also brought the experimental and simulation results within statistical error of each other.

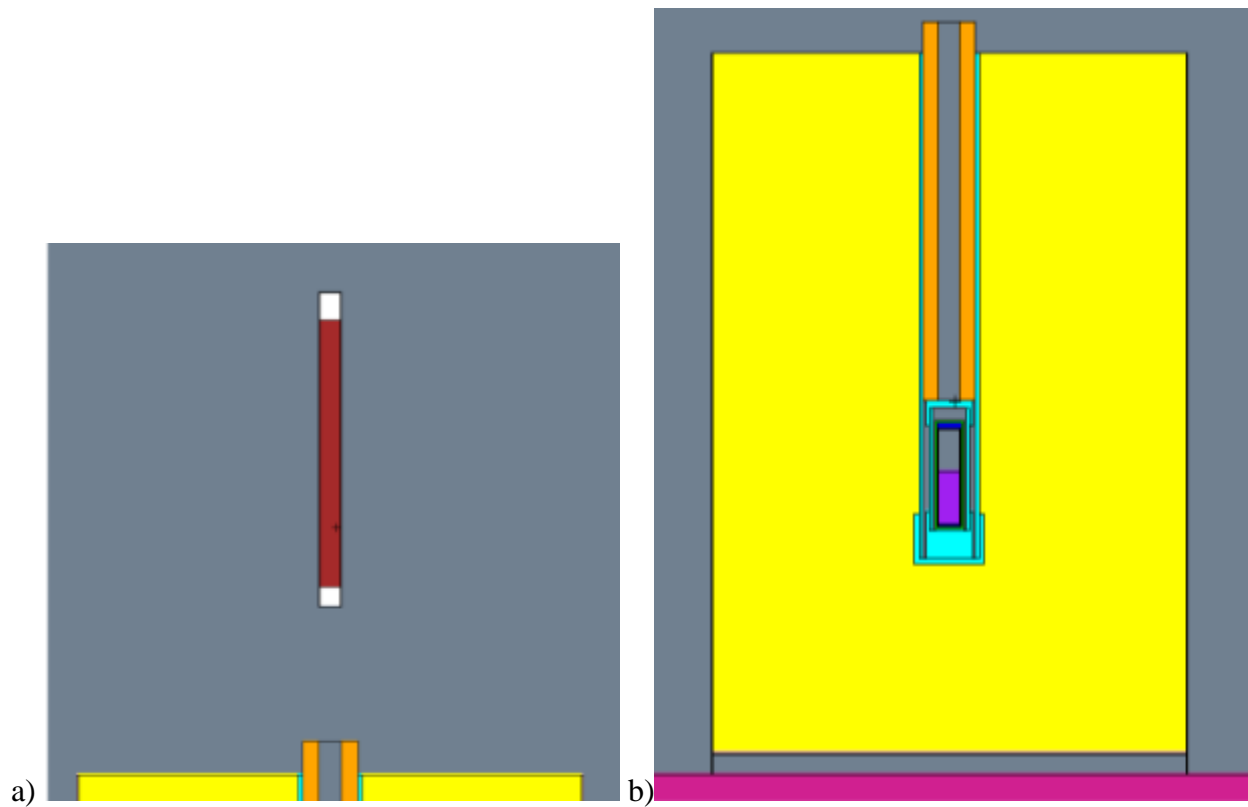


Figure 7-29 a) MCNP plotter depiction of the final ^3He detector geometry. b) Depiction of the final drum/collimator geometry.

7.5.4 Simulation Results with Comparison to Experimental

After much effort in refining the input files to match reality, the simulations results were much improved. A plot showing the comparison of experimental data for the unshielded and shielded setups, with experimental errors, to simulated results for the same setups is shared in Figure 7-30. The plot shows that statistically the simulations are consistent with experimental data.

It is noted that the order of materials seems to make some difference in the effectiveness of the shield. This was also shown in the gamma-ray experiments, though the material order for most effective is different for the two cases. For neutrons the order shows preference of having borated polyethylene as the furthest material from the source, while gamma-rays prefer having tungsten carbide furthest from the source.

Table 7–XVI: Counts per second calculated from MCNP F4 tally data and computed to experimental ratios.

Shielding Setup	Counts per Second	$\pm\sigma$ of CPS	C/E
No shielding	386.0	86.4	1.018
SSBPCWC	378.9	74.4	1.161
SSBPWCC	381.1	75.0	1.159
SSCBPWC	377.9	75.2	1.147
SSCWCBP	377.6	73.5	1.171
SSWCBPC	381.6	75.0	1.161
SSWCCBP	377.3	73.3	1.173

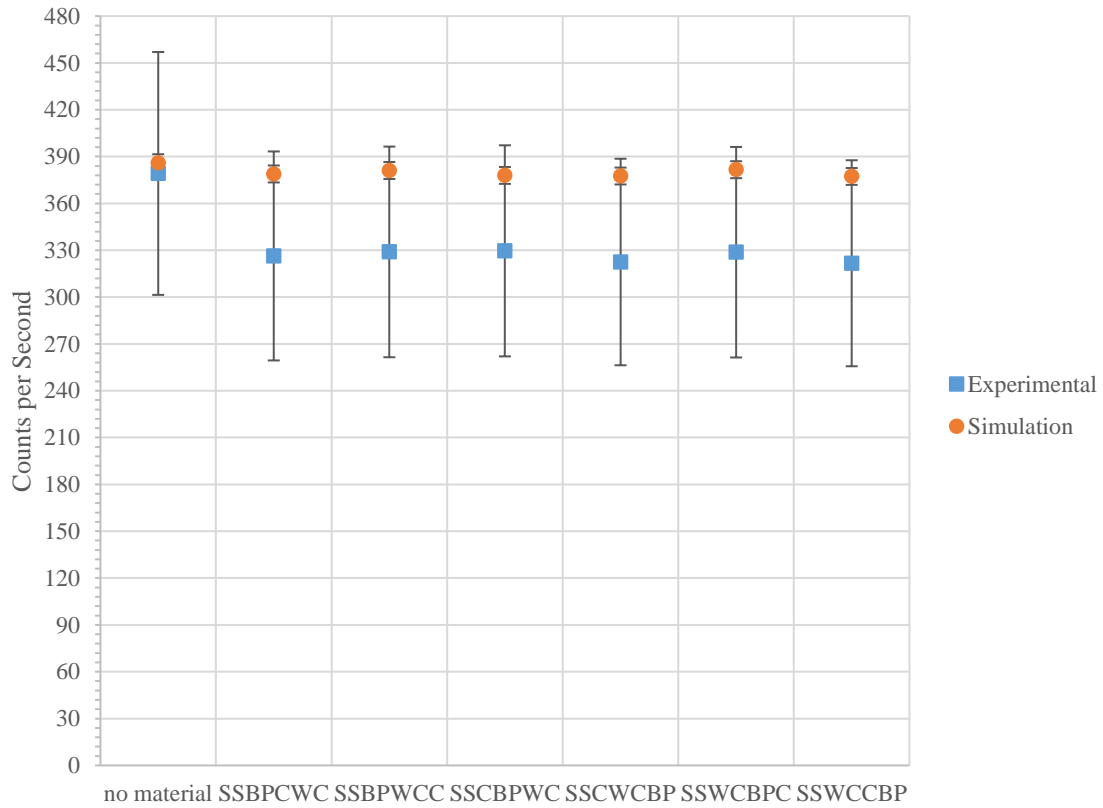


Figure 7-30 Plot of neutron experimental and simulated results with associated errors.

8 Shielding Optimization

Ideally there is an optimum thickness for each layer of the shield. The optimal thickness of each layer will be different for neutrons and gamma-rays, individually. Finding the optimal thickness of each layer to provide the necessary protection for both gamma-rays and neutrons is the goal.

This section discusses the simulations performed to find the optimal thickness of the layers as compared to conventional monolithic concrete shielding. The monolithic concrete shield was used for comparison because it is the standard method of shielding for the types of facilities being considered in this work, namely hot cells where used nuclear fuel is handled in preparation for pyroprocessing. This research may be extrapolated to other facilities performing similar work with used nuclear fuel.

Much of the work on the optimization was performed by an assistant. This work aided in the completion of requirements for the assistant's senior design class. Both the optimization and parts of the gamma-ray and neutron simulations were occurring at the same time. Realization of changes needed occurred regularly. Great efforts to maintain good communication was made so modifications could be implemented in a timely manner.

8.1 Optimization Design

The first stage of the optimization was to determine the range of concrete thicknesses to consider. Typical hot cells have concrete walls of four feet (1.2 m) thick, though there are some facilities having walls as thick as eight feet (2.4 m). These two values were set as the bounding thicknesses, though comparisons will be made to the four foot (122 cm) thick wall, since it is the more common thickness.

The second stage was to determine the source term for gamma-rays and neutrons. A Westinghouse 17x17 fuel bundle was chosen as the gamma-ray source to represent the day to day operational handling within a hot cell. A sphere of plutonium was selected as the neutron source to represent a worst-case criticality accident scenario.

The third stage was to determine the detectors to use. The detector material descriptions used came directly from the experimental/simulations discussed in Chapter 7. The tallies for gamma-rays and neutrons were selected as the modified F4 for reaction rate. These tallies were selected because they can be used with variance reduction techniques which the F8 tallies could not. Also, using the F4 tally for neutron simulations allowed for use of multi-threading when the F8 would not because of the presence of non-standard particles. For the gamma-ray case, it is known the F4 reaction rate tally affords an answer greater than 2.5 times higher than the F8 tally. This is not problematic from the standpoint of desiring to shield the radiation for protection of those working at the hot cell, but rather is conservative and builds in a significant engineering safety factor to the shield for protection purposes.

The final stage was to determine how to create the input files and run them for analysis. Initially, the design was to produce a MatLab code that would start with an initial input file, run it in MCNP, extract the tally result and compare it to a given value and proceed by adding more material and running iteratively until the criteria for completion were met. Due to time and coding ability constraints, the MatLab code design was modified to perform the functions of writing a series of input files with constant thickness of concrete and stainless steel, varying thicknesses of tungsten carbide and borated polyethylene, extract data from each output file and produce an output file with the consolidated data for further analysis.

A given order of shielding materials was selected from those indicating best efficiency in experimental results. The order of shielding material from source to detector was stainless steel, concrete, tungsten carbide, and borated polyethylene.

The thickness of stainless steel was set as a constant at 1.27 cm (0.5 in). The concrete thickness was also held constant at 30 cm (~12 in). The thickness of tungsten carbide was varied from 0 – 15 cm (0 – ~6 in). Likewise, the borated polyethylene was varied from 0 – 15.24 cm (0 - 6 in). Why the additional 0.24 cm on the borated polyethylene? Because borated polyethylene comes in one inch (2.54 cm) slabs and 15.24 cm is an equivalent multiple of inches in centimeters. The tungsten carbide comes in plates up to 5 cm thick.

The source and detector distance from the shield was held constant. For the gamma-ray optimizations the source was placed 30 cm from one side of the shield and rose from the floor 365.76 cm. The detector was placed 30 cm from the other side of the shield. For the neutron optimizations the source was placed so the edge of the sphere was at 30 cm from one side of the shield sitting on the floor with a radius of 5.93 cm. The detector was placed 30 cm from the other side of the shield.

Atom densities for all of the non-shielding materials came from the PNNL compendium. The concrete and stainless steel shielding materials also came from the PNNL compendium. The tungsten carbide and borated polyethylene atom densities were calculated using manufacturer information on the specification sheets. These more general atom densities were selected for WC and BP because more specific information regarding the future production of such materials cannot be known due to variations in the manufacturing processes.

This work focused on single layers of each type of material in the layered shield. Depiction of the monolithic concrete and layered shield for gamma-ray simulations are shown in Figure 8-1. These depictions show the initial setup style where the source and detector were centered with respect to the shield in an air atmosphere and the shield between them.

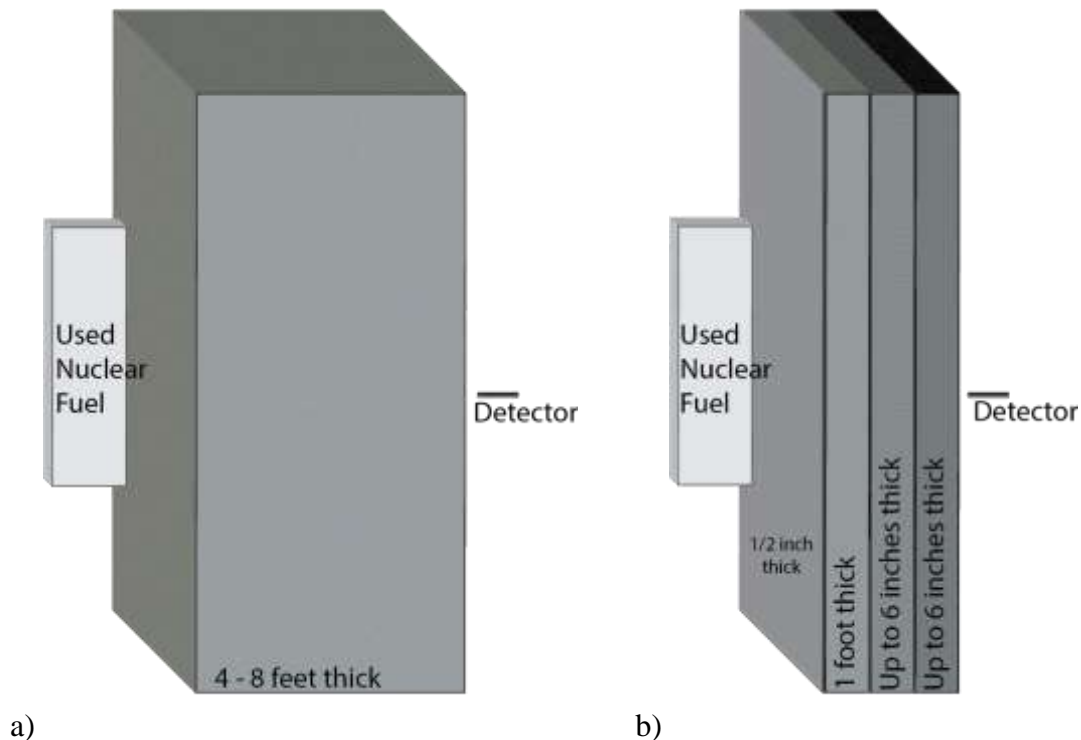
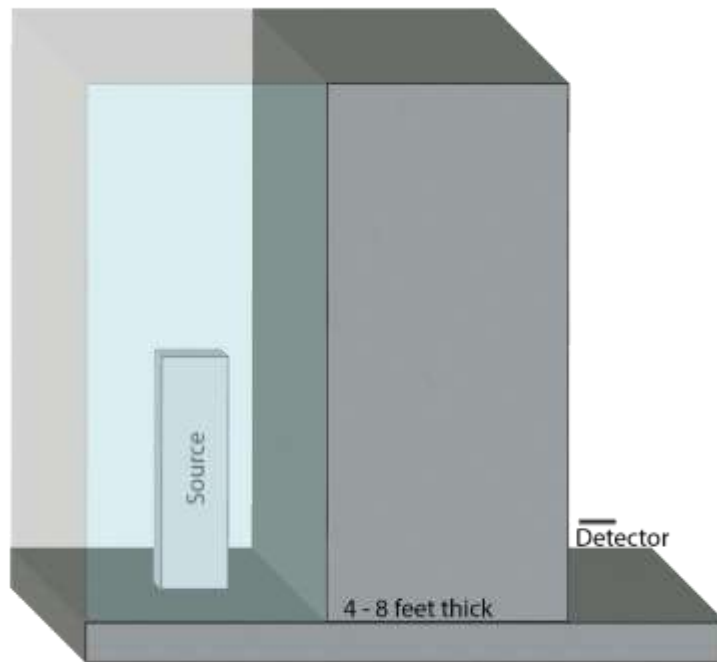
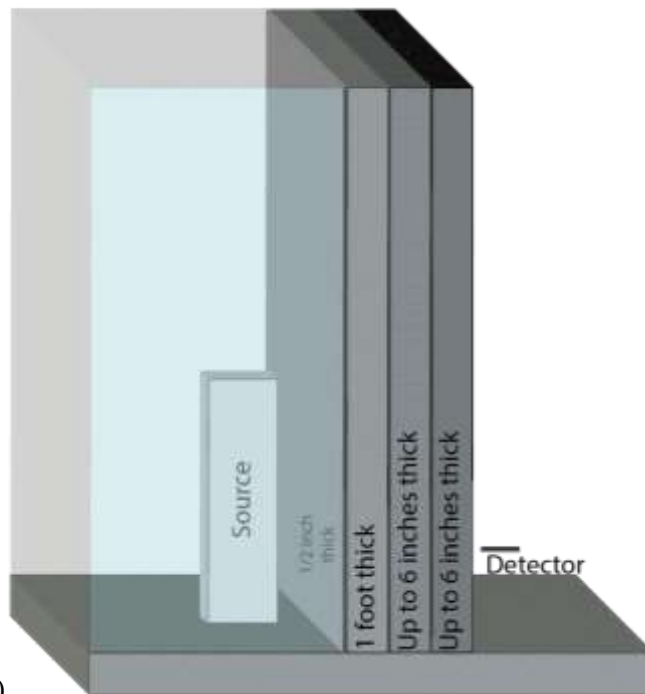


Figure 8-1 a) depiction of a concrete shield as used in the initial setup of the optimizations. b) depiction of the multilayered shield as used initially in the optimizations.

After discovering the importance of more room detail, especially for neutrons, a floor was added and the source was placed on the floor and the detector placed a nominal distance above the floor as though a human was holding it, 147 cm above the floor. An argon atmosphere was also added to the source side of the problem to better represent reality because a hot cell would contain an inert environment. The more current depictions are shown in Figure 8-2.



a)



b)

Figure 8-2 a) Depiction of the concrete shield of the models reported. b) Depiction of the multilayered shield used in reported optimizations.

8.2 Results

To obtain the results for the optimization 171 input files were generated and run in MCNP. These files include five for gamma-ray concrete simulations, five for neutron concrete simulations, 112 for gamma-ray multilayered simulations, and 49 for neutron multilayered simulations. Each input file was remade several times as various modifications were made to improve the results. The final iteration of the input files included a STOP card to run the simulation until the statistical error became less than 1% of the tally mean.

8.2.1 Gamma-Ray Monolithic Concrete Shield

These simulations consisted of a single slab of concrete sitting on a floor, the gamma-ray source, an argon atmosphere on the source side, a detector, and an air atmosphere on the detector side. The thickness of the slab was varied from 122 – 244 cm (4 – 8 ft) to provide five data points for comparison to the multilayered shielding configuration. However, the four foot (122 cm) thick shield will be used as the standard.

The simulation results of the monolithic concrete followed the expected pattern for attenuation of gamma-rays by a single shielding material. The semilogarithmic plot is shown in Figure 8-3. The negatively sloped linear form on a semilogarithmic plot indicates an exponential decrease in the detector response relative to thickness. An exponential fit was applied to show the goodness of the data. The R^2 value is nearly unity for this fit indicating a good fit.

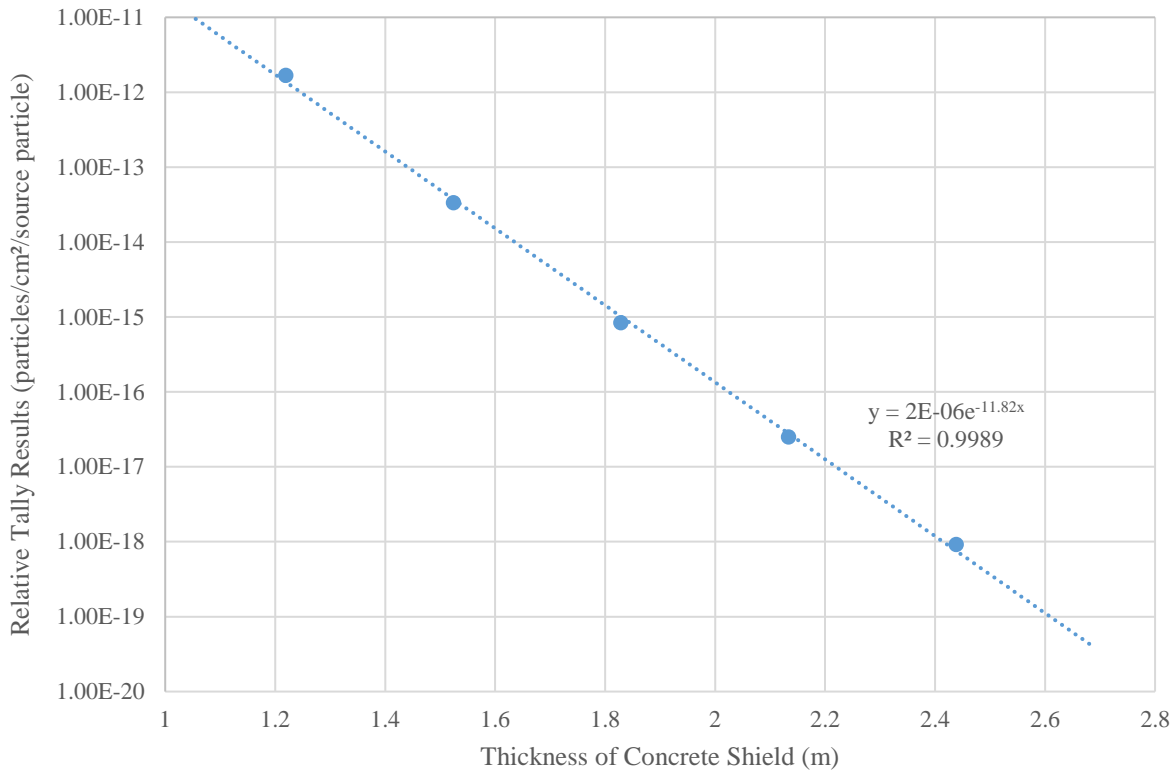


Figure 8-3 Plot of the gamma-ray tally results from the monolithic concrete shielding for various thicknesses.

8.2.2 Gamma-Ray Multi-Layered Multi-Material Shield

The setup for the multilayered shield consists of the source, a shield, a detector and an atmosphere on each side of the shield. The atmosphere on the source side is argon and the atmosphere on the detector side is air. The layers of the shield consist of 1.27 cm of stainless steel (constant thickness), 30 cm of concrete (constant thickness), and a varying thickness of tungsten carbide and borated polyethylene.

The multilayered shield optimization comprised of 112 input files providing 112 data points. These results are plotted on a 3-D semilogarithmic surface plot, Figure 8-4. Each vertex of the grid is a data point corresponding to a detector response value. The false color indicates orders of magnitude on the plot and lines between colors are iso-magnitude lines. For comparison the iso-

magnitude line closest to the four foot (122 cm) thick concrete result is the line at 1.00×10^{-12} p/cm²/sp (between red and grey).

The results show a slight concave curve with respect to the addition of tungsten carbide on the semilogarithmic plot indicating there is a slightly less than exponential decay to the results.

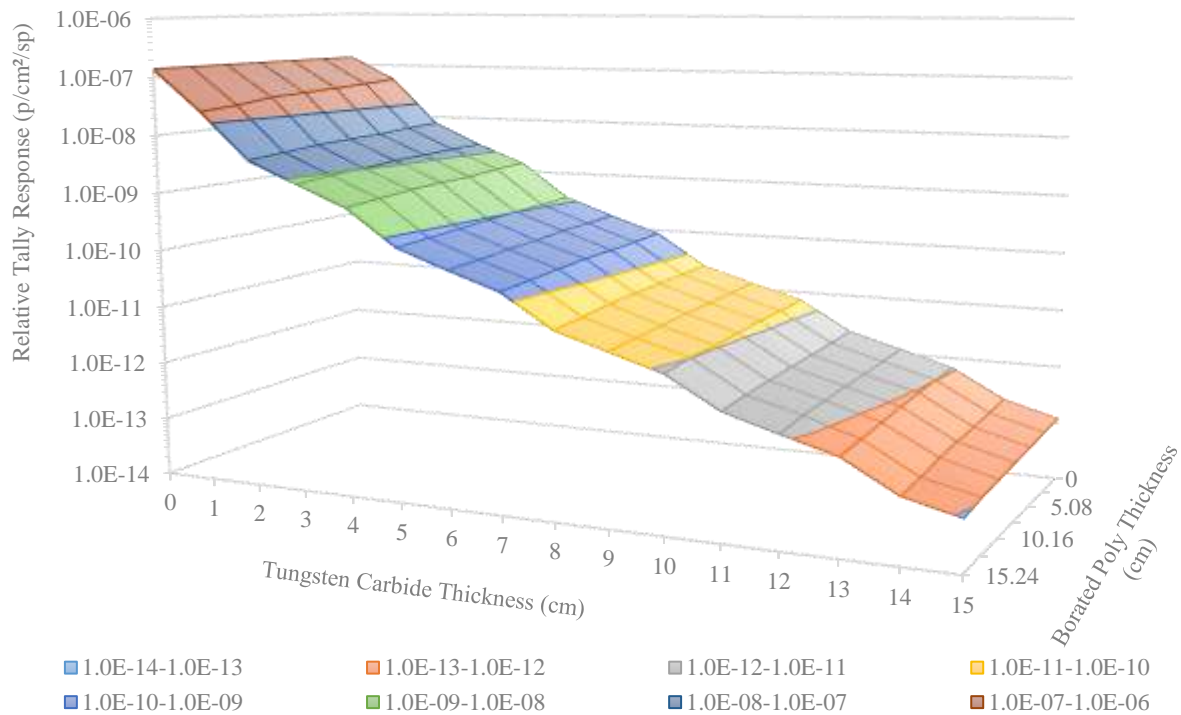


Figure 8-4 Plot of the gamma-ray tally response for the multilayered shield versus the thickness variations of tungsten carbide and borated polyethylene.

8.2.3 Neutron Monolithic Concrete Shield

The tally results for neutron simulations for a monolithic concrete shield are shown in Figure 8-5. The detector response was plotted on a semilogarithmic scale. The results appear to be a linear response on the semilogarithmic scale indicating an exponential response, which is expected for the attenuation of neutrons through a shield. An exponential fit was performed on the response, also shown on the plot. The R^2 value is unity indicating an excellent fit.

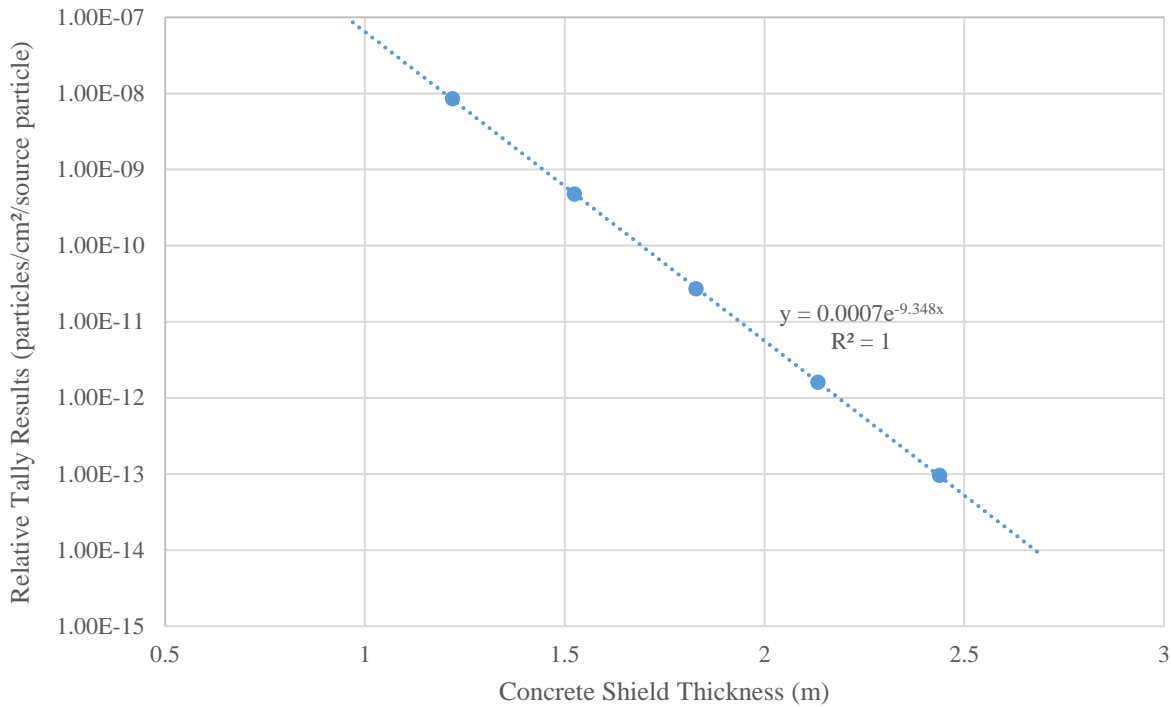


Figure 8-5 Plot of the neutron tally results for the monolithic concrete shield.

8.2.4 Neutron Multi-Layered Multi-Material Shield

The setup of the multilayered neutron optimization simulations was similar to that of the gamma-ray version, except the added layers of tungsten carbide were thicker and fewer input files were necessary, with 49 input files. The constant layer thickness for stainless steel and concrete remain the same, as well as the varying of the tungsten carbide and borated polyethylene thicknesses.

The right rectangular parallelepiped gamma-ray source is replaced with a sphere of plutonium to act as the neutron source. It is still positioned at the same distance from the shield. The detector is modeled as a ^3He tube positioned on the opposite side of the shield from the source.

The simulated detector response is plotted on a 3-D semilogarithmic surface plot. The vertexes of the grid are the location of the plotted responses. The false color bands represent orders of magnitude while the lines separating the colors are iso-magnitude lines. These results do not quite

succeed in achieving the attenuation of the four foot (122 cm) thick concrete wall. The addition of more layers of either BP or WC or both, to a thickness of about 20 cm, would achieve this result.

Similar to the gamma-ray results there appears to be a slightly concave curve to the results with respect to the borated polyethylene thickness. This curve represents a less than exponential trend on the semilogarithmic plot. Also, the data for no borated polyethylene, with varying thickness of tungsten carbide does not follow the expected trend. There is a leveling off for five of the data points at higher tungsten carbide thicknesses and a peak at no shielding except the stainless steel and concrete. The only point to keep the trend is the 2.5 cm of added tungsten carbide and no borated polyethylene.

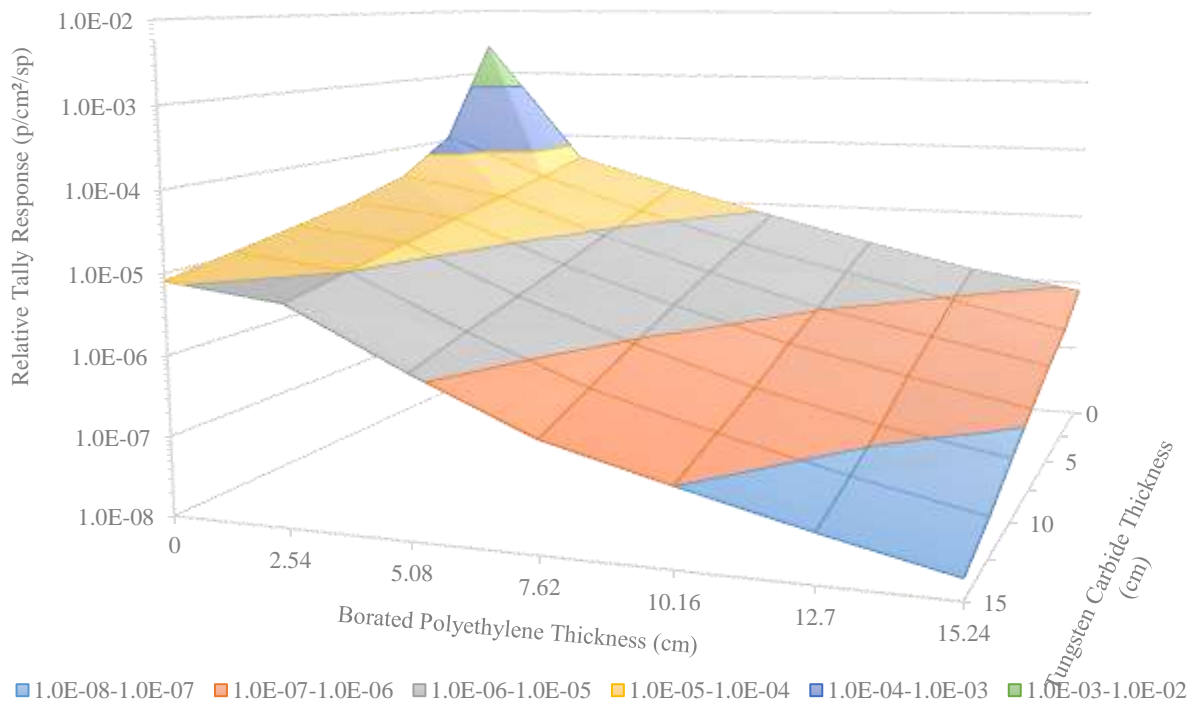


Figure 8-6 Plot of the neutron tally result for the layered shield for varying thicknesses of tungsten carbide and borated polyethylene.

The current hypothesis for tally data not following the trend of the rest of the tally data for the neutron optimization relies upon understanding of the materials and how the neutrons interact with them. The hypothesis for the single point representing no borated polyethylene and no tungsten carbide resulting in a peak is that there is a significantly reduced neutron absorption occurring because of the lack of borated polyethylene and a reduction in scattering away from the detector by the lack of tungsten carbide. The total fluence of neutrons toward the detector is significantly higher than when shielding material is present, thus increasing the probability of tally. The hypothesis for the five data points having no borated polyethylene and varying thicknesses of tungsten carbide, showing a reduced signal from the trend exhibited by the rest of the data, is the lack of borated polyethylene effectively hardens the neutron spectrum relative to setups having borated polyethylene thus effecting the detector efficiency and reducing the number of neutrons tallied. The spectrum is hardened enough to seem more effective than adding borated polyethylene for absorbing neutrons.

The optimal thickness of the multi-layered shield was found to be 61.25 cm. Compare this to a thickness of 121.92 cm of concrete used in the monolithic shield. In terms of thickness this is a significant improvement, though this is not the only metric required when determining how to build a shield.

8.2.5 Weight Comparison and Rudimentary Cost Estimate

In addition to the comparison of shield thickness, weight and costs were compared. To compare the weight of the two shields, some assumptions were needed about building design. The assumptions applying to both the monolithic concrete shield and the multilayered shield are: the shield weight is based upon the wall being 50 feet (15.25 m) tall, only explicitly stated materials are included in the estimates, no labor or shipping/transportation costs are included. The weight is

per linear foot of material for a 50 foot (15.25 m) high wall. The cost is per square foot of wall surface area.

The monolithic concrete shield is also assumed to be poured concrete requiring a rebar structure for integrity. The costs of rebar and labor to emplace the rebar is not included. The only cost included is the material cost of the concrete. The shield is assumed to be 4 feet (122 cm) thick. The density of concrete is assumed to be 2.30 g/cm³. The weight of the concrete shield is 13.02 metric tons per linear foot (mt/lf). The cost of the concrete is between \$19 and \$23 per square foot (ft²).

The multilayered shield assumes the concrete is prestressed prefabricated wall slabs ready to put in place. The prefabricated wall slabs have the necessary strength for construction requirements built in to them that the poured wall does not have without the addition of the rebar. The densities of the materials are assumed to be: SS = 8.03 g/cm³, concrete = 2.30 g/cm³, WC = 14.93 g/cm³, and BP = 1.40 g/cm³. No other structural requirements are included in the weight or cost estimates. The weight of each component and the total weight are: 0.37 mt/lf SS, 3.26 mt/lf concrete, 7.63 mt/lf WC, 1.24 mt/lf BP, and 12.14 mt/lf total. The costs are: \$28/ft² SS, \$25/ft² concrete, \$4950/ft² WC, \$402/ft² BP, and a total of \$5405/ft². See Table 8–I for a comparison.

Table 8–I: Comparison of shielding weight and costs.

	Monolithic Weight (mt/lf)	Multi-layer Weight (mt/lf)	Monolithic Cost (/ft ²)	Multi-layered Cost (/ft ²)
Concrete	13.02	3.26	\$ 21	\$ 25
Stainless Steel	-	0.37	-	\$ 28
Tungsten Carbide	-	7.63	-	\$ 4950
Borated Polyethylene	-	1.24	-	\$ 402
Total	13.02	12.14	\$ 21	\$ 5405

There are several other cost factors that would need to be considered in a full cost analysis but are beyond the scope of this work. However, it is useful to mention an example to help qualitatively understand how they affect the overall costs and potentially level the cost field. For example, one cost that is not included is labor and time required for construction. The time and man power required to construct the monolithic shield is significantly more than using prefabricated components that would be assembled on site, as would be done in the multi-layered shield. This increased manpower and time increases the overall costs of the construction process for the monolithic shield as compared to the multi-layered shield.

9 Conclusions

The hypothesis of this work was to determine if creating a layered shield of unique materials would afford a more reasonable shield thickness for use in hot cells working with used nuclear fuel. A comparison of point kernel calculations and simulations were used to decide which Monte Carlo simulation to use for comparison to experiments and to perform the optimization. Then a set of experiments were designed to obtain physical data to compare to simulations. Finally, an optimization using the Monte Carlo software was performed to find the thickness of the layers as compared to a monolithic concrete wall.

9.1 Point Kernel Calculations and Simulations

A basic isotropic 1 MeV source placed at the center of a sphere of shield material design was used to compare results from point kernel and Monte Carlo calculations. Two Monte Carlo software packages were used for the comparisons, MCNP and SCALE. The results indicated that MCNP was more functional for the needs of this work and was selected for use in the remainder of the research.

9.2 Experiments and Simulations

The contrived experiments consisted of using either a ^{137}Cs gamma-ray source or an AmBe neutron source. The sources were collimated and the shielding materials were placed in the beam path. Data was collected for an unshielded and several shielded versions of the setup for both the gamma-ray and neutron sources. Simulations of each setup were created in MCNP and results of the simulations were compared to experimental data. The primary metric for analysis was the ratio of computed to experimental (C/E) result. Ideally the result would be unity for a perfect simulation of the result. The goal was to have a ratio between $0.95 \leq C/E \leq 1.05$. If meeting this criterium was not possible, then meeting the goal of having the simulation result fall within the errors of the

experimental data was the next desired goal. The purpose of these criteria is to make sure the Monte Carlo software is capable of providing reliable results for the proposed optimization.

The results for the gamma-ray simulations all met the first criterium of being within 5% of unity for the C/E ratio as well as the simulation results being within the experimental errors associated with the data. This provides great confidence the MCNP simulations of the optimization will afford excellent results. Unexpectedly, the experimental and simulation results indicated a dependence on material order. Material order selection then became a need for the optimization simulations but neutron results were needed as well before the decision could be made.

The neutron results met a varied conclusion with respect to the primary criterium of being within 5% of unity for the C/E ratio. The unshielded setup met this criterium with a ratio = 1.017. However, the shielded setups did not meet this criterium having a C/E around 1.16. The results did meet the second criterium of falling within the experimental uncertainties. These results also showed a dependency on material order but it was different from the gamma-ray order. Though the results may be a little less definitive than the gamma-ray results, MCNP will still afford good results for the optimization.

The collection of excellent results for gamma-rays and reasonable results for neutrons meets the expectations of this research. It is more imperative to have excellent results for the gamma-ray experiments, simulations, and optimizations because gamma-rays present an ever-present hazard. The results for the neutrons are sufficient because they are only a hazard for an event that has a very rare probability of occurring.

9.3 Optimization

Design of the optimization simulation includes a fuel bundle as the source for gamma-rays and a plutonium sphere for the neutrons. The shield is placed between the source and detector with a material order of stainless steel, concrete, tungsten carbide, and borated polyethylene. An appropriate detector was provided on the opposite side of the shield, NaI for gamma-rays and ^3He for neutrons. The concrete and stainless steel thicknesses were held constant while the tungsten carbide and borated polyethylene were incrementally changed to discover the effect each had on the simulated result. This was done to determine the optimum thickness of each of those two layers.

The source and detector were also simulated with a concrete shield of varying thickness for both gamma-rays and neutrons. The shield thickness varied from four to eight feet (1.2 - 2.4 m). Four feet (1.2 m) of concrete shielding was used as the standard for comparison for effectiveness of the shield and optimum thickness of the materials in the layered shield.

The gamma-ray tally selected provides a result that is higher than what experiment would give by a factor of approximately 2.5. This naturally builds in a safety factor and will be kept for expression of results. The results indicate tungsten carbide provides the greater attenuation, which was expected. In addition to the stainless steel and concrete, the addition of 11 – 12 cm of tungsten carbide is needed to achieve the same attenuation factor as four feet (1.2 m) of concrete, regardless of how much borated polyethylene is added. This would make the layered shield 42.25 – 43.25 cm total thickness, compared to 121.92 cm for concrete alone, to attenuate gamma-rays to the decided metric. This is approximately $\frac{1}{3}$ the thickness of concrete needed.

Neutron simulations indicate both tungsten carbide and borated polyethylene have significant attenuating capabilities with borated polyethylene being more effective, as was expected. Though the plotted data does not achieve an attenuation equivalence to the four foot (122 cm) concrete

shield, extrapolation can be used to obtain the necessary thicknesses of borated polyethylene. If 11 – 12 cm of tungsten carbide is added to the stainless steel and concrete, as is required for attenuation of the gamma-rays, extrapolation indicates a need of 18 - 19 cm of added borated polyethylene to achieve the same attenuation of neutrons as four feet (1.2 m) of concrete. Inclusion of this much borated polyethylene in the layered shield allows for narrowing the tungsten carbide thickness to 11 cm corresponding to a borated polyethylene thickness of 19 cm needed. This makes the optimal total thickness of stainless steel, concrete, tungsten carbide, and borated polyethylene to be 61.25 cm. The optimal thickness is approximately $\frac{1}{2}$ the thickness of the 121.92 cm concrete used as a metric for the amount of attenuation needed, which is a significant reduction in the wall thickness. A comparison of the two shields is shown in Figure 9-1.

The application of this type of shield is widely varied. This study specifically looked at this shield being used for hot cells where used nuclear fuel is being handled. This design of shield could be used for the walls and ceiling of such a hot cell. It is possible to extrapolate the uses beyond this specific study to other areas where mixed gamma-ray and neutron sources are being used. For example, this design could be made into portable or movable shields for use in nuclear research facilities. Given the cost estimate in Section 8.2.5, this shielding is unlikely to be used in the full construction of a large facility, but rather to shield explicit locations within the facility or as a mobile shield in a laboratory.

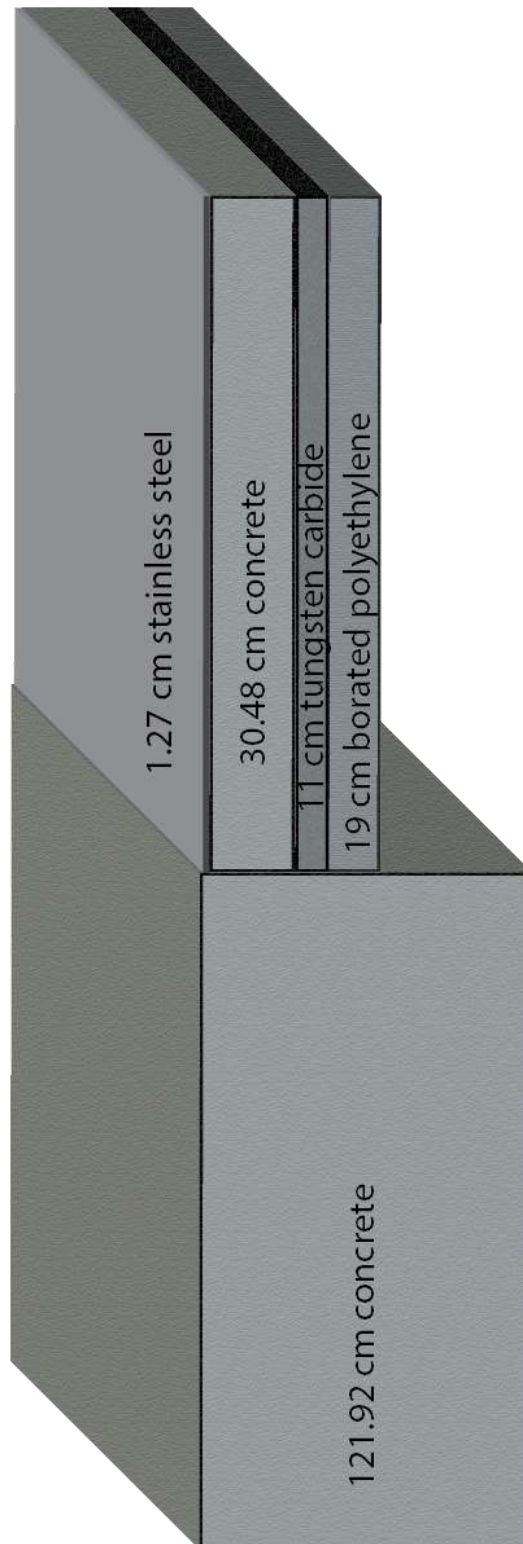


Figure 9-1: Comparison of the optimized SSCWCBP shield to the concrete shield.

10 Further Work

As there is with any research there are always improvements to be made to the experiments and simulations and further ideas that come up as the work is being done. These facets provide the basis for future time investment to refine the information gleaned from the work and to afford further knowledge to the scientific community. This work is no exception. Improvements and future ideas came from this work and they are discussed below.

10.1 Improvements to Experiments

There are three main ideas for improvement to the experiments. Two of these apply to both the gamma-ray and neutron experiments, despite the good agreement between simulation and experiment for gamma-rays, while the third applies exclusively to the neutron experiment.

The first recommended improvement is to better isolate the experiments. The neutron simulations indicated a fair amount of scattering being caused by the shielding materials and also from the concrete walls and floor. Isolating the experiment from such scattering would improve understanding of the unknown bias noted between the experiments and the simulations. Isolation could be done through moving the experiments to a more open environment, such as at the airport or the open field areas near the Idaho Accelerator Center. Isolation could also be achieved through use of an absorbing medium, such as a gadolinium paint on a surface surrounding the experiments.

The second recommended improvement to the experiments is to obtain larger surface areas to shielding components. The tungsten carbide was the limiting factor for size in these experiments. Manufacturers in the United States are capable of making 10.16 cm x 10.16 cm blanks. These were used for time and convenience. Manufacturers in China are capable of making 30 cm x 30 cm blanks, but the lead time for shipping is two weeks and shipping is by boat making a lengthy

delivery time. Either way, the solution to making a surface area sufficient for the shield in these experiments would require tiling the tungsten carbide. All other shielding materials, concrete, stainless steel, and borated polyethylene, may be purchased or made with significant surface area sufficient for the experimental improvements. This improvement would also assist in minimizing scattered radiation being detected after circumventing the shield.

The third improvement is better characterization of the neutron source. The neutron source utilized was manufactured in 1963. Some of the necessary and desired information has been lost to time regarding how it was manufactured and assumptions were made from robust parametric simulations for comparison to the experiments. Some information could be obtained by in-house characterization of the source, such as exposing photographic medium to the surface of the source and developing it. However, this would still provide limited information. The best course of action would be to purchase a new, well characterized source and perform the experiments with this new source and under better experimental environmental conditions.

10.2 Improvements to Simulations

When discussing the biased results of the neutron simulations with a colleague, a recommendation was provided from personal experience. The recommendation was in regards to which cross section set to use. In particular, this colleague had previously performed a study using tungsten. When using the most current cross sections for tungsten their simulation was disparate from the expected results. They received the recommendation of using the older cross sections and reran the simulation using these older set of cross sections. Upon doing so their simulation was much more in line with the expected results.

10.3 Future Related Work Ideas

Shielding designs in this work were partially motivated by the published works of Greene [39], Maruyama [40], and Whetstone [41]. In particular, the repeated structure of multi-layering materials, similar to the way Whetstone [41] studied material layering, could be an enhancement to the shielding efficiency and efficacy. Investigation into this may show a benefit of even thinner walls and less material use.

This design focused on the use of borated polyethylene and tungsten carbide in conjunction with stainless steel and concrete. Other shielding materials were considered (see Section 5.1). Investigation into these other shielding materials would be a natural extension of the work.

Tungsten carbide has great potential as a shielding material for gamma-rays and as a shielding material or reflector for neutrons. A study of the gamma-ray shielding properties of tungsten alloys, such as tungsten carbide, has been published [54] and tungsten carbide has been used as a shielding material in many ways for both gamma-rays and neutrons. Nothing was found regarding the cross section data for tungsten carbide in a basic literature search. There is potential for further study of attenuation information and cross section data for tungsten carbide.

Additional simulation studies into the seemingly abnormal response received in the neutron optimization would be beneficial. Recall in Figure 8-6 there is a peak at the point where there is no WC and no BP and the divergence from the normal trend for the measurements having no BP as compared to when BP is present. Adapting the tallies to determine energy spectra of neutrons as the cross certain boundaries as well as relative magnitudes of neutrons crossing those boundaries could help determine why there is a tendency away from the trend presented in the rest of the data results.

11 References

- [1] E.-S. A. Abdo, M. A. M. Ali, and M. R. Ismail, "Natural Fibre High-Density Polyethylene and Lead Oxide Composites for Radiation Shielding," *Radiat. Phys. Chem.*, vol. 66, no. 3, pp. 185–195, 2003.
- [2] M. Celli, F. Grazzi, and M. Zoppi, "A New Ceramic Material for Shielding Pulsed Neutron Scattering Instruments," *Nucl. Instruments Methods Phys. Res. Sect. A Accel. Spectrometers, Detect. Assoc. Equip.*, vol. 565, no. 2, pp. 861–863, 2006.
- [3] M. Erdem, O. Baykara, M. Doğru, and F. Kuluöztürk, "A Novel Shielding Material Prepared from Solid Waste Containing Lead for Gamma Ray," *Radiat. Phys. Chem.*, vol. 79, no. 9, pp. 917–922, 2010.
- [4] T. Hayashi, K. Tobita, Y. Nakamori, and S. Orimo, "Advanced Neutron Shielding Material Using Zirconium Borohydride and Zirconium Hydride," *J. Nucl. Mater.*, vol. 386, pp. 119–121, 2009.
- [5] H. Hu *et al.*, "Study on Composite Material for Shielding Mixed Neutron and γ -Rays," *IEEE Trans. Nucl. Sci.*, vol. 55, no. 4, pp. 2376–2384, 2008.
- [6] R. Y. Moghaddam, R. L. Motavalli, and M. H. Hakimabad, "Shielding Optimization in an In Vivo Activation Analysis Setup," *J. Radioanal. Nucl. Chem.*, vol. 295, no. 1, pp. 157–162, 2013.
- [7] Y. Sakurai, A. Sasaki, and T. Kobayashi, "Development of Neutron Shielding Material Using Metathesis-Polymer Matrix," *Nucl. Instruments Methods Phys. Res. Sect. A Accel. Spectrometers, Detect. Assoc. Equip.*, vol. 522, no. 3, pp. 455–461, 2004.
- [8] K. Singh *et al.*, "Gamma-Ray Attenuation Coefficients in Bismuth Borate Glasses," *Nucl. Instruments Methods Phys. Res. Sect. B Beam Interact. with Mater. Atoms*, vol. 194, no. 1, pp. 1–6, 2002.
- [9] K. J. Singh, N. Singh, R. S. Kaundal, and K. Singh, "Gamma-Ray Shielding and Structural Properties of PbO-SiO₂ Glasses," *Nucl. Instruments Methods Phys. Res. Sect. B Beam Interact. with Mater. Atoms*, vol. 266, no. 6, pp. 944–948, 2008.
- [10] N. Singh, K. J. Singh, K. Singh, and H. Singh, "Comparative Study of Lead Borate and Bismuth Lead Borate Glass Systems as Gamma-Radiation Shielding Materials," *Nucl. Instruments Methods Phys. Res. Sect. B Beam Interact. with Mater. Atoms*, vol. 225, no. 3, pp. 305–309, 2004.
- [11] S. Singh, A. Kumar, D. Singh, K. S. Thind, and G. S. Mudahar, "Barium-Borate-Flyash Glasses: As Radiation Shielding Materials," *Nucl. Instruments Methods Phys. Res. Sect. B Beam Interact. with Mater. Atoms*, vol. 266, no. 1, pp. 140–146, 2008.
- [12] C. Xiaozhou *et al.*, "Mechanical Properties of UHMWPE/Sm₂O₃ Composite Shielding Material," *J. Rare Earths*, vol. 28, no. SUPPL. 1, pp. 482–484, 2010.
- [13] The Aberdeen Group, "High Density Concretes for Radiation Shielding," 1960.
- [14] I. Akkurt and A. M. El-khayatt, "The Effect of Barite Proportion on Neutron and Gamma-

- Ray Shielding,” *Ann. Nucl. Energy*, vol. 51, pp. 5–9, 2013.
- [15] I. I. Bashter, A. E. S. Abdo, and M. S. Abdel-Azim, “Magnetite Ores with Steel or Basalt for Concrete Radiation Shielding,” *Japanese J. Appl. Physics, Part 1 Regul. Pap. Short Notes Rev. Pap.*, vol. 36, no. 6 A, pp. 3692–3696, 1997.
 - [16] F. C. de Beer, M. J. Radebe, B. Schillinger, R. Nshimirimana, M. A. Ramushu, and T. Modise, “Upgrading the Neutron Radiography Facility in South Africa (SANRAD): Concrete Shielding Design Characteristics,” *Phys. Procedia*, vol. 69, no. 2015, pp. 115–123, 2015.
 - [17] E. Gallego, A. Lorente, and H. R. Vega-Carrillo, “Testing of a High-Density Concrete as Neutron Shielding Material,” *Nucl. Technol.*, vol. 168, no. 2, pp. 399–404, 2009.
 - [18] T. Korkut, A. Karabulut, G. Budak, B. Aygün, O. Gencel, and A. Hançerlioğullari, “Investigation of Neutron Shielding Properties Depending on Number of Boron Atoms for Colemanite, Ulexite and Tincal Ores by Experiments and FLUKA Monte Carlo Simulations,” *Appl. Radiat. Isot.*, vol. 70, no. 1, pp. 341–345, 2012.
 - [19] A. S. Makarious, I. I. Bashter, A. E.-S. Abdo, M. S. A. Azim, and W. A. Kansouh, “On the Utilization of Heavy Concrete for Radiation Shielding,” *Ann. Nucl. Energy*, vol. 23, no. 3, pp. 195–206, 1996.
 - [20] K. Okuno, M. Kawai, and H. Yamada, “Development of Novel Neutron Shielding Concrete,” *Nucl. Technol.*, vol. 168, no. 2, pp. 545–552, 2009.
 - [21] B. Oto, A. Gür, E. Kavaz, T. Çakır, and N. Yaltay, “Determination of Gamma and Fast Neutron Shielding Parameters of Magnetite Concretes,” *Prog. Nucl. Energy*, vol. 92, pp. 71–80, 2016.
 - [22] T. Piotrowski, D. B. Tefelski, A. Polański, and J. Skubalski, “Monte Carlo Simulations for Optimization of Neutron Shielding Concrete,” *Cent. Eur. J. Eng.*, vol. 2, no. 2, pp. 296–303, 2012.
 - [23] T. Piotrowski, M. Mazgaj, A. Zak, and J. Skubalski, “Importance of Atomic Composition and Moisture Content of Cement Based Composites in Neutron Radiation Shielding,” *Procedia Eng.*, vol. 108, pp. 616–623, 2015.
 - [24] M. J. Radebe, S. Korochinsky, W. J. Strydom, and F. C. De Beer, “Au Foil Activation Measurement and Simulation of the Concrete Neutron Shielding Ability for the Proposed New SANRAD Facility,” *Phys. Procedia*, vol. 69, pp. 392–398, 2015.
 - [25] B. L. Broadhead, J. S. Tang, R. L. Childs, C. V Parks, and H. Taniuchi, “Evaluation of Shielding Analysis Methods in Spent-Fuel Cask Environments,” *Nucl. Technol.*, vol. 117, no. 2, pp. 206–222, 1997.
 - [26] E. Calzada, F. Grünauer, B. Schillinger, and H. Türck, “Reusable Shielding Material for Neutron- and Gamma-Radiation,” *Nucl. Instruments Methods Phys. Res. Sect. A Accel. Spectrometers, Detect. Assoc. Equip.*, vol. 651, no. 1, pp. 77–80, 2011.
 - [27] F. A. Dilmanian *et al.*, “Improvement of the Prompt-Gamma Neutron Activation Facility at Brookhaven National Laboratory,” *Phys. Med. Biol.*, vol. 43, no. 2, pp. 339–349, 1998.

- [28] M. R. Gilbert, Z. Ghani, J. E. McMillan, and L. W. Packer, "Optimising the Neutron Environment of Radiation Portal Monitors: A Computational Study," *Nucl. Instruments Methods Phys. Res. Sect. A Accel. Spectrometers, Detect. Assoc. Equip.*, vol. 795, pp. 174–185, 2015.
- [29] A. Infantino *et al.*, "Accurate Monte Carlo Modeling of Cyclotrons for optimization of Shielding and Activation Calculations in the Biomedical Field," *Radiat. Phys. Chem.*, vol. 116, pp. 231–236, 2015.
- [30] K. V Subbaiah, L. Thilagam, R. Sarangapani, and D. K. Mohapatra, "An Inverse Calculation Technique for Optimization of Gamma Ray Shielding Designs," *Ann. Nucl. Energy*, vol. 57, pp. 246–255, 2013.
- [31] H. Taniuchi and B. L. Broadhead, "Simple Geometry Dose Rate Benchmarks for Spent Fuel Cask Analysis," in *Proceedings of the 8th International Conference on Radiation Shielding*, 1994, p. 746.
- [32] A. Turner *et al.*, "Nuclear Analysis and Shielding Optimisation in Support of the ITER In-Vessel Viewing System Design," *Fusion Eng. Des.*, vol. 89, no. 9–10, pp. 1949–1953, 2014.
- [33] A. Turner *et al.*, "Shielding Optimisation of the ITER ICH&CD Antenna for Shutdown Dose Rate," *Fusion Eng. Des.*, vol. 96–97, pp. 357–360, 2015.
- [34] G. F. Knoll, *Radiation Detection and Measurement*, 3rd ed. Hoboken, New Jersey: John Wiley & Sons Inc., 2000.
- [35] H. Cember and T. E. Johnson, *Introduction to Health Physics*, 4th ed. New York: McGraw Hill, Inc., 2009.
- [36] J. R. Lamarsh, *Introduction to Nuclear Engineering*, 2nd ed. Reading, MA: Addison-Wesley Publishing Company, 1983.
- [37] J. C. Courtney, "Handout Materials for NS-7530 Nuclear Shielding Analysis and Design." Kinko's Professor Publishing, Baton Rouge, p. 256, 1989.
- [38] K. Shibata *et al.*, "JENDL-4.0: A New Library for Nuclear Science and Engineering," *J. Nucl. Sci. Technol.*, vol. 48, no. 1, pp. 1–30, 2012.
- [39] D. Greene and R. L. Thomas, "The Attenuation of 14 MeV Neutrons in Steel and Polyethylene," *Phys. Med. Biol.*, vol. 14, no. 1, pp. 45–54, 1969.
- [40] T. Maruyama and C. J. Bouts, "Attenuation of 15 MeV Neutrons in Multilayer Shields Composed of Steel, Polyethylene and Borated Materials," *Phys. Med. Biol.*, vol. 17, no. 3, pp. 420–424, 1972.
- [41] Z. D. Whetstone and K. J. Kearfott, "Use of Multiple Layers of Repeating Material to Effectively Collimate an Isotropic Neutron Source," *Nucl. Technol.*, vol. 176, no. 3, pp. 395–413, 2011.
- [42] J. T. Goorley *et al.*, *MCNP6 User's Manual, Version 1.0, LA-CP-13-00634*, Rev. 0. Los Alamos, NM: Los Alamos National Laboratory, 2013.

- [43] X-5 Monte Carlo Team, *MCNP - A General Monte Carlo N-Particle Transport Code, Version 5 Volume I: Overview and Theory*, 2008 Rev., vol. I. Los Alamos, NM: Los Alamos Nuclear Laboratory, 2005.
- [44] B. T. Rearden and M. A. Jessee, Eds., *SCALE Code System*, 6.2.2. Oak Ridge, Tennessee: Oak Ridge National Laboratory, 2017.
- [45] ISO, “Reference Neutron Radiations--Part 2: Calibration Fundamentals of Radiation Protection Devices Related to the Basic Quantities Characterizing the Radiation Field.” International Organization for Standards, Geneva, p. 38, 2000.
- [46] R. J. J. McConn, C. J. Gesh, R. T. Pagh, R. A. Rucker, and R. G. I. Williams, “Compendium of Material Composition Data for Radiation Transport Modeling,” *PNNL-15870 Rev 1*. Pacific Northwest National Laboratory, Richland, WA, p. 375, 2011.
- [47] C. Pope and S. Robison, “Spent Fuel Gamma Ray Shielding Using Concrete,” Pocatello, ID, 2017.
- [48] T. E. Johnson and B. K. Birky, *Health Physics and Radiological Health*, 4th ed. Baltimore, MD: Lippincott Williams & Wilkins, Wolters Kluwer, 2012.
- [49] J. H. Hubbell and S. M. Seltzer, “X-Ray Mass Attenuation Coefficients,” 2004. [Online]. Available: <https://www.nist.gov/pml/x-ray-mass-attenuation-coefficients>. [Accessed: 01-May-2017].
- [50] *Radiological Health Handbook*. Rockville, MD: Bureau of Radiologica Health, U.S. Department of Health, Education, and Welfare: Public Health Service: Food and Drug Administration, 1970.
- [51] J. K. Shultis and R. E. Faw, *Fundamentals of Nuclear Science and Engineering*, 2nd ed. Boca Raton, Fl: CRC Press, Taylor & Francis Group, LLC, 2007.
- [52] T. Wilcox, “MCNP6 Advanced Tallies Tutorial,” in *American Nuclear Society Topical Meeting: Radiation Protection and Shielding Division*, 2014, p. 64.
- [53] E. Baum, H. D. Knox, and T. R. Miller, Eds., *Nuclides and Isotopes: Chart of the Nuclides*, 17th ed. Knolls Atomic Power Laboratory, 2010.
- [54] S. Kobayashi, N. Hosoda, and R. Takashima, “Tungsten Alloys as Radiation Protection Materials,” *Nucl. Instruments Methods Phys. Res. Sect. A Accel. Spectrometers, Detect. Assoc. Equip.*, vol. 390, no. 3, pp. 426–430, 1997.
- [55] Saint Gobain Crystals, “Scintillation Materials and Assemblies,” 2016.
- [56] Saint Gobain Crystals, “NaI(Tl) and Polyscin® NaI(Tl) Sodium Iodide Scintillation Material,” 2016.
- [57] *SCALE: Getting Started with SCALE 6.2.2*. Oak Ridge National Laboratory, 2017.

12 Appendix A: Atom Densities

Weight fractions and atom densities are necessary inputs to Monte Carlo codes. These values provide the code the necessary proportion of each element or isotope to make the appropriate statistical choices for particle interactions and to use the correct cross sections. Weight fractions were used in the point kernel problem and atom densities were used in the simulations of the experiments and the optimization problem. The weight fractions for the point kernel problem are shared in tabular form in Section 12.1, atom densities used in the simulations of experiments are shared in tabular form in Section 12.2, and atom densities used in the optimization problem are shared in tabular form in Section 12.3.

Atom densities used in this work are of two varieties. These varieties are standard composition, such as those found in the SCALE 6.2 manual [42] or in the PNNL Compendium [46], and hand calculated compositions. All atom densities used in the final models for both gamma ray and neutron experiments are tabulated in this appendix.

12.1 Point Kernel and Code Validation

The code validation input files used weight fractions as opposed to atom densities. Table 12–I shows the weight fractions used for each material in the input files. The weight fractions were obtained from the SCALE 6.2 manual [44].

Table 12–I: Standard composition weight fractions used in code verification input files.

		Weight Fraction
Dry Air		
Nitrogen	7000	-0.77
Oxygen	8000	-0.23
Aluminum		
Aluminum	13000	-1.00
Iron		
Iron	26000	-1.00
Lead		

Lead	82000	-1.00
Regular Concrete		
Hydrogen	1000	-0.010
Oxygen	8000	-0.532
Sodium	11000	-0.029
Aluminum	13000	-0.034
Silicon	14000	-0.337
Calcium	20000	-0.044
Iron	26000	-0.014

12.2 Experimental Simulation Model Atom Densities

All of the standard compositions used in this work came from the Compendium of Material Composition Data for Radiation Transport Modeling [46]. Many of the atom densities were hand calculated, especially for the neutron problem to account for actual densities of materials and to change from elemental to isotopic abundances. The practice of changing from elemental to isotopic abundance was necessary to make sure the most recent ENDF/B files were selected by MCNP6. This section provides the atom densities used in the final simulations of the gamma-ray and neutron experiments as well as an example of performing a hand calculation of the atom density. The tables are broken down by material.

12.2.1 Gamma-ray Experiments

Table 12–II: Regular concrete standard composition atom densities used for gamma-ray models.

Regular Concrete	Density = 2.30 g/cm ³	Atom Densities
Hydrogen	1000	0.013742
Oxygen	8000	0.046056
Sodium	11000	0.001747
Aluminum	13000	0.001745
Silicon	14000	0.016620
Calcium	20000	0.001521
Iron	26000	0.000347

Table 12–III: Lead standard composition atom densities used for gamma-ray models.

Lead	Density = 11.35 g/cm ³	Atom Densities
Lead	82000	0.32988

Table 12–IV: Aluminum standard composition atom densities used for gamma-ray models.

Aluminum	Density = 2.6989 g/cm ³	Atom Densities
Aluminum	13000	0.060238

Table 12–V: Dry air standard composition atom densities used for gamma-ray models.

Dry Air	Density = 0.001225 g/cm ³	Atom Densities
Nitrogen	7000	0.000039
Oxygen	8000	0.000011

Table 12–VI: Stainless steel 304 standard composition atom densities used for gamma-ray models.

Stainless Steel 304	Density = 8.03 g/cm ³	Atom Densities
Carbon	6000	0.000160
Silicon	14000	0.000858
Phosphorus	15000	0.000036
Sulfur	16000	0.000023
Chromium	24000	0.017605
Manganese	25000	0.000877
Iron	26000	0.060538
Nickel	28000	0.007593

Table 12–VII: Borated polyethylene hand calculated atom densities for gamma-ray models.

Borated Polyethylene (HD, 5% B)	Density = 1.4783 g/cm ³	Atom Densities
Hydrogen	1000	0.1205911
Boron	5000	0.0041173
Carbon	6000	0.0602956

Table 12–VIII: Tungsten carbide hand calculated atom densities for gamma-ray models.

Tungsten Carbide	Density = 14.842 g/cm ³	Atom Densities
Carbon	6000	0.0427164
Oxygen	8000	0.0008380
Vanadium	23000	0.0002632
Iron	26000	0.0001601
Cobalt	27000	0.0090999
Tungsten	74000	0.0427165

Table 12–IX: Cesium chloride glass hand calculated atom densities for gamma-ray models. Weight fractions were obtained of elements comprising more than 1% were obtained from Eckert & Ziegler.

Cesium Chloride Glass	Density = 1.580968 g/cm ³	Atom Densities
-----------------------	--------------------------------------	----------------

Boron	5000	0.0058780
Oxygen	8000	0.0330873
Sodium	11000	0.0009213
Silicon	14000	0.0118795
Chlorine	17000	0.0000023
Potassium	19000	0.0001010
Cesium	55000	0.0000023

Table 12–X: Sodium iodide hand calculated atom densities for gamma-ray models. Approximate thallium weight fraction was obtained by correspondence with Saint Gobain.

Sodium Iodide (TI)	Density = 3.76 g/cm ³	Atom Densities
Sodium	11000	0.0150794
Iodine	53000	0.0150794
Thallium	81000	0.0000196

Table 12–XI: Mu metal hand calculated atom densities for gamma-ray models. Weight fractions, density, and composition were obtained from www.mumetal.com/mumetal-specifications.php.

Mu Metal	Density = 8.747 g/cm ³	Atom Densities
Carbon	6000	0.0000877
Silicon	14000	0.0006564
Manganese	25000	0.0004794
Iron	26000	0.0140827
Nickel	28000	0.0717977
Molybdenum	42000	0.0023060

Table 12–XII: Hand calculated atom densities used in the gamma-ray simulations for the concrete used as shielding made in-house.

Shielding Concrete	Density = 2.3462 g/cm ³	Atom Densities
Hydrogen	1000	0.0140180
Oxygen	8000	0.0469811
Sodium	11000	0.0017821
Aluminum	13000	0.0017801
Silicon	14000	0.0169538
Calcium	20000	0.0015516
Iron	26000	0.0003540

Table 12–XIII: Hand calculated atom densities used in the gamma-ray simulations for the stainless steel used as shielding.

Shielding Stainless Steel 304	Density = 7.9394 g/cm ³	Atom Densities
Carbon	6000	0.0001582
Silicon	14000	0.0008483
Phosphorus	15000	0.0000356

Sulfur	16000	0.0000227
Chromium	24000	0.0174064
Manganese	25000	0.0008671
Iron	26000	0.0598550
Nickel	28000	0.0075073

12.2.2 Neutron Experiments

Table 12–XIV: Regular concrete standard composition atom densities with isotopic abundance modifications for neutron models.

Regular Concrete	Density = 2.30 g/cm ³	Atom Density
Hydrogen	1001	0.0137404197
	1002	0.0000015803
Oxygen	8016	0.0460382693
	8017	0.0000175372
Sodium	11023	0.001747
Aluminum	13027	0.001745
Silicon	14028	0.0153285761
	14029	0.0007783478
	14030	0.0005130926
Calcium	20040	0.0014744726
	20042	0.0000098409
	20043	0.0000020534
	20044	0.0000317271
Iron	20046	0.0000000608
	20048	0.0000028443
	26054	0.0000202822
	26056	0.0003183864
	26057	0.0000073529
	26058	0.0000009785

Table 12–XV: Stainless steel 304 standard composition atom densities with isotopic abundance modifications for neutron models.

Stainless Steel 304	Density = 8.03 g/cm ³	Atom Density
Carbon	6000	0.000160
Silicon	14028	0.0007913308
	14029	0.0000401819
	14030	0.0000264882
Phosphorus	15031	0.000036
Sulfur	16032	0.0000218339
	16033	0.0000001748
	16034	0.0000009867
	16036	0.0000000046
Chromium	24050	0.0007649373
	24052	0.0147510535

	24053	0.0016726511
	24054	0.0004163583
Manganese	25055	0.000877
Iron	26054	0.0035384461
	26056	0.0555460365
	26057	0.0012828002
	26058	0.0001707172
Nickel	28058	0.0051690790
	28060	0.0019911200
	28061	0.0000865526
	28062	0.0002759676
	28064	0.0000702808

Table 12–XVI: Lead standard composition atom densities with isotopic abundance modifications for neutron models.

Lead	Density = 11.35 g/cm ³	Atom Density
Lead	82204	0.0004618320
	82206	0.0079501080
	82207	0.0072903480
	82208	0.0172857120

Table 12–XVII: PVC standard composition atom densities with isotopic abundance modifications for neutron models.

Polyvinyl Chloride (PVC)	Density = 1.406 g/cm ³	Atom Density
Hydrogen	1001	0.0406383261
	1002	0.0000046739
Carbon	6000	0.027096
Chlorine – 35	17035	0.010264
Chlorine – 37	17037	0.003284

Table 12–XVIII: Iron standard composition atom densities with isotopic abundance modifications for neutron models.

Iron	Density = 7.874 g/cm ³	Atom Density
Iron	26054	0.0049630480
	26056	0.0779092389
	26057	0.0017992641
	26058	0.0002394490

Table 12–XIX: Dry air standard composition atom densities with isotopic abundance modifications for neutron models.

Dry Air	Density = 0.001225 g/cm ³	Atom Density
Nitrogen	7014	0.0000388565
	7015	0.0000001435
Oxygen	8016	0.0000109958
	8017	0.0000000042

Table 12–XX: Borated polyethylene hand calculated atom densities for neutron models. Weight fractions obtained from ShieldWrx.

Borated Polyethylene (HD, 5% B)	Density = 1.4783 g/cm ³	Atom Density
Hydrogen	1001	0.1205772320
	1002	0.0000138680
Boron – 10	5010	0.0008194
Boron – 11	5011	0.0032980
Carbon	6000	0.0602956

Table 12–XXI: Tungsten carbide hand calculated atom densities for neutron models. Weight fractions of materials above 1 w/o were obtained from H. B Carbide.

Tungsten Carbide	Density = 14.842 g/cm ³	Atom Density
Carbon	6000	0.0429698
Oxygen	8016	0.0008376774
	8017	0.0000003191
Vanadium – 50	23050	0.0000007
Vanadium – 51	23051	0.0002640
Iron – 54	26054	0.0000094
Iron – 56	26056	0.0001477
Iron – 57	26057	0.0000034
Iron – 58	26058	0.0000004
Cobalt – 59	27059	0.0091538
Tungsten – 180	74180	0.0000516
Tungsten – 182	74182	0.0113870
Tungsten – 183	74183	0.0061490
Tungsten – 184	74184	0.0131660
Tungsten – 186	74186	0.0122163

Table 12–XXII: Shielding concrete mixed in-house. Atom densities are from standard composition modified for both measured density and isotopic abundance for neutron models.

Concrete Shielding	Density = 2.3462 g/cm ³	Atom Density
Hydrogen	1001	0.0140163879
	1002	0.0000016121
Oxygen	8016	0.0469630131
	8017	0.0000178894
Sodium	11023	0.0017821
Aluminum	13027	0.0017801
Silicon	14028	0.0156364389
	14029	0.0007939804
	14030	0.0005233977
Calcium	20040	0.0015041366
	20042	0.0000100389

	20043	0.0000020947
	20044	0.0000323664
	20046	0.0000000621
	20048	0.0000029015
Iron	26054	0.0000206913
	26056	0.0003248092
	26057	0.0000075013
	26058	0.0000009983

Table 12–XXIII: Shielding stainless steel 304 from McMaster Carr. Atom densities are from standard composition modified for both measured density and isotopic abundance for neutron models.

Stainless Steel 304	Density = 7.9394 g/cm ³	Atom Density
Carbon	6000	0.0001582
Silicon	14028	0.0007823845
	14029	0.0000397276
	14030	0.0000261887
Phosphorus	15031	0.0000356
Sulfur	16032	0.0000215491
	16033	0.0000001725
	16034	0.0000009738
	16036	0.0000000045
Chromium	24050	0.0007563081
	24052	0.0145846485
	24053	0.0016537821
	24054	0.0004116614
Manganese	25055	0.0008671
Iron	26054	0.0034985248
	26056	0.0549193567
	26057	0.0012683275
	26058	0.0001687911
Nickel	28058	0.0051107371
	28060	0.0019686468
	28061	0.0000855757
	28062	0.0002728528
	28064	0.0000694876

Table 12–XXIV: Paraffin wax weight fractions were obtained from NIST. The atom densities were then modified for isotopic abundance for neutron models.

Paraffin Wax	Density = 0.92 g/cm ³	Atom Density
Hydrogen	1001	0.0817128019
	1002	0.0000093981
Carbon	6000	0.0392727

Table 12–XXV: Polyethylene weight fractions were obtained from NIST. The atom densities were then modified for isotopic abundance for neutron models.

Polyethylene	Density = 0.94 g/cm ³	Atom Density
Hydrogen	1001	0.0790217115
	1002	0.0000090885
Carbon	6000	0.0394984

Table 12–XXVI: These atom densities are based on the 14 g being the mass of AmO₂ weighed out and mixed with 57.6 g of Be powder. The density is based upon the mass fractions and component densities using an alloy density equation. Other atom densities were calculated for a comparative study based on different assumptions regarding the source.

Americium-Beryllium	Density = 2.214403 g/cm ³	Atom Density
Beryllium	4009	0.1479713726
Oxygen	8016	0.0833413036
	8017	0.0000298791
Americium	95241	0.0055320804

Table 12–XXVII: These ³He atom densities are based upon the assumption that CO₂ is 2% of the gas. This is the upper bound of CO₂ concentration according to GE Reuter Stokes.

Helium – 3 (4 atm) 2% CO ₂	Density = 0.000622 g/cm ³	Atom Density
Helium – 3	2003	0.0001326651
Carbon	6000	0.0000074934
Oxygen	8016	0.0000112457
	8017	0.0000000043

12.2.3 Hand Calculation Examples

The fundamental equation for calculating an atom density is

$$N = \frac{\rho N_A}{M}$$

Equation 12-1: The fundamental equation for atom density calculations.

where N is the atom density [$atoms/cm^3$], ρ is the mass density [g/cm^3], N_A is Avogadro's number [$atoms/mol$], and M is the molecular weight [g/mol]. The standard units for atom density in Monte Carlo codes is [$atoms/barn \cdot cm$] and thus a conversion factor is applied to Avogadro's number.

$$6.022141 \times 10^{23} \left[\frac{\text{atoms}}{\text{mol}} \right] \cdot 1 \times 10^{-24} \left[\frac{\text{cm}^2}{\text{b}} \right] = 0.6022141 \left[\frac{\text{atoms} \cdot \text{cm}^2}{\text{mol} \cdot \text{b}} \right]$$

Equation 12-2: Conversion applied to Avogadro's number to obtain proper units for use in Monte Carlo codes.

The atom density calculation for ^3He in the neutron proportional counter detector utilized Equation 12-1. The following demonstrates this calculation.

Known values:

$$\rho = 0.00067795 \left[\frac{\text{g}}{\text{cm}^3} \right]$$

$$N_A = 0.6022141 \left[\frac{\text{atoms} \cdot \text{cm}^2}{\text{b} \cdot \text{mol}} \right]$$

$$M(^3\text{He}) = 3.0160293 \left[\frac{\text{g}}{\text{mol}} \right]$$

the molar mass of ^3He is used because the proportional counter contains only ^3He .

$$\begin{aligned} N &= \frac{0.00067795 \left[\frac{\text{g}}{\text{cm}^3} \right] \cdot 0.6022141 \left[\frac{\text{atoms} \cdot \text{cm}^2}{\text{b} \cdot \text{mol}} \right]}{3.0160293 \left[\frac{\text{g}}{\text{mol}} \right]} \\ &= 1.353671 \times 10^{-4} \left[\frac{\text{atoms}}{\text{b} \cdot \text{cm}} \right] \end{aligned}$$

Equation 12-3: Example calculation of ^3He atom density in the neutron proportional counter detector.

For some atom density calculations use of the fundamental equation is insufficient. Inclusion of weight percent or isotopic abundance may be needed. The equation used to account for weight percent is

$$N_i = \frac{\omega_i \rho N_A}{100 M_i}$$

Equation 12-4: Atom density equation used when weight percent of individual components are known.

where N_i is the atom density for the i^{th} component of the material, M_i is the molecular weight of the i^{th} component, and $\frac{\omega_i}{100}$ is the weight percent.

If the weight percent of each component is not known or given, it may be calculated using the following equation.

$$\frac{\omega_i}{100} = \frac{mM_x}{mM_x + nM_y}$$

Equation 12-5: Equation for calculating weight percent of a molecule or alloy.

where m is the number of atoms of element x in the molecule or alloy, n is the number of atoms of element y in the molecule or alloy, M_x is the molecular weight of element x , and M_y is the molecular weight of element y .

The atom density calculation for hydrogen and carbon in the paraffin wax used in the neutron experiments is good example of using Equation 12-4. The manufacturer of the paraffin wax provided the weight percent of H and C, so it was not necessary to calculate these values.

Known values:

$$\rho = 0.92 \left[\frac{g}{cm^3} \right]$$

$$N_A = 0.6022141 \left[\frac{atoms \cdot cm^2}{b \cdot mol} \right]$$

$$M(H) = 1.00747 \left[\frac{g}{mol} \right]$$

$$\frac{\omega_H}{100} = 0.148605$$

$$M(C) = 12.011 \left[\frac{g}{mol} \right]$$

$$\frac{\omega_C}{100} = 0.851395$$

$$\begin{aligned} N_H &= \frac{0.148605 \cdot 0.92 \left[\frac{g}{cm^3} \right] \cdot 0.6022141 \left[\frac{atoms \cdot cm^2}{b \cdot mol} \right]}{1.00747 \left[\frac{g}{mol} \right]} \\ &= 0.0817222 \left[\frac{atoms}{b \cdot cm} \right] \end{aligned}$$

$$N_C = \frac{0.851395 \cdot 0.92 \left[\frac{g}{cm^3} \right] \cdot 0.6022141 \left[\frac{atoms \cdot cm^2}{b \cdot mol} \right]}{12.011 \left[\frac{g}{mol} \right]}$$

$$= 0.0392727 \left[\frac{atoms}{b \cdot cm} \right]$$

Equation 12-6: Example calculation of the hydrogen and carbon atom densities in paraffin wax.

When considering isotopic abundance in an atom density the following equation is used.

$$N_i = \frac{\gamma_i \rho N_A}{M}$$

Equation 12-7: Atom density equation when considering isotopic abundance.

where N_i is the atom density of the i^{th} isotope, γ_i is the isotopic abundance of the i^{th} isotope, and the other components are previously defined. Isotopic abundances can be found on the Chart of the Nuclides [53].

Borated polyethylene is used in both the gamma ray and neutron experiments as a shielding material. When calculating the atom densities for the gamma ray experiments weight percent of each element was used. However, boron is very important when neutrons are involved. The isotopic abundance of boron was considered for the atom densities in neutron models. First the atom density for atomic boron was determined based on the weight percent of boron in the borated polyethylene (not shown). Then the isotopic abundance was included.

Previously calculated:

$$N(B) = 0.0038993 \left[\frac{atom}{b \cdot cm} \right]$$

Known values:

$$\gamma(^{10}B) = 0.199$$

$$\gamma(^{11}B) = 0.801$$

$$N(^{10}B) = 0.199 \cdot 0.0038993 \left[\frac{atom}{b \cdot cm} \right]$$

$$= 0.0007760 \left[\frac{atom}{b \cdot cm} \right]$$

$$\begin{aligned}
N(^{11}\text{B}) &= 0.801 \cdot 0.0038993 \left[\text{atom}/\text{b} \cdot \text{cm} \right] \\
&= 0.0031233 \left[\text{atom}/\text{b} \cdot \text{cm} \right]
\end{aligned}$$

Equation 12-8: Example of atom density calculation considering isotopic abundance of boron in borated polyethylene.

12.3 Shielding Optimization

The following sections provide tables of atom densities used in the optimization simulations. The values for concrete, stainless steel, tungsten carbide, and borated polyethylene are based upon the general properties provided by the manufacturer rather than the specifically measured values for the experiments. This is because materials purchased to build a facility would not be identical to the materials purchased for the experiments.

12.3.1 Gamma-ray Models

The source used in the gamma-ray simulation is uranium dioxide, based on the materials used in the manufacture of typical fuel assemblies for the nuclear industry. Instead of making a detailed model of a fuel assembly the total mass of fuel was homogenized over the volume of a 17 x 17 Westinghouse assembly. The mass density for uranium dioxide was modified for this homogenization purposes from 10.96 g/cm³ to 5.485 g/cm³.

Table 12–XXVIII: Modified mass density uranium dioxide atom densities from the SCALE standard atom density tables.

Uranium Dioxide	Density = 5.485 g/cm ³	Atom Density
Oxygen – 16	8016	0.002440578
Oxygen – 17	8017	0.000009296786
Oxygen – 18	8018	0.00005015371
Uranium – 234	92234	0.0000006605612
Uranium – 235	92235	0.00008812375
Uranium – 238	92238	0.01214383

Table 12–XXIX: Regular concrete atom densities from standard composition.

Regular Concrete	Density = 2.30 g/cm ³	Atom Densities
Hydrogen	1000	0.013742
Oxygen	8000	0.046056
Sodium	11000	0.001747

Aluminum	13000	0.001745
Silicon	14000	0.016620
Calcium	20000	0.001521
Iron	26000	0.000347

Table 12–XXX: Borated polyethylene atom densities calculated from manufacturer provided density and abundances.

Borated Polyethylene (HD, 5% B)	Density = 1.40 g/cm ³	Atom Densities
Hydrogen	1000	0.1142039
Boron	5000	0.0038993
Carbon	6000	0.0571019

Table 12–XXXI: Tungsten carbide atom densities calculated from manufacturer provided density and abundances.

Tungsten Carbide	Density = 14.93 g/cm ³	Atom Densities
Carbon	6000	0.0429698
Oxygen	8000	0.0008429
Vanadium	23000	0.0002647
Iron	26000	0.0001610
Cobalt	27000	0.0091538
Tungsten	74000	0.0429698

Table 12–XXXII: Stainless steel 304 atom densities from standard composition.

Stainless Steel 304	Density = 8.03 g/cm ³	Atom Densities
Carbon	6000	0.000160
Silicon	14000	0.000858
Phosphorus	15000	0.000036
Sulfur	16000	0.000023
Chromium	24000	0.017605
Manganese	25000	0.000877
Iron	26000	0.060538
Nickel	28000	0.007593

Table 12–XXXIII: Aluminum atom densities from standard composition.

Aluminum	Density = 2.6989 g/cm ³	Atom Densities
Aluminum	13000	0.060238

Table 12–XXXIV: Sodium iodide atom densities calculated from information provided by the manufacturer.

Sodium Iodide (TI)	Density = 3.76 g/cm ³	Atom Densities
Sodium	11000	0.0150794
Iodine	53000	0.0150794

Thallium	81000	0.0000196
----------	-------	-----------

Table 12–XXXV: Mu metal atom densities determined from weight fractions given by www.mumetal.com/mumetal-specifications.php

Mu Metal	Density = 8.747 g/cm ³	Atom Densities
Carbon	6000	0.0000877
Silicon	14000	0.0006564
Manganese	25000	0.0004794
Iron	26000	0.0140827
Nickel	28000	0.0717977
Molybdenum	42000	0.0023060

Table 12–XXXVI: Argon gas atom densities from standard composition.

Argon	Density = 0.001662 g/cm ³	Atom Densities
Argon	18000	0.000025

Table 12–XXXVII: Dry air atom densities from standard composition.

Dry Air	Density = 0.001225 g/cm ³	Atom Densities
Nitrogen	7000	0.000039
Oxygen	8000	0.000011

12.3.2 Neutron Models

Similar to the neutron simulations of the experiments isotopic density modifications were made to standard compositions to make sure MCNP was using the most current ENDF cross sections. Unlike the photon optimization the updated atom densities, based upon measured values, were used for borated polyethylene and tungsten carbide.

The source for the neutron optimization simulation is considered to be plutonium. The mass of plutonium was calculated in a SCALE/ORIGEN depletion analysis. This mass was converted to a mass of plutonium oxide and then used in conjunction with the density of PuO₂ to calculate the volume of a sphere. All other material from the fuel bundle was arbitrarily removed affording a more severe case of a criticality; for example, no self-shielding. The plutonium dioxide atom densities were obtained from the Compendium [46].

Table 12–XXXVIII: Plutonium dioxide atom densities from standard composition modified for isotopic abundance.

Plutonium Dioxide	Density = 11.46 g/cm ³	Atom Density
Oxygen – 16	8016	0.050910
Plutonium – 238	94238	0.000013
Plutonium – 239	94239	0.023807
Plutonium – 240	94240	0.001521
Plutonium – 241	94241	0.000101
Plutonium – 242	94242	0.000013

Table 12–XXXIX: Regular concrete atom densities from standard composition modified for isotopic abundance.

Regular Concrete	Density = 2.30 g/cm ³	Atom Density
Hydrogen	1001	0.0137404197
	1002	0.0000015803
Oxygen	8016	0.0460382693
	8017	0.0000175372
Sodium	11023	0.001747
Aluminum	13027	0.001745
Silicon	14028	0.0153285761
	14029	0.0007783478
	14030	0.0005130926
Calcium	20040	0.0014744726
	20042	0.0000098409
	20043	0.0000020534
	20044	0.0000317271
	20046	0.0000000608
	20048	0.0000028443
Iron	26054	0.0000202822
	26056	0.0003183864
	26057	0.0000073529
	26058	0.0000009785

Table 12–XL: Borated polyethylene atom densities calculated from measured density and modified for isotopic abundances.

Borated Polyethylene (HD, 5% B)	Density = 1.4783 g/cm ³	Atom Density
Hydrogen	1001	0.1205772320
	1002	0.0000138680
Boron – 10	5010	0.0008194
Boron – 11	5011	0.0032980
Carbon	6000	0.0602956

Table 12–XLI: Tungsten carbide atom densities calculated from measured density and modified for isotopic abundances.

Tungsten Carbide	Density = 14.842 g/cm ³	Atom Density
------------------	------------------------------------	--------------

Carbon	6000	0.0427165
Oxygen	8016	0.0008376774
	8017	0.0000003191
Vanadium – 50	23050	0.0000006
Vanadium – 51	23051	0.0002625
Iron – 54	26054	0.0000094
Iron – 56	26056	0.0001468
Iron – 57	26057	0.0000034
Iron – 58	26058	0.0000004
Cobalt – 59	27059	0.0090999
Tungsten – 180	74180	0.0000512
Tungsten – 182	74182	0.0113199
Tungsten – 183	74183	0.0061127
Tungsten – 184	74184	0.0130883
Tungsten – 186	74186	0.0121443

Table 12–XLII: Stainless steel 304 atom densities from standard composition modified for isotopic abundance.

Stainless Steel 304	Density = 8.03 g/cm ³	Atom Density
Carbon	6000	0.000160
Silicon	14028	0.0007913308
	14029	0.0000401819
	14030	0.0000264882
Phosphorus	15031	0.000036
Sulfur	16032	0.0000218339
	16033	0.0000001748
	16034	0.0000009867
	16036	0.0000000046
Chromium	24050	0.0007649373
	24052	0.0147510535
	24053	0.0016726511
	24054	0.0004163583
Manganese	25055	0.000877
Iron	26054	0.0035384461
	26056	0.0555460365
	26057	0.0012828002
	26058	0.0001707172
Nickel	28058	0.0051690790
	28060	0.0019911200
	28061	0.0000865526
	28062	0.0002759676
	28064	0.0000702808

Table 12–XLIII: ^3He atom densities based upon manufacturer provided data and modified for isotopic abundances.

Helium – 3 (4 atm) 2% CO ₂	Density = 0.000622 g/cm ³	Atom Density
Helium – 3	2003	0.0001326651
Carbon	6000	0.0000074934
Oxygen	8016	0.0000112457
	8017	0.0000000043

Table 12–XLIV: Dry air atom densities from standard composition modified for isotopic abundance.

Dry Air	Density = 0.001225 g/cm ³	Atom Density
Nitrogen	7014	0.0000388565
	7015	0.0000001435
Oxygen	8016	0.0000109958
	8017	0.0000000042

Table 12–XLV: Argon atom densities from standard composition modified for isotopic abundance.

Argon	Density = 0.001662 g/cm ³	Atom Density
Argon	18036	0.0000000834
	18038	0.0000000157
	18040	0.0000249009

13 Appendix B: Shielding Material Information

This appendix contains all of the material data provided by the manufacturers.

13.1 Concrete

This concrete was made in-house at ISU. The specifications for material mix are provided in Table 13–I.

Table 13–I: Concrete made in-house at ISU for shielding material.

CONCRETE MIX DESIGN						
	Volume (ft ³)	Weight (lbs)	4x4x3 Bricks			
			Volume (ft ³)	Weight (lbs)	Total Weight (4 bricks)	Total Weight (+30%)
Air	0.0555		0.00154			
Water	0.1722	11.5540	0.0048	0.3209	1.2838	1.6689
Cement	0.1393	24.6250	0.0039	0.6840	2.7361	3.5569
CA	0.3926	64.6741	0.0109	1.7965	7.1860	9.3418
FA	0.2407	39.3582	0.0067	1.0933	4.3731	5.6851
Total	1.0003	140.3734	0.0278	3.8948	15.5790	20.2528
w/c	0.47		0.47			

Specimen Size	Length (ft)	Width (ft)	Thickness (ft)	Volume (ft ³)
4x4x3 Brick	0.33	0.33	0.2500	0.0278

Table 13–II: Mass, dimensions, and density of the concrete blocks made in-house for shielding.

Brick	Mass (g)	Length (cm)	Width (cm)	Height (cm)	Density (g/cm ³)
1	1938.9 ± 0.1	10.622 ± 0.001	10.309 ± 0.001	7.489 ± 0.001	2.3643 ± 0.0001
2	2004.6 ± 0.1	10.662 ± 0.001	10.298 ± 0.001	7.811 ± 0.001	2.3462 ± 0.0001
3	1945.8 ± 0.1	10.606 ± 0.001	10.305 ± 0.001	7.590 ± 0.001	2.3456 ± 0.0001
4	1970.1 ± 0.1	10.589 ± 0.001	10.311 ± 0.001	7.754 ± 0.001	2.3256 ± 0.0001

13.2 Stainless steel 304 (McMaster Carr)

\$10.19 Each

Item #: 8983K118 <https://www.mcmaster.com/#8983k118/=1chhpcq>

Table 13–III: Stainless steel properties

Material	304 Stainless Steel	Density	0.29 lbs./cu. in.
Cross Section Shape	Rectangle	Surface Resistivity	469 ohm-cir. mil/ft.
Construction	Solid	Melting Point Temperature	2400° F
Appearance	Plain	Modulus of Elasticity	28 ksi $\times 10^3$
Thickness	0.12"	Thermal Conductivity	100 Btu/hr. \times in./sq. ft./°F @ 212° F
Thickness Tolerance	-0.007" to 0.007"	Elongation	50%
Tolerance Rating	Standard	Material Composition	
Width	6"	Iron	53.48-74.5%
Width Tolerance	-1/8" to 1/8"	Carbon	0-0.08%
Length	6"	Chromium	17.5-24%
Length Tolerance	-1/8" to 1/8"	Cobalt	0-0.29%
Yield Strength	30,000 psi	Copper	0-1%
Fabrication	Cold Worked	Manganese	0-2%
Hardness	Rockwell B80 (Medium)	Molybdenum	0-2.5%
Temper Rating	Softened (Annealed)	Nickel	8-15%
Heat Treatable	No	Nitrogen	0-0.1%
Min. Temperature	Not Rated	Phosphorus	0-0.2%
Maximum Temperature	1500° F	Silicon	0-1%
Specifications Met	ASTM A240	Sulfur	0-0.35%
Flatness Tolerance	Not Rated		

13.3 Borated Polyethylene (ShieldWerx)

The borated polyethylene used in this work was model SWX-207HD5-U. The specification sheet can be found at [http://www.shieldwerx.com/assets/swx-207hd\(5\).pdf](http://www.shieldwerx.com/assets/swx-207hd(5).pdf)


NEUTRON SHIELDING

SWX-207HD & 207HD5

Self-Extinguishing Borated Polyethylene

Specifications

Composition Data	207HD	207HD5
Hydrogen atom density / cm ³ :	6.10×10^{22}	6.35×10^{22}
Hydrogen weight percent:	6.01 %	6.65 %
Hydrogen natural isotope distribution:	99.98 % ¹ H	99.98 % ¹ H
Boron atom density / cm ³ :	8.14×10^{20}	4.19×10^{21}
Boron natural isotope distribution:	19.6 % ¹⁰ B & 80.4 % ¹¹ B	19.6 % ¹⁰ B & 80.4 % ¹¹ B
Boron weight percent:	0.86 %	4.71 %
Total Density:	1.70 g / cm ³ (106 lbs / ft ³)	1.60 g / cm ³ (99.8 lbs / ft ³)
Radiation Properties		
Macroscopic thermal neutron cross section:	0.64 (cm ⁻¹)	3.19 (cm ⁻¹)
Gamma resistance:	5×10^8 rad	5×10^8 rad
Neutron resistance:	2.5×10^{17} n/cm ²	2.5×10^{17} n/cm ²
Physical Properties		
State:	Sheets, bricks	Sheets, bricks
Color:	Grey/Tan	Grey/Black
Odor:	No odor	No odor
Machinability:	Excellent	Excellent
Thermal Properties		
Recommended Temperature Limit:	200 °F (93.3 °C)	200 °F (93.3 °C)
Chemical Properties		
Chemical Name & Synonyms:	Borated Polyethylene	Borated Polyethylene
Trade Name & Synonyms:	SWX-207HD	SWX-207HD5
Chemical Family:	Polyolefins	Polyolefins
Formula:	Mixture (CH ²) _n , B	Mixture (CH ²) _n , B
Solubility in Water:	Negligible	Negligible



A Division of Bladewerx LLC

4529 Arrowhead Ridge Dr. SE
Rio Rancho, New Mexico 87124
United States of America
Phone: +01.505.892.5144
Fax: +01.505.890.8319
Email: sales@shieldwerx.com
Data Sheet Revision: Nov 2015

Figure 13-1 Borated polyethylene specification sheet from ShieldWerx.

13.4 Tungsten Carbide (H. B Carbide)



H.B. Carbide Company
A Subsidiary of Star Cutter Company
4210 Doyle Drive - Lewiston, MI 49756
Phone: (800) 459-8521 / (989) 786-4223
Fax: (800) 459-8547 / (989) 786-4494

Material Lot Certification

Order Details:

Customer: Idaho State University / School of Engineering
H.B. Shop Order Reference: J000288167- 0
H.B. Order Reference: SHB0097844-1
Customer Order Number: VERBAL
Tool Number: .125" x 4" x 4" Flat Stock
Grade: HB-2
Number of Pieces: 8
Lot Number: j00028617800001

Physical Properties:

A Porosity: 00
B Porosity: 00
C Porosity: 00
HB-Density (g/cc) : 14.93
HB-Grain Size (Micron): 1.5
HB-Hardness (ASTM): 92.10
Transverse Rupture Strength (PSI): 530,000

Chemical Properties:

Cobalt (%): 6
Others (%): 0.1 - 0.5
Tungsten Carbide (%): BALANCE
Tantalum Carbide (%) : NONE
Titanium Carbide (%): NONE

*This is to certify that the above mentioned pieces have been inspected, tested,
and conform to relevant H.B. Carbide and customer specifications.*

Signed: Kurt Hutchison

Figure 13-2 Tungsten carbide specification sheet from H B Carbide.

Other (%) were provided as vanadium (0.15%), oxygen (0.15%), and iron (0.1%).

14 Appendix C: Current Source Strengths and Source Certificates

Two radiation sources were used for the experiments. One was a gamma ray emitter, cesium-137 (^{137}Cs) and the other was a neutron emitter, americium-241/beryllium ($^{241}\text{Am/Be}$). In order to convert the Monte Carlo results to match the values measured in the experiments the results must be multiplied by the current emission rate of the source used. The following calculations determine the current emission rates.

The equation for determining the current strength is

$$I(t) = \gamma \cdot A(t) = \gamma \cdot A(0)e^{\frac{-\ln(2) \cdot t}{t_{1/2}}}$$

Equation 14-1: Decay equation for determining current activity.

where $I(t) \left[\frac{\text{particles}}{\text{s}} \right]$ is the current particle emission rate $A(t)$ [Bq or Ci] is the current activity, $A(0)$ [Bq or Ci] is the original activity, $t_{1/2}$ is the half life, t is the amount of time from the original assay to the date of experimentation, and γ is the particle yield. Both half life and time need to be in the same units. Both calculations used years. The units of activity depend on γ .

14.1 Current Gamma Ray Emission Rate

Known values:

$$\gamma = 0.8510 \left[\frac{\gamma}{\text{disintegration}} \right]$$

$$A(0) = 3.7 \times 10^7 \text{ [Bq]} = 3.7 \times 10^7 \text{ [disintegrations/s]}$$


$$t_{1/2} = 30.07 \text{ [y]}$$

$$t = 1.670089 \text{ [y]}$$

$$I(t) = 0.8510 \left[\frac{\gamma}{d} \right] \cdot 3.7 \times 10^7 \left[\frac{d}{s} \right] \cdot e^{\frac{-\ln(2) \cdot 1.670089 \text{ [y]}}{30.07 \text{ [y]}}} = 3.02979 \times 10^7 \left[\frac{\gamma}{s} \right]$$

Equation 14-2: Calculation of current gamma emission rate from the ^{137}Cs source.

14.2 ^{137}Cs Certificate



Eckert & Ziegler
Isotope Products

24937 Avenue Tibbitts
Valencia, California 91355

Tel 661•309•1010
Fax 661•257•8303

NOMINAL SOURCE CERTIFICATE

Customer: Idaho State University
Purchase Order No.: P0019693
Model No.: 193
Catalog No.: CS73011/40001M
Capsule Type: A3011-4-1
Active Diameter: 0.125" (3.18 mm)
Cover: Stainless Steel
Backing: Stainless Steel

Certificate Date: 10-Feb-16
Quantity: 1
SS&DR No.: CA0406S126S
ISO/ANSI Classification: ANSI 77C86545
Special Form No.: USA/0353/S-96 Rev 8
Nuclide Half Life: 30.17 ± 0.16 years
Recommended Working Life: 15 years

Nuclide	Source No.	Activity	Radiation Output	Reference Date
Cs-137	N3-540	1 mCi (37 MBq)	Not Applicable	1-Mar-16


Impurities: None detected.

Leak Test Information is on Reverse Side:

Remarks:

- This document uses the numerical convention where 1.000 = 1 and 1,000 = 10³.
- Nuclear data were taken from IAEA-TECDOC-619, 1991.
- ANSI classification is equivalent to ISO2919.

Matthew Dey
Name


Signature

16 Feb 16
Date

Notebook Page: 1854-48

Medical Imaging Laboratory

24937 Avenue Tibbitts Valencia, California 91355

ISO 9001 CERTIFIED

Industrial Gauging Laboratory

1800 North Keystone Street Burbank, California 91504

Figure 14-1 A copy of the 1 mCi ^{137}Cs source certificate.

14.3 AmBe Certificate

07/26/69 09:37 FAX 5262548 RESL 001					
MONSANTO RESEARCH CORPORATION A SUBSIDIARY OF MONSANTO CHEMICAL COMPANY NUCLEAR SOURCES DEPARTMENT 1818 NICHOLAS ROAD DAYTON, OHIO					
Mail Address: Station B, Dayton 7, Ohio	Phone 202-5461- Area Code 513				
TO <div style="border: 1px solid black; padding: 5px; margin: 5px;"> FISCAL SECTION P.O. BOX 2067 IDAHO FALLS, IDAHO 83401 P.O. C-3266 </div>	<div style="border: 1px solid black; padding: 5px; margin: 5px;"> SHIPPING DATA FORM DATE OF CALIBRATION AND SHIPMENT <div style="text-align: center; font-weight: bold;">8-25-65</div> <table border="1" style="width: 100%; border-collapse: collapse;"> <tr> <td style="width: 50%;">VIA</td> <td style="width: 50%;">S/L NUMBER</td> </tr> <tr> <td style="text-align: center;">MOTOR FREIGHT</td> <td style="text-align: center;">03120</td> </tr> </table> SHIPPING ADDRESS: PHILLIPS PETROLEUM CO. ATOMIC ENERGY DIVISION CENTRAL FACILITIES WAREHOUSE NATIONAL REACTOR TESTING STATION SCOVILLE, IDAHO </div>	VIA	S/L NUMBER	MOTOR FREIGHT	03120
VIA	S/L NUMBER				
MOTOR FREIGHT	03120				
MONSANTO RESEARCH CORPORATION LICENSE NUMBER SNM-567					
Accountability data					
License No. NR	S. S. Allotment Quota No.				
Remarks:					
Monsanto Research Corporation Customer P. O. No. C-3266 Nuclear Source No. MRC-N-SS-W-AmBe-262 Job No. 3					
Type of source Americium-beryllium Neutron Source					
Amount and chemical form of isotope	14.0 g Am				
Weight and composition of target (in neutron sources)	57.6 gm Be				
Emission rate	1.02×10^8 n/sec				
Max. energy of emitted alpha or beta particles					
Source container description material:	dimensions: 1.0 x 4.5 1.06 x 4.65				
304 stainless steel alpha or beta source cover material:	cover thickness: 1.145 x 5.0 1.40 x 5.25				
Shipping container description:	75-gal paraffin-filled drum N-130				
Remarks:	SOURCE \$ 2700.00 Value of shipping container \$ 150.00(N-13) Total price of source \$ 2850.00 MONSANTO RESEARCH CORPORATION By <u>J.L. Richmond</u> Title Manager, Nuclear Source Date 26 August 1965				

Figure 14-2 A copy of the AmBe source certificate – page 1 of 4. Source strength specifications.

	gender	no. of cases	%
male	60	78.9%	
female	16	21.1%	

157

SOURCE EQUIPMENT SURVEY RECORD

Date 8-25-65
 Type of source(s) in container AmBe No. of sources 1
 Type of radiation emitted gamma Shielding material Pb
 Shipping container: Drum Steel pot Other Other
 Size of container 15 gal Container No. N-130
 Carrier: REA Air Express Motor Freight ✓ Air Freight Other

Source Data

Source No.	Neutron flux (n/sec)	Curie Value	Wipe (μ c)
<u>MBC-N-33-N-130</u>	<u>262</u>	<u>1.02Y10⁸</u>	<u>46.6</u>
			<u>6.4X10⁻⁶</u>

Total 46.6

Neutron and Gamma Survey

	Surface	1 meter
Fast neutron (n/cm ² /sec)	<u>100</u>	<u>1.18</u> mrad/hr
Gamma (mr/hr)	<u>18</u>	<u>2.0</u> mrad/hr
Total	<u>118</u> mrad/hr	<u>2.55</u> mrad/hr

Shipping Container Survey

Outer surfaces	(μ c wipe)	Center pipe(s) or pipe nipple	Holder(s)
<u>2.7X10⁻⁶</u>	<u>-</u>	<u>0</u>	<u>8.2X10⁻⁶</u>

Direct: All direct readings are less than 1000 disintegrations per minute

Survey Instruments Used

Direct alpha - Eberline PAC 15A
 Gamma - Jordan AGB-50B-SR
 Fast neutron - Eberline FN-1A

Health Instructions Enclosed ☒
 Container Properly Labelled ☒

Shipment approved by:

L. Campbell
 Health Physics

• MONSANTO RESEARCH CORPORATION •

Figure 14-4 A copy of the AmBe source certificate – page 3 of 4. Shipment survey record.

-2-

The above described sources have been calibrated within the deep well configuration used for routine instrument calibration utilizing a Victoreen R-Meter Model 70 certified by the NBS to an uncertainty of $\pm 5\%$.

3. Americium-241 Beryllium-9 Neutron Source

Source Description as certified by the manufactures certificate*

Source number - MRC-W-55-W-AmBe-262

Amount of Isotope - 14.0 g Am

Weight and Composition of target - 57.6 g Be

Emission Rate - 1.02×10^6 n/sec

Date of Calibration - 8/25/65

Half-life - 458.1 years

*Monsanto Research Corp.

Figure 14-5 A copy of the AmBe source certificate – page 4 of 4. Source description summary.

14.4 Current Neutron Emission Rate

Known values:

$$\gamma = 2.20 \times 10^6 \left[\frac{\eta}{s \cdot Ci} \right]$$

$$A(0) = 47.6 [Ci]$$

$$t_{1/2} = 432.2 [yr]$$

$$t = 50.846 [yr]$$

$$I(t) = 2.20 \times 10^6 \left[\frac{\eta}{s \cdot Ci} \right] \cdot 47.6 [Ci] \cdot e^{\frac{-\ln(2) \cdot 50.846 [yr]}{432.2 [yr]}} = 9.65195 \times 10^7 \left[\frac{\eta}{s} \right]$$

Equation 14-3: Calculation of the current neutron emission rate from the $^{241}\text{Am}/\text{Be}$ source.

15 Appendix D: Detector Data Sheets

15.1 NaI(Tl) Scintillation Detector for Gamma-Rays

Standard Assemblies

Saint-Gobain Crystals offers four basic detector designs: a packaged scintillator, a scintillator integrally mounted to a light-sensing device [such as a photomultiplier tube (PMT)], a scintillator with a demountable PMT and a scintillator array. Each of those basic detector configurations can be designed with one or more of the various options listed. To discuss which options may suit your application, contact our customer service department.

Basic Packaged Scintillator -

The packaged scintillator is a scintillation crystal mounted in a low-mass metal container (usually aluminum). For NaI(Tl) and other hygroscopic crystals, the package is hermetically sealed. Reflector material is placed between the scintillator and the container walls. An optical window is incorporated into one end. A wide variety of sizes and shapes (including cylindrical and rectangular) can be produced. This type of detector requires a user-supplied, externally-coupled light-sensing device.

Packaged scintillators are appropriate for certain experimental or manufacturing situations where different scintillator-PMT combinations may be required on a regular basis.

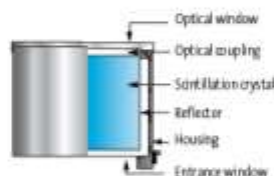


Illustration of Basic Packaged Scintillator

Integrally Mounted Scintillator/Light-sensing Device Assembly -

In this integral design, the light-sensing device (usually a PMT) is optically coupled directly to the scintillator. The scintillator is mounted in a container (usually aluminum) and a mu-metal shield is fitted over the PMT. The detector package is hermetically sealed when a hygroscopic scintillator, such as NaI(Tl), is used. The scintillator container and mu-metal shield are sealed together to form a low-mass and light-tight housing for the detector.

This design usually yields better and more consistent energy resolution. Therefore, these are the detectors of choice for spectroscopy and radioisotope assay.

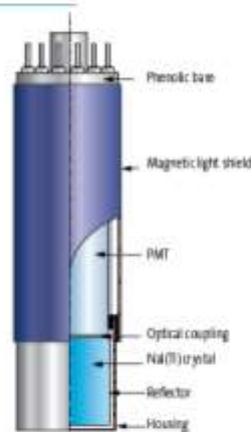


Illustration of Integrally Mounted Scintillator/PMT Assembly



Detector Assembly Options -

- Rectangular and other shapes
- Light-sensing device selection
- Integrated, low-background voltage divider and preamplifier bases
- Thin aluminum or beryllium radiation entrance windows
- Special flanges, O-rings, mounting fixtures or other modifications
- End well and transversal well geometries
- Low background stainless steel or copper containers and other components

Figure 15-1 Sodium Iodide detector overview provided by Saint Gobain Crystals.[55]

Nal(Tl) and Polyscin® Nal(Tl) Sodium Iodide Scintillation Material

Of all available scintillators, Nal(Tl) is the most extensively used material. Nal(Tl) has a very high luminescence (scintillation) efficiency and is available in single crystal or polycrystalline forms in a wide variety of sizes and geometries. The material exhibits no significant self-absorption of the scintillation light.

Single Crystal Nal(Tl) -

Figure 1 shows the emission spectrum of Nal(Tl). The emission maximum is well matched to the sensitivity curve of photomultiplier tubes (PMTs) with alkali photocathodes.

Nal(Tl) produces one of the highest signals in a PMT per amount of radiation absorbed. It is second only to our BrilLanCe®380 scintillator. Under optimum conditions, an average of 1×10^4 photoelectrons are produced per MeV γ -rays.

The relation between the scintillation intensity and the temperature is shown in Figure 2 for two main amplifier shaping times. For most applications, a 1 μ s shaping time is used for temperatures around room temperature and above. The small difference in PH between the 1 μ s and 12 μ s shaping times does not affect energy resolution for these temperatures.

Nal(Tl) exhibits several decay time constant components. The primary single exponential decay constant is 250ns at room temperature. As the temperature increases, the longer time constant components decrease in intensity and the 1 μ s and 12 μ s response curves become identical (Figure 2). The relation between the effective decay time and the temperature is presented in Figure 3. [IEEE NSS NS-30, 380 (1983)].

Nal(Tl) is susceptible to radiation damage, i.e. prolonged exposure to intense radiation degrades the scintillation performance. Radiation damage has been observed above levels of 1 Gray (10^2 rad). The crystal should not be exposed to ultraviolet radiation from fluorescent lamps or sunlight.

Scintillation crystals of Nal(Tl) are routinely grown with a potassium content of less than 0.5 ppm, and are appropriate for low background applications.

Nal(Tl) crystals are widely used for radiation detection: in nuclear medicine, for environmental monitoring, in nuclear physics, aerial survey, well logging and in many other applications.

Properties

Density [g/cm ³]	3.67
Melting point [K]	924
Thermal expansion coefficient [C ⁻¹]	47.4×10^{-6}
Cleavage plane	<100>
Hardness (Mho)	2
Hygroscopic	yes
Wavelength of emission max [nm]	415
Refractive index @ emission max.	1.85
Primary decay time [ns]	250
Light yield [photons/keV γ]	38
Temperature coefficient of light yield	-0.3%/C ^o

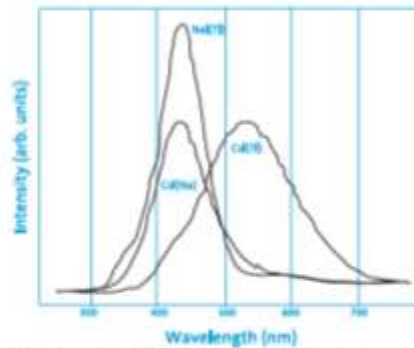


Figure 1. Scintillation emission spectrum of Nal(Tl) and other scintillation materials (1990)

CRYSTALS

SAINT-GOBAIN

Nal(Tl) Sodium Iodide Scintillation Material

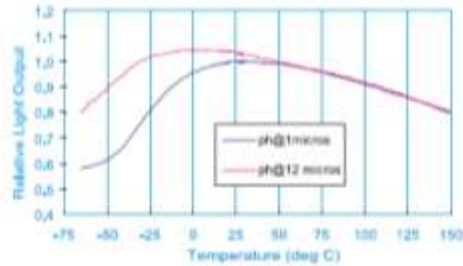


Figure 2. Temperature response of Nal(Tl)

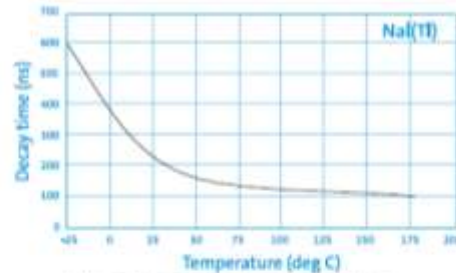


Figure 3. Temperature dependence of the decay time of Nal(Tl)

Polyscin® Nal(Tl) -

Polyscin® Nal(Tl) crystals are widely recognized as suitable alternatives to single crystal scintillators in many applications where thermal and mechanical shock are encountered. This crystal offers ruggedness combined with a scintillation performance identical to single crystal Nal(Tl). Current applications include aerospace research, oil well logging, geophysical survey and radiation environmental monitoring.

The polycrystalline structure of Polyscin® Nal(Tl) is derived from a unique manufacturing process in which single crystal ingots are recrystallized under heat and pressure. The resulting material may be characterized as a polycrystalline material with randomly oriented crystal grains in a mosaic structure. The density of Nal is not changed in the process. The characteristic improves mechanical strength but has no effect on the scintillation performance since the material is optically equivalent to single crystal Nal(Tl).

Any fractures produced by thermal or mechanical shock in Polyscin® Nal(Tl) are normally blocked or confined to the small local volumes called grains. Because the cleavage planes of the grains are randomly oriented, it is unlikely that a small fracture would propagate across the grain

boundaries. This makes Polyscin® Nal(Tl) the material of choice where ruggedness is important, such as well logging, MWD and aerospace applications.

In contrast, single crystals can cleave along <100> planes under similar shock conditions. In a detector assembly fabricated from single crystal material, even a small crack may propagate along the entire crystal, interfering with the light collection and degrading the pulse height resolution.

Another feature of Polyscin® Nal(Tl) is the possibility to manufacture complicated detector geometries directly without extensive machining. Special geometries currently offered include hexagonal, square and rectangular detector assemblies and large diameter slabs.

Polyscin® Nal(Tl) has been used to construct long crystals of $10 \times 10 \times 100\text{cm}^3$ ($4'' \times 4'' \times 40''$) and large flat crystals of $60\text{cm} \times 90\text{cm}$ area ($24'' \times 36''$). The use of long continuous bars eliminates the discontinuity encountered by interfacing two or more shorter crystals, improving the scintillation characteristics. Long crystals may be used as position sensitive detectors while at the same time providing spectroscopic data. Detectors of this kind have been fabricated in steel and low background aluminum housings.



Manufacturer reserves the right to alter specifications.
©2005-2016 Saint-Gobain Ceramics & Plastics, Inc. All rights reserved.

(08-16)

Figure 15-3 Information regarding Nal(Tl) detectors. Page 2 of 2.

15.2 ^3He Proportional Counting Detector for Neutrons

Sales Specifications

Model Number: SA- P4-0812-217

Rev:

NC

HE-3 NEUTRON DETECTOR

Mechanical

Maximum diameter: SEE DRAWING
Maximum overall length: SEE DRAWING
Connector Type: HN

Material

Body Material: 304 S.S.
Connector Material: BRASS, SILVER PLATED
Connector Insulator: TEFLON
Internal Insulator: ALUMINA CERAMIC
Coating Material: NONE
Primary Gas: He-3
Total Pressure: 60 psia (0.41 MPa)

Electrical

Resistance : 1.00E+12 ohms
Capacitance: 10 pF±20%

Maximum Ratings

Maximum Voltage: 2000 volts
Maximum Temperature: 175 °C

Operating Characteristics

Thermal neutron flux range: 1.30E-04 to 1.30E+03 nv
Thermal neutron sensitivity: 38 cps/nv ± %
Voltage Range: 1000 to 1500 volts
Resolution (FWHM): < 10 %
Temperature range: -25 °C to 150 °C

GE Reuter-Stokes reserves the right to
improve or modify designs and/or
specifications without notice.

29-Oct-10

GE PROPRIETARY AND CONFIDENTIAL, UNCONTROLLED WHEN PRINTED OR TRANSMITTED ELECTRONICALLY

Figure 15-5 Model P4-0812-217 He-3 detector specifications provided by GE Reuter Stokes.

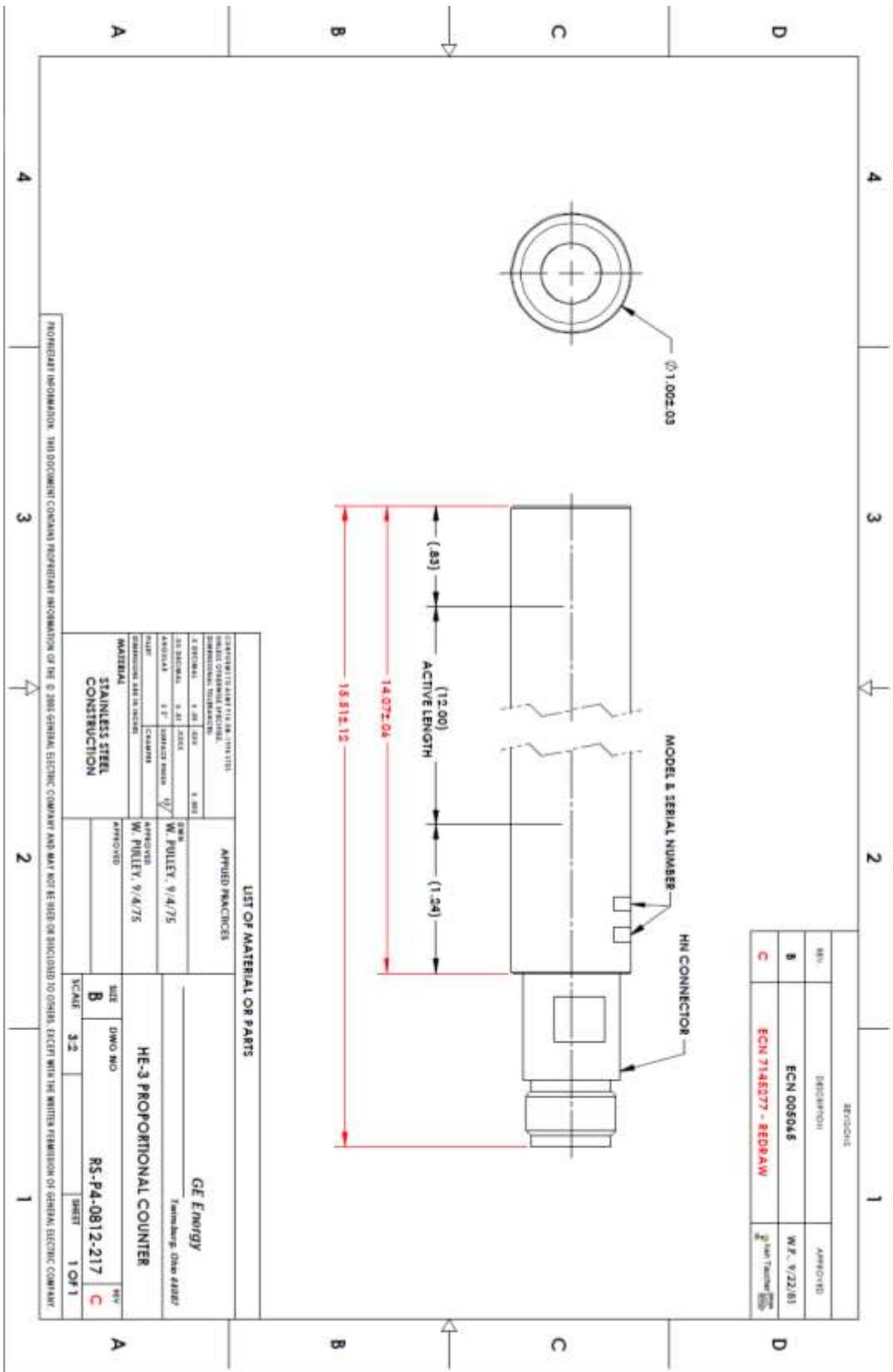


Figure 15-6 Model P4-0812-217 GE Reuter Stokes ³He detector diagram. Provided by Ge Reuter Stokes.

16 Appendix E: Point Kernel Hand Calculation Example

A set of contrived shielding geometries were selected to compare point kernel calculations to Monte Carlo computations using both MCNP and SCALE. These comparisons were multifaceted in purpose. The comparisons aided in teaching Monte Carlo input file design skills, offered confidence to the experimenter, and aided in developing experimental parameters and limits.

The basic geometry of the contrived problem consists of a point source at the center of a shield of 20 cm radius, a small volume or point detector placed 100 cm from the source. Four shielding materials were investigated; aluminum, iron, lead, and concrete. The source strength was set to be 1 Curie and the photon energy emitted was set to 1 MeV. The atmosphere was assumed a basic mixture of nitrogen and oxygen. A representation of the geometry is shown in Figure 16-1. A step by step description of and an example of the point kernel calculation for aluminum follows. The density of aluminum was set to 2.702 g/cm^3 and the density of air was set to 0.001205 g/cm^3 . Mass attenuation values were obtained from five sources Health Physics and Radiological Health Handbook (HPRH) [48], National Institute of Standards and Technology (NIST) [49], Fundamentals of Nuclear Science and Engineering [51], Introduction to Nuclear Engineering [36], and Radiological Health Handbook (RHH) [50]. The linear attenuation coefficient was calculated from the mass attenuation coefficient and the density. The flux at the edge of the shield and then at the detector was calculated using the linear attenuation coefficient, activity of the source, and distances from the source. The particle fluence rate was calculated from the particle flux. This particle fluence rate is comparable to the uncollided flux from a Monte Carlo next event point detector, such as the F5 tally in MCNP. The total particle fluence rate is then calculated from the particle fluence rate using extrapolated build up factors from both HPRH [48] and Introduction to Nuclear Engineering [36]. The total particle fluence rate was compared to the total flux from tallies

in both MCNP and SCALE. These tallies were cell track length estimators such as a MCNP F4 tally and next event point detectors.

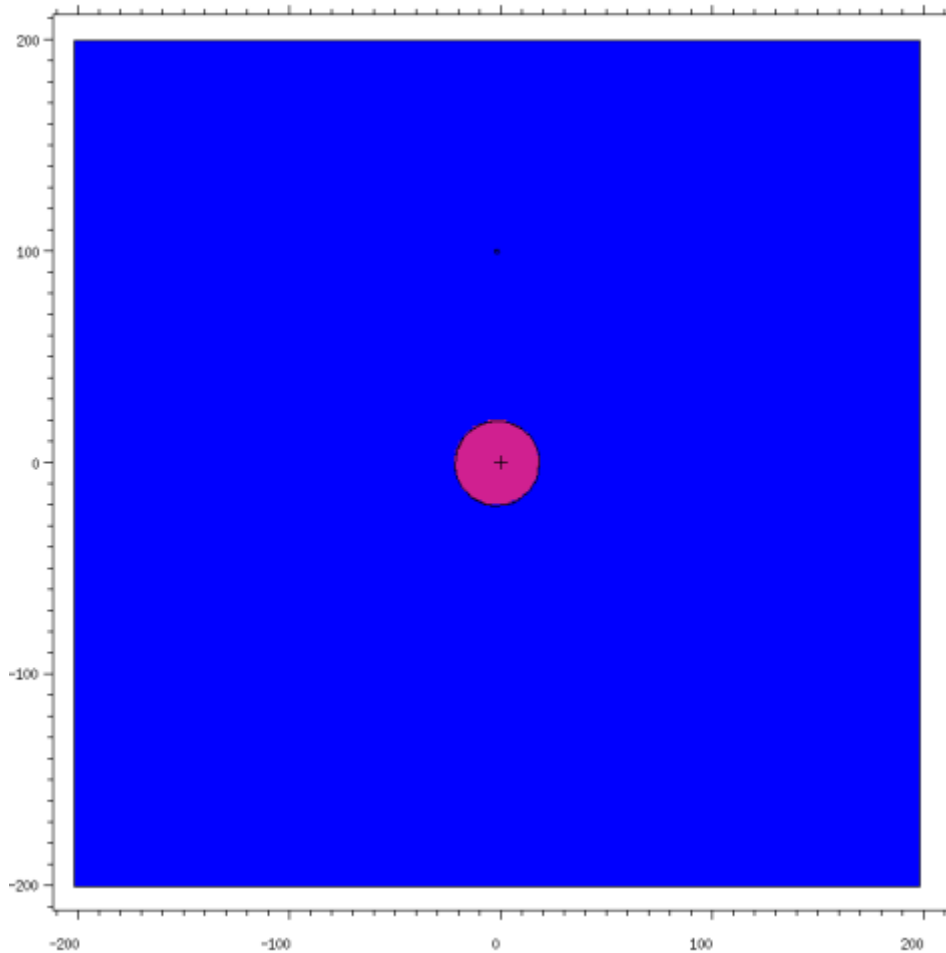


Figure 16-1 Elevation plot of the MCNP geometry used in the code verification of the point kernel calculations. It provides a graphical representation of the contrived problem.

EXAMPLE:

Calculated values will be shown for HPRH and Lamarsh.

Given quantities:

Aluminum density (ρ) = 2.703 g/cm³

Air density (ρ) = 0.001205 g/cm³

Aluminum mass attenuation coefficients (μ/ρ)

HPRH = 6.146×10^{-2} cm²/g

Lamarsh = 6.140×10^{-2} cm²/g

Air mass attenuation coefficients (μ/ρ)

$$\text{HPRH} = 6.358 \times 10^{-2} \text{ cm}^2/\text{g}$$

$$\text{Lamarsh} = 6.360 \times 10^{-2} \text{ cm}^2/\text{g}$$

Aluminum buildup factors (B)

$$\text{HPRH} = 8.9743$$

$$\text{Lamarsh} = 9.334$$

Equations and calculated values:

Begin by calculating the linear attenuation coefficients.

$$\mu[\text{cm}^{-1}] = \frac{\mu}{\rho} [\text{cm}^2/\text{g}] \cdot \rho [\text{g}/\text{cm}^3]$$

Equation 16-1: Linear attenuation calculated from mass attenuation and density

$$\mu(\text{Al, HPRH}) = 1.661 \times 10^{-1} \text{ cm}^{-1}, \mu(\text{Al, Lamarsh}) = 1.659 \times 10^{-1} \text{ cm}^{-1}$$

$$\mu(\text{Air, HPRH}) = 7.661 \times 10^{-5} \text{ cm}^{-1}, \mu(\text{Air, Lamarsh}) = 7.664 \times 10^{-5} \text{ cm}^{-1}$$

Then calculate the flux at the edge of the shield followed by the flux at the detector.

$$\dot{N} = A \cdot e^{-(\mu \cdot x)}$$

Equation 16-2: Equation for calculating flux at a distance from the source through a material.

where $\dot{N} [\text{Y}/\text{s}]$ is the flux at a point $x [\text{cm}]$ away from the source, $A [\text{s}^{-1}]$ is the activity, and $\mu [\text{cm}^{-1}]$ is the linear attenuation coefficient for the material between the source and the point x .

The values for the flux at the edge of the 20 cm Al shield are:

$$\dot{N} (\text{shield, HPRH}) = 1.336 \times 10^9 [\text{Y}/\text{s}], \dot{N} (\text{shield, Lamarsh}) = 1.340 \times 10^9 [\text{Y}/\text{s}]$$

The values for flux at the detector after passing through 80 cm of air are:

$$\dot{N} (\text{detector, HPRH}) = 1.328 \times 10^9 [\text{Y}/\text{s}], \dot{N} (\text{detector, Lamarsh}) = 1.332 \times 10^9 [\text{Y}/\text{s}]$$

Then we calculate the particle fluence rate or particle flux density at the detector from the flux.

$$\dot{\Phi} = \frac{\dot{N}}{4 \cdot \pi \cdot r^2}$$

Equation 16-3: Equation for calculating particle fluence rate or particle flux density.

where $\dot{\Phi} \left[\gamma / s \cdot cm^2 \right]$ is the particle fluence rate or particle flux density, and r is the radial distance between the source and the location where the particle fluence rate is determined. These values are compared to the uncollided flux as calculated in MCNP and SCALE.

$$\dot{\Phi} \text{ (HPRH)} = 1.057 \times 10^4 \left[\gamma / s \cdot cm^2 \right], \dot{\Phi} \text{ (Lamarsh)} = 1.060 \times 10^4 \left[\gamma / s \cdot cm^2 \right]$$

$$\dot{\Phi} \text{ (MCNP, F5)} = 1.0747 \times 10^4 \pm 1.0747 \left[\gamma / s \cdot cm^2 \right]$$

$$\dot{\Phi} \text{ (SCALE)} = 1.22763 \times 10^4 \pm 6.657 \times 10^{-5} \left[\gamma / s \cdot cm^2 \right]$$

Next the total particle fluence rate is calculated from the buildup factor and the particle fluence rate.

$$\dot{\Phi}_{tot} = B \cdot \dot{\Phi}$$

Equation 16-4: Equation for calculating the total particle fluence rate.

where $\dot{\Phi}_{tot} \left[\gamma / s \cdot cm^2 \right]$ is the total particle fluence rate and B is the buildup factor. These values are compared to the total flux as calculated by MCNP and SCALE.

$$\dot{\Phi}_{tot} \text{ (HPRH)} = 9.482 \times 10^4 \left[\gamma / s \cdot cm^2 \right], \dot{\Phi}_{tot} \text{ (Lamarsh)} = 9.894 \times 10^4 \left[\gamma / s \cdot cm^2 \right]$$

$$\dot{\Phi}_{tot} \text{ (MCNP, F4)} = 8.75420 \times 10^4 \pm 796.6 \left[\gamma / s \cdot cm^2 \right]$$

$$\dot{\Phi}_{tot} \text{ (MCNP, F5)} = 8.81784 \times 10^4 \pm 8.817 \left[\gamma / s \cdot cm^2 \right]$$

$$\dot{\Phi}_{tot} \text{ (SCALE)} = 9.39376 \times 10^4 \pm 8.31 \left[\gamma / s \cdot cm^2 \right]$$

17 Appendix F: Monte Carlo Neutron Particle (MCNP) Input Files

The following sections contain example input files created for simulation and modeling of point kernel calculations, gamma ray and neutron experiments, and hot cell optimizations. Included in the optimization section is a copy of the Matlab® code used to automate the creation of shielding optimization input files.

17.1 Point Kernel Models

The example input file provided here was used in modeling the point kernel calculations for gamma rays. Though aluminum, iron, lead and concrete shields were studied, only the final input file for aluminum is shown. The primary difference between aluminum and the other material input files is the number of particle splitting/roulette boundaries and the importance assigned to each cell.

MCNP Code validation compared to hand calculation

c This input file creates an aluminum sphere of 20 cm radius around a 1.0 MeV
c point source. The sphere is surrounded by air. A point detector is placed
c 1 meter from the source. An F4 tally is used for particle fluence rate.

c

c CELL CARDS

c

```
=====
100 100 -2.7020 -10          $ Aluminum sphere
200 200 -0.0012 -30          $ Detector sphere
300 200 -0.0012 10 30 20 -21 22 -23 24 -25    $ Atmosphere
400 0      -20:21:-22:23:-24:25    $ Kill zone
```

c SURFACE CARDS

c

```
=====
10 so 20  $ Aluminum Sphere
20 px -200 $ Air & Kill boundaries
21 px 200
22 py -200
23 py 200
24 pz -200
25 pz 200
30 sx 100 1 $ Detector sphere
```

c DATA CARDS

c

c Material Cards

c

```
m100 $ Aluminum
    13000 -1.00
M200 $ Dry Air from SCALE manual
    7000 -0.77
```

```

      8000   -0.23
c =====
c Source Definition Card
c
c This source is a piont source with energy of 1.0 MeV at the origin/center
c of the concrete sphere. It is directionally biased to the positive X
c direction with a Power Law directional transform.
mode p
nps 1e9
sdef erg 1.0
c
c =====
c Random Number Generator Card
c
rand gen=2
c
c =====
c Variance Reduction Card
c -----
c Weight Windows
c
c WWG 6 0 0 J J J J 0
c MESH
c   geom=rec ref=0 0 0 origin=-200 -200 -200
c   imesh=200 iints=41
c   jmesh=200 jints=41
c   kmesh=200 kints=41
c
c -----
c Exponential Transform
c
c ext:p sv2 sv2 sv2 0 0 0
c vect v2 100 0 0
c
c -----
c Importance
c
imp:p 1 1 1 0
c
c -----
c Forced Collisions
c
c fcl:p 0 0 0 0 1 0
c
c -----
c DXTRAN Sphere
c
c dxt:p 100 0 0 5 5 0 0
c dxc:p 1 1 1 0 1 0
c
c -----
c Energy Splitting
c
c esplt:p 0.5 5 0.5 1 0.5 0.3 0.5 0.1 0.5 0.03
c
c =====
c Tally Cards
c
c Particle Fluence Rate
f4:p 200
c
c Dose Conversion to ANSI 1991 Isotropic

```

```

f14:p 200
df14 IU=2 FAC=1.0 LOG IC=35
c
c Dose Conversion to ANSI 1977 Clairborne & Trubey
f24:p 200
df24 IU=2 FAC=1.0 LOG IC=20
c
c -----
c This point detector determines the flux at the center of the head
f5:p 100 0 0 5
c
c Dose Conversion to ANSI 1991 Isotropic
f15:p 100 0 0 5
df15 IU=2 FAC=1.0 LOG IC=35
c
c Dose Conversion to ANSI 1977 Clairborne & Trubey
f25:p 100 0 0 5
df25 IU=2 FAC=1.0 LOG IC=20
c
c -----
c Energy Deposition detector
c f6:p 200
c -----
c Energy Deposition detector with a multiplier to determine dose rate in rad/hr
c f16:p 200
c fm16 2.134102e6
c
c =====
c Other Optional Cards
c -----
c Plotting
c mplot freq 5e6 tally 6 tfc m
c
c -----
c Cutoffs: Time Energy and Weight
c cut:p 1.0e123 0.001 -0.5 -0.25
c
c -----
c Computer time cutoff
c CTME 45
c
c -----
c Printing
c prints all tables pertinent to the problem
print

```

17.2 Gamma Ray Experiment Models

17.2.1 Unshielded Setup

Simplified Model for Gamma Interactions Calculations

```

c This tallies the interactions within the NaI crystal from a Cs-137 source.
c The tally is from an F8 using the PHL special treatment to simulate photon
c and electron interactions within the detector volume. It gains additional
c information from an F6 electron heating and using the special detector
c responses built in with the NAI-1.
c There are no shielding materials between the source and the detector.
c

```

CELL CARDS

```

c =====
c Source

```

100 300 -1.580968 -1 -5 6 \$ CsCl source material
 101 104 -8.03 (1:5:-6) -2 -4 7 \$ SS source containment
 102 104 -8.03 -3 -7 8 \$ SS source nut
 103 104 -8.03 -2 -8 9 \$ SS threaded bolt
 c Lead Pig/Collimator
 200 201 -11.35 (20:-9:23) -21 22 -23 \$ Pb pig
 201 500 -0.001225 -20 9 -23 (2:4:-7)(3:7:-8)(2:8:-9) \$ air around source inside Pb pig
 c Concrete Block Stand and Floor
 300 101 -2.30 -22 30 -31 32 -33 34 \$ Concrete blocks
 301 101 -2.30 -30 91 -92 93 -94 95 \$ Concrete floor
 c NaI(Tl) Detector
 400 401 -3.76 -40 43 -44 \$ NaI detector medium
 401 0 -40 44 -45 \$ Vacuum of PMT
 402 403 -2.6989 (40:-43:44) -41 42 -44 \$ Al can of NaI detector
 403 404 -8.7470 (40:-44:45) -41 44 -46 \$ Mu metal can of PMT
 c Room Atmosphere
 800 500 -0.001225 (41:-42:46)(21:-22:23)(22:-30:31:-32:33:-34) -90 30 -92 93 &
 -94 95 \$ Room air
 c End of Universe/Kill Zone
 900 0 90:-91:92:-93:94:-95 \$ kill zone

c SURFACE CARDS

c =====
 c Source
 1 cx 0.15875 \$ cylinder of source (CsCl glass)
 2 cx 0.3175 \$ cylinder of source containment and threaded bolt (SS)
 3 cx 0.442 \$ cylinder of source nut (SS)
 4 px 0.102 \$ top of source SS containment and air inside pig interface
 5 px 0 \$ top of source and inner top source SS containment interface
 6 px -0.2286 \$ bottom of source and SS containment interface
 7 px -2.487 \$ bottom of SS containment and top of SS nut
 8 px -2.987 \$ bottom of SS nut top of SS threaded bolt
 9 px -3.487 \$ bottom of SS threaded bolt and top of Pb inner lead pig
 c Lead pig/collimator
 20 cx 1.27 \$ inner air chamber of pig (Pb)
 21 cx 5.08 \$ outer edge of Pb pig and outside air
 22 px -6.661 \$ bottom of Pb pig top of concrete blocks
 23 px 5.215 \$ top of Pb pig air interface
 c Concrete block stand
 30 px -47.301 \$ bottom of concrete blocks and concrete floor interface
 31 py 8.89 \$ edge of concrete block
 32 py -8.89 \$ edge of concrete block
 33 pz 10.16 \$ edge of concrete block
 34 pz -10.16 \$ edge of concrete block
 c NaI(Tl) detector
 40 cx 2.54 \$ detector (NaI) and PMT radius
 41 cx 2.591 \$ Al detector can outer radius
 42 px 43.972 \$ Al detector can bottom
 43 px 44.015 \$ Al can NaI interface
 44 px 49.103 \$ NaI PMT interface and Al Mu interface
 45 px 62.336 \$ PMT vacuum Mu can interface
 46 px 62.387 \$ Mu can top air interface
 c End of Universe
 90 px 162 \$ air kill zone interface
 91 px -78 \$ concrete floor kill zone interface
 92 py 109 \$ air kill zone interface
 93 py -109 \$ air kill zone interface
 94 pz 110 \$ air kill zone interface
 95 pz -110 \$ air kill zone interface

c DATA CARDS

c =====

c

c Material Cards

c The ZA and atom densities come from PNNL compendium except BP, WC, CsCl, and
c He-3 which are hand calculated.

c

m101 \$ regular concrete (shielding material), density=2.30 g/cc

1000 0.013742
8000 0.046056
11000 0.001747
13000 0.001745
14000 0.016620
20000 0.001521
26000 0.000347

m102 \$ borated polyethylene (shielding material), density=1.40 g/cc

1000 0.1142039
5000 0.0038993
6000 0.0571019

m103 \$ tungsten carbide (shielding material), density=14.93 g/cc

6000 0.0429698
8000 0.0008429
23000 0.0002647
26000 0.0001610
27000 0.0091538
74000 0.0429698

m104 \$ stainless steel 304 (shielding material, source container, and detector can), density=8.03 g/cc

6000 0.000160
14000 0.000858
15000 0.000036
16000 0.000023
24000 0.017605
25000 0.000877
26000 0.060538
28000 0.007593

m201 \$ lead (source container), density=11.35 g/cc

82000 0.032988

m202 \$ Iron (source container), density=7.874 g/cc

26000 0.084911

m300 \$ Cesium Chloride Glass (Cs-137 source material), density=1.580968 g/cc

5000 0.0058780
8000 0.0330873
11000 0.0009213
14000 0.0118795
17000 0.0000023
19000 0.0001010
55000 0.0000023

m401 \$ sodium iodide (detector medium - photon), density=3.76 g/cc

11000 0.0150794
53000 0.0150794
81000 0.0000196

m402 \$ helium 3 (detector medium - neutron) - P=4 atm, P4-0812-217, density=0.00067795 g/cc

2000 0.000134

m403 \$ aluminum (detector can of NaI), density=2.6989 g/cc

13000 0.060238

m404 \$ mu metal (detector can of PMT vacuum), density=8.747 g/cc

6000 0.0000877
25000 0.0004794
14000 0.0006564
28000 0.0717977
42000 0.0023060
26000 0.0140827

m500 \$ dry air (within source and around the whole assembly), density=0.001225 g/cc

7000 0.000039

```

8000 0.000011
c =====
c
c Source Definition Card
c
mode p e
nps 1e9
sdef ERG=d6 POS=-0.2286 0 0 RAD=d2 EXT=d4 AXS=1 0 0 PAR=p
si2 0 0.15875
sp2 -21 1
si4 0 0.2286
sp4 0 1
si6 L 0.661650
sp6 1
c =====
c
c Random Number Generator Card
c
rand gen=2 stride=210321
c =====
c
c Importances
IMP:p 1 1 1 1 1 1 1 1 1 1 1 1 0
IMP:e 0 0 0 0 0 0 0 0 1 0 1 1 0
c
c Physics Cards
c
c PHYS:p J 1 5J
c =====
c
c Tally Cards
c
c GEB values for a, b, and c come from MCNP detector class handout b-93_detectors.pdf
c
c GEB values for a, b, and c were calculated for the NaI(Tl) detector used
c
F8:e 400
E8 0 1e-5 0.015 255I 0.745
FT8 GEB -0.0141448 0.0897491 0.191194 &
PHL 1 6 1 NAI-1
F6:e 400
c
F24:p 400
FM24 -1 401 -5
SD24 1
c
FMESH4:p GEOM=xyz ORIGIN=-78 -109 -110
IMESH 162 IINTS 501
JMESH 109 JINTS 101
KMESH 110 KINTS 101
c
FMESH14:p GEOM=xyz ORIGIN=-78 -109 -110
IMESH 162 IINTS 501
JMESH 109 JINTS 101
KMESH 110 KINTS 101
FM14 -1 0 -5
c =====
c
c Optional Cards
c
c -----
c Plotting

```



```

c mplot freq 5e6 tally 4 tfc m
c
c -----
c Cutoffs: Time, Energy, and Weight
c cut:p 1.0e123 0.001 -0.5 -0.25
c
c -----
c Computer Time Cutoff
c CTME 45
c
c -----
c Printing
c Prints all tables pertinent to the problem
print
c .....
c sets the frequency of tally and runtpe dumps
prdump 2e8 2e8

```

17.2.2 Shielded Setups

An example of a single layered shield and an example of a multi-layered shield are provided. The other input files for single layer modify the material and the thickness based upon the material (stainless steel = 1/8 inch (0.3175 cm), borated polyethylene = 1 inch (2.54 cm), tungsten carbide = 1/8 inch (0.3175 cm), and concrete = 3 inches (7.62 cm)). These thicknesses are the actual thickness of the manufactured materials used. The additional input files for the multi-layered shields modify the order of the material with corresponding thicknesses.

17.2.2.1 Single Material, Single Layer

```

Simplified Model for Gamma Interactions Calculations
c This tallies the interactions within the NaI crystal from a Cs-137 source.
c The tally is from an F8 using the PHL special treatment to simulate photon
c and electron interactions within the detector volume. It gains additional
c information from an F6 electron heating and using the special detector
c responses built in with the NAI-1.
c There is 1/8" stainless steel shielding materials between the source and the detector.
c
c CELL CARDS
c =====
c Source
100 300 -1.580968 -1 -5 6 $ CsCl source material
101 104 -8.03 (1:5:-6) -2 -4 7 $ SS source containment
102 104 -8.03 -3 -7 8 $ SS source nut
103 104 -8.03 -2 -8 9 $ SS threaded bolt
c Lead Pig/Collimator
200 201 -11.35 (20:-9:23) -21 22 -23 $ Pb pig
201 500 -0.001225 -20 9 -23 (2:4:-7)(3:7:-8)(2:8:-9) $ air around source inside Pb pig
c Concrete Block Stand and Floor
300 101 -2.30 -22 30 -31 32 -33 34 $ Concrete blocks
301 101 -2.30 -30 91 -92 93 -94 95 $ Concrete floor
c NaI(Tl) Detector

```

400 401 -3.76 -40 43 -44 \$ NaI detector medium
 401 0 -40 44 -45 \$ Vacuum of PMT
 402 403 -2.6989 (40:-43:44) -41 42 -44 \$ Al can of NaI detector
 403 404 -8.7470 (40:-44:45) -41 44 -46 \$ Mu metal can of PMT
 c Shielding Materials
 500 106 -7.9394 -50 23 -51 52 -53 54 \$ Stainless steel shield
 c Room Atmosphere
 800 500 -0.001225 (41:-42:46)(21:-22:23)(22:-30:31:-32:33:-34) -90 30 -92 93 &
 -94 95 (50:-23:51:-52:53:-54) \$ Room air
 c End of Universe/Kill Zone
 900 0 90:-91:92:-93:94:-95 \$ kill zone

c SURFACE CARDS

c =====

c Source

1 cx 0.15875 \$ cylinder of source (CsCl glass)
 2 cx 0.3175 \$ cylinder of source containment and threaded bolt (SS)
 3 cx 0.442 \$ cylinder of source nut (SS)
 4 px 0.102 \$ top of source SS containment and air inside pig interface
 5 px 0 \$ top of source and inner top source SS containment interface
 6 px -0.2286 \$ bottom of source and SS containment interface
 7 px -2.487 \$ bottom of SS containment and top of SS nut
 8 px -2.987 \$ bottom of SS nut top of SS threaded bolt
 9 px -3.487 \$ bottom of SS threaded bolt and top of Pb inner lead pig

c Lead pig/collimator

20 cx 1.27 \$ inner air chamber of pig (Pb)
 21 cx 5.08 \$ outer edge of Pb pig and outside air
 22 px -6.661 \$ bottom of Pb pig top of concrete blocks
 23 px 5.215 \$ top of Pb pig air interface

c Concrete block stand

30 px -47.301 \$ bottom of concrete blocks and concrete floor interface
 31 py 8.89 \$ edge of concrete block
 32 py -8.89 \$ edge of concrete block
 33 pz 10.16 \$ edge of concrete block
 34 pz -10.16 \$ edge of concrete block

c NaI(Tl) detector

40 cx 2.54 \$ detector (NaI) and PMT radius
 41 cx 2.591 \$ Al detector can outer radius
 42 px 43.972 \$ Al detector can bottom
 43 px 44.015 \$ Al can NaI interface
 44 px 49.103 \$ NaI PMT interface and Al Mu interface
 45 px 62.336 \$ PMT vacuum Mu can interface
 46 px 62.387 \$ Mu can top air interface

c Shielding Materials

50 px 5.517 \$ outer edge of shield
 51 py 5.08 \$ edge of shield
 52 py -5.08 \$ edge of shield
 53 pz 5.08 \$ edge of shield
 54 pz -5.08 \$ edge of shield

c End of Universe

90 px 162 \$ air kill zone interface
 91 px -78 \$ concrete floor kill zone interface
 92 py 109 \$ air kill zone interface
 93 py -109 \$ air kill zone interface
 94 pz 110 \$ air kill zone interface
 95 pz -110 \$ air kill zone interface

c DATA CARDS

c =====

c

c Material Cards

c The ZA and atom densities come from PNNL compendium except BP, WC, CsCl, and

c He-3 which are hand calculated.

c

m101 \$ regular concrete (walls, stand, and floor), density=2.30 g/cc

1000 0.013742
8000 0.046056
11000 0.001747
13000 0.001745
14000 0.016620
20000 0.001521
26000 0.000347

m102 \$ borated polyethylene (shielding material), density=1.4783 g/cc

1000 0.1205911
5000 0.0041173
6000 0.0602956

m103 \$ tungsten carbide (shielding material), density=14.842 g/cc

6000 0.0427164
8000 0.0008380
23000 0.0002632
26000 0.0001601
27000 0.0090999
74000 0.0427165

m104 \$ stainless steel 304 (source container), density=8.03 g/cc

6000 0.000160
14000 0.000858
15000 0.000036
16000 0.000023
24000 0.017605
25000 0.000877
26000 0.060538
28000 0.007593

m105 \$ concrete shield, density=2.3462 g/cc

1000 0.0140180
8000 0.0469811
11000 0.0017821
13000 0.0017801
14000 0.0169538
20000 0.0015516
26000 0.0003540

m106 \$ SS304 shield, density=7.9394 g/cc

6000 0.0001582
14000 0.0008483
15000 0.0000356
16000 0.0000227
24000 0.0174064
25000 0.0008671
26000 0.0598550
28000 0.0075073

m201 \$ lead (source container), density=11.35 g/cc

82000 0.032988

m202 \$ Iron (source container), density=7.874 g/cc

26000 0.084911

m300 \$ Cesium Chloride Glass (Cs-137 source material), density=1.580968 g/cc

5000 0.0058780
8000 0.0330873
11000 0.0009213
14000 0.0118795
17000 0.0000023
19000 0.0001010
55000 0.0000023

m401 \$ sodium iodide (detector medium - photon), density=3.76 g/cc

11000 0.0150794
53000 0.0150794

```

      81000 0.0000196
m402 $ helium 3 (detector medium - neutron) - P=4 atm, P4-0812-217, density=0.00067795 g/cc
      2000 0.000134
m403 $ aluminum (detector can of NaI), density=2.6989 g/cc
      13000 0.060238
m404 $ mu metal (detector can of PMT vacuum), density=8.747 g/cc
      6000 0.0000877
      25000 0.0004794
      14000 0.0006564
      28000 0.0717977
      42000 0.0023060
      26000 0.0140827
m500 $ dry air (within source and around the whole assembly), density=0.001225 g/cc
      7000 0.000039
      8000 0.000011

```

```

c =====
c
c Source Definition Card
c
mode p e
nps 1e9
sdef ERG=d6 POS=-0.2286 0 0 RAD=d2 EXT=d4 AXS=1 0 0 PAR=p
si2 0 0.15875
sp2 -21 1
si4 0 0.2286
sp4 0 1
si6 L 0.661650
sp6 1
c =====
c
c Random Number Generator Card
c
rand gen=2 stride=210321
c =====
c
c Importances
IMP:p 1 1 1 1 1 1 1 1 1 1 1 1 1 1 0
IMP:e 0 0 0 0 0 0 0 0 1 0 1 1 0 0 0
c
c Physics Cards
c
c PHYS:p J 1 5J
c =====
c
c Tally Cards
c
c GEB values for a, b, and c were calculated for the NaI(Tl) detector used
c
F8:e 400
E8 0 1e-5 0.015 255I 0.745
FT8 GEB -0.0141448 0.0897491 0.191194 &
PHL 1 6 1 NAI-1
F6:e 400
c
F24:p 400
FM24 -1 401 -5
SD24 1
c
FMESH4:p GEOM=xyz ORIGIN=-78 -109 -110
      IMESH 162 IINTS 501
      JMESH 109 JINTS 101
      KMESH 110 KINTS 101

```

```

c
FMESH14:p GEOM=xyz ORIGIN=-78 -109 -110
  IMESH 162 IINTS 501
  JMESH 109 JINTS 101
  KMESH 110 KINTS 101
FM14 -1 0 -5
c =====
c
c Optional Cards
c
c -----
c Plotting
c mplot freq 5e6 tally 4 tfc m
c
c -----
c Cutoffs: Time, Energy, and Weight
c cut:p 1.0e123 0.001 -0.5 -0.25
c
c -----
c Computer Time Cutoff
c CTME 45
c
c -----
c Printing
c Prints all tables pertinent to the problem
print
c .....
c sets the frequency of tally and runtpe dumps
prdmp 2e8 2e8

```

17.2.2.2 Multi-material, Multi-layered

```

Simplified Model for Gamma Interactions Calculations
c This tallies the interactions within the NaI crystal from a Cs-137 source.
c The tally is from an F8 using the PHL special treatment to simulate photon
c and electron interactions within the detector volume. It gains additional
c information from an F6 electron heating and using the special detector
c responses built in with the NAI-1.
c There is a 1/8" SS + 1/8" WC + 3" C + 1" BP shield between source and
c detector.
c
c CELL CARDS
c =====
c Source
100 300 -1.580968 -1 -5 6 $ CsCl source material
101 104 -8.03 (1:5:-6) -2 -4 7 $ SS source containment
102 104 -8.03 -3 -7 8 $ SS source nut
103 104 -8.03 -2 -8 9 $ SS threaded bolt
c Lead Pig/Collimator
200 201 -11.35 (20:-9:23) -21 22 -23 $ Pb pig
201 500 -0.001225 -20 9 -23 (2:4:-7)(3:7:-8)(2:8:-9) $ air around source inside Pb pig
c Concrete Block Stand and Floor
300 101 -2.30 -22 30 -31 32 -33 34 $ Concrete blocks
301 101 -2.30 -30 91 -92 93 -94 95 $ Concrete floor
c NaI(Tl) Detector
400 401 -3.76 -40 43 -44 $ NaI detector medium
401 0 -40 44 -45 $ Vacuum of PMT
402 403 -2.6989 (40:-43:44) -41 42 -44 $ Al can of NaI detector
403 404 -8.7470 (40:-44:45) -41 44 -46 $ Mu metal can of PMT
c Shielding Materials
500 106 -7.9394 -50 23 -54 55 -56 57 $ SS shield
501 103 -14.842 50 -51 -54 55 -56 57 $ WC shield

```

502 105 -2.3462 51 -52 -54 55 -56 57 \$ Con shield
 503 102 -1.4783 52 -53 -54 55 -56 57 \$ BP shield
 c Room Atmosphere
 800 500 -0.001225 (41:-42:46)(21:-22:23)(22:-30:31:-32:33:-34) -90 30 -92 93 &
 -94 95 (53:-23:54:-55:56:-57) \$ Room air
 c End of Universe/Kill Zone
 900 0 90:-91:92:-93:94:-95 \$ kill zone

c SURFACE CARDS

c =====

c Source

1 cx 0.15875 \$ cylinder of source (CsCl glass)
 2 cx 0.3175 \$ cylinder of source containment and threaded bolt (SS)
 3 cx 0.442 \$ cylinder of source nut (SS)
 4 px 0.102 \$ top of source SS containment and air inside pig interface
 5 px 0 \$ top of source and inner top source SS containment interface
 6 px -0.2286 \$ bottom of source and SS containment interface
 7 px -2.487 \$ bottom of SS containment and top of SS nut
 8 px -2.987 \$ bottom of SS nut top of SS threaded bolt
 9 px -3.487 \$ bottom of SS threaded bolt and top of Pb inner lead pig

c Lead pig/collimator

20 cx 1.27 \$ inner air chamber of pig (Pb)
 21 cx 5.08 \$ outer edge of Pb pig and outside air
 22 px -6.661 \$ bottom of Pb pig top of concrete blocks
 23 px 5.215 \$ top of Pb pig air interface

c Concrete block stand

30 px -47.301 \$ bottom of concrete blocks and concrete floor interface
 31 py 8.89 \$ edge of concrete block
 32 py -8.89 \$ edge of concrete block
 33 pz 10.16 \$ edge of concrete block
 34 pz -10.16 \$ edge of concrete block

c NaI(Tl) detector

40 cx 2.54 \$ detector (NaI) and PMT radius
 41 cx 2.591 \$ Al detector can outer radius
 42 px 43.972 \$ Al detector can bottom
 43 px 44.015 \$ Al can NaI interface
 44 px 49.103 \$ NaI PMT interface and Al Mu interface
 45 px 62.336 \$ PMT vacuum Mu can interface
 46 px 62.387 \$ Mu can top air interface

c Shielding Materials

50 px 5.517 \$ outer edge of SS shield 1st material
 51 px 5.911 \$ outer edge of shield 2nd material
 52 px 13.722 \$ outer edge of shield 3rd material
 53 px 16.255 \$ outer edge of shield last material
 54 py 5.08 \$ edge of concrete shield
 55 py -5.08 \$ edge of concrete shield
 56 pz 5.08 \$ edge of concrete shield
 57 pz -5.08 \$ edge of concrete shield

c End of Universe

90 px 162 \$ air kill zone interface
 91 px -78 \$ concrete floor kill zone interface
 92 py 109 \$ air kill zone interface
 93 py -109 \$ air kill zone interface
 94 pz 110 \$ air kill zone interface
 95 pz -110 \$ air kill zone interface

c DATA CARDS

c =====

c

c Material Cards

c The ZA and atom densities come from PNNL compendium except BP, WC, CsCl, and
 c He-3 which are hand calculated.

c

m101 \$ regular concrete (walls, stand, and floor), density=2.30 g/cc

1000 0.013742
8000 0.046056
11000 0.001747
13000 0.001745
14000 0.016620
20000 0.001521
26000 0.000347

m102 \$ borated polyethylene (shielding material), density=1.4783 g/cc

1000 0.1205911
5000 0.0041173
6000 0.0602956

m103 \$ tungsten carbide (shielding material), density=14.842 g/cc

6000 0.0427164
8000 0.0008380
23000 0.0002632
26000 0.0001601
27000 0.0090999
74000 0.0427165

m104 \$ stainless steel 304 (source container), density=8.03 g/cc

6000 0.000160
14000 0.000858
15000 0.000036
16000 0.000023
24000 0.017605
25000 0.000877
26000 0.060538
28000 0.007593

m105 \$ concrete shield, density=2.3462 g/cc

1000 0.0140180
8000 0.0469811
11000 0.0017821
13000 0.0017801
14000 0.0169538
20000 0.0015516
26000 0.0003540

m106 \$ SS304 shield, density=7.9394 g/cc

6000 0.0001582
14000 0.0008483
15000 0.0000356
16000 0.0000227
24000 0.0174064
25000 0.0008671
26000 0.0598550
28000 0.0075073

m201 \$ lead (source container), density=11.35 g/cc

82000 0.032988

m202 \$ Iron (source container), density=7.874 g/cc

26000 0.084911

m300 \$ Cesium Chloride Glass (Cs-137 source material), density=1.580968 g/cc

5000 0.0058780
8000 0.0330873
11000 0.0009213
14000 0.0118795
17000 0.0000023
19000 0.0001010
55000 0.0000023

m401 \$ sodium iodide (detector medium - photon), density=3.76 g/cc

11000 0.0150794
53000 0.0150794
81000 0.0000196

m402 \$ helium 3 (detector medium - neutron) - P=4 atm, P4-0812-217, density=0.00067795 g/cc

2000 0.000134

m403 \$ aluminum (detector can of NaI), density=2.6989 g/cc

13000 0.060238

m404 \$ mu metal (detector can of PMT vacuum), density=8.747 g/cc

6000 0.0000877

25000 0.0004794

14000 0.0006564

28000 0.0717977

42000 0.0023060

26000 0.0140827

m500 \$ dry air (within source and around the whole assembly), density=0.001225 g/cc

7000 0.000039

8000 0.000011

c =====

c

c Source Definition Card

c

mode p e

nps 1e9

sdef ERG=d6 POS=-0.2286 0 0 RAD=d2 EXT=d4 AXS=1 0 0 PAR=p

si2 0 0.15875

sp2 -21 1

si4 0 0.2286

sp4 0 1

si6 L 0.661650

sp6 1

c =====

c

c Random Number Generator Card

c

rand gen=2 stride=210321

c =====

c

c Importances

IMP:p 1 1 1 1 1 1 1 1 1 1 1 1 1 1 1 1 0

IMP:e 0 0 0 0 0 0 0 0 1 0 1 1 0 0 0 0 0

c

c Physics Cards

c

c PHYS:p J 1 5J

c =====

c

c Tally Cards

c

c GEB values for a, b, and c were calculated for the NaI(Tl) detector used

c

F8:e 400

E8 0 1e-5 0.015 255I 0.745

FT8 GEB -0.0141448 0.0897491 0.191194 &

PHL 1 6 1 NAI-1

F6:e 400

c

F24:p 400

FM24 -1 401 -5

SD24 1

c

FMESH4:p GEOM=xyz ORIGIN=-78 -109 -110

IMESH 162 IINTS 501

JMESH 109 JINTS 101

KMESH 110 KINTS 101

c


```
FMESH14:p GEOM=xyz ORIGIN=-78 -109 -110
```

```
IMESH 162 IINTS 501
```

```
JMESH 109 JINTS 101
```

```
KMESH 110 KINTS 101
```

```
FM14 -1 0 -5
```

```
c =====
```

```
c
```

```
c Optional Cards
```

```
c
```

```
c -----
```

```
c Plotting
```

```
c mplot freq 5e6 tally 4 tfc m
```

```
c
```

```
c -----
```

```
c Cutoffs: Time, Energy, and Weight
```

```
c cut:p 1.0e123 0.001 -0.5 -0.25
```

```
c
```

```
c -----
```

```
c Computer Time Cutoff
```

```
c CTME 45
```

```
c
```

```
c -----
```

```
c Printing
```

```
c Prints all tables pertinent to the problem
```

```
print
```

```
c .....
```

```
c sets the frequency of tally and runtpe dumps
```

```
prdump 2e8 2e8
```

17.2.3 Gaussian Energy Broadening

The following code was written to determine the Gaussian Energy Broadening coefficients for the MCNP F8 PHL GEB modifier. The GEB coefficients are unique to each detector and can be found from experimental results by capturing the location and full width half maximum of each peak for that NaI detector. The code was written in Wolfram's Mathematica version 11.1.1.0 Student Edition. The entry for "data" is the energy of the full energy peak paired with the FWHM of that peak. The "fit" is the function to solve. The last line provides the output solution to "fit", which are also the values for "a", "b", and "c" used with the F8 tally.

Finding the GEB Coefficients

Data Pairs (Emev, Fres)

```
data = {{1.3203, 0.099}, {1.2529, 0.0907}, {1.1713, 0.1059}, {0.6686, 0.0578}, {0.5188, 0.0524}, {0.3701, 0.047}, {0.1372, 0.0196}, {0.0933, 0.0127}};
```

```
fit = FindFit[data, a+b*Sqrt[x+c*x^2], {a, b, c}, x]
```

```
{a->-0.0141448,b->0.0897491,c->0.191194}
```

17.3 Neutron Experiment Models

17.3.1 Unshielded Setup

Simplified Model for Neutron Fluence Calculations

c This is the newest version of the neutron model. It accounts for the actual
c size of the drum and source cradle, as well as source placement. It can be
c modified to have the shielding material placed over the hole.

c

c CELL CARDS

c =====

c -----

c source material and Pb/SS capsule

c -----

100 300 -2.214403 -1 2 -3 \$ AmO2/Be13 source material

101 500 -0.001225 -1 3 -4 \$ air inside SS1 capsule

110 104 -8.03 (1:-2:4)(-5 7 -8) \$ SS1 capsule

111 500 -0.001225 5 -6 7 -8 \$ air between SS1/SS2

120 104 -8.03 (6:-7:8)(-9 11 -12) \$ SS2 capsule

121 500 -0.001225 9 -10 11 -12 \$ air between SS2/Pb

130 202 -11.35 (10:-11:12)(-13 14 -15) \$ Pb capsule

132 500 -0.001225 (13:-14:15)(-20 14 -22) \$ air outside Pb/inside 1.5" PVC cradle

c -----

c PVC cradle

c -----

140 203 -1.406 20 -21 14 -22 \$ 1.5" PVC pipe of cradle

141 203 -1.406 (21:-14:27)(-25 26 -27) \$ 1.5" bottom PVC cap

142 203 -1.406 (21:-28:22)(-25 28 -29) \$ 1.5" top PVC cap

143 500 -0.001225 (25:-28:29)(25:-26:27)(21 -30 26 -29) \$ air around PVC capsule inside 2.5" PVC tube of collimator

c -----

c Collimator

c -----

150 500 -0.001225 -1 29 -31 \$ air inside polyethylene tube

151 204 -0.94 1 -30 29 -31 \$ polyethylene tube

152 203 -1.406 30 -32 26 -33 \$ 2.5" PVC tube of collimator

153 203 -1.406 (32:-26:37)(-35 36 -37) \$ 2.5" PVC cap

c -----

c Drum and paraffin wax

c -----

160 201 -0.92 (35:-36:37)(32:-36:33)(-40 44 -33) \$ Paraffin wax inside drum

165 205 -8.03 40 -41 42 -33 \$ Steel drum wall

166 205 -8.03 -40 43 -44 \$ Steel drum bottom

167 500 -0.001225 -40 42 -43 \$ air under drum

c -----

c Shielding Blocks

c -----

c 200

c -----

c Detector

c -----

300 104 -8.03 (60:-62:65)(-1 61 -66) \$ SS detector can

310 403 -0.000622 -60 63 -64 \$ He-3/CO2 fill gas

320 0 -60 62 -63 \$ lower inactive region

330 0 -60 64 -65 \$ upper inactive region

c -----

c Floor, Walls, and Room Atmosphere

c -----

400 101 -2.30 90 -91 -92 93 94 -95 (82:-83:81:-80:-42:84) \$ concrete floor and building walls

401 101 -2.30 (80 -75 76 -77 42 -73) \$ concrete bricks of reactor - facing drum

402 101 -2.30 (77 -78 74 -75 42 -73) \$ concrete bricks of reactor - facing console

403 101 -2.30 (80 -75 76 -78 73 -79) \$ concrete bricks of reactor - top

405 101 -2.30 70 -71 72 -82 42 -73 \$ concrete bricks of additional wall
 800 500 -0.001225 (41:-42:33)(30:31:-33)(1:-61:66)(-70:71:-72:82:-42:73)
 (-80:75:-76:77:-42:73)(-76:78:-74:75:-42:73)(-80:75:-76:78:-73:79)
 (42 -84 -82 83 80 -81) \$ Room air

c -----

c End of Universe

c -----

900 0 -90:91:92:-93:-94:95 \$ kill space

c SURFACE CARDS

c =====

c -----

c source and capsule

c -----

1 cz 1.27 \$ source material & air/SS interface, collimator ID, detector OD

2 pz 30.2082 \$ bottom of source material/inner bottom SS1

3 pz 36.5894 \$ source material/air interface

4 pz 41.6382 \$ air/inner top SS1

5 cz 1.3462 \$ outer SS1/air

6 cz 1.35128 \$ air/inner SS2

7 pz 30.0177 \$ SS1 outer bottom/SS2 inner bottom

8 pz 41.8287 \$ SS1 outer top/SS2 inner top

9 cz 1.45415 \$ outer SS2/air

10 cz 1.4605 \$ air/inner Pb

11 pz 29.7637 \$ outer bottom SS2/inner bottom Pb

12 pz 42.4637 \$ outer top SS2/inner top Pb

13 cz 1.778 \$ outer Pb/air

14 pz 29.4462 \$ outer bottom Pb, inner bottom PVC cap of cradle

15 pz 42.7812 \$ outer top Pb

c -----

c PVC cradle

c -----

20 cz 2.047 \$ ID 1.5" PVC tube of cradle

21 cz 2.40 \$ OD 1.5" PVC tube of cradle

22 pz 44.21 \$ top of 1.5" PVC tube/inner top PVC cap

25 cz 2.8375 \$ OD 1.5" PVC caps

26 pz 26.035 \$ outer bottom PVC cap, inner bottom PVC cap of collimator

27 pz 31.6712 \$ top edge of 1.5" PVC bottom cap

28 pz 41.985 \$ bottom edge of 1/5" PVC top cap

29 pz 45.085 \$ outer top of 1.5" PVC top cap, bottom of poly collimator tube

c -----

c Collimator

c -----

30 cz 3.134 \$ OD poly tube/ID 2.5" PVC tube

31 pz 90.805 \$ top of poly tube

32 cz 3.65 \$ OD 2.5" PVC tube/ID 2.5" PVC cap

33 pz 86.995 \$ top of 2.5" PVC tube, top of drum/paraffin wax

35 cz 4.24 \$ OD 2.5" PVC cap

36 pz 25.445 \$ outer bottom 2.5" PVC cap

37 pz 31.455 \$ top edge of 2.5" PVC cap

c -----

c Drum and Paraffin Wax

c -----

40 cz 28.575 \$ ID drum/OD wax

41 cz 28.7401 \$ OD drum/atmosphere

42 pz 0 \$ bottom of drum bottom rim

43 pz 2.413 \$ outer bottom of drum/air

44 pz 2.5781 \$ inner bottom of drum/wax

c -----

c Shielding Blocks

c -----

c 50 py -5.0800 \$ front edge of shielding

c 51 py 5.0800 \$ back edge of shielding
 c 52 px -5.0800 \$ top edge of shielding
 c 53 px 5.0800 \$ bottom edge of shielding
 c 55 pz 91.107 \$ outer SS inner BP
 c 56 pz 93.64 \$ outer BP inner C
 c 57 pz 101.451 \$ outer C inner WC
 c 58 pz 101.845 \$ outer WC

c -----
 c Detector

c -----
 60 cz 1.2192 \$ ID of detector/fill gas
 61 pz 106.045 \$ outer bottom of SS detector can
 62 pz 106.096 \$ inner bottom of SS can/inactive region
 63 pz 108.2042 \$ inactive region/fill gas
 64 pz 138.5824 \$ fill gas/inactive region
 65 pz 141.732 \$ inactive region/inner top SS can
 66 pz 141.783 \$ outer top SS can

c -----
 c Floor and Walls

c -----
 70 px 91.44 \$ additional concrete brick walls
 71 px 131.90 \$ additional concrete brick walls
 72 py 398.78 \$ additional concrete brick walls
 73 pz 243.84 \$ additional concrete brick walls
 74 px -30.30 \$ reactor concrete brick walls
 75 px 10.16 \$ reactor concrete brick walls
 76 py 247.98 \$ reactor concrete brick walls
 77 py 288.44 \$ reactor concrete brick walls
 78 py 502.92 \$ reactor concrete brick walls
 79 pz 320.04 \$ reactor concrete brick walls
 80 px -350.52 \$ inner wall of building
 81 px 502.92 \$ inner wall of building
 82 py 601.98 \$ inner wall of building
 83 py -251.46 \$ inner wall of building
 84 pz 701.04 \$ inner wall of building

c -----
 c End of Universe

c -----
 90 pz -40 \$ kill
 91 pz 716.28 \$ kill
 92 py 632.46 \$ kill
 93 py -281.94 \$ kill
 94 px -381.00 \$ kill
 95 px 533.40 \$ kill

c DATA CARDS

c =====

c
 c Material Cards

c The ZA and atom densities come from PNNL compendium except WC, which is self-
 c calculated.

c
 m101 \$ regular concrete (floor, walls), den=2.30 g/cc

1001 0.0137404197
 1002 0.0000015803
 8016 0.0460382693
 8017 0.0000175372
 11023 0.001747
 13027 0.001745
 14028 0.0153285761
 14029 0.0007783478
 14030 0.0005130926

20040 0.0014744726
 20042 0.0000098409
 20043 0.0000020534
 20044 0.0000317281
 20046 0.0000000608
 20048 0.0000028443
 26054 0.0000202822
 26056 0.0003183864
 26057 0.0000073529
 26058 0.0000009785
 m102 \$ borated polyethylene (shielding material), den=1.4783 g/cc
 1001 0.1205772320
 1002 0.0000138680
 5010 0.0008194
 5011 0.0032980
 6000 0.0602956
 m103 \$ tungsten carbide (shielding material), den=14.842 g/cc
 6000 0.0427165
 8016 0.0008376774
 8017 0.0000003191
 23050 0.0000006
 23051 0.0002625
 26054 0.0000094
 26056 0.0001468
 26057 0.0000034
 26058 0.0000004
 27059 0.0090999
 74180 0.0000512
 74182 0.0113199
 74183 0.0061127
 74184 0.0130883
 74186 0.0121443
 m104 \$ stainless steel 304 (source container, and detector can), den=8.03 g/cc
 6000 0.000160
 14028 0.0007913308
 14029 0.0000401819
 14030 0.0000264882
 15031 0.000036
 16032 0.0000218339
 16033 0.0000001748
 16034 0.0000009867
 16036 0.0000000046
 24050 0.0007649373
 24052 0.0147510535
 24053 0.0016726511
 24054 0.0004163583
 25055 0.000877
 26054 0.0035384461
 26056 0.0555460365
 26057 0.0012828002
 26058 0.0001707172
 28058 0.0051690790
 28060 0.0019911200
 28061 0.0000865526
 28062 0.0002759676
 28064 0.0000702808
 m105 \$ shielding concrete, den=2.3462 g/cc
 1001 0.0140163879
 1002 0.0000016121
 8016 0.0469630131
 8017 0.0000178894
 11023 0.0017821

13027 0.0017801
 14028 0.0156364389
 14029 0.0007939804
 14030 0.0005233977
 20040 0.0015041366
 20042 0.0000100389
 20043 0.0000020947
 20044 0.0000323664
 20046 0.0000000621
 20048 0.0000029015
 26054 0.0000206913
 26056 0.0003248092
 26057 0.0000075013
 26058 0.0000009983
 m106 \$ stainless steel 304 (shielding material), den=7.9394 g/cc
 6000 0.0001582
 14028 0.0007823845
 14029 0.0000397276
 14030 0.0000261887
 15031 0.0000356
 16032 0.0000215491
 16033 0.0000001725
 16034 0.0000009738
 16036 0.0000000045
 24050 0.0007563081
 24052 0.0145846485
 24053 0.0016537821
 24054 0.0004116614
 25055 0.0008671
 26054 0.0034985248
 26056 0.0549193567
 26057 0.0012683275
 26058 0.0001687911
 28058 0.0051107371
 28060 0.0019686468
 28061 0.0000855757
 28062 0.0002728528
 28064 0.0000694876
 m201 \$ paraffin wax (collimator/drum), den=0.92
 1001 0.0817128019
 1002 0.0000093981
 6000 0.0392727
 m202 \$ lead (source container), den=11.35 g/cc
 82204 0.0004618320
 82206 0.0079501080
 82207 0.0072903480
 82208 0.0172857120
 m203 \$ PVC (collimator/drum), den=1.406 g/cc
 1001 0.0406383261
 1002 0.0000046739
 6000 0.027096
 17035 0.010264
 17037 0.003284
 m204 \$ Polyethylene (collimator/drum), den=0.94 g/cc
 1001 0.0790217115
 1002 0.0000090885
 6000 0.0394984
 m205 \$ Iron (collimator/drum), den=7.874 g/cc
 26054 0.0049630480
 26056 0.0779092389
 26057 0.0017992641
 26058 0.0002394490


```

c F16:t 310
c
F24:n 310
FM24 -1 403 103
SD24 1
c
c F2:n 80 85 86 T
c E2 1e-7 1e-6 1e-5 1e-4 1e-3 1e-2 0.1 1 2 3 4 5 6 7 8 9 10 100
c C2 0 1
c
c FMESH4:n GEOM=xyz ORIGIN=-381 -281.94 -40
c   IMESH 533.4 IINTS 1
c   JMESH 632.46 JINTS 500
c   KMESH 716.28 KINTS 500
c
c FMESH14:n GEOM=xyz ORIGIN=-381 -281.94 -40
c   IMESH 533.4 IINTS 1
c   JMESH 632.46 JINTS 500
c   KMESH 716.28 KINTS 500
c FM14 -1 0 103
c =====
c
c Optional Cards
c
c -----
c Plotting
c mplot freq 5e6 tally 4 tfc m
c
c -----
c Cutoffs: Time, Energy, and Weight
c cut:n 1.0e123 1e-4 -0.5 -0.25
c CUT:h J 0.001
c CUT:t J 0.001
c
c -----
c Computer Time Cutoff
c CTME 45
c
c -----
c Printing
c Prints all tables pertinent to the problem
print
c .....
c sets the frequency of tally and runtpe dumps
prdump 1e8 1e8

```

17.3.2 Shielded Setups

17.3.2.1 Multi-material, Multi-layered

Simplified Model for Neutron Fluence Calculations

c This is the newest version of the neutron model. It accounts for the actual
c size of the drum and source cradle, as well as source placement. It can be
c modified to have the shielding material placed over the hole.

c

c CELL CARDS

c =====

c -----

c source material and Pb/SS capsule

c -----

100 300 -2.214403 -1 2 -3 \$ AmO2/Be13 source material

101 500 -0.001225 -1 3 -4 \$ air inside SS1 capsule
 110 104 -8.03 (1:-2:4)(-5 7 -8) \$ SS1 capsule
 111 500 -0.001225 5 -6 7 -8 \$ air between SS1/SS2
 120 104 -8.03 (6:-7:8)(-9 11 -12) \$ SS2 capsule
 121 500 -0.001225 9 -10 11 -12 \$ air between SS2/Pb
 130 202 -11.35 (10:-11:12)(-13 14 -15) \$ Pb capsule
 132 500 -0.001225 (13:-14:15)(-20 14 -22) \$ air outside Pb/inside 1.5" PVC cradle
 c -----
 c PVC cradle
 c -----
 140 203 -1.406 20 -21 14 -22 \$ 1.5" PVC pipe of cradle
 141 203 -1.406 (21:-14:27)(-25 26 -27) \$ 1.5" bottom PVC cap
 142 203 -1.406 (21:-28:22)(-25 28 -29) \$ 1.5" top PVC cap
 143 500 -0.001225 (25:-28:29)(25:-26:27)(21 -30 26 -29) \$ air around PVC capsule inside 2.5" PVC tube of collimator
 c -----
 c Collimator
 c -----
 150 500 -0.001225 -1 29 -31 \$ air inside polyethylene tube
 151 204 -0.94 1 -30 29 -31 \$ polyethylene tube
 152 203 -1.406 30 -32 26 -33 \$ 2.5" PVC tube of collimator
 153 203 -1.406 (32:-26:37)(-35 36 -37) \$ 2.5" PVC cap
 c -----
 c Drum and paraffin wax
 c -----
 160 201 -0.92 (35:-36:37)(32:-36:33)(-40 44 -33) \$ Paraffin wax inside drum
 165 205 -8.03 40 -41 42 -33 \$ Steel drum wall
 166 205 -8.03 -40 43 -44 \$ Steel drum bottom
 167 500 -0.001225 -40 42 -43 \$ air under drum
 c -----
 c Shielding Blocks
 c -----
 200 106 -7.9394 31 -55 50 -51 52 -53 \$ SS shielding
 210 102 -1.4783 55 -56 50 -51 52 -53 \$ BP shielding
 220 103 -14.842 57 -58 50 -51 52 -53 \$ WC shielding
 230 105 -2.3462 56 -57 50 -51 52 -53 \$ C shielding
 c -----
 c Detector
 c -----
 300 104 -8.03 (60:-62:65)(-1 61 -66) \$ SS detector can
 310 403 -0.000622 -60 63 -64 \$ He-3/CO2 fill gas
 320 0 -60 62 -63 \$ lower inactive region
 330 0 -60 64 -65 \$ upper inactive region
 c -----
 c Floor, Walls, and Room Atmosphere
 c -----
 400 101 -2.30 90 -91 -92 93 94 -95 (82:-83:81:-80:-42:84) \$ concrete floor and building walls
 401 101 -2.30 (80 -75 76 -77 42 -73) \$ concrete bricks of reactor - facing drum
 402 101 -2.30 (77 -78 74 -75 42 -73) \$ concrete bricks of reactor - facing console
 403 101 -2.30 (80 -75 76 -78 73 -79) \$ concrete bricks of reactor - top
 405 101 -2.30 70 -71 72 -82 42 -73 \$ concrete bricks of additional wall
 800 500 -0.001225 (41:-42:33)(30:31:-33)(1:-61:66)(-70:71:-72:82:-42:73)
 (-80:75:-76:77:-42:73)(-76:78:-74:75:-42:73)(-80:75:-76:78:-73:79)
 (42 -84 -82 83 80 -81)(-31:-50:51:-52:53:58) \$ Room air
 c -----
 c End of Universe
 c -----
 900 0 -90:91:92:-93:-94:95 \$ kill space

 c SURFACE CARDS
 c =====
 c -----
 c source and capsule

c -----

1 cz 1.27 \$ source material & air/SS interface, collimator ID, detector OD
2 pz 30.2082 \$ bottom of source material/inner bottom SS1
3 pz 36.5894 \$ source material/air interface
4 pz 41.6382 \$ air/inner top SS1
5 cz 1.3462 \$ outer SS1/air
6 cz 1.35128 \$ air/inner SS2
7 pz 30.0177 \$ SS1 outer bottom/SS2 inner bottom
8 pz 41.8287 \$ SS1 outer top/SS2 inner top
9 cz 1.45415 \$ outer SS2/air
10 cz 1.4605 \$ air/inner Pb
11 pz 29.7637 \$ outer bottom SS2/inner bottom Pb
12 pz 42.4637 \$ outer top SS2/inner top Pb
13 cz 1.778 \$ outer Pb/air
14 pz 29.4462 \$ outer bottom Pb, inner bottom PVC cap of cradle
15 pz 42.7812 \$ outer top Pb

c -----

c PVC cradle

c -----

20 cz 2.047 \$ ID 1.5" PVC tube of cradle
21 cz 2.40 \$ OD 1.5" PVC tube of cradle
22 pz 44.21 \$ top of 1.5" PVC tube/inner top PVC cap
25 cz 2.8375 \$ OD 1.5" PVC caps
26 pz 26.035 \$ outer bottom PVC cap, inner bottom PVC cap of collimator
27 pz 31.6712 \$ top edge of 1.5" PVC bottom cap
28 pz 41.985 \$ bottom edge of 1/5" PVC top cap
29 pz 45.085 \$ outer top of 1.5" PVC top cap, bottom of poly collimator tube

c -----

c Collimator

c -----

30 cz 3.134 \$ OD poly tube/ID 2.5" PVC tube
31 pz 90.805 \$ top of poly tube
32 cz 3.65 \$ OD 2.5" PVC tube/ID 2.5" PVC cap
33 pz 86.995 \$ top of 2.5" PVC tube, top of drum/paraffin wax
35 cz 4.24 \$ OD 2.5" PVC cap
36 pz 25.445 \$ outer bottom 2.5" PVC cap
37 pz 31.455 \$ top edge of 2.5" PVC cap

c -----

c Drum and Paraffin Wax

c -----

40 cz 28.575 \$ ID drum/OD wax
41 cz 28.7401 \$ OD drum/atmosphere
42 pz 0 \$ bottom of drum bottom rim
43 pz 2.413 \$ outer bottom of drum/air
44 pz 2.5781 \$ inner bottom of drum/wax

c -----

c Shielding Blocks

c -----

50 py -5.0800 \$ front edge of shielding
51 py 5.0800 \$ back edge of shielding
52 px -5.0800 \$ top edge of shielding
53 px 5.0800 \$ bottom edge of shielding
55 pz 91.107 \$ outer SS inner BP
56 pz 93.64 \$ outer BP inner C
57 pz 101.451 \$ outer C inner WC
58 pz 101.845 \$ outer WC

c -----

c Detector

c -----

60 cz 1.2192 \$ ID of detector/fill gas
61 pz 106.045 \$ outer bottom of SS detector can
62 pz 106.096 \$ inner bottom of SS can/inactive region

63 pz 108.2042 \$ inactive region/fill gas
 64 pz 138.5824 \$ fill gas/inactive region
 65 pz 141.732 \$ inactive region/inner top SS can
 66 pz 141.783 \$ outer top SS can

c -----

c Floor and Walls

c -----

70 px 91.44 \$ additional concrete brick walls
 71 px 131.90 \$ additional concrete brick walls
 72 py 398.78 \$ additional concrete brick walls
 73 pz 243.84 \$ additional concrete brick walls
 74 px -30.30 \$ reactor concrete brick walls
 75 px 10.16 \$ reactor concrete brick walls
 76 py 247.98 \$ reactor concrete brick walls
 77 py 288.44 \$ reactor concrete brick walls
 78 py 502.92 \$ reactor concrete brick walls
 79 pz 320.04 \$ reactor concrete brick walls
 80 px -350.52 \$ inner wall of building
 81 px 502.92 \$ inner wall of building
 82 py 601.98 \$ inner wall of building
 83 py -251.46 \$ inner wall of building
 84 pz 701.04 \$ inner wall of building

c -----

c End of Universe

c -----

90 pz -40 \$ kill
 91 pz 716.28 \$ kill
 92 py 632.46 \$ kill
 93 py -281.94 \$ kill
 94 px -381.00 \$ kill
 95 px 533.40 \$ kill

c DATA CARDS

c =====

c

c Material Cards

c The ZA and atom densities come from PNNL compendium except WC, which is self-
 c calculated.

c

m101 \$ regular concrete (floor, walls), den=2.30 g/cc

1001 0.0137404197
 1002 0.0000015803
 8016 0.0460382693
 8017 0.0000175372
 11023 0.001747
 13027 0.001745
 14028 0.0153285761
 14029 0.0007783478
 14030 0.0005130926
 20040 0.0014744726
 20042 0.0000098409
 20043 0.0000020534
 20044 0.0000317281
 20046 0.0000000608
 20048 0.0000028443
 26054 0.0000202822
 26056 0.0003183864
 26057 0.0000073529
 26058 0.0000009785

m102 \$ borated polyethylene (shielding material), den=1.4783 g/cc

1001 0.1205772320
 1002 0.0000138680

5010 0.0008194
 5011 0.0032980
 6000 0.0602956
 m103 \$ tungsten carbide (shielding material), den=14.842 g/cc
 6000 0.0427165
 8016 0.0008376774
 8017 0.0000003191
 23050 0.0000006
 23051 0.0002625
 26054 0.0000094
 26056 0.0001468
 26057 0.0000034
 26058 0.0000004
 27059 0.0090999
 74180 0.0000512
 74182 0.0113199
 74183 0.0061127
 74184 0.0130883
 74186 0.0121443
 m104 \$ stainless steel 304 (source container, and detector can), den=8.03 g/cc
 6000 0.000160
 14028 0.0007913308
 14029 0.0000401819
 14030 0.0000264882
 15031 0.000036
 16032 0.0000218339
 16033 0.0000001748
 16034 0.0000009867
 16036 0.0000000046
 24050 0.0007649373
 24052 0.0147510535
 24053 0.0016726511
 24054 0.0004163583
 25055 0.000877
 26054 0.0035384461
 26056 0.0555460365
 26057 0.0012828002
 26058 0.0001707172
 28058 0.0051690790
 28060 0.0019911200
 28061 0.0000865526
 28062 0.0002759676
 28064 0.0000702808
 m105 \$ shielding concrete, den=2.3462 g/cc
 1001 0.0140163879
 1002 0.0000016121
 8016 0.0469630131
 8017 0.0000178894
 11023 0.0017821
 13027 0.0017801
 14028 0.0156364389
 14029 0.0007939804
 14030 0.0005233977
 20040 0.0015041366
 20042 0.0000100389
 20043 0.0000020947
 20044 0.0000323664
 20046 0.0000000621
 20048 0.0000029015
 26054 0.0000206913
 26056 0.0003248092
 26057 0.0000075013

26058 0.0000009983
 m106 \$ stainless steel 304 (shielding material), den=7.9394 g/cc
 6000 0.0001582
 14028 0.0007823845
 14029 0.0000397276
 14030 0.0000261887
 15031 0.0000356
 16032 0.0000215491
 16033 0.0000001725
 16034 0.0000009738
 16036 0.0000000045
 24050 0.0007563081
 24052 0.0145846485
 24053 0.0016537821
 24054 0.0004116614
 25055 0.0008671
 26054 0.0034985248
 26056 0.0549193567
 26057 0.0012683275
 26058 0.0001687911
 28058 0.0051107371
 28060 0.0019686468
 28061 0.0000855757
 28062 0.0002728528
 28064 0.0000694876
 m201 \$ paraffin wax (collimator/drum), den=0.92
 1001 0.0817128019
 1002 0.0000093981
 6000 0.0392727
 m202 \$ lead (source container), den=11.35 g/cc
 82204 0.0004618320
 82206 0.0079501080
 82207 0.0072903480
 82208 0.0172857120
 m203 \$ PVC (collimator/drum), den=1.406 g/cc
 1001 0.0406383261
 1002 0.0000046739
 6000 0.027096
 17035 0.010264
 17037 0.003284
 m204 \$ Polyethylene (collimator/drum), den=0.94 g/cc
 1001 0.0790217115
 1002 0.0000090885
 6000 0.0394984
 m205 \$ Iron (collimator/drum), den=7.874 g/cc
 26054 0.0049630480
 26056 0.0779092389
 26057 0.0017992641
 26058 0.0002394490
 m300 \$ AmBe [14 g Am, 57.6 g Be] (AmBe source material) den=2.214403 g/cc
 4009 0.1479713726
 8016 0.0833413036
 8017 0.0000298791
 95241 0.0055320804
 m403 \$ helium 3 w/ 2% CO2 (detector medium - neutron) - P=4 atm, P4-0812-217, den=0.000622 g/cc
 2003 0.0001326651
 6000 0.0000074934
 8016 0.0000112457
 8017 0.0000000043
 m500 \$ dry air (within source and around the whole assembly), den=0.001225 g/cc
 7014 0.0000388565
 7015 0.0000001435


```

c    KMESH 716.28 KINTS 500
c
c FMESH14:n GEOM=xyz ORIGIN=-381 -281.94 -40
c    IMESH 533.4 IINTS 1
c    JMESH 632.46 JINTS 500
c    KMESH 716.28 KINTS 500
c FM14 -1 0 103
c =====
c
c Optional Cards
c -----
c Plotting
c mplot freq 5e6 tally 4 tfc m
c -----
c Cutoffs: Time, Energy, and Weight
c cut:n 1.0e123 1e-4 -0.5 -0.25
c CUT:h J 0.001
c CUT:t J 0.001
c -----
c Computer Time Cutoff
c CTME 45
c -----
c Printing
c Prints all tables pertinent to the problem
print
c .....
c sets the frequency of tally and runtime dumps
prdump 1e8 1e8

```

17.4 Gamma Ray Hot Cell Optimization Models

17.4.1 Concrete Only

Gamma Shielding Optimization

c This input file creates a concrete wall X (4 - 7) ft thick and
c placed a 3D fuel assembly on one side as a source using a photon distribution
c given from ORIGEN. A mesh detector is placed on the side of the wall opposite
c the source representing a human body. The tallies are weighted to give dose in
c each boxel of the mesh. There is a point detector at the head of the person.

c CELL CARDS

100	101	-2.3000	1 -2 50 -51 3 -4	\$ Concrete Wall section 1
101	101	-2.3000	1 -2 51 -52 3 -4	\$ Concrete Wall section 2
102	101	-2.3000	1 -2 52 -53 3 -4	\$ Concrete Wall section 3
103	101	-2.3000	1 -2 53 -54 3 -4	\$ Concrete Wall section 4
104	101	-2.3000	1 -2 54 -55 3 -4	\$ Concrete Wall section 5
105	101	-2.3000	1 -2 55 -56 3 -4	\$ Concrete Wall section 6
106	101	-2.3000	1 -2 56 -57 3 -4	\$ Concrete Wall section 7
107	101	-2.3000	1 -2 57 -58 3 -4	\$ Concrete Wall section 8
108	101	-2.3000	1 -2 58 -59 3 -4	\$ Concrete Wall section 9
109	101	-2.3000	1 -2 59 -60 3 -4	\$ Concrete Wall section 10
110	101	-2.3000	1 -2 60 -61 3 -4	\$ Concrete Wall section 11
111	101	-2.3000	1 -2 61 -62 3 -4	\$ Concrete Wall section 12
112	101	-2.3000	1 -2 62 -63 3 -4	\$ Concrete Wall section 13
113	101	-2.3000	1 -2 63 -64 3 -4	\$ Concrete Wall section 14
114	101	-2.3000	1 -2 64 -65 3 -4	\$ Concrete Wall section 15
115	101	-2.3000	1 -2 65 -66 3 -4	\$ Concrete Wall section 16
116	101	-2.3000	1 -2 66 -67 3 -4	\$ Concrete Wall section 17

117	101	-2.3000	1 -2 67 -68 3 -4	\$ Concrete Wall section 18
118	101	-2.3000	1 -2 68 -69 3 -4	\$ Concrete Wall section 19
119	101	-2.3000	1 -2 69 -70 3 -4	\$ Concrete Wall section 20
120	101	-2.3000	1 -2 70 -71 3 -4	\$ Concrete Wall section 21
121	101	-2.3000	1 -2 71 -72 3 -4	\$ Concrete Wall section 22
122	101	-2.3000	1 -2 72 -73 3 -4	\$ Concrete Wall section 23
123	101	-2.3000	1 -2 73 -74 3 -4	\$ Concrete Wall section 24
124	101	-2.3000	1 -2 74 -75 3 -4	\$ Concrete Wall section 25
125	101	-2.3000	1 -2 75 -76 3 -4	\$ Concrete Wall section 26
126	101	-2.3000	1 -2 76 -77 3 -4	\$ Concrete Wall section 27
127	101	-2.3000	1 -2 77 -78 3 -4	\$ Concrete Wall section 28
128	101	-2.3000	1 -2 78 -79 3 -4	\$ Concrete Wall section 29
129	101	-2.3000	1 -2 79 -80 3 -4	\$ Concrete Wall section 30
200	300	-5.4850	10 -11 12 -13 14 -15	\$ Fuel Bundle/Source
400	401	-3.76	-40 -43 44	\$ NaI detector medium
401	0		-40 -44 45	\$ Vacuum of PMT
402	403	-2.6989	(40:43:-44) -41 -42 44	\$ Al can of NaI detector
403	404	-8.7470	(40:44:-45) -41 -44 46	\$ Mu metal can of PMT
500	501	-0.001662	1 -2 80 -31 5 -4 (-10:11:-12:13:-14:15)	\$ Argon
501	500	-0.0012	1 -2 30 -50 5 -4 (41:42:-46)	\$ Atmosphere
600	101	-2.3000	1 -2 80 -31 3 -5	\$ Floor
601	101	-2.3000	1 -2 30 -50 3 -5	\$ Floor
700	0		-1:2:-30:31:-3:4	\$ Kill Zone

c SURFACE CARDS

1	px 0	\$concrete boundary
2	px 1000	\$concrete boundary
3	pz -317	\$concrete boundary
4	pz 683	\$concrete boundary
5	pz -277	\$floor boundary
10	px 490.905	\$source boundary
11	px 509.095	\$source boundary
12	py 180	\$source boundary
13	py 198.19	\$source boundary
14	pz -277	\$source boundary
15	pz 88.76	\$source boundary
30	py -135	\$kill boundary
31	py 337	\$kill boundary
40	c/y 500 -127 2.54	\$ detector (NaI) and PMT radius
41	c/y 500 -127 2.591	\$ Al detector can outer radius
42	py -30	\$ Al detector can bottom
43	py -30.043	\$ Al can NaI interface
44	py -35.131	\$ NaI PMT interface and Al Mu interface
45	py -48.364	\$ PMT vacuum Mu can interface
46	py -48.415	\$ Mu can top air interface
50	py 0	\$concrete boundary
51	py 5	\$concrete boundary
52	py 10	\$concrete boundary
53	py 15	\$concrete boundary
54	py 20	\$concrete boundary
55	py 25	\$concrete boundary
56	py 30	\$concrete boundary
57	py 35	\$concrete boundary
58	py 40	\$concrete boundary
59	py 45	\$concrete boundary
60	py 50	\$concrete boundary
61	py 55	\$concrete boundary
62	py 60	\$concrete boundary
63	py 65	\$concrete boundary
64	py 70	\$concrete boundary
65	py 75	\$concrete boundary
66	py 80	\$concrete boundary

67 py 85 \$concrete boundary
 68 py 90 \$concrete boundary
 69 py 95 \$concrete boundary
 70 py 100 \$concrete boundary
 71 py 105 \$concrete boundary
 72 py 110 \$concrete boundary
 73 py 115 \$concrete boundary
 74 py 120 \$concrete boundary
 75 py 125 \$concrete boundary
 76 py 130 \$concrete boundary
 77 py 135 \$concrete boundary
 78 py 140 \$concrete boundary
 79 py 145 \$concrete boundary
 80 py 150 \$concrete boundary

c DATA CARDS

c

c Material Cards

c

m101 \$ regular concrete (shielding material), density=2.30 g/cc

1000 0.013742
 8000 0.046056
 11000 0.001747
 13000 0.001745
 14000 0.016620
 20000 0.001521
 26000 0.000347

m102 \$ borated polyethylene (shielding material), density=1.40 g/cc

1000 0.1142039
 5000 0.0038993
 6000 0.0571019

m103 \$ tungsten carbide (shielding material), density=14.93 g/cc

6000 0.0429698
 8000 0.0008429
 23000 0.0002647
 26000 0.0001610
 27000 0.0091538
 74000 0.0429698

m104 \$ stainless steel 304 (shielding material, source container, and detector can), density=8.03 g/cc

6000 0.000160
 14000 0.000858
 15000 0.000036
 16000 0.000023
 24000 0.017605
 25000 0.000877
 26000 0.060538
 28000 0.007593

c I obtained the UO2 definition from Seth Roberson. I think we should check it.

m300 \$ UO2 from SCALE Manual, density set to 5.485 g/cc instead of 10.96 g/cc for homogenization purposes

8016 2.440578e-2
 8017 9.296786e-6
 8018 5.015371e-5
 92234 6.605612e-7
 92235 8.812375e-5
 92238 1.214383e-2

m401 \$ sodium iodide (detector medium - photon), density=3.76 g/cc

11000 0.0150794
 53000 0.0150794
 81000 0.0000196

m403 \$ aluminum (detector can of NaI), density=2.6989 g/cc

13000 0.060238

m404 \$ mu metal (detector can of PMT vacuum), density=8.747 g/cc

```

6000 0.0000877
25000 0.0004794
14000 0.0006564
28000 0.0717977
42000 0.0023060
26000 0.0140827
m500 $ dry air (within source and around the whole assembly), density=0.001225 g/cc
7000 0.000039
8000 0.000011
m501 $ Argon, density = 0.001662 g/cc
18000 0.000025
c
c Source Definition Cards
c
c This source is an approximation of a SCALE calculated Westinghouse 17x17 fuel
c bundle with 60 GWd burnup over 3 cycles plus 10 years of cooling. Original
c enrichment was 6 w%.
mode p e
stop f24 0.01
sdef x d1 y d2 z d3 erg d4
si1 490.905 509.095
sp1 0 1
si2 180 198.19
sp2 0 1
si3 -277 88.76
sp3 0 1
si4 H 0.01 0.05 0.1 0.2 0.3 0.4 0.6 0.8 1 1.33 1.67 2 2.5 3 4 5
6.5 8 10
sp4 0 0.266728003144 0.074693960431 0.055137928740 0.016180577719
0.010403676527 0.048915378105 0.485281106843 0.026383809300 0.014246186685
0.001984696877 0.000033312782 0.000010555470 0.000000738241 0.000000064876
0.000000002847 0.000000001143 0.000000000224 0.000000000048
c
c Variance Reduction
c
c Importance Card
c
IMP:p 2147483648
1073741824
536870912
268435456
134217728
67108864
33554432
16777216
8388608
4194304
2097152
1048576
524288
262144
131072
65536
32768
16384
8192
4096
2048
1024
512
256
128

```



```

c   JMESH= -10 0 130 137 219 238   JINTS= 6 1 65 7 8 19   $ 4 cm in tissue, 10 cm in air, 1&2 cm in concrete, 1 cm in
fuel
c   KMESH= 683   KINTS= 500           $ 2 cm mesh intervals
c
c Exponential Transform
c
c EXT:p  SV2 SV2 0 0 0 0
c VECT  V2 500 -22.5 179
c
c
c Tally Cards
c
c GEB values for a, b, and c come from MCNP detector class handout b-93_detectors.pdf
c
c Cell numbers for all F8, F6, and F4 tallies must be altered to match the new input file
c
c F8:e 400
c E8 0 1e-5 0.015 81911 0.745
c FT8 GEB 0.0 0.0586 0.30486 &
c PHL 1 6 1 NAI-1
c F6:e 400
c
c The 401 in F24 must be altered to match the material number for the NaI detector
c
F24:p 400
FM24 -1 401 -5
SD24 1
c
c Origin, IJKMESH and IJKINTS must all be altered to match new input file.
c
c FMESH4:p GEOM=xyz ORIGIN=-78 -109 -110
c   IMESH 162 IINTS 501
c   JMESH 109 JINTS 101
c   KMESH 110 KINTS 101
c
c FMESH14:p GEOM=xyz ORIGIN=-78 -109 -110
c   IMESH 162 IINTS 501
c   JMESH 109 JINTS 101
c   KMESH 110 KINTS 101
c FM14 -1 0 -5
c
c Optional Cards
c
c -----
c Plotting
c mplot freq 5e6 tally 4 tfc m
c
c -----
c Cutoffs: Time, Energy, and Weight
c cut:p 1.0e123 0.001 -0.5 -0.25
c
c -----
c Computer Time Cutoff
c CTME 45
c
c -----
c Printing
c Prints all tables pertinent to the problem
print
c .....
c sets the frequency of tally and runtpe dumps
c this must be altered to a reasonable number relative to NPS in the new input file

```

prdmp 1e9 1e9

17.4.2 Multi-material, Multi-layered

Gamma Shielding Optimization

c This input file creates a concrete wall X (4 - 7) ft thick and
c placed a 3D fuel assembly on one side as a source using a photon distribution
c given from ORIGEN. A mesh detector is placed on the side of the wall opposite
c the source representing a human body. The tallies are weighted to give dose in
c each boxel of the mesh. There is a point detector at the head of the person.

c CELL CARDS

100	104	-8.0300	1 -2 40 -41 3 -4	\$ stainless steel section
200	101	-2.3000	1 -2 41 -42 3 -4	\$ concrete section 1
201	101	-2.3000	1 -2 42 -43 3 -4	\$ concrete section 2
202	101	-2.3000	1 -2 43 -44 3 -4	\$ concrete section 3
203	101	-2.3000	1 -2 44 -45 3 -4	\$ concrete section 4
204	101	-2.3000	1 -2 45 -46 3 -4	\$ concrete section 5
205	101	-2.3000	1 -2 46 -47 3 -4	\$ concrete section 6
300	103	-14.930	1 -2 47 -48 3 -4	\$ WC section 1
301	103	-14.930	1 -2 48 -49 3 -4	\$ WC section 2
302	103	-14.930	1 -2 49 -50 3 -4	\$ WC section 3
303	103	-14.930	1 -2 50 -51 3 -4	\$ WC section 4
304	103	-14.930	1 -2 51 -52 3 -4	\$ WC section 5
305	103	-14.930	1 -2 52 -53 3 -4	\$ WC section 6
306	103	-14.930	1 -2 53 -54 3 -4	\$ WC section 7
307	103	-14.930	1 -2 54 -55 3 -4	\$ WC section 8
308	103	-14.930	1 -2 55 -56 3 -4	\$ WC section 9
309	103	-14.930	1 -2 56 -57 3 -4	\$ WC section 10
310	103	-14.930	1 -2 57 -58 3 -4	\$ WC section 11
311	103	-14.930	1 -2 58 -59 3 -4	\$ WC section 12
312	103	-14.930	1 -2 59 -60 3 -4	\$ WC section 13
313	103	-14.930	1 -2 60 -61 3 -4	\$ WC section 14
314	103	-14.930	1 -2 61 -62 3 -4	\$ WC section 15
315	103	-14.930	1 -2 62 -63 3 -4	\$ WC section 16
316	103	-14.930	1 -2 63 -64 3 -4	\$ WC section 17
317	103	-14.930	1 -2 64 -65 3 -4	\$ WC section 18
318	103	-14.930	1 -2 65 -66 3 -4	\$ WC section 19
319	103	-14.930	1 -2 66 -67 3 -4	\$ WC section 20
400	102	-1.4000	1 -2 67 -68 3 -4	\$ BP section 1
401	102	-1.4000	1 -2 68 -69 3 -4	\$ BP section 2
402	102	-1.4000	1 -2 69 -70 3 -4	\$ BP section 3
403	102	-1.4000	1 -2 70 -71 3 -4	\$ BP section 4
404	102	-1.4000	1 -2 71 -72 3 -4	\$ BP section 5
405	102	-1.4000	1 -2 72 -73 3 -4	\$ BP section 6
2000	300	-5.4850	10 -11 -12 13 14 -15	\$ Fuel Bundle/Source
4000	401	-3.76	-20 23 -24	\$ NaI detector medium
4001	0		-20 24 -25	\$ Vacuum of PMT
4002	403	-2.6989	(20:-23:24) -21 22 -24	\$ Al can of NaI detector
4003	404	-8.7470	(20:-24:25) -21 24 -26	\$ Mu metal can of PMT
5000	500	-0.0012	1 -2 73 -31 5 -4 (21:-22:26)	\$ Atmosphere
5001	501	-0.001662	1 -2 30 -40 5 -4 (-10:11:12:-13:-14:15)	\$ Argon
6000	101	-2.3000	1 -2 73 -31 3 -5	\$ Floor
6001	101	-2.3000	1 -2 30 -40 3 -5	\$ Floor
7000	0		-1:2:-30:31:-3:4	\$ Kill Zone

c SURFACE CARDS

1	px 0	\$concrete boundary
2	px 1000	\$concrete boundary
3	pz -317	\$concrete boundary
4	pz 683	\$concrete boundary
5	pz -277	\$floor boundary
10	px 490.905	\$source boundary

11 px 509.095 \$source boundary
 12 py -31.27 \$source boundary
 13 py -49.46 \$source boundary
 14 pz -277 \$source boundary
 15 pz 88.76 \$source boundary
 20 c/y 503 -130 2.54 \$ detector (NaI) and PMT radius
 21 c/y 503 -130 2.591 \$ Al detector can outer radius
 22 py 90.24 \$ Al detector can bottom
 23 py 90.283 \$ Al can NaI interface
 24 py 95.371 \$ NaI PMT interface and Al Mu interface
 25 py 108.604 \$ PMT vacuum Mu can interface
 26 py 108.655 \$ Mu can top air interface
 30 py -135 \$skill boundary
 31 py 178.19 \$skill boundary
 40 py -1.27 \$stainless steel/atmosphere boundary
 41 py 0 \$concrete/stainless steel boundary
 42 py 5 \$concrete boundary
 43 py 10 \$concrete boundary
 44 py 15 \$concrete boundary
 45 py 20 \$concrete boundary
 46 py 25 \$concrete boundary
 47 py 30 \$concrete/BP boundary
 48 py 30.75 \$WC boundary
 49 py 31.5 \$WC boundary
 50 py 32.25 \$WC boundary
 51 py 33 \$WC boundary
 52 py 33.75 \$WC boundary
 53 py 34.5 \$WC boundary
 54 py 35.25 \$WC boundary
 55 py 36 \$WC boundary
 56 py 36.75 \$WC boundary
 57 py 37.5 \$WC boundary
 58 py 38.25 \$WC boundary
 59 py 39 \$WC boundary
 60 py 39.75 \$WC boundary
 61 py 40.5 \$WC boundary
 62 py 41.25 \$WC boundary
 63 py 42 \$WC boundary
 64 py 42.75 \$WC boundary
 65 py 43.5 \$WC boundary
 66 py 44.25 \$WC boundary
 67 py 45 \$WC boundary
 68 py 47.54 \$BP boundary
 69 py 50.08 \$BP boundary
 70 py 52.62 \$BP boundary
 71 py 55.16 \$BP boundary
 72 py 57.7 \$BP boundary
 73 py 60.24 \$BP boundary

c DATA CARDS

c

c Material Cards

c

m101 \$ regular concrete (shielding material), density=2.30 g/cc

1000 0.013742

8000 0.046056

11000 0.001747

13000 0.001745

14000 0.016620

20000 0.001521

26000 0.000347

m102 \$ borated polyethylene (shielding material), density=1.40 g/cc

```

1000 0.1142039
5000 0.0038993
6000 0.0571019
m103 $ tungsten carbide (shielding material), density=14.93 g/cc
6000 0.0429698
8000 0.0008429
23000 0.0002647
26000 0.0001610
27000 0.0091538
74000 0.0429698
m104 $ stainless steel 304 (shielding material, source container, and detector can), density=8.03 g/cc
6000 0.000160
14000 0.000858
15000 0.000036
16000 0.000023
24000 0.017605
25000 0.000877
26000 0.060538
28000 0.007593
c I obtained the UO2 definition from Seth Roberson. I think we should check it.
m300 $ UO2 from SCALE Manual, density set to 5.485 g/cc instead of 10.96 g/cc for homogenization purposes
8016 2.440578e-2
8017 9.296786e-6
8018 5.015371e-5
92234 6.605612e-7
92235 8.812375e-5
92238 1.214383e-2
m401 $ sodium iodide (detector medium - photon), density=3.76 g/cc
11000 0.0150794
53000 0.0150794
81000 0.0000196
m403 $ aluminum (detector can of NaI), density=2.6989 g/cc
13000 0.060238
m404 $ mu metal (detector can of PMT vacuum), density=8.747 g/cc
6000 0.0000877
25000 0.0004794
14000 0.0006564
28000 0.0717977
42000 0.0023060
26000 0.0140827
m500 $ dry air (within source and around the whole assembly), density=0.001225 g/cc
7000 0.000039
8000 0.000011
m501 $ Argon, density = 0.001662 g/cc
18000 0.000025
c
c Source Definition Cards
c
c This source is an approximation of a SCALE calculated Westinghouse 17x17 fuel
c bundle with 60 GWd burnup over 3 cycles plus 10 years of cooling. Original
c enrichment was 6 w%.
mode p e
stop f24 0.05
sdef x d1 y d2 z d3 erg d4
si1 490.905 509.095
sp1 0 1
si2 150 168.19
sp2 0 1
si3 -277 88.76
sp3 0 1
si4 H 0.01 0.05 0.1 0.2 0.3 0.4 0.6 0.8 1 1.33 1.67 2 2.5 3 4 5
6.5 8 10

```

sp4 0 0.266728003144 0.074693960431 0.055137928740 0.016180577719
0.010403676527 0.048915378105 0.485281106843 0.026383809300 0.014246186685
0.001984696877 0.000033312782 0.000010555470 0.000000738241 0.000000064876
0.000000002847 0.000000001143 0.000000000224 0.000000000048

c

c Variance Reduction

c

c Importance Card

c

IMP:p 4

8

16

32

64

128

256

512

1024

2048

4096

8192

16384

32768

65536

131072

262144

524288

1048576

2097152

4194304

8388608

16777216

33554432

67108864

134217728

268435456

536870912

1073741824

2147483648

4294967296

8589934592

17179869184

1 137438953472 68719476736 68719476736

68719476736 34359738368 2 34359738368 2 0

IMP:e 0

0

0

0

0

0

0

0

0

0

0

0

0

0

0

0

0

0


```

F24:p 4000
FM24 -1 401 -5
SD24 1
c
c Origin, IJKMESH and IJKINTS must all be altered to match new input file.
c
c FMESH4:p GEOM=xyz ORIGIN=-78 -109 -110
c   IMESH 162 IINTS 501
c   JMESH 109 JINTS 101
c   KMESH 110 KINTS 101
c
c FMESH14:p GEOM=xyz ORIGIN=-78 -109 -110
c   IMESH 162 IINTS 501
c   JMESH 109 JINTS 101
c   KMESH 110 KINTS 101
c FM14 -1 0 -5
c
c Optional Cards
c
c -----
c Plotting
c mplot freq 5e6 tally 4 tfc m
c
c -----
c Cutoffs: Time, Energy, and Weight
c cut:p 1.0e123 0.001 -0.5 -0.25
c
c -----
c Computer Time Cutoff
c CTME 45
c
c -----
c Printing
c Prints all tables pertinent to the problem
print
c .....
c sets the frequency of tally and runtpe dumps
c this must be altered to a reasonable number relative to NPS in the new input file
prdmp 1e9 1e9

```

17.5 Neutron Hot Cell Optimization Models

17.5.1 Concrete Only

Neutron Shielding Optimization

```

c This input file creates a concrete wall X (4 - 7) ft thick and
c placed a 3D fuel assembly on one side as a source using a photon distribution
c given from ORIGEN. A mesh detector is placed on the side of the wall opposite
c the source representing a human body. The tallies are weighted to give dose in
c each boxel of the mesh. There is a point detector at the head of the person.

```

c CELL CARDS

100	101	-2.3000	1 -2 40 -41 3 -4	\$ Concrete Wall section 1
101	101	-2.3000	1 -2 41 -42 3 -4	\$ Concrete Wall section 2
102	101	-2.3000	1 -2 42 -43 3 -4	\$ Concrete Wall section 3
103	101	-2.3000	1 -2 43 -44 3 -4	\$ Concrete Wall section 4
104	101	-2.3000	1 -2 44 -45 3 -4	\$ Concrete Wall section 5
105	101	-2.3000	1 -2 45 -46 3 -4	\$ Concrete Wall section 6
106	101	-2.3000	1 -2 46 -47 3 -4	\$ Concrete Wall section 7
107	101	-2.3000	1 -2 47 -48 3 -4	\$ Concrete Wall section 8
108	101	-2.3000	1 -2 48 -49 3 -4	\$ Concrete Wall section 9
109	101	-2.3000	1 -2 49 -50 3 -4	\$ Concrete Wall section 10
110	101	-2.3000	1 -2 50 -51 3 -4	\$ Concrete Wall section 11

111	101	-2.3000	1 -2 51 -52 3 -4	\$ Concrete Wall section 12
112	101	-2.3000	1 -2 52 -53 3 -4	\$ Concrete Wall section 13
113	101	-2.3000	1 -2 53 -54 3 -4	\$ Concrete Wall section 14
114	101	-2.3000	1 -2 54 -55 3 -4	\$ Concrete Wall section 15
115	101	-2.3000	1 -2 55 -56 3 -4	\$ Concrete Wall section 16
116	101	-2.3000	1 -2 56 -57 3 -4	\$ Concrete Wall section 17
117	101	-2.3000	1 -2 57 -58 3 -4	\$ Concrete Wall section 18
118	101	-2.3000	1 -2 58 -59 3 -4	\$ Concrete Wall section 19
119	101	-2.3000	1 -2 59 -60 3 -4	\$ Concrete Wall section 20
2000	200	-11.460	-10	\$ Fuel Bundle/Source
3000	104	-8.03	(21:23:-24)(-20 -22 25)	\$ SS304 detector can
3100	403	-0.000622	-21 -23 24	\$ He-3 fill gas of detector
5000	501	-0.001662	1 -2 60 -31 5 -4 10	\$ Atmosphere
5001	500	-0.0012	1 -2 30 -40 5 -4 (20:22:-25)	\$ Atmosphere
6000	101	-2.3000	1 -2 60 -31 3 -5	\$ Floor
6001	101	-2.3000	1 -2 30 -40 3 -5	\$ Floor
7000	0		-1:2:-30:31:-3:4	\$ Kill Zone

c SURFACE CARDS

1	px 0	\$concrete boundary
2	px 1000	\$concrete boundary
3	pz -317	\$concrete boundary
4	pz 683	\$concrete boundary
5	pz -277	\$floor boundary
10	s 500 185.93 -271.07 5.93	\$source boundary
20	c/y 503 -130 1.27000	\$ AmBe and collimator inner hole in polyethylene
21	c/y 503 -130 1.2192	\$ detector fill gas diameter
22	py -31.2700	\$ detector Al casing outer lower
23	py -31.3210	\$ detector Al casing inner lower/fill gas
24	py -66.9570	\$ detector fill gas/Al casing inner upper
25	py -67.0080	\$ detector Al casing outer upper
30	py -135	\$kill boundary
31	py 337	\$kill boundary
40	py 0	\$concrete boundary
41	py 7.5	\$concrete boundary
42	py 15	\$concrete boundary
43	py 22.5	\$concrete boundary
44	py 30	\$concrete boundary
45	py 37.5	\$concrete boundary
46	py 45	\$concrete boundary
47	py 52.5	\$concrete boundary
48	py 60	\$concrete boundary
49	py 67.5	\$concrete boundary
50	py 75	\$concrete boundary
51	py 82.5	\$concrete boundary
52	py 90	\$concrete boundary
53	py 97.5	\$concrete boundary
54	py 105	\$concrete boundary
55	py 112.5	\$concrete boundary
56	py 120	\$concrete boundary
57	py 127.5	\$concrete boundary
58	py 135	\$concrete boundary
59	py 142.5	\$concrete boundary
60	py 150	\$concrete boundary

c DATA CARDS

c

c

c Material Cards

c The ZA and atom densities come from PNNL compendium except WC, which is self-calculated.

c

m101 \$ regular concrete (floor, walls), den=2.30 g/cc

1001	0.0137404197
1002	0.0000015803
8016	0.0460382693
8017	0.0000175372
11023	0.001747
13027	0.001745
14028	0.0153285761
14029	0.0007783478
14030	0.0005130926
20040	0.0014744726
20042	0.0000098409
20043	0.0000020534
20044	0.0000317281
20046	0.0000000608
20048	0.0000028443
26054	0.0000202822
26056	0.0003183864
26057	0.0000073529
26058	0.0000009785

m102 \$ borated polyethylene (shielding material), den=1.4783 g/cc

1001	0.1205772320
1002	0.0000138680
5010	0.0008194
5011	0.0032980
6000	0.0602956

m103 \$ tungsten carbide (shielding material), den=14.842 g/cc

6000	0.0427165
8016	0.0008376774
8017	0.0000003191
23050	0.0000006
23051	0.0002625
26054	0.0000094
26056	0.0001468
26057	0.0000034
26058	0.0000004
27059	0.0090999
74180	0.0000512
74182	0.0113199
74183	0.0061127
74184	0.0130883
74186	0.0121443

m104 \$ stainless steel 304 (source container, and detector can), den=8.03 g/cc

6000	0.000160
14028	0.0007913308
14029	0.0000401819
14030	0.0000264882
15031	0.000036
16032	0.0000218339
16033	0.0000001748
16034	0.0000009867
16036	0.0000000046
24050	0.0007649373
24052	0.0147510535
24053	0.0016726511
24054	0.0004163583
25055	0.000877
26054	0.0035384461
26056	0.0555460365
26057	0.0012828002
26058	0.0001707172
28058	0.0051690790

28060 0.0019911200
 28061 0.0000865526
 28062 0.0002759676
 28064 0.0000702808
 m200 \$ plutonium from PNNL compendium, den=11.46 g/cc
 8016 0.050910
 94238 0.000013
 94239 0.023807
 94240 0.001521
 94241 0.000101
 94242 0.000013
 m403 \$ helium 3 w/ 2% CO2 (detector medium - neutron) - P=4 atm, P4-0812-217, den=0.000622 g/cc
 2003 0.0001326651
 6000 0.0000074934
 8016 0.0000112457
 8017 0.0000000043
 m500 \$ dry air (within source and around the whole assembly), den=0.001225 g/cc
 7014 0.0000388565
 7015 0.0000001435
 8016 0.0000109958
 8017 0.0000000042
 m501 \$ argon, den=0.001662 g/cc
 18036 0.0000000834
 18038 0.0000000157
 18040 0.0000249009
 c Source Definition Card
 c
 c NOTE: if F8 with PHL is removed keeping only F4 then mode can be altered to just n
 c
 mode n
 stop f14 0.05
 c pos and rad may need to be altered to match new input file
 sdef POS=500 185.93 -271.07 RAD=d2 ERG=d4
 si2 0 5.93 \$ this gives the range of the radius to sample
 sp2 -21 2 \$ this power law samples the sphere
 sp4 -3 0.966 2.842 \$ this is the Pu-239 Watt Fission Spectrum
 c the radius of 5.93 is an estimate from 1 MTIHM burnup yielding 0.52%Pu239
 c 0.21%Pu240, 0.1%Pu241, 0.05%Pu242, converted to PuO2 mass then vol of sphere.
 c
 c Variance Reduction
 c
 c Importance Card
 c
 IMP:n 2097152
 1048576
 524288
 262144
 131072
 65536
 32768
 16384
 8192
 4096
 2048
 1024
 512
 256
 128
 64
 32
 16
 8

```

4
1 16777216 8388608 2 4194304 2 4194304 0
c
c
c
c Random Number Generator Card
c
rand gen=2 stride=15291700
c
c
c Physics Cards
c PHYS:n 100 5J 5 $ elastic recoil and neutron capture ion algorithm (NCIA)
c PHYS:h 100 3J 1 $ continuous slow down for straggling charged particles
c PHYS:t 100 3J 1 $ same as phys:h
c
c Forced Collisions
c
c FCL:p 1 1 1 1 1 1 1 1 1 1 0
c
c
c Weight Windows
c
WWG 14 0 0 J J J J
MESH
    GEOM=REC REF= 500.1 159 -94 ORIGIN= -0.1 -135.1 -317.1
    IMESH= 1000.1 IINTS= 100          $ 10 cm mesh intervals
    JMESH= 337.1 JINTS= 50           $ 9.44 cm mesh intervals
    KMESH= 683.1 KINTS= 100          $ 10 cm mesh intervals
c
c Exponential Transform
c
EXT:n SV2 19R 0 7R
VECT V2 503 -49.139 -130
c
c
c Tally Cards
c
c NOTE: cell values will need to be altered to match detector cell in new input file
c
F14:n 3100
FM14 -1 403 103
SD14 1
c
c we may consider dropping F8/F6 tally so variance reduction can be used.
c
c F6:h 3000
c FT6 GEB 0.0 0.06 0.0
c F16:t 3000
c FT16 GEB 0.0 0.06 0.0
c F8:n 3000
c FT8 GEB 0.0 0.06 0.0 &
c PHL 2 6 1 16 1 HE3-1
c E8 0 1e-5 0.01 2047i 2.0 100
c
c consider adding the FMESH, if we do, Origin IJKMESH and IJKINTS will need to be altered
c
c FMESH4:n GEOM=xyz ORIGIN=-100 -127.4701 -127.4701
c   IMESH 181.2800 IINTS 500
c   JMESH 127.4701 JINTS 500
c   KMESH 127.4701 KINTS 1
c
c =====

```

```

c
c Optional Cards
c
c -----
c Plotting
c mplot freq 5e6 tally 4 tfc m
c
c -----
c Cutoffs: Time, Energy, and Weight
c cut:n 1.0e123 1e-4 -0.5 -0.25
c
c these cut cards will be eliminated if mode is reduced to just n
c
c CUT:h J 0.001
c CUT:t J 0.001
c
c -----
c Computer Time Cutoff
c CTME 45
c
c -----
c Printing
c Prints all tables pertinent to the problem
print
c .....
c sets the frequency of tally and runtpe dumps
c
c these values will need to be altered to appropriate values based on NPS
c
prdump 1e9 1e9

```

17.5.2 Multi-material, Multi-layered

Neutron Shielding Optimization

c This input file creates a concrete wall X (4 - 7) ft thick and placed a 3D fuel assembly on one side as a source using a photon distribution given from ORIGEN. A mesh detector is placed on the side of the wall opposite the source representing a human body. The tallies are weighted to give dose in each boxel of the mesh. There is a point detector at the head of the person.

c CELL CARDS

100	104	-8.0300	1 -2 40 -41 3 -4	\$ stainless steel section
200	101	-2.3000	1 -2 41 -42 3 -4	\$ concrete section 1
201	101	-2.3000	1 -2 42 -43 3 -4	\$ concrete section 2
202	101	-2.3000	1 -2 43 -44 3 -4	\$ concrete section 3
203	101	-2.3000	1 -2 44 -45 3 -4	\$ concrete section 4
204	101	-2.3000	1 -2 45 -46 3 -4	\$ concrete section 5
205	101	-2.3000	1 -2 46 -47 3 -4	\$ concrete section 6
300	103	-14.930	1 -2 47 -48 3 -4	\$ WC section 1
301	103	-14.930	1 -2 48 -49 3 -4	\$ WC section 2
302	103	-14.930	1 -2 49 -50 3 -4	\$ WC section 3
303	103	-14.930	1 -2 50 -51 3 -4	\$ WC section 4
304	103	-14.930	1 -2 51 -52 3 -4	\$ WC section 5
305	103	-14.930	1 -2 52 -53 3 -4	\$ WC section 6
400	102	-1.4000	1 -2 53 -54 3 -4	\$ BP section 1
401	102	-1.4000	1 -2 54 -55 3 -4	\$ BP section 2
402	102	-1.4000	1 -2 55 -56 3 -4	\$ BP section 3
403	102	-1.4000	1 -2 56 -57 3 -4	\$ BP section 4
404	102	-1.4000	1 -2 57 -58 3 -4	\$ BP section 5
405	102	-1.4000	1 -2 58 -59 3 -4	\$ BP section 6
2000	200	-11.460	-10	\$ Fuel Bundle/Source
3000	104	-8.03	(21:-23:24)(-20 22 -25)	\$ SS304 detector can
3100	403	-0.000622	-21 23 -24	\$ He-3 fill gas of detector

5000 500 -0.0012 1 -2 59 -31 5 -4 (20:-22:25) \$ Atmosphere
 5001 501 -0.001662 1 -2 30 -40 5 -4 10 \$ Atmosphere
 6000 101 -2.3000 1 -2 59 -31 3 -5 \$ Floor
 6001 101 -2.3000 1 -2 30 -40 3 -5 \$ Floor
 7000 0 -1:2:-30:31:-3:4 \$ Kill Zone

c SURFACE CARDS

1 px 0 \$concrete boundary
 2 px 1000 \$concrete boundary
 3 pz -317 \$concrete boundary
 4 pz 683 \$concrete boundary
 5 pz -277 \$floor boundary
 10 s 500 -37.20 -271.07 5.93 \$ source boundary
 20 c/y 503 -130 1.27000 \$ AmBe and collimator inner hole in polyethylene
 21 c/y 503 -130 1.2192 \$ detector fill gas diameter
 22 py 90.24 \$ detector Al casing outer lower
 23 py 90.291 \$ detector Al casing inner lower/fill gas
 24 py 125.927 \$ detector fill gas/Al casing inner upper
 25 py 125.978 \$ detector Al casing outer upper
 30 py -135 \$kill boundary
 31 py 337 \$kill boundary
 40 py -1.27 \$stainless steel/atmosphere boundary
 41 py 0 \$concrete/stainless steel boundary
 42 py 5 \$concrete boundary
 43 py 10 \$concrete boundary
 44 py 15 \$concrete boundary
 45 py 20 \$concrete boundary
 46 py 25 \$concrete boundary
 47 py 30 \$concrete/BP boundary
 48 py 32.5 \$WC boundary
 49 py 35 \$WC boundary
 50 py 37.5 \$WC boundary
 51 py 40 \$WC boundary
 52 py 42.5 \$WC boundary
 53 py 45 \$WC boundary
 54 py 47.54 \$BP boundary
 55 py 50.08 \$BP boundary
 56 py 52.62 \$BP boundary
 57 py 55.16 \$BP boundary
 58 py 57.7 \$BP boundary
 59 py 60.24 \$BP boundary

c DATA CARDS

c

c

c Material Cards

c The ZA and atom densities come from PNNL compendium except WC, which is self-calculated.

c

m101 \$ regular concrete (floor, walls), den=2.30 g/cc

1001 0.0137404197
 1002 0.0000015803
 8016 0.0460382693
 8017 0.0000175372
 11023 0.001747
 13027 0.001745
 14028 0.0153285761
 14029 0.0007783478
 14030 0.0005130926
 20040 0.0014744726
 20042 0.0000098409
 20043 0.0000020534

20044 0.0000317281
 20046 0.0000000608
 20048 0.0000028443
 26054 0.0000202822
 26056 0.0003183864
 26057 0.0000073529
 26058 0.0000009785
 m102 \$ borated polyethylene (shielding material), den=1.4783 g/cc
 1001 0.1205772320
 1002 0.0000138680
 5010 0.0008194
 5011 0.0032980
 6000 0.0602956
 m103 \$ tungsten carbide (shielding material), den=14.842 g/cc
 6000 0.0427165
 8016 0.0008376774
 8017 0.0000003191
 23050 0.0000006
 23051 0.0002625
 26054 0.0000094
 26056 0.0001468
 26057 0.0000034
 26058 0.0000004
 27059 0.0090999
 74180 0.0000512
 74182 0.0113199
 74183 0.0061127
 74184 0.0130883
 74186 0.0121443
 m104 \$ stainless steel 304 (source container, and detector can), den=8.03 g/cc
 6000 0.000160
 14028 0.0007913308
 14029 0.0000401819
 14030 0.0000264882
 15031 0.000036
 16032 0.0000218339
 16033 0.0000001748
 16034 0.0000009867
 16036 0.0000000046
 24050 0.0007649373
 24052 0.0147510535
 24053 0.0016726511
 24054 0.0004163583
 25055 0.000877
 26054 0.0035384461
 26056 0.0555460365
 26057 0.0012828002
 26058 0.0001707172
 28058 0.0051690790
 28060 0.0019911200
 28061 0.0000865526
 28062 0.0002759676
 28064 0.0000702808
 m403 \$ helium 3 w/ 2% CO2 (detector medium - neutron) - P=4 atm, P4-0812-217, den=0.000622 g/cc
 2003 0.0001326651
 6000 0.0000074934
 8016 0.0000112457
 8017 0.0000000043
 m200 \$ plutonium from PNNL compendium, den=11.46 g/cc
 8016 0.050910
 94238 0.000013
 94239 0.023807

```

94240 0.001521
94241 0.000101
94242 0.000013
m500 $ dry air (within source and around the whole assembly), den=0.001225 g/cc
7014 0.0000388565
7015 0.0000001435
8016 0.0000109958
8017 0.0000000042
m501 $ argon, den=0.001662 g/cc
18036 0.0000000834
18038 0.0000000157
18040 0.0000249009
c Source Definition Card
c
c NOTE: if F8 with PHL is removed keeping only F4 then mode can be altered to just n
c
mode n
stop f14 0.05
c pos and rad may need to be altered to match new input file
sdef POS=500 -37.20 -271.07 RAD=d2 ERG=d4
si2 0 5.93 $ this gives the range of the radius to sample
sp2 -21 2 $ this power law samples the sphere
sp4 -3 0.966 2.842 $ this is the Pu-239 Watt Fission Spectrum
c the radius of 5.93 is an estimate from 1 MTIHM burnup yielding 0.52%Pu239
c 0.21%Pu240, 0.1%Pu241, 0.05%Pu242, converted to PuO2 mass then vol of sphere.
c
c Variance Reduction
c
c Importance Card
c
IMP:n 4
8
16
32
64
128
256
512
1024
2048
4096
8192
16384
32768
65536
131072
262144
524288
1048576
1 8388608 16777216
4194304 2 4194304 2 0
c
c
c
c Random Number Generator Card
c
rand gen=2 stride=15291700
c
c
c Physics Cards
c PHYS:n 100 5J 5 $ elastic recoil and neutron capture ion algorithm (NCIA)
c PHYS:h 100 3J 1 $ continuous slow down for straggling charged particles

```

```

c PHYS:t 100 3J 1 $ same as phys:h
c
c Forced Collisions
c
c FCL:p 1 1 1 1 1 1 1 1 1 1 0
c
c
c Weight Windows
c
WWG 14 0 0 J J J J
MESH
  GEOM=REC REF= 500.1 159 -94 ORIGIN= -0.1 -135.1 -317.1
  IMESH= 1000.1 IINTS= 100          $ 10 cm mesh intervals
  JMESH= 337.1 JINTS= 50           $ 9.44 cm mesh intervals
  KMESH= 683.1 KINTS= 100          $ 10 cm mesh intervals
c
c Exponential Transform
c
EXT:n SV2 18R 0 7R
VECT V2 503 108.109 -130
c
c
c Tally Cards
c
c NOTE: cell values will need to be altered to match detector cell in new input file
c
F14:n 3000
FM14 -1 403 103
SD14 1
c
c we may consider dropping F8/F6 tally so variance reduction can be used.
c
c F6:h 3000
c FT6 GEB 0.0 0.06 0.0
c F16:t 3000
c FT16 GEB 0.0 0.06 0.0
c F8:n 3000
c FT8 GEB 0.0 0.06 0.0 &
c PHL 2 6 1 16 1 HE3-1
c E8 0 1e-5 0.01 2047i 2.0 100
c
c consider adding the FMESH, if we do, Origin IJKMESH and IJKINTS will need to be altered
c
c FMESH4:n GEOM=xyz ORIGIN=-100 -127.4701 -127.4701
c   IMESH 181.2800 IINTS 500
c   JMESH 127.4701 JINTS 500
c   KMESH 127.4701 KINTS 1
c
c =====
c
c Optional Cards
c
c -----
c Plotting
c mplot freq 5e6 tally 4 tfc m
c
c -----
c Cutoffs: Time, Energy, and Weight
c cut:n 1.0e123 1e-4 -0.5 -0.25
c
c these cut cards will be eliminated if mode is reduced to just n
c

```

```

c CUT:h J 0.001
c CUT:t J 0.001
c -----
c Computer Time Cutoff
c CTME 45
c -----
c Printing
c Prints all tables pertinent to the problem
print
c .....
c sets the frequency of tally and runtpe dumps
c
c these values will need to be altered to appropriate values based on NPS
c
prdmp 1e9 1e9

```

18 Appendix G: Other Codes Utilized in Conjunction with MCNP

Several other codes were created or used to assist in generating components of the MCNP files, such as the GEB coefficients, or optimization, by automating input file creation and scripts to automate running of input files. These codes are provided in the following sections.

18.1 Matlab® Codes for Shielding Optimization Input File Generation

Matlab® was used to develop code for generating input files for the optimization studies to aid in quick changes to cell changes for variance reduction purposes. Copies of each code used is provided in the following sections.

18.1.1 Gamma-ray Concrete Shielding

```
% % This is the final iteration of the uni-layered gamma Matlab file.
% % I did not save multiple versions -- I edited the same file time and
% % time again. This file was designed to write, run, and extract output
% % from the "baseline" MCNP files. The file is commented accordingly.
% % File last edited by Sarah Black on 4/28/18.

% % Here is where I directed to the actual main folder in my file
cd(['C:\Users\Ben Black\Documents\College Senior ISU 2018\Senior Design'...
   '\Shielding'])
shielding = 'gammashielding';
% % brk indicates portions of the baseline MCNP file in which to insert
% % cells, surfaces, importances, etc.
brk = 'c BREAK';
mkdir(shielding)
batchID = fopen('shielding.bat');
batchFileArray = cell(5, 1);
    for index = 1:5
        batchFileArray{index, 1} = fgetl(batchID);
    end
fclose(batchID);

% % create single place to determine the width variation
loopStart = 4.5;
loopIteration = 1;
loopEnd = 5.5;
loopCount = (loopEnd - loopStart)/ loopIteration + 1;
% % track which loop we're on in order to index arrays
count = 0;
% % create array for outp values
outpValueArray = zeros(loopCount, 3);

for index = loopStart:loopIteration:loopEnd
```

```

count = count + 1; % for indexing arrays
cd(['C:\Users\Ben Black\Documents\College Senior ISU 2018\Senior'...
    'Design\Shielding'])
% %make directory
dirname = ['shielding',num2str(index)];
mkdirname = [shielding,'\', dirname];
mkdir(mkdirname)
% %make text files with proper width
copyfile([shielding,'.txt'],[shielding, '\', dirname,'\...',
    dirname,'.txt']);
fID = fopen([shielding, '\', dirname,'\', dirname,'.txt'], 'r');
tline = fgetl(fID);
mfp = 5.0;
foot = 30;
input = textscan(fID, '%s', 'Delimiter', '\n', 'Whitespace','');
input = input{1};
N = length(input);
fclose(fID);

% % figure out how many cells need to be made
width = index * foot;
widthSection = width / mfp;
widthNumber = widthSection;
newFArray = cell(3 * widthNumber + N, 1);
% % populate cells that stay the same
m = 1;
n = 1;
while m <= N && strcmp(input{n,1}, brk) == 0
    newFArray{m, 1} = input{n,1};
    m = m + 1;
    n = n + 1;
end
n = n + 1; %skip brk line

j = 1;
% % create the cells
for j = 1:widthNumber
    newFArray{m, 1} = [num2str(99 + j),' 101 -2.3000 1 -2 ',...
        num2str(49 + j), ' ', num2str(-50 - j),...
        ' 3 -4 $ Concrete Wall section ', num2str(j)];
    m = m + 1;
end
% % populate cells 200 - 499
sourceYWidth = 18.19;
while strcmp(input{n,1}, brk, 3) == 0
    % % recreate cell 5000 to match final surface number
    if strcmp(input{n,1}, '500', 3)
        newFArray{m, 1} = ['500 501 -0.001662 1 -2 ',...
            num2str(50 + widthNumber),...
            ' -31 5 -4 (-10:11:-12:13:-14:15) $ Argon'];
    elseif strcmp(input{n,1}, '600', 3)
        newFArray{m, 1} = ['600 101 -2.3000 1 -2 ',...
            num2str(50 + widthNumber),' -31 3 -5 $ Floor'];
    elseif strcmp(input{n,1}, '12 py ', 5)
        newFArray{m, 1} = ['12 py ',...
            num2str(widthNumber * mfp + foot),...
            ' $source boundary'];
    elseif strcmp(input{n,1}, '13 py ', 5)
        newFArray{m, 1} = ['13 py ',...
            num2str(widthNumber * mfp + foot + sourceYWidth),...
            ' $source boundary'];

```

```

else
    newFArray{m, 1} = input{n, 1};
end
n = n + 1;
m = m + 1;
end
n = n + 1; % skip brk line
% % create the surfaces
for k = 1:widthNumber + 1
    newFArray{m, 1} = [num2str(49 + k), ' py ',...
        num2str((k - 1) * mfp), ' $concrete boundary'];
    m = m + 1;
end
% % copy data cards up to importances
while strcmp(input{n, 1}, brk, 3) == 0
    % % recreate si2 to match final surface number
    if strcmp(input{n, 1}, 'si2', 3)
        newFArray{m, 1} = ['si2 ',...
            num2str(widthNumber * mfp + foot), ' ',...
            num2str(widthNumber * mfp + foot + sourceYWidth)];
    else
        newFArray{m, 1} = input{n, 1};
    end
    n = n + 1;
    m = m + 1;
end
% % make importances
for l = 1:widthNumber
    if l == 1
        newFArray{m, 1} = ['IMP:p ', num2str(2^(widthNumber + 2 - l))];
    else
        newFArray{m, 1} = [' ', num2str(2^(widthNumber + 2 - l))];
    end
    m = m + 1;
end
newFArray{m, 1} = [' ', '1 ', num2str(2^(widthNumber + 4)),...
    ' ', num2str(2^(widthNumber + 3)), ' ',...
    num2str(2^(widthNumber + 3))];
m = m + 1;
newFArray{m, 1} = [' ', num2str(2^(widthNumber + 3)),...
    '2 ', num2str(2^(widthNumber + 2)), '2 ',...
    num2str(2^(widthNumber + 2)), '0'];
m = m + 1;

% % make electron importances
for l = 1:widthNumber
    if l == 1
        newFArray{m, 1} = ['IMP:e ', num2str(0)];
    else
        newFArray{m, 1} = [' ', num2str(0)];
    end
    m = m + 1;
end
newFArray{m, 1} = [' ', '0 ', num2str(1), ' ', num2str(1), ' ',...
    num2str(1), ' ', num2str(1), '0 ', num2str(0), '000'];
m = m + 1;
n = n + 1;
% % copy rest of cards
while n <= N && ischar(input{n, 1})
    newFArray{m, 1} = input{n, 1};
    m = m + 1;
    n = n + 1;
end

```

```

end

otherfID = fopen([shielding, '\', dirname, '\', dirname, '.txt'], 'w');
fprintf(otherfID, '%s\n', newFArray{:,1});
fclose(otherfID);

% % make appropriate batch file
copyfile('shielding.bat', [shielding, '\', dirname, 'shielding.bat']);
bID = fopen([shielding, '\', dirname, 'shielding.bat'], 'w');
batchFileArray{4, 1} = ['cd C:\Users\Ben Black\Documents\College'...
    'Senior ISU 2018\Senior Design\Shielding\', shielding,...
    '\', dirname];
batchFileArray{5, 1} = ['E:\my_mcnp\MCNP_CODE\bin\mcnp6.exe i=',...
    dirname, '.txt tasks 7'];
fprintf(bID, '%s\n', batchFileArray{:,1});
fclose(bID);
% % run batch file
directoryName = ['C:\Users\Ben Black\Documents\College Senior'...
    'ISU 2018\Senior Design\Shielding\', shielding, '\', dirname, '\'];
system([directoryName, 'shielding.bat']);
% % rename outp file as openable text file
movefile([shielding, '\', dirname, 'outp'], [shielding, '\',...
    dirname, 'outp.txt'], 'f')
% % open outp file, put results in an array
outpID = fopen([shielding, '\', dirname, 'outp.txt']);
output = textscan(outpID, '%s', 'Delimiter', '\n');
output = output{1};
% % search for final result
nps = regexp(output, 'nps\s+=\s+(\S+)', 'tokens');
nps = [nps{:}];
fileNPS = cell2mat(nps{length(nps)});
outpSearch = regexp(output, [fileNPS,...
    '\s+(\d{1}.\d{4})\S+)\s+(\d{1}.\d{4})\s+...'
    '(\d{1}.\d{4})\s+(\d.\d)\s+', 'tokens');
outpSearch = [outpSearch{:}];
format short e
outpValueArray(count, 1) = index; % thickness (ft)
outpValueArray(count, 2) = str2double(outpSearch{size(outpSearch,...
    2)}{1}); % final result
outpValueArray(count, 3) = str2double(outpSearch{size(outpSearch,...
    2)}{2}) * outpValueArray(count, 2); % error
fclose(outpID);

end

% % plot data
plotaxes = axes;
plotaxes.YScale = 'log';
xlim([3.5 8.5])
hold all
errorbar(outpValueArray(:, 1), outpValueArray(:, 2), outpValueArray(:, 3))
xlabel('thickness (ft)')
ylabel('fluence (p/cm2)')
savefig(['Results\', shielding, 'results'])

csvwrite(['Results\', shielding, 'matrix.csv'], outpValueArray);

```

18.1.2 Gamma-ray Multi-layered Shielding

```

% % This is the final iteration of the multi-layered gamma Matlab file.
% % I did not save multiple versions -- I edited the same file time and
% % time again. This file was designed to write, run, and extract output
% % from the "baseline" MCNP files. The file is commented accordingly.

```



```

% % File last edited by Sarah Black on 4/28/18.

% % Here is where I directed to the actual main folder in my file
cd('C:\Users\Ben Black\Documents\College Senior ISU 2018\Senior Design'\...
    '\Shielding')
shielding = 'multigammashielding';
% % brk indicates portions of the baseline MCNP file in which to insert
% % cells, surfaces, importances, etc.
brk = 'c BREAK';
mkdir(shielding)
batchID = fopen('shielding.bat');
batchFileArray = cell(5, 1);
    for BPindex = 1:5
        batchFileArray{BPindex, 1} = fgetl(batchID);
    end
fclose(batchID);
CSSNumber = 7;

% % create single place to determine the width variation
BPloopStart = 0;
BPloopSteps = 2.54;
BPloopEnd = 15.24;
BPloopCount = round((BPloopEnd - BPloopStart)/ BPloopSteps + 1);
WCloopStart = 0.0;
WCloopSteps = 1.0;
WCloopEnd = 15.0;
% % track which loop we're on in order to index arrays
count = 0;
% % create array for outp values
outpValueArray = zeros(BPloopCount, 3);

for BPindex = BPloopStart:BPloopSteps:BPloopEnd
    for WCindex = WCloopStart:WCloopSteps:WCloopEnd
        count = count + 1; % for indexing arrays
        cd(['C:\Users\Ben Black\Documents\College Senior ISU 2018\Senior'...
            '\Design\Shielding'])
        % % make directory
        dirname = ['shielding', 'WC', num2str(WCindex), 'BP', num2str(BPindex)];
        mkdirname = [shielding, '\', dirname];
        mkdir(mkdirname)
        % % make text files with proper radius
        copyfile([shielding, '.txt'], [shielding, '\', dirname, '\', dirname, ...
            '.txt']);
        fID = fopen([shielding, '\', dirname, '\', dirname, '.txt'], 'r');
        tline = fgetl(fID);
        BPmfp = 2.54;
        WCmfp = 0.5;
        foot = 30;
        input = textscan(fID, '%s', 'Delimiter', '\n', 'Whitespace', '');
        input = input{1};
        N = length(input);
        fclose(fID);

        % % figure out how many cells need to be made
        BPwidth = BPindex;
        BPwidthSection = BPwidth / BPmfp;
        BPwidthNumber = round(BPwidthSection);
        WCwidth = WCindex;
        WCwidthSection = WCwidth / WCmfp;

```

```

WCwidthNumber = round(WCwidthSection);
FArray = cell(3 * (BPwidthNumber + WCwidthNumber) + N, 1);
% % populate cells that stay the same
m = 1;
n = 1;
while m <= N && strcmp(input{n,1}, brk) == 0
    FArray{m, 1} = input{n,1};
    m = m + 1;
    n = n + 1;
end
n = n + 1; %skip brk line

% % create the cells
for s = 1:WCwidthNumber
    FArray{m, 1} = [num2str(299 + s), ' 103 -14.930 1 -2 ',...
        num2str(46 + s), ', ', num2str(-47 - s), ...
        ' 3 -4 $ WC section ', num2str(s)];
    m = m + 1;
end
for j = 1:BPwidthNumber
    FArray{m, 1} = [num2str(399 + j), ' 102 -1.4000 1 -2 ',...
        num2str(46 + WCwidthNumber + j), ', ', ...
        num2str(-47 - WCwidthNumber - j),...
        ' 3 -4 $ BP section ', num2str(j)];
    m = m + 1;
end
% % populate cells 200 - 499
sourceYWidth = 18.19;
while strncmp(input{n,1}, brk, 3) == 0
    % % recreate cell 5000 to match final surface number
    if strcmp(input{n,1}, '5000', 4)
        FArray{m, 1} = ['5000 500 -0.0012 1 -2 ',...
            num2str(47 + BPwidthNumber + WCwidthNumber),...
            ' -31 5 -4 (21:-22:26) $ Atmosphere'];
    elseif strcmp(input{n,1}, '6000', 4)
        FArray{m, 1} = ['6000 101 -2.3000 1 -2 ',...
            num2str(47 + BPwidthNumber + WCwidthNumber),...
            ' -31 3 -5 $ Floor'];
    % % surface 22
    elseif strcmp(input{n,1}, '22 py', 5)
        FArray{m,1} = ['22 py ', num2str(BPwidthNumber * BPmfp +...
            WCwidthNumber * WCmfp + 2 * foot + 0),...
            ' $ Al detector can bottom'];
    % % surface 23
    elseif strcmp(input{n,1}, '23 py', 5)
        FArray{m,1} = ['23 py ', num2str(BPwidthNumber * BPmfp +...
            WCwidthNumber * WCmfp + 2 * foot + 0.043),...
            ' $ Al can NaI interface'];
    % % surface 24
    elseif strcmp(input{n,1}, '24 py', 5)
        FArray{m,1} = ['24 py ', num2str(BPwidthNumber * BPmfp...
            + WCwidthNumber * WCmfp + 2 * foot + 5.131),...
            ' $ NaI PMT interface and Al Mu interface'];
    % % surface 25
    elseif strcmp(input{n,1}, '25 py', 5)
        FArray{m,1} = ['25 py ', num2str(BPwidthNumber * BPmfp +...
            WCwidthNumber * WCmfp + 2 * foot + 18.364),...
            ' $ PMT vaccum Mu can interface'];
    % % surface 26
    elseif strcmp(input{n,1}, '26 py', 5)
        FArray{m,1} = ['26 py ', num2str(BPwidthNumber * BPmfp +...
            WCwidthNumber * WCmfp + 2 * foot + 18.415),...

```

```

    '    $ Mu can top air interface'];
else
    FArray{m, 1} = input{n, 1};
end
n = n + 1;
m = m + 1;
end
n = n + 1; % skip brk line
% % create the surfaces
for r = 1:WCwidthNumber
    FArray{m, 1} = [num2str(47 + r), 'py',...
        num2str(foot + r * WCmfp), '    $WC boundary'];
    m = m + 1;
end
for k = 1:BPwidthNumber
    FArray{m, 1} = [num2str(47 + WCwidthNumber + k), 'py',...
        num2str(foot + WCwidth + k * BPmfp), '    $BP boundary'];
    m = m + 1;
end
% % copy data cards up to importances
while strcmp(input{n,1}, brk, 3) == 0
    FArray{m, 1} = input{n, 1};
    n = n + 1;
    m = m + 1;
end
% % make importances
for l = 1:(BPwidthNumber + WCwidthNumber + CSSNumber)
    if l == 1
        FArray{m, 1} = ['IMP:p ', num2str(2^(l+1))];
    else
        FArray{m, 1} = [' ', num2str(2^(l + 1))];
    end
    m = m + 1;
end
FArray{m, 1} = [' ', '1 ', num2str(2^(BPwidthNumber + ...
    WCwidthNumber + CSSNumber + 4)), ' ', num2str(2^(BPwidthNumber...
    + WCwidthNumber + CSSNumber + 3)), ' ', num2str(2^(BPwidthNumber...
    + WCwidthNumber + CSSNumber + 3))];
m = m + 1;
FArray{m, 1} = [' ', num2str(2^(BPwidthNumber + WCwidthNumber...
    + CSSNumber + 3)), ' ', num2str(2^(BPwidthNumber + ...
    WCwidthNumber + CSSNumber + 2)), '2 ', num2str(2^(BPwidthNumber...
    + WCwidthNumber + CSSNumber + 2)), '2 0'];
m = m + 1;

% % make electron importances
widthNumber = BPwidthNumber + WCwidthNumber + CSSNumber;
for l = 1:widthNumber
    if l == 1
        FArray{m, 1} = ['IMP:e ', num2str(0)];
    else
        FArray{m, 1} = [' ', num2str(0)];
    end
    m = m + 1;
end
FArray{m, 1} = [' ', '0 ', num2str(1), ' ', num2str(1), ' ',...
    num2str(1), ' ', num2str(1), '0 ', num2str(0), '0 ',...
    num2str(0), '0'];
m = m + 1;
n = n + 1;

```

```

% % copy rest of cards
while n <= N && ischar(input{n, 1})
    FArray{m, 1} = input{n, 1};
    m = m + 1;
    n = n + 1;
end

otherfID = fopen([shielding, '\', dirname, '\', dirname, '.txt'], 'w');
fprintf(otherfID, '%s\n', FArray{:,1});
fclose(otherfID);

% % make appropriate batch file
copyfile('shielding.bat', [shielding, '\', dirname, 'shielding.bat']);
bID = fopen([shielding, '\', dirname, 'shielding.bat'], 'w');
batchFileArray{4, 1} = ['cd C:\Users\Ben Black\Documents\...
    'College Senior ISU 2018\Senior Design\Shielding\', shielding,...
    '\', dirname];
batchFileArray{5, 1} = ['E:\my_mcn\MCNP_CODE\bin\mcnp6.exe i=',...
    dirname, '.txt tasks 7'];
fprintf(bID, '%s\n', batchFileArray{:,1});
fclose(bID);
% % run batch file
directoryName = ['C:\Users\Ben Black\Documents\College Senior ISU'...
    '2018\Senior Design\Shielding\', shielding, '\', dirname, '\'];
system([directoryName, 'shielding.bat']);
% % rename outp file as openable text file
movefile([shielding, '\', dirname, 'outp'], [shielding,...
    '\', dirname, 'outp.txt'], 'f')
% % open outp file, put results in an array
outpID = fopen([shielding, '\', dirname, 'outp.txt']);
output = textscan(outpID, '%s', 'Delimiter', '\n');
output = output{1};
% % search for NPS
endnps = regexp(output, 'nps\s+=\s+(\d+)', 'tokens');
endnps = [endnps{:}];
fileNPS = cell2mat(endnps{length(endnps)});
% % search for final result
outpSearch = regexp(output, [fileNPS,...
    '\s+(\d{1}.\d{4})E-(\d{2})\s+(\d{1}.\d{4})'], 'tokens');
outpSearch = [outpSearch{:}];
format short e
outpValueArray(count, 1) = WCindex; % thickness (ft)
outpValueArray(count, 2) = BPindex;
outpValueArray(count, 3) = str2double(outpSearch{size(outpSearch,...
    2)}{1}); % final result
outpValueArray(count, 4) = str2double(outpSearch{size(outpSearch,...
    2)}{2})* outpValueArray(count, 3); % error
fclose(outpID);
end
end

% % the plots commented out were not used due to lack of readability
%plot data
% plotaxes = axes;
% plotaxes.ZScale = 'log';
% hold all
% scatter3(outpValueArray(:, 1), outpValueArray(:, 2), outpValueArray(:,3))
% title('concrete thickness optimization')
% xlabel('WC thickness (cm)')
% ylabel('BP thickness (cm)')
% zlabel('fluence')
% savefig(['Results\', shielding, 'results'])

```

```
csvwrite(['Results\'], shielding, 'matrix.csv', outpValueArray);
```

18.1.3 Neutron Concrete Shielding

```
% % This is the final iteration of the uni-layered neutron Matlab file.
% % I did not save multiple versions -- I edited the same file time and
% % time again. This file was designed to write, run, and extract output
% % from the "baseline" MCNP files. The file is commented accordingly.
% % File last edited by Sarah Black on 4/28/18.
```

```
% % Here is where I directed to the actual main folder in my file
cd(['C:\Users\Ben Black\Documents\College Senior ISU 2018\Senior '...
'Design\Shielding'])
shielding = 'neutronshielding';
% % brk indicates portions of the baseline MCNP file in which to insert
% % cells, surfaces, importances, etc.
brk = 'c BREAK';
mkdir(shielding)
batchID = fopen('shielding.bat');
batchFileArray = cell(5, 1);
for index = 1:5
    batchFileArray{index, 1} = fgetl(batchID);
end
fclose(batchID);
```

```
% % create single place to determine the width variation
indexarray = [4 4.5 5 6 7 8];
loopCount = length(indexarray);
% % track which loop we're on in order to index outp arrays
count = 0;
% % create array for outp values
outpValueArray = zeros(loopCount, 3);
```

```
for index = indexarray
    count = count + 1; % for indexing arrays
    cd(['C:\Users\Ben Black\Documents\College Senior ISU 2018\Senior '...
'Design\Shielding'])
    % % make directory
    dirname = ['shielding', num2str(index)];
    mkdirname = [shielding, '\', dirname];
    mkdir(mkdirname)
    % % make text files with proper width
    copyfile([shielding, '.txt'], [shielding, '\', dirname, '\', dirname, ...
'.txt']);
    fID = fopen([shielding, '\', dirname, '\', dirname, '.txt'], 'r');
    tline = fgetl(fID);
    mfp = 7.5;
    foot = 30;
    input = textscan(fID, '%s', 'Delimiter', '\n', 'Whitespace', '');
    input = input{1};
    N = length(input);
    fclose(fID);
```

```
% % figure out how many cells need to be made
width = index * foot;
widthSection = width / mfp;
widthNumber = round(widthSection);
```

```

newFArray = cell(3 * widthNumber + N, 1);
% % populate cells that stay the same
m = 1;
n = 1;
while m <= N && strcmp(input{n,1}, brk) == 0
    newFArray{m, 1} = input{n,1};
    m = m + 1;
    n = n + 1;
end
n = n + 1; %skip brk line

j = 1;
% % create the cells
for j = 1:widthNumber
    newFArray{m, 1} = [num2str(99 + j), ' 101 -2.3000 1 -2 ',...
        num2str(39 + j), ' ', num2str(-40 - j),...
        ' 3 -4 $ Concrete Wall section ', num2str(j)];
    m = m + 1;
end
% % populate cells 200 - 499
PuRadius = 5.93;
sourceYWidth = PuRadius * 2;
while strcmp(input{n,1}, brk, 3) == 0
    % % recreate cell 5000 to match final surface number
    if strcmp(input{n,1}, '5000', 4)
        newFArray{m, 1} = ['5000 501 -0.001662 1 -2 ',...
            num2str(40 + widthNumber),...
            ' -31 5 -4 10 $ Atmosphere'];
    elseif strcmp(input{n,1}, '6000', 4)
        newFArray{m, 1} = ['6000 101 -2.3000 1 -2 ',...
            num2str(40 + widthNumber), ' -31 3 -5 $ Floor'];
    elseif strcmp(input{n,1}, '10 s', 4)
        newFArray{m, 1} = ['10 s ', num2str(500), ' ',...
            num2str(widthNumber * mfp + foot + PuRadius), ' ',...
            num2str(-271.07), ' ', num2str(PuRadius),...
            ' $source boundary'];
    else
        newFArray{m, 1} = input{n, 1};
    end
    n = n + 1;
    m = m + 1;
end
n = n + 1; % skip brk line
% % create the surfaces
for k = 1:widthNumber + 1
    newFArray{m, 1} = [num2str(39 + k), ' py ', ...
        num2str((k - 1) * mfp), ' $concrete boundary'];
    m = m + 1;
end
% % copy data cards up to importances
while strcmp(input{n,1}, brk, 3) == 0
    if strcmp(input{n,1}, 'sdef', 4)
        newFArray{m, 1} = ['sdef POS=',...
            num2str(mean([490.905 509.095])), ' ',...
            num2str(widthNumber * mfp + foot + sourceYWidth/2), ' ',...
            num2str(mean([0 365.76])), ' RAD=d2 ERG=d4'];
    else
        newFArray{m, 1} = input{n, 1};
    end
    n = n + 1;
    m = m + 1;
end
end

```

```

% % make importances
for l = 1:widthNumber
    if l == 1
        newFArray{m, 1} = ['TMP:n ', num2str(2^(widthNumber + 2 - l))];
    else
        newFArray{m, 1} = [' ', num2str(2^(widthNumber + 2 - l))];
    end
    m = m + 1;
end
newFArray{m, 1} = [' ', '1 ', num2str(2^(widthNumber + 4)), ' ', ...
    num2str(2^(widthNumber + 3)), ' 2 ', ...
    num2str(2^(widthNumber + 2)), ' 2 ', ...
    num2str(2^(widthNumber + 2)), ' 0'];
m = m + 1;
n = n + 1;
% % copy rest of cards
while n <= N && ischar(input{n, 1})
    newFArray{m, 1} = input{n, 1};
    m = m + 1;
    n = n + 1;
end

otherfID = fopen([shielding, '\', dirname, '\', dirname, '.txt'], 'w');
fprintf(otherfID, '%s\n', newFArray{:,1});
fclose(otherfID);

% % make appropriate batch file
copyfile('shielding.bat', [shielding, '\', dirname, 'shielding.bat']);
bID = fopen([shielding, '\', dirname, 'shielding.bat'], 'w');
batchFileArray{4, 1} = ['cd C:\Users\Ben Black\Documents\'...
    'College Senior ISU 2018\Senior Design\Shielding\', shielding,...
    '\', dirname];
batchFileArray{5, 1} = ['E:\my_mcn\MCNP_CODE\bin\mcnp6.exe i=', ...
    dirname, '.txt tasks 7'];
fprintf(bID, '%s\n', batchFileArray{:,1});
fclose(bID);
% % run batch file
directoryName = ['C:\Users\Ben Black\Documents\College Senior ISU'...
    '2018\Senior Design\Shielding\', shielding, '\', dirname, '\'];
system([directoryName, 'shielding.bat']);
% % rename outp file as openable text file
movefile([shielding, '\', dirname, 'outp'], [shielding, '\', ...
    dirname, 'outp.txt'], 'F')
% % open outp file, put results in an array
outpID = fopen([shielding, '\', dirname, 'outp.txt']);
output = textscan(outpID, '%s', 'Delimiter', '\n');
output = output{1};
% % search for final result
outpSearch = regexp(output, '5000000\s+(\S+)\s+(\S+)', 'tokens');
outpSearch = [outpSearch{:}];
format short e
outpValueArray(count, 1) = index; % thickness (ft)
outpValueArray(count, 2) = str2double(outpSearch{size(outpSearch,...
    2) - 2}{1}); % final result
outpValueArray(count, 3) = str2double(outpSearch{size(outpSearch,...
    2) - 2}{2}) * outpValueArray(count, 2); % error
fclose(outpID);
end

% % plot data
plotaxes = axes;
plotaxes.YScale = 'log';

```

```

xlim([3.5 8.5])
hold all
errorbar(outpValueArray(:, 1), outpValueArray(:, 2), outpValueArray(:, 3))
xlabel('thickness (ft)')
ylabel('fluence (n/cm2)')
savefig(['Results\', shielding, 'results'])

```

```

csvwrite(['Results\', shielding, 'matrix.csv'], outpValueArray);

```

18.1.4 Neutron Multi-layered Shielding

```

% % This is the final iteration of the multi-layered neutron Matlab file.
% % I did not save multiple versions -- I edited the same file time and
% % time again. This file was designed to write, run, and extract output
% % from the "baseline" MCNP files. The file is commented accordingly.
% % File last edited by Sarah Black on 4/28/18.

% % Here is where I directed to the actual main folder in my file
cd 'C:\Users\Ben Black\Documents\College Senior ISU 2018\Senior Design'...
    '\Shielding'
shielding = 'multineutronshielding';
% % brk indicates portions of the baseline MCNP file in which to insert
% % cells, surfaces, importances, etc.
brk = 'c BREAK';
mkdir(shielding)
batchID = fopen('shielding.bat');
batchFileArray = cell(5, 1);
    for BPindex = 1:5
        batchFileArray{BPindex, 1} = fgetl(batchID);
    end
fclose(batchID);
CSSNumber = 7;

% % create single place to determine the width variation
BPloopStart = 0;
BPloopSteps = 2.54;
BPloopEnd = 15.24;
BPloopCount = round((BPloopEnd - BPloopStart)/ BPloopSteps + 1);
WCloopStart = 0.0;
WCloopSteps = 2.5;
WCloopEnd = 15.0;
% % track which loop we're on in order to index arrays
count = 0;
% % create array for outp values
outpValueArray = zeros(BPloopCount, 3);

for BPindex = BPloopStart:BPloopSteps:BPloopEnd
    for WCindex = WCloopStart:WCloopSteps:WCloopEnd
        count = count + 1; % for indexing arrays
        cd 'C:\Users\Ben Black\Documents\College Senior ISU 2018\Senior '...
            '\Design\Shielding'
        % % make directory
        dirname = ['shielding', 'WC', num2str(WCindex), 'BP', num2str(BPindex)];
        mkdirname = [shielding, '\', dirname];
        mkdir(mkdirname)
        % % make text files with proper width
        copyfile([shielding, '.txt'], [shielding, '\', dirname, '\', dirname, '.txt']);
        fID = fopen([shielding, '\', dirname, '\', dirname, '.txt', 'r');
        tline = fgetl(fID);
        BPmfp = 2.54;
    end
end

```



```

WCmfp = 2.5;
foot = 30;
input = textscan(fid, '%s', 'Delimiter', '\n', 'Whitespace', '');
input = input{1};
N = length(input);
fclose(fid);

% % figure out how many cells need to be made
BPwidth = BPindex;
BPwidthSection = BPwidth / BPmfp;
BPwidthNumber = round(BPwidthSection);
WCwidth = WCindex;
WCwidthSection = WCwidth / WCmfp;
WCwidthNumber = round(WCwidthSection);
FArray = cell(3 * (BPwidthNumber + WCwidthNumber) + N, 1);
% % populate cells that stay the same
m = 1;
n = 1;
while m <= N && strcmp(input{n,1}, brk) == 0
    FArray{m, 1} = input{n,1};
    m = m + 1;
    n = n + 1;
end
n = n + 1; %skip brk line

% % create the cells
for s = 1:WCwidthNumber
    FArray{m, 1} = [num2str(299 + s), ' 103 -14.930 1 -2 ', ...
        num2str(46 + s), ' ', num2str(-47 - s), ...
        ' 3 -4 $ WC section ', num2str(s)];
    m = m + 1;
end
for j = 1:BPwidthNumber
    FArray{m, 1} = [num2str(399 + j), ' 102 -1.4000 1 -2 ', ...
        num2str(46 + WCwidthNumber + j), ' ', ...
        num2str(-47 - WCwidthNumber - j), ...
        ' 3 -4 $ BP section ', num2str(j)];
    m = m + 1;
end
% % populate cells 200 - 499
sourceYWidth = 18.19;
while strncmp(input{n,1}, brk, 3) == 0
    % % recreate cell 5000 to match final surface number
    if strncmp(input{n,1}, '5000', 4)
        FArray{m, 1} = ['5000 500 -0.0012 1 -2 ', ...
            num2str(47 + BPwidthNumber + WCwidthNumber), ...
            ' -31 5 -4 (20:-22:25) $ Atmosphere'];
    elseif strncmp(input{n,1}, '6000', 4)
        FArray{m, 1} = ['6000 101 -2.3000 1 -2 ', ...
            num2str(47 + BPwidthNumber + WCwidthNumber), ...
            ' -31 3 -5 $ Floor'];
    elseif strncmp(input{n,1}, '22 py ', 5)
        FArray{m, 1} = ['22 py ', num2str(BPwidthNumber * BPmfp ...
            + WCwidthNumber * WCmfp + 2 * foot + 0), ...
            ' $ detector Al casing outer lower'];
    elseif strncmp(input{n,1}, '23 py ', 5)
        FArray{m, 1} = ['23 py ', num2str(BPwidthNumber * ...
            BPmfp + WCwidthNumber * WCmfp + 2 * foot + 0.051), ...
            ' $ detector Al casing inner lower/fill gas'];
    elseif strncmp(input{n,1}, '24 py ', 5)
        FArray{m, 1} = ['24 py ', num2str(BPwidthNumber * BPmfp + ...

```

```

        WCwidthNumber * WCmfp + 2 * foot + 35.687) ,...
        '$ detector fill gas/Al casing inner upper'];
elseif strcmp(input(n,1), '25 py ', 5)
    FArray{m,1} = ['25 py ', num2str(BPwidthNumber * BPmfp ...
        + WCwidthNumber * WCmfp + 2 * foot + 35.738) , ...
        '$ detector Al casing outer upper'];
else
    FArray{m, 1} = input{n, 1};
end
n = n + 1;
m = m + 1;
end
n = n + 1; % skip brk line
% % create the surfaces
for r = 1:WCwidthNumber
    FArray{m, 1} = [num2str(47 + r), ' py ', num2str(foot + ...
        r * WCmfp), ' $WC boundary'];
    m = m + 1;
end
for k = 1:BPwidthNumber
    FArray{m, 1} = [num2str(47 + WCwidthNumber + k), ' py ', ...
        num2str(foot + WCwidth + k * BPmfp), ' $BP boundary'];
    m = m + 1;
end
% % copy data cards up to importances
while strcmp(input{n,1}, brk, 3) == 0
    FArray{m, 1} = input{n, 1};
    n = n + 1;
    m = m + 1;
end
% % make importances
for l = 1:(BPwidthNumber + WCwidthNumber + CSSNumber)
    importance = 2;
    if l == 1
        FArray{m, 1} = ['IMP:n ', num2str(importance^(l+1))];
    else
        FArray{m, 1} = [' ', num2str(importance^(l + 1))];
    end
    m = m + 1;
end
FArray{m, 1} = [' ', '1 ', num2str(importance^(BPwidthNumber + ...
    WCwidthNumber + CSSNumber + 4)), ' ', ...
    num2str(importance^(BPwidthNumber + WCwidthNumber + ...
    CSSNumber + 5)), ' '];
m = m + 1;
FArray{m, 1} = [' ', ...
    num2str(importance^(BPwidthNumber + WCwidthNumber + ...
    CSSNumber + 3)) , ' ', num2str(importance) , ' ', ...
    num2str(importance^(BPwidthNumber + WCwidthNumber ...
    + CSSNumber + 3)) , ' ', num2str(importance) , '0'];
m = m + 1;
n = n + 1;
% % copy rest of cards
while n <= N && ischar(input{n, 1})
    FArray{m, 1} = input{n, 1};
    m = m + 1;
    n = n + 1;
end

otherfID = fopen([shielding, '\', dirname, '\', dirname, '.txt'], 'w');
fprintf(otherfID, '%s\n', FArray{:,1});
fclose(otherfID);

```

```

% % make appropriate batch file
copyfile('shielding.bat', [shielding, '\', dirname, 'shielding.bat']);
bID = fopen([shielding, '\', dirname, 'shielding.bat'], 'w');
batchFileArray{4, 1} = ['cd C:\Users\Ben Black\Documents\College'...
    'Senior ISU 2018\Senior Design\Shielding\', shielding, '\', dirname];
batchFileArray{5, 1} = ['E:\my_mcnp\MCNP_CODE\bin\mcnp6.exe i=', ...
    dirname, '.txt tasks 7'];
fprintf(bID, '%s \n', batchFileArray{:,1});
fclose(bID);
% % run batch file
directoryName = ['C:\Users\Ben Black\Documents\College Senior ISU',...
    '2018\Senior Design\Shielding\', shielding, '\', dirname, '\'];
system([directoryName, 'shielding.bat']);
% % rename outp file as openable text file
movefile([shielding, '\', dirname, 'outp'], [shielding, '\',...
    dirname, 'outp.txt'], 'f')
% % open outp file, put results in an array
outpID = fopen([shielding, '\', dirname, 'outp.txt']);
output = textscan(outpID, '%s', 'Delimiter', '\n');
output = output{1};
% % search for final result
outpSearch = regexp(output, '5000000\s+(\S+)\s+(\S+)', 'tokens');
outpSearch = [outpSearch{:}];
format short e
outpValueArray(count, 1) = WCindex; % thickness (cm)
outpValueArray(count, 2) = BPindex; % thickness (cm)
outpValueArray(count, 3) = str2double(outpSearch{size(outpSearch,...
    2) - 2}{1}); % final result
outpValueArray(count, 4) = str2double(outpSearch{size(outpSearch,...
    2) - 2}{2}) * outpValueArray(count, 3); % error
fclose(outpID);
end
end

% % these plots commented out below were not used as they were
% % difficult to read
%plot data
% plotaxes = axes;
% plotaxes.ZScale = 'log';
% hold all
% colormap(jet)
% colorbar
% scatter3(outpValueArray(:, 1), outpValueArray(:, 2),...
%     outpValueArray(:, 3), 10, log10(outpValueArray(:, 3)), 'filled')
% title('concrete thickness optimization')
% xlabel('WC thickness (cm)')
% ylabel('BP thickness (cm)')
% zlabel('fluence')
% view(45, 45)
% savefig(['Results\', shielding, 'results'])

```

```

csvwrite(['Results\', shielding, 'matrix.csv'], outpValueArray);

```

18.1.5 Example Continue Run and Data Analysis

```

cd 'C:\Users\Ben Black\Documents\College Senior ISU 2018\Senior Design\Shielding'
shielding = 'gammashielding';
count = 0;

%read batch file to array
batchID = fopen('continue.bat');

```

```

batchFileArray = cell(5, 1);
for index = 1:5
    batchFileArray{index, 1} = fgetl(batchID);
end
fclose(batchID);

indexarray = [4 4.5 5 5.5 6 7 8];
loopCount = length(indexarray);
outpValueArray = zeros(loopCount, 3);

for index = indexarray
    count = count + 1;
    cd 'C:\Users\Ben Black\Documents\College Senior ISU 2018\Senior Design\Shielding\'
    dirname = ['shielding', num2str(index)];
    % make appropriate batch file
    copyfile('continue.bat', [shielding, '\', dirname, '\continue.bat']);
    bID = fopen([shielding, '\', dirname, '\continue.bat'], 'w');
    batchFileArray{4, 1} = ['cd C:\Users\Ben Black\Documents\College Senior ISU 2018\Senior Design\Shielding\'
shielding, '\', dirname];
    fprintf(bID, '%s\n', batchFileArray{:,1});
    fclose(bID);
    % copy continue.txt to folder
    copyfile('continue.txt', [shielding, '\', dirname, '\continue.txt']);
    % run batch file
    % directoryName = ['C:\Users\Ben Black\Documents\College Senior ISU 2018\Senior Design\Shielding\'
dirname, '\',
    % system([directoryName, '\continue.bat']);

    % rename outp file as openable text file
    if exist([shielding, '\', dirname, '\outp'], 'file')
        movefile([shielding, '\', dirname, '\outp'], [shielding, '\', dirname, '\outp2.txt'], 'f')
    elseif exist([shielding, '\', dirname, '\outp2.txt'], 'file')
    else
        copyfile([shielding, '\', dirname, '\outp.txt'], [shielding, '\', dirname, '\outp2.txt'])
    end
    % open outp file, put results in an array
    outp2ID = fopen([shielding, '\', dirname, '\outp2.txt']);
    output2 = textscan(outp2ID, '%s', 'Delimiter', '\n');
    output2 = output2{1};
    % search for NPS
    nps = regexp(output2, 'nps\s+|=|s+(\S+)', 'tokens');
    nps = [nps{:}];
    fileNPS = cell2mat(nps{length(nps)});
    outp2Search = regexp(output2, [fileNPS, '\s+(\d{1}.\d{4})\S+)\s+(\d{1}.\d{4})\s+(\d{1}.\d{4})\s+(\d.\d)\s+', 'tokens');
    outp2Search = [outp2Search{:}];
    format short e
    outpValueArray(count, 1) = index; % thickness (ft)
    outpValueArray(count, 2) = str2double(outp2Search{size(outp2Search, 2)}{1}); % final result
    outpValueArray(count, 3) = str2double(outp2Search{size(outp2Search, 2)}{2}) * outpValueArray(count, 2); % error
    fclose(outp2ID);
end

%plot data
plotaxes = axes;
plotaxes.YScale = 'log';
xlim([3.5 8.5])
hold all
errorbar(outpValueArray(:, 1), outpValueArray(:, 2), outpValueArray(:, 3))
xlabel('thickness (ft)')
ylabel('fluence (p/cm2)')
savefig(['Results\_', shielding, 'results'])

```

```
csvwrite(['Results\'], shielding, 'matrix.csv'], outpValueArray);
```

18.2 Scripts and Batch Files

Batch scripts were written to aid in consecutively running MCNP input files without having to check when each run was complete. Examples of these scripts and other files used in conjunction with the .bat file are shared in the following sections.

18.2.1 Example .bat File for Windows System

```
for /F "tokens=*" %%A in (neutronfiles.txt) do (
    %%A
)
```

18.2.2 Example Read File for .bat

```
mcnp6 name=shielding4.txt tasks 31
mcnp6 name=shielding5.txt tasks 31
mcnp6 name=shielding6.txt tasks 31
mcnp6 name=shielding7.txt tasks 31
mcnp6 name=shielding8.txt tasks 31
```

18.2.3 Example .sh File for Linux System

```
mcnp6 name=shieldingBP0WC0.txt tasks 31
mcnp6 name=shieldingBP0WC1.txt tasks 31
mcnp6 name=shieldingBP0WC2.txt tasks 31
mcnp6 name=shieldingBP0WC3.txt tasks 31
mcnp6 name=shieldingBP0WC4.txt tasks 31
mcnp6 name=shieldingBP0WC5.txt tasks 31
mcnp6 name=shieldingBP0WC6.txt tasks 31
mcnp6 name=shieldingBP0WC7.txt tasks 31
mcnp6 name=shieldingBP0WC8.txt tasks 31
mcnp6 name=shieldingBP0WC9.txt tasks 31
mcnp6 name=shieldingBP0WC10.txt tasks 31
mcnp6 name=shieldingBP0WC11.txt tasks 31
mcnp6 name=shieldingBP0WC12.txt tasks 31
mcnp6 name=shieldingBP0WC13.txt tasks 31
mcnp6 name=shieldingBP0WC14.txt tasks 31
mcnp6 name=shieldingBP0WC15.txt tasks 31
```

18.3 Special Treatment for Tally Gaussian Energy Broadening Coefficients

The method used for solving the GEB coefficients was to create a Mathematica file that would perform a least squares fit to solve the equation provided in the MCNP manual for the data collected using the detector. The code with all the array values and the solution is provided here.

Finding the GEB Coefficients

Data Pairs (Emev, Fres)

```
data = {{1.3203, 0.099}, {1.2529, 0.0907}, {1.1713, 0.1059}, {0.6686, 0.0578}, {0.5188,  
0.0524}, {0.3701, 0.047}, {0.1372, 0.0196}, {0.0933, 0.0127}};
```

```
fit = FindFit[data, a+b*Sqrt[x+c*x^2], {a, b, c}, x]
```

```
{a->-0.0141448,b->0.0897491,c->0.191194}
```

19 Appendix H: SCALE Input Files

The following section provides an input file created in SCALE for modeling and simulating hand calculations.

19.1 Point Kernel Models

Similar to the MCNP input files, only the aluminum input file is shown.

```
=mavric
' TITLE BLOCK
SCALE code verification Compare to hand calculations
' This input file creates an aluminum sphere of 20 cm radius around a 1.0 MeV
' point source. The sphere is surrounded by air. A point detector is placed 1
' meter from the source to measure particle fluence rate.
'
' CROSS SECTION BLOCK
v7-200n47g
' COMPOSITION BLOCK
read composition
' composition 1 is the standard composition of regulatory concrete listed in
' the SCALE manual.
aluminum 1 end
' composition 2 is dry air for filling the problem volume
dry-air 2 end
end composition
' GEOMETRY BLOCK
read geometry
global unit 1
com="Unit 1"
' This sphere is filled with concrete and has a 20 cm radius.
sphere 1 20
' This sphere is the kill sphere. It has a 2m radius.
cuboid 2 -200 200 -200 200 -200 200
' This sphere is the vacuum around the point detector.
sphere 3 0.5 origin x=100 y=0 z=0
' Material 1 (concrete) is placed inside sphere 1.
media 1 1 1
' Material 2 (dry air) fills the boundary but not the objects
media 2 1 -1 2 -3
' Media 0 (void) is placed inside of sphere 3
media 0 1 3
' The problem boundry is the surface of cuboid 2
boundary 2
end geometry
' DEFINITIONS BLOCK
read definitions
' Location 1 defines the detector location. It is located relative to the
' center of the fuel bundle, but on the opposite side of the concrete wall.
' It is located 1 cm from the wall.
location 1
title="point detector at the center of the person's head"
position 100 0 0
end location
response 2
photon
```

```

bounds 1000.0 2.0e7 end
values 1.0 1.0 end
end response
' Response 9502 applies Henderson conversion factors -> rad/hr
' response 9502
' specialdose=9502
' end response
' Response 9503 applies Claiborne-Trubey conversion factors -> rad/hr
' response 9503
' specialdose=9503
' end response
' Response 9504 applies ANSI/ANS-6.1.1-1977 conversion factors -> rem/hr
response 9504
specialdose=9504
end response
' Response 9505 applies ANSI/ANS-6.1.1-1991 conversion factors -> rem/hr
response 9505
specialdose=9505
end response
' Response 9506 applies ICRU-57 Air Kerma conversion factors -> Gy/hr
' response 9506
' specialdose=9506
' end response
' Response 9510 applies ICRU-57 Effective dose conversion factors -> Sv/hr
' response 9510
' specialdose=9510
' end response
' Distribution 1 creates the PDF for a point source emitting 1 MeV gammas.
distribution 1
title="1 MeV point source"
discrete 1e6 end
truepdf 1 end
end distribution
' Grid Geometry 5 will be used in the importance mapping calculation
gridGeometry 5
xLinear 40 -200 200
yLinear 40 -200 200
zLinear 40 -200 200
end gridGeometry
end definitions
' SOURCE BLOCK
read sources
' Point source placed in cuboid 3 distributed according to the ORIGIN file
src 1
strength=3.7E10
photons
origin x=0 y=0 z=0
edistributionid=1
end src
end sources
' TALLY BLOCK
read tallies
' Point detector 1 is a photon detector at Location 1
pointDetector 1
photon
title="point detector 1"
locationID=1
responseIDs 2 9504 9505 end
end pointDetector
end tallies
' PARAMETERS BLOCK
read parameters

```



```

' The first random seed is listed. There are 250000 histories per batch
' and 50 batches
randomSeed=0000000100000001
perBatch=2000000
batches=500
end parameters
' IMPORTANC MAP BLOCK
read importanceMap
'Adjoint source must have same responseID as the detector it is optimizing
'for point detectors the LocationID must also be the same as the detector
'The grid geometry used to optimize detector 1 will be gridGeometry5
adjointSource 1
locationID=1
responseIDs 2 9504 9505 end
end adjointSource
gridGeometryID=5
end importanceMap
end data
end

```

20 Appendix I: SCALE Message Passing Interface (MPI) Build

NOTE: “The internal frameworks for launching SCALE jobs in parallel are experimental in this release. Users must accept all responsibility for using these parallel capabilities on their systems.”

[44] The term “this release” being SCALE 6.2 and 6.2.1. OpenMP is the recommended parallel capability. OpenMP is available for all platforms (Windows, Linux, and Mac).

SCALE 6.2.1 offers the option to install a message passing interface (MPI) version of the software using the source code. Installation, or more properly build, of the MPI version allows the user to leverage parallel processing in several of the SCALE sequences and modules. Example sequences where parallel processing is accessible with a MPI build are SAMPLER and ORIGAMI, whereas examples modules are KENO Va, KENO VI. Similarly, any sequence implementing these modules may operate in parallel, such as CSAS and TSUNAMI. See Table 20–I for a more thorough list of sequences and modules capable of utilizing MPI.

Building the MPI version of SCALE may afford challenges. The MPI build may only be installed on Linux or Mac operating systems (OS). Building MPI is not available for Windows OS for this version, or previous versions, of SCALE. If the researcher is not already familiar with Linux or Mac, then they must also learn how to use this new OS in conjunction with building SCALE MPI.

Before building a SCALE MPI one must order the source code from RSICC. After being approved RSICC will send the code. If you already have an executable version the source code will be sent without the data files. If you do not already have SCALE the source code and the data files will be sent together.

Table 20–I A list of SCALE modules and sequences capable of parallel processing after building with MPI.

Modules or Sequences	Notes
CSAS5	
CSAS6	Automatically invokes parallel KENO-VI
DENOVO	Serial when run as part of MAVRIC
KENO V.a	
KENO-VI	
ORIGAMI	
ORIGEN	
POLARIS	
RUNNER	
SAMPLER	
T6-DEPL	Automatically invokes parallel KENO-VI
TRITON	
TSUMANI-3D-K6	Automatically invokes parallel KENO-VI

This description for building SCALE MPI is based on Linux OS. CentOS 7 was the OS installed on the system. However, CentOS 7 is not explicitly supported by SCALE help. See Table 20–II for a list of supported OSs. Though the build for Mac OS is similar, please refer to README literature [57] provided on the disc with the software or pose questions to scalehelp@ornl.gov.

Table 20–II SCALE Supported operating systems.

Operating Platform	Supported OS
Linux	Red Hat Enterprise Linux (RHEL) 6 64-bit
Mac	OS X (Darwin) 10.9.5 or newer
Windows	Windows 7, 64-bit or newer

20.1 Building SCALE MPI

This section contains many direct quotes from the README pdf, as well as notes and comments to assist the reader in building their SCALE MPI. These notes and comments are compiled from the experience of the author while performing the build and learning Linux at the same time. Direct quotes from the README will be indicated by the use of quotation marks (“ ”).

The README begins with the following

“These instructions are only for those who wish to recompile their SCALE binaries. If you are running SCALE using the precompiled binary executable files distributed with SCALE, please disregard this section.

“For SCALE 6.2, the build configuration has been completely renewed relative to all previous versions. The SCALE build is now based on CMake from KitWare, which supports a consistent experience on Linux, Mac, and Windows.”

So, if you want to venture into the experience of compiling the binaries for a parallel version of SCALE continue reading. The author recommends you consider the need for parallel processing carefully. If it is not a necessity or the sequence/module will not make use of the parallel capabilities, do not proceed. Just install the precompiled binaries. However, if you need parallel processing or really like to experience an adventure continue on.

According to the README

“There are four main steps to create and install SCALE binaries

1. Install compilers and third-party libraries (TPLs)
2. CMake configuration - This generates a native build tree
3. Compilation - This compiles all executables and libraries
4. Installation - This deploys all executables into a configuration ready for execution”

Sounds simple enough. Each step is shown in detail.

20.1.1 Installing Compilers and Third-party Libraries (TPLs)

The steps for installing compilers and third-party libraries (TPLs) will not be discussed. The user will need to follow the recommended installation steps provided with the compiler or library. Rather this section will discuss of which compilers and TPLs are recommended.

This is the most difficult step in the process. The user must make sure all TPLs are compatible with SCALE. This means the user must validate the compiler and TPL version number installed with the OS, or the version number selected for installation (if not installed with the OS), are the recommended versions for SCALE, otherwise SCALE may not be able to interact or use the version installed. This validation of version numbers is absolutely crucial for the build (configuration, compilation, and installation). Neglecting to perform this validation will result in the build not completing or the installation not functioning properly.

The recommended compilers listed in the README are

1. “Fortran Compiler
 - a. Linux –
 - i. Intel Fortran compiler 14.1+
 - ii. GNU gfortran 4.8.3+ compiler
 - b. Mac OS – GNU gfortran 4.8.5+ compiler
 - c. Windows – Intel Fortran compiler 15.0
2. “C/C++ Compiler
 - a. Linux –
 - i. Intel C/C++ compiler 14.1+
 - ii. GNU g++/gcc 4.8.3+ compiler
 - b. Mac OS – GNU g++/gcc 4.8.5+ compiler
 - c. Windows – Intel C/C++ compiler 15.0
3. “CMake 2.8.12.2+ - Platform independent build configuration.”

SCALE also requires installation of the following libraries: QT, LAPACK and BLAS. LAPACK and BLAS come together in a package. They are linear algebra packages used in the computations made by SCALE. The installed versions of these libraries are QT 4.8.5 and LAPACK/BLAS 3.4.2. In order for the configuration to be successful the path to each of the TPLs will need to be modified in the configure file in order for the configuration to find where these libraries are installed. This is also true for other software, if there are more than one version installed, or the software is installed in a unique location. Specifics regarding how to do this will be discussed in Section 20.1.3.

In order to perform parallel processing with this build installation of another program is required, OpenMPI. The supported versions of OpenMPI is 1.8.x or 1.10.x. CentOS 7 automatically installed a more current version, OpenMPI 2.0.2. For some reason, unknown to the author and not specified by SCALE Help, this version is not compatible with and is not supported by SCALE. Removal of version 2.0.2 and installation of 1.10.x was required before the configuration worked properly.

20.1.2 Pre-configuration

After making sure the correct compilers and libraries are installed and notes made about the location of installation the next step is to create a directory for the SCALE discs. Once made copy the SCALE files from the discs to this directory. The author created a second directory and unpacked the source code, SCALE-6.2-serial-6.2.1-Source.zip, into this directory. For the remainder of this document the directory with the unpacked source code will be referred to as <SCALE_SRC_ROOT>. The SCALE README.pdf also refers to this directory in the same fashion.

Within <SCALE_SRC_ROOT> the user will need to create a directory. The README.pdf calls this directory “build”. Within the build directory create a sub-directory. The README calls this subdirectory “gcc”.

If you are using a Linux OS graphics user interface (GUI) then creation of directories is done the same way as in Windows by clicking the right button on the mouse and selecting “new folder” followed by renaming the folder. If you are using the command prompt to create directories open a command prompt and change directories to <SCALE_SRC_ROOT>. Once in this directory the specific command for creating the build and gcc directories simultaneously is as follows

```
<SCALE_SRC_ROOT>$ mkdir -p build/gcc
```

Next make a copy of the configuration file, `configure_scale_mpi.sh`, and save it in the `build/gcc` directory. The configuration file may found in `<SCALE_SRC_ROOT>/script`. If using GUI right click and “copy” from the script directory and then navigate back to `build/gcc` and right click and select “paste”. If using command prompt use the following command from the root directory

```
<SCALE_SRC_ROOT>$ cp script/configure_scale_mpi.sh build/gcc
```

20.1.3 CMake Configuration

The CMake configuration consists of four steps: altering the file `configure_scale_mpi.sh`, making `configure_scale_mpi.sh` executable, altering a very specific `CMakeLists.txt` file, and executing the configuration. The first step is the most complicated and care must be taken to provide the correct paths to the libraries. Failure to provide the correct paths will result in failure of the configuration and ultimately installation failure. Attention to detail is important on this step.

STEP 1 Altering the configuration file:

Open the copy of `configure_scale_mpi.sh` from the `build/gcc` directory in a text editor for alterations. Do not alter the original in the script directory. It may be needed to undo errors made on the copy.

The first changes to make are for the libraries. Scroll down the file until you see the section titled “# TPLs”. Under this you will see “`MPI=/home/...`” and “`LAPACK=/opt/...`” The path after the equal sign will need to be altered to the correct path for the location where OpenMPI and LAPACK were installed. On the author’s machine these were altered to read

```
MPI=/usr/local/bin  
LAPACK=/usr/lib64
```

The following alterations were required on the author's configuration because the author has two versions of QT and CMake installed. These may not be required for the typical user. However, if multiple versions of libraries are installed these types of alterations are probable.

Near the top of the configure file is a line reading "export INSTALL_PATH=\${PWD}/INSTALL". After this line the author included a new path to the version of CMake to use. These lines read

```
# use a newer cmake
CMAKE=/opt/cmake/bin/cmake
```

Additionally, under the "# TPLs" the following line was added for the QT path

```
QT=/usr/lib64/qt4
```

The final alteration to the configure file is in the last section of the file. The first line, "cmake \" is changed to

```
${CMAKE} \
```

And the following line is added to the end of the "-D" list, prior to the "\$*"

```
-D CMAKE_PREFIX_PATH:PATH=${QT} \
```

Save the file when the alterations are complete.

STEP 2 Making the configuration file executable:

Open a command prompt window and navigate to <SCALE_SRC_ROOT>/build/gcc. Type the following command and press enter.

```
chmod u+x configure_scale_mpi.sh
```

The command "chmod" is short for change mode. The "u" indicates to make this change only for the current user/owner.

STEP 3 Altering the CMakeLists.txt file.

Open a folder and navigate to <SCALE_SRC_ROOT>/Trilinos/packages/anasazi/src directory. Open the CMakeLists.txt file from this folder in a text editor. The README provided by SCALE says to modify a single line in this file by commenting out this one line. NOTE: This is incorrect and has not been updated. There are three lines to comment out. Find the following three lines and simply add a “#” at the beginning of the line to comment them out.

```
ASSERT_DEFINED(Anasazi_ENABLE_ThyraEpetraAdapters)
ASSERT_DEFINED(Anasazi_ENABLE_ThyraCore)
ASSERT_DEFINED(Anasazi_ENEBLE_Tpetra)
```

Save the file after these lines have been commented out.

STEP 4 Executing the configuration:

Open a command window and navigate to <SCALE_SRC_ROOT>/build/gcc. Type the following command and press enter.

```
./configure_scale_mpi.sh ../..
```

A lot of output will follow the entering of this command. If all of the necessary alterations were made successfully and the configuration is successful the final few lines of the output will read similar to

```
Finished configuring SCALE!
Removing .h5.inp input files...
Generating bsxml regression script file...
Generationg bsxml sample problem script file...
Adding sample problems...
- - Configuring done
- - Generating done
- - Build files have been written to:
/home/.../<SCALE_SRC_ROOT>/build/gcc
```

20.1.4 Compilation and Installation

Compilation is completed by use of the command “make”. This command will build the necessary targets for the installation. In this document, ALL of the SCALE modules and components are build and installed. For information on how to build and install individual modules independently see the README.pdf or ask SCALEHELP. Installation takes the built targets and installs all of the binaries for use. Compilation and installation may be performed with a single command line entry. From the command prompt in the build/gcc directory type and press enter

```
make install
```

After pressing enter a lot of output will follow. You should see a percent progress [%1] at the beginning of each line of output until it reaches 100%. At this point the compilation is complete and the installation begins and more output follows. Typical lines read

```
-- Installing: /some path/.../some file name.extension
```

Compilation and installation will take some time. It took several hours on the author’s machine.

20.2 Installing DATA Files

This section details the steps for installing the data files associated with SCALE. These steps are a direct quote of those in the README provided with the discs. In addition to the installation the data will need to be associated with the MPI built SCALE. The steps to make this association are also provided.

“To begin installation of SCALE 6.2 data, **copy the scale-6.2-data-setup.jar to your local disk. Double-click this jar file. If the installer does not start** then bring up a command prompt or terminal window and issue the following command:

```
java -jar scale-6.2-data-setup.jar
```

in the location where the installer jar file was copied.”

The author created a folder in the build/gcc directory called “data” and unpacked the scale-6.2-data-setup.jar to this folder.

“After launching the installer, a dialog should appear as shown below.

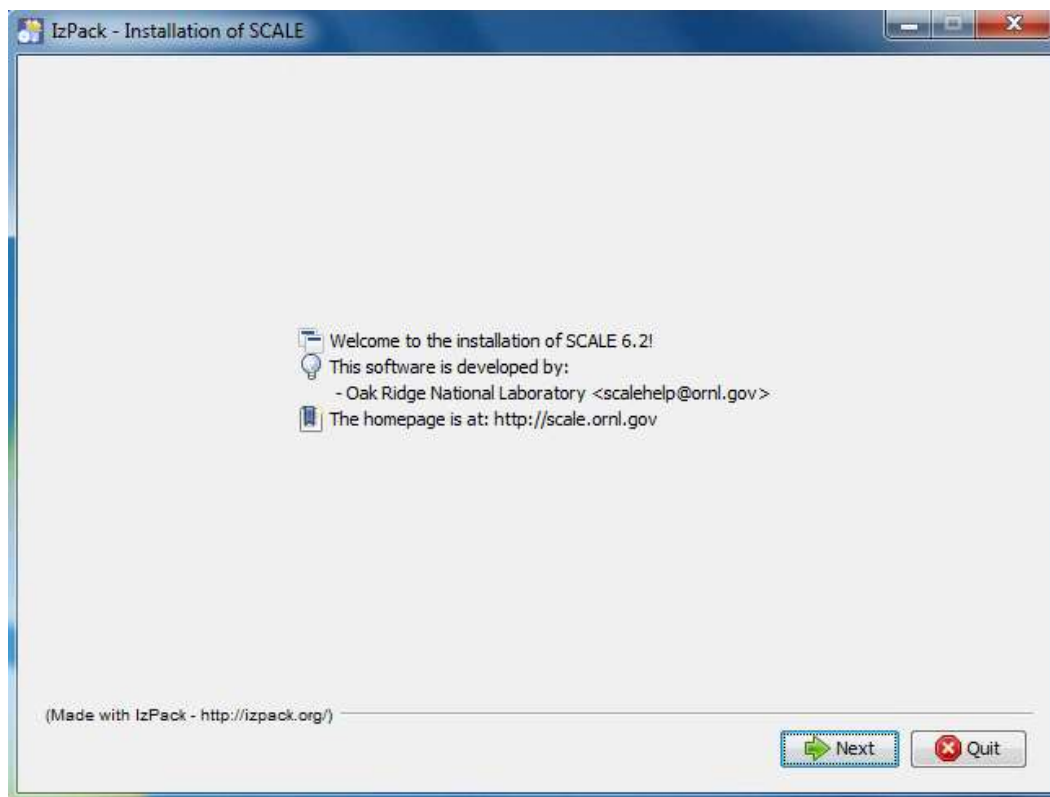


Figure 20-1 SCALE 6.2 data installer welcome dialog.

“Please continue by pressing *Next*.

“You will be prompted to review and accept the terms of the license agreement.

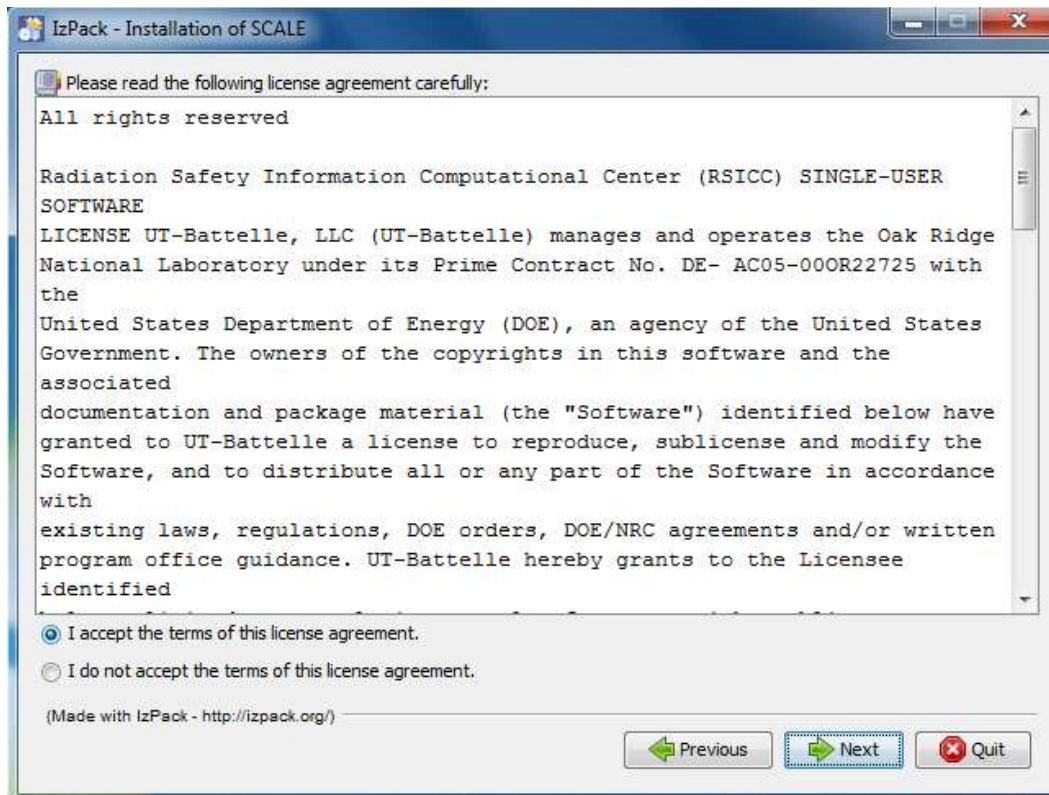


Figure 20-2 SCALE license agreement.

“To proceed, check that you accept the terms and press next.

“You will be prompted to choose the destination of your installation.

“For Windows users, the recommended installation path is inside your SCALE-6.2 directory:

c:\SCALE-6.2

“For Linux, a typical location is:

/scale/scale6.2

“For Mac, a typical location is:

/Applications/SCALE-6.2.app/Contents/Resources

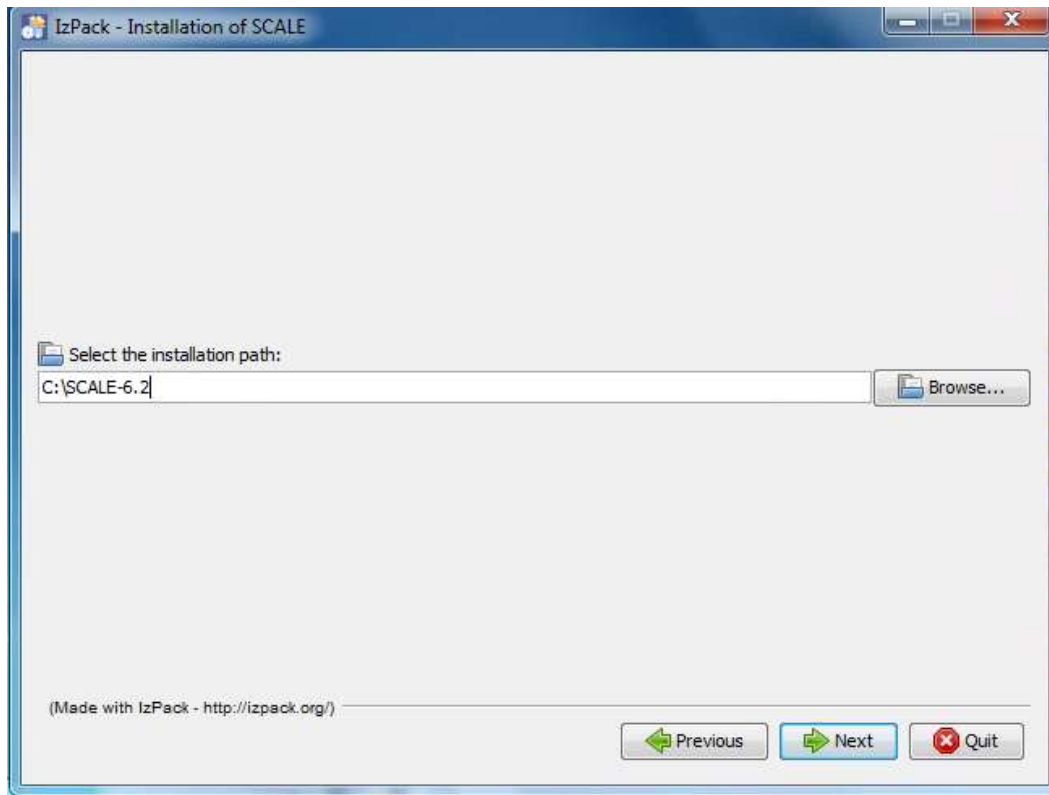


Figure 20-3 Setting typical data installation path on Windows.

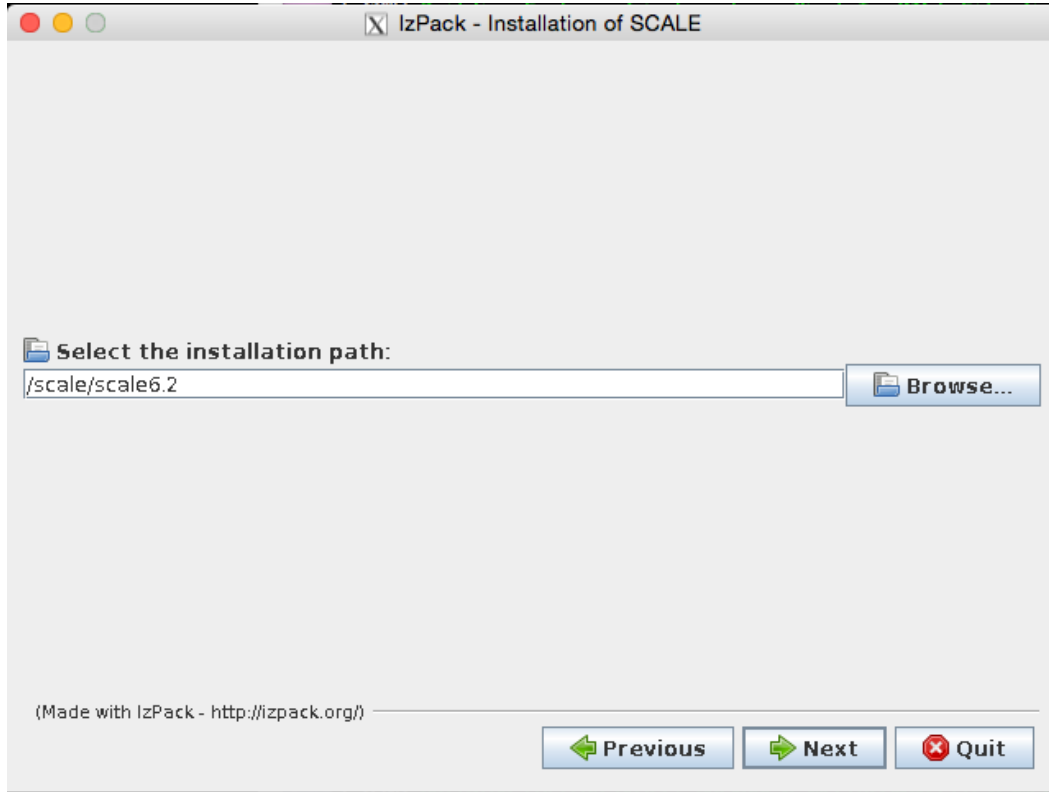


Figure 20-4 Setting a typical data installation path on Linux.

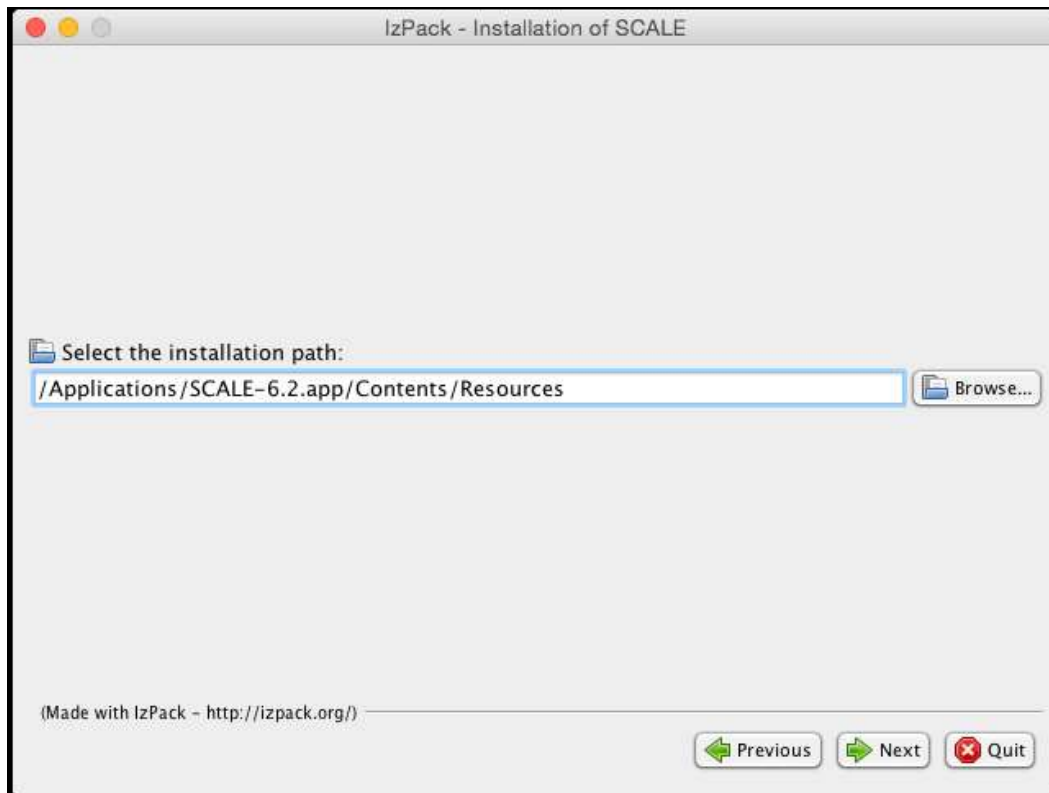


Figure 20-5 Setting a typical data installation path on Mac.

“For some systems, the installer will not be allowed to create a new directory. If you encounter a message like the one shown below, simply create the directory manually (e.g. using Windows Explorer) then return to the installer and continue.

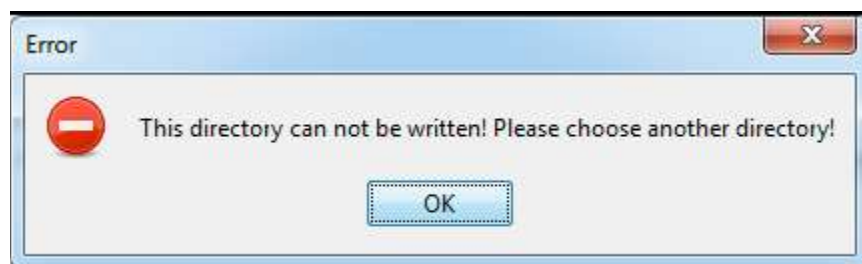


Figure 20-6 Data installer directory creation error message.

“In most cases, the installer will present a prompt to confirm the creation of a new directory; if that target directory is correct you can simply press *OK*.

“If the directory was manually created, the installer will notify you that it is about to overwrite any previous contents. Press *Yes* to continue.



Figure 20-7 Directory overwrite dialog.

“The installer then presents a dialog for available data sets you wish to install.

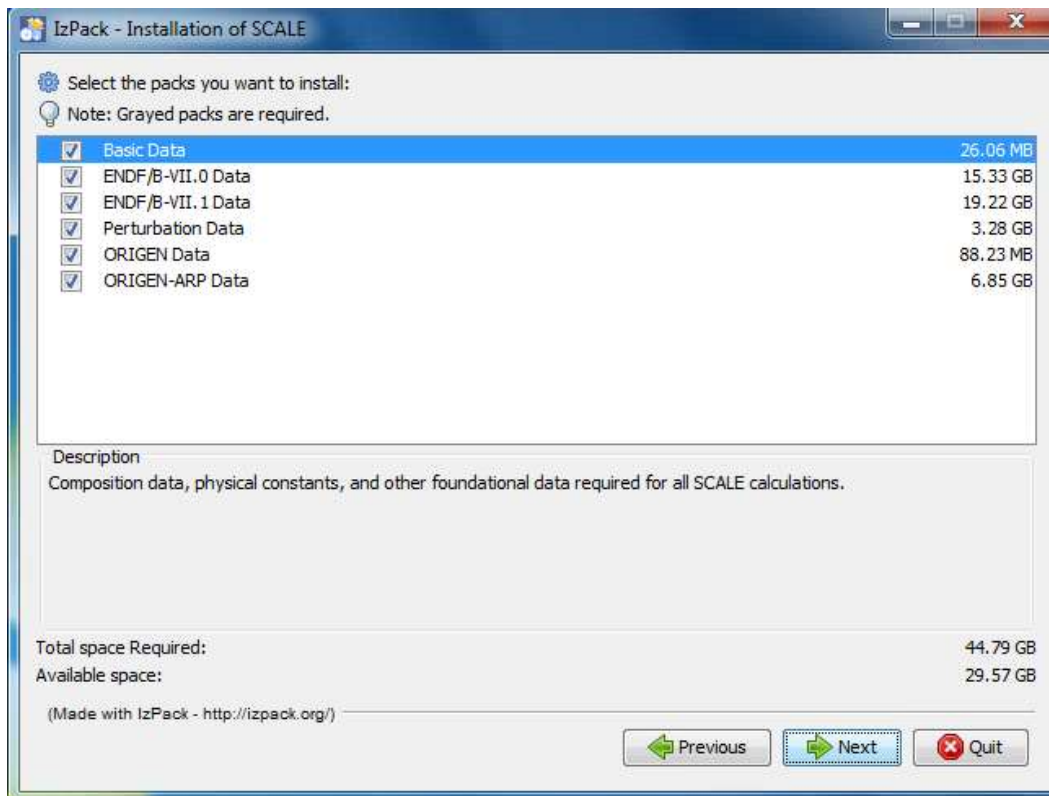


Figure 20-8 Data selection dialog.

“Please select the data needed to perform your desired SCALE calculations.

- Basic Data — Composition data, physical constants, and other foundational data required for all SCALE calculations.

- ENDF/B-VII.0 Data — Nuclear Data from ENDF/B-VII.0 for continuous-energy and multi-group calculations; Coupled n-gamma data from ENDF/B-VII.0 for multi-group calculations;

SCALE 6.0/6.1 44-group neutron covariance data. Optional for most calculations, but provided for backwards compatibility.

- ENDF/B-VII.1 Data — Nuclear Data from ENDF/B-VII.1 for continuous-energy and multi-group calculations; Coupled n-gamma data from ENDF/B-VII.1 for multi-group calculations; ENDF/B-VII.1 neutron covariance data. Recommended for most calculations and required to run the SCALE sample problems.

- Perturbation data — 1000 samples of data each for: ENDF/B-VII.1 neutron covariance data, SCALE 6.0/6.1 neutron covariance data, fission product yield covariance data, and radioactive decay covariance data. Required for Sampler calculations.

- ORIGEN Data — Activation, depletion and decay data from ENDF/V-VII.1 and JEFF 3.1. Required for activation, depletion and decay calculations.

- ORIGEN-ARP Data — Pre-generated ORIGEN reactor libraries for many fuel types. Required for spent fuel characterization and source terms calculations.

“Next, the installer may ask for the location of the data *.pak* files that are unpacked during the installation process. Please direct the installer to the location of these data files, which are part of the SCALE distribution and may be on the distribution media or copies to a local directory as shown below.

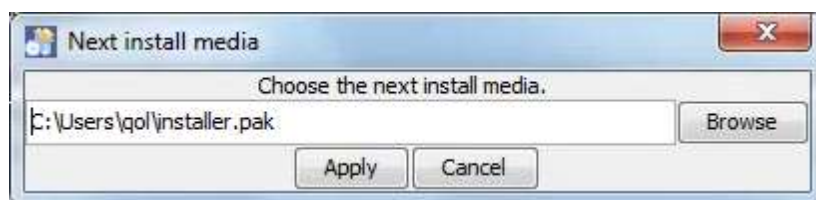


Figure 20-9 Media selection dialog.

“The installer will post the progress of the installation. If installing from a DVD set, part way through the installation you will be prompted for installer.pak.1. Please insert the PAK.1 disk and click *Apply*.

“The installation from PAK.1 will complete and prompt for installer.pak.2. Please insert the PAK.2 disk and click *Apply*.

“PAK.2 will finish. Proceed with all DVDs or files in the delivery until you have completed your installation of SCALE 6.2.”

In order to associate the data files with SCALE the user will need to open Fulcrum. From the “file” menu select “settings”.

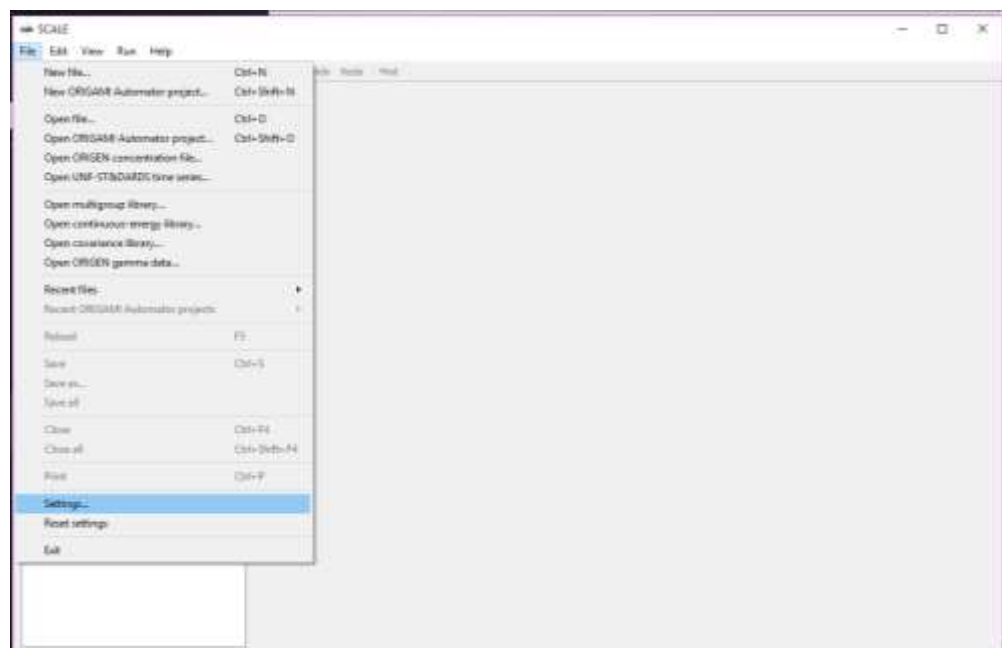


Figure 20-10 Location of the “settings” option in Fulcrum.

Selecting settings opens a dialog box.

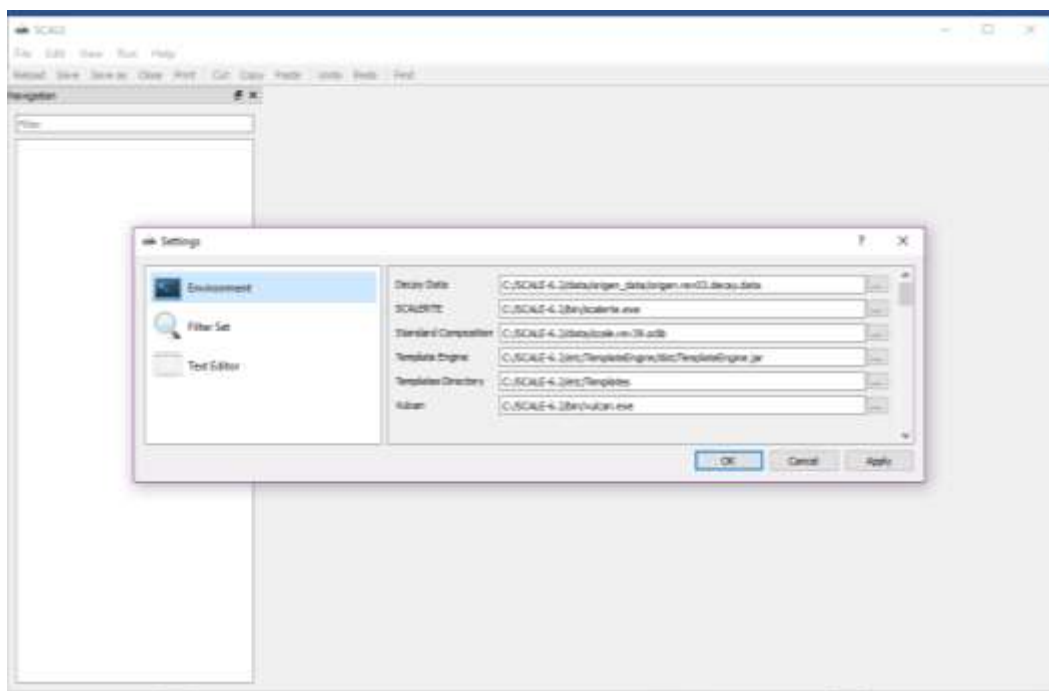


Figure 20-11 Settings dialog box.

Figure 20-11 is a representation from a Windows installation, but in a Linux installation it will look the same. When you perform an MPI build the data installation will fill each of these boxes with a default directory. Many of them will be highlighted in red. ALL of the entries highlighted in RED must be altered to the correct directory for the file listed. For example, the user will need to search for the file “origen.rev03.decay.data” and then replace the listed path in the “Decay Data” field. On the author’s machine this path was

```
/home/user/<SCALE_SRC_ROOT>/build/gcc/data/data/origen_data/origen.rev03.decay.data
```

If an entry is not highlighted in red, do not change it. Users do not need to make alterations to any other tabs in the settings.

20.3 Implementing Parallel Processing

This section discusses notation in the input file and customization configuration in the Fulcrum GUI needed for invoking parallel processing.

NOTE: Parallel code execution is currently available on Linux and Mac systems but is NOT AVAILABLE on Windows PCs.

“SCALE 6.2 contains five modules and sequences that have distributed memory (MPI) parallelism; KENO V.a, KENO-VI, Sampler, ORIGAMI, and Runner...

“Control modules, like CSAS6, T6-DEPL, and TSUNAMI-3D-K6, automatically initiate the parallel version of KENO-VI in a parallel SCALE build if the user provides the required arguments as summarized below. When running a standalone code in parallel (such as KENO-VI), a “%” prefix on the sequence specification record in the input file (e.g. =%keno-vi).” For example, the first line of the input file should look like Figure 20-12.

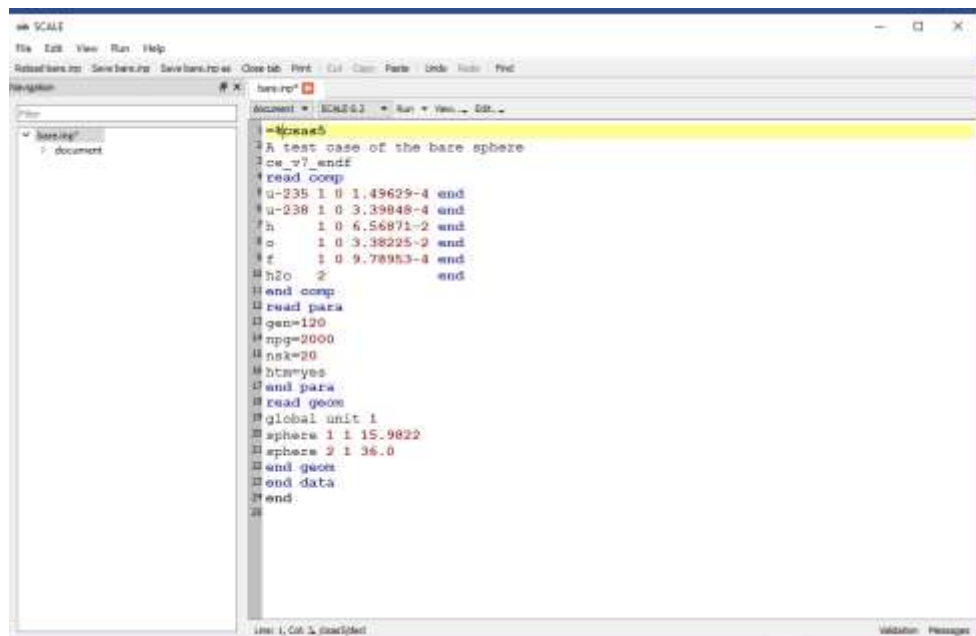


Figure 20-12 First line input file argument used to initiate parallel processing.

In addition to adding the notation on the first line the user needs to customize the arguments associated with SCALE. In order to do this, click on the “SCALE 6.2” tab just above the input file text then select “customize...”. See Figure 20-13.

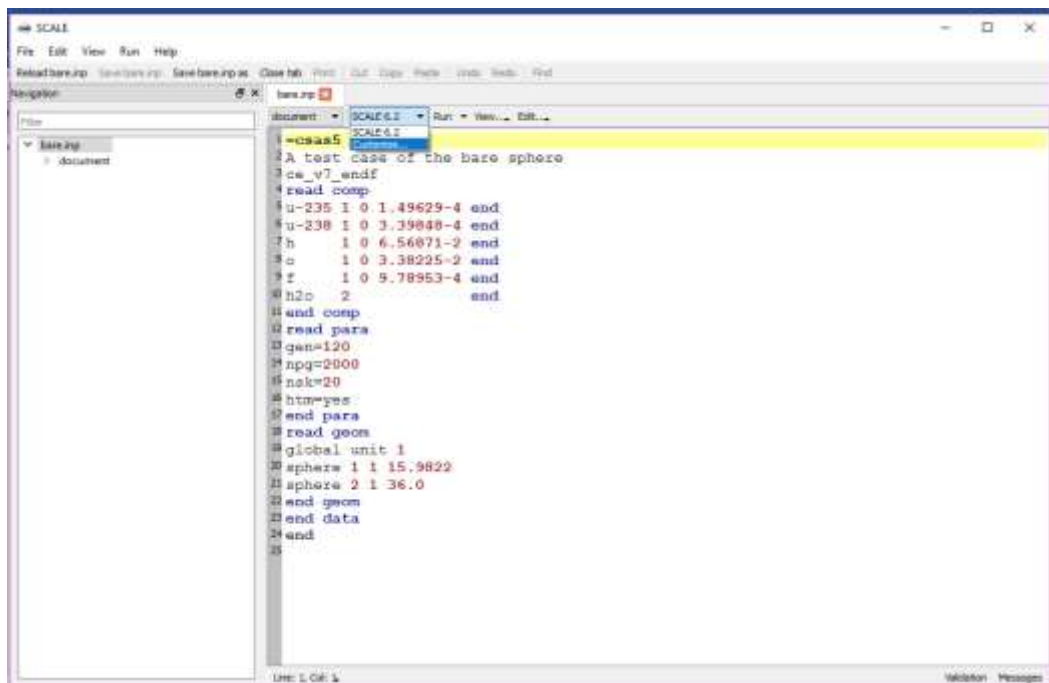


Figure 20-13 Location of the customize options in Fulcrum.

Selection of the “customize...” option will open a dialog box similar to the one in Figure 20-14.

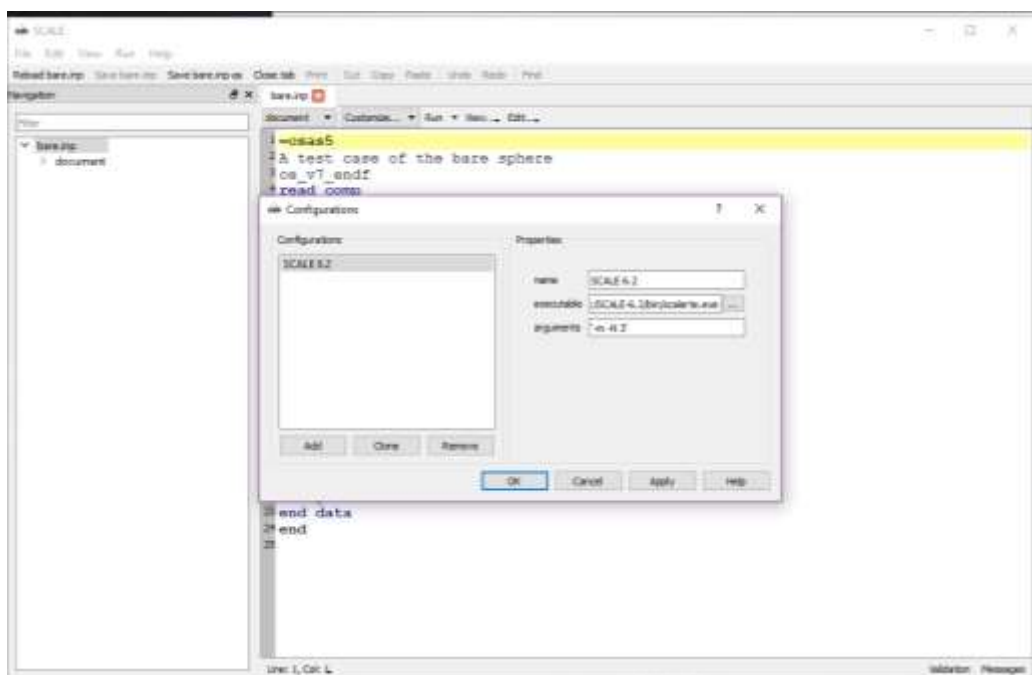


Figure 20-14 Customize dialog box.

The “arguments” field will most likely have only the argument “-m” in the field. In order to specify the number of parallel threads, the user must add the argument “-N #”, where # is the

number of threads to use. In Figure 20-14 the author indicated 3 threads are to be used for this CSAS5 calculation.

If the threads/processors are located on more than one node in a computer cluster, further arguments are required. Please refer to the README or contact SCALEHelp for assistance on this topic.